



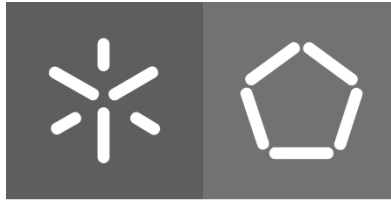
Universidade do Minho
Escola de Engenharia

Design of a wearable active ankle-foot orthosis for both sides

Catarina Enes Ribeiro

**Design of a wearable active ankle-foot
orthosis for both sides**





Universidade do Minho

Escola de Engenharia

Catarina Enes Ribeiro

Design of a wearable active ankle-foot orthosis for both sides

Dissertação de mestrado

Mestrado Integrado em Engenharia Biomédica

Ramo de Biomateriais, Reabilitação e

Biomecânica

Trabalho efetuado sob orientação do(a)

Professor Doutor Eurico Augusto Rodrigues

Seabra

Professor Doutor Luís Fernando Sousa Ferreira

Silva

abril 2021

COPYRIGHTS AND TERMS OF USE OF WORK BY THIRD PARTIES

This is an academic work that can be used by third parties as long as the rules and regulations internationally accepted good practices with regard to copyright and related rights, are respected.

Thus, the present work can be used under the terms provided for in the license indicated below.

If the user needs permission to be able to use the work under unforeseen conditions in the indicated licensing, you should contact the author, through the RepositóriUM of the University of Minho.

License granted to users of this work



**Atribuição-NãoComercial-SemDerivações
CC BY-NC-ND**

<https://creativecommons.org/licenses/by-nc-nd/4.0/>

ACKNOWLEDGEMENTS

First thing first, I wanted to acknowledge the tremendous support of the Orthos XXI design team, namely Engineer André Ribeiro, who always found time within his busy days to help me, not only with the design but also with this master thesis. I also want to thank Engineer António Ribeiro for providing me the opportunity to fulfil my master's degree in biomedical engineering in a company that dedicates its work to precisely this area. With the curricular internship, I was able to get an insight into how a Portuguese engineering company works and, specially, was able to improve capabilities with regard to CAD drawing in the SolidWorks® tool. On this matter, I would have to also thank the designers working at the same company, who always found time to aid me and clarify my doubts.

To the rest of the SmartOs design team, Joana Figueiredo, Mihai Popescu and Professor Mário Vaz, a big thank you for being an excellent team to work with and for providing me the opportunity to learn more not only about mechanical design but also about teamwork.

To the people who were always eager to share their acquired knowledge and expertise on the matters of human anatomy and biomechanics, Dra. Rita Proença from the Santa Luzia Hospital of Viana do Castelo, and Professor João Paulo Vilas-Boas, director of LABIOMEP.

I would like to thank my supervisors, Professor Eurico Seabra and Professor Luis Ferreira da Silva, for the constant support and teachings on the area of mechanical design. I hope everything turns out well and that life treats you amazingly, as you deserve.

To the people on the rearward, with whom I found the tranquillity and laughter during the times I most needed it. My friends who were going through the same life phase as me that, with the shared stories concerning the past year about all the times of adversity and moments of success, were able to transform this atypical year into something bearable and strangely fun. I couldn't help but thank also to the ones who were not experiencing the same academic circumstance but could always find a soothing word, which definitely helped putting things into a more rational, pragmatic, and comfortable perspective. My parents and brother, who always provided me with the support one needs to tackle all sort of challenges during a lifetime. To the rest of my family, my uncle,

aunt, and cousins who found their ways to make my experience in a new city more comfortable and fuller of the confectionery a girl requires. To Hugo for being my best of friends. Because a dog is indeed a human's best friend, I want to acknowledge my dogs for being the most precious creatures inhabiting this planet and for ameliorating all life even without knowing it.

A big warm thank you to everyone with whom I got the pleasure to share this existence.

“Perhaps the most indispensable thing we can do as human beings, every day of our lives, is remind ourselves and others of our complexity, fragility, finiteness, and uniqueness.”

- António R. Damásio

STATEMENT OF INTEGRITY

I hereby declare having conducted this academic work with integrity. I confirm that I have not used plagiarism or any form of undue use of information or falsification of results along the process leading to its elaboration.

I further declare that I have fully acknowledged the Code of Ethical Conduct of the University of Minho.

RESUMO

Portugal é o país da Europa ocidental com maior taxa de mortalidade por acidente vascular cerebral (AVC), sendo que, dos que sofrem acidentes vasculares cerebrais, 40% apresentam uma deficiência que pode manifestar-se por sequelas motoras, nomeadamente o pé pendente. Uma ortótese do tornozelo é recomendada frequentemente para acomodar passivamente esses problemas motores; no entanto, exoesqueletos ativos são também uma solução adequada para pacientes pós-AVC. Devido à alta complexidade da articulação do tornozelo humano, um dos problemas associados a esses dispositivos ativos é o desalinhamento que ocorre entre o dispositivo de reabilitação e a articulação humana, que é uma causa de forças parasitas, desconforto e dor.

A presente dissertação de mestrado propõe o desenvolvimento de uma ortótese ativa do tornozelo ajustável e vestível, que seja capaz de resolver esse problema de desalinhamento relativo aos dispositivos ortóticos de membros inferiores disponíveis comercialmente. Este trabalho está integrado no projeto SmartOs - *Smart, Stand-alone Active Orthotic System* - projeto que propõe uma tecnologia robótica inovadora (*wearable mobile lab*) direcionada para a reabilitação da marcha.

O projeto conceptual de uma versão padrão da ortótese ativa vestível do projeto SmartOs foi iniciado com a análise de outra ortótese do tornozelo – Exo-H2 (*Technaid*) - a partir da qual foram implementadas as alterações de projeto necessárias, visando o aprimoramento do dispositivo estabelecido. Para se chegar a uma solução conceptual, tanto o conhecimento prático da equipa de projeto da Orthos XXI como os diversos métodos de projeto foram utilizados para garantir o cumprimento dos requisitos definidos. O processo do desenho detalhado da versão padrão da ortótese ativa SmartOs será também divulgado. Com o objetivo de validar o projeto, os componentes críticos foram simulados com os recursos disponíveis no SolidWorks® e as adaptações necessárias do modelo CAD foram implementadas para garantir um projeto fidedigno e seguro. O projeto apresentado está atualmente em preparação para produção na empresa Orthos XXI, depois do qual se seguem os ensaios mecânicos obrigatórios.

Palavras-chave: Pé pendente; Projeto mecânico, Reabilitação; Ortótese ativa vestível.

ABSTRACT

Portugal is the west European country with the highest rate of stroke-related mortality, being that, of those who suffer cerebrovascular accidents, 40% feature an impairment which can manifest itself through motor sequelae, namely drop foot. An ankle-foot orthosis is often recommended to passively accommodate these motor problems; however, active/powered exoskeletons are also a suitable solution for post-stroke patients. Due to the high complexity of the human ankle joint, one of the problems regarding these active devices is the misalignment occurring between the rehabilitation device and the human joint, which is a cause of parasitic forces, discomfort, and pain.

The present master dissertation proposes the development of an adjustable wearable active ankle-foot orthosis that is able to tackle this misalignment issue concerning commercially available lower limb orthotic devices. This work is integrated on the SmartOs – *Smart, Stand-alone Active Orthotic System* – project that proposes an innovative robotic technology (a wearable mobile lab) oriented to gait rehabilitation.

The conceptual design of a standard version of the SmartOs wearable active orthosis was initiated with the analysis of another ankle-foot orthosis – Exo-H2 (Technaid) – from which the necessary design changes were implemented, aiming at the improvement of the established device. In order to achieve a conceptual solution, both the practical knowledge of the Orthos XXI design team and several design methods were used to ensure the accomplishment of the defined requirements. The detailed design process of the standard SmartOs wearable active orthosis prototype is disclosed. With the purpose of validating the design, the critical components were simulated with the resources available in SolidWorks®, and the necessary CAD model's adaptations were implemented to guarantee a reliable and safe design. The presented design is currently set for further production in Orthos XXI, followed by the mandatory mechanical tests.

Keywords: Drop foot; Mechanical design; Rehabilitation; Wearable active orthosis.

TABLE OF CONTENTS

1.	Introduction	1
1.1	Context and Motivation	2
1.2	Objectives.....	3
1.3	Orthos XXI.....	4
1.4	SmartOs Project	5
1.5	Thesis organization.....	6
2.	Biomechanics of the ankle joint and foot.....	8
2.1	Ankle joint complex.....	8
2.1.1	Anatomy of the ankle and foot.....	8
2.1.2	Biomechanics of the normal ankle joint	12
2.2	Human gait	16
2.2.1	Kinetics of normal human walking	17
2.2.2	Kinematics of normal human walking	21
2.3	Biomechanics of impaired ankle joint.....	23
2.3.1	Ankle joint post-stroke.....	24
2.3.2	Impaired human gait.....	25
3.	Rehabilitative lower limb orthotic devices	29
3.1	Gait rehabilitation	29
3.2	Passive, semi-active and active orthoses.....	34
3.3	Wearable active lower limb exoskeletons and ankle-foot orthoses	37
3.3.1	Conventional actuation in exoskeletons and active orthoses.....	39
3.3.2	Safety mechanisms	42
3.3.3	Electronic control systems	44
3.3.4	Active lower limb orthotic devices	47
3.4	Orthoses articulation compliance	51

3.4.1	Self-alignment mechanisms.....	51
3.4.2	Multiple degrees of freedom AFOs.....	52
3.5	User-orthosis attachment system.....	56
3.5.1	Design of the geometrical shape	56
3.5.2	Materials	58
3.5.3	Production method.....	59
4.	Conceptual Design	64
4.1	The objective tree method.....	64
4.2	The function analysis method.....	68
4.3	The performance specification method.....	71
4.4	The morphological chart method	73
4.4.1	Conceptual solutions	81
4.5	The weighted objectives method.....	84
5.	Detailed Design	92
5.1	SmartOs design organization	92
5.1.1	Anthropometric dimensions.....	94
5.2	Computational modelling of the solution.....	96
5.2.1	Actuation/Articulation system.....	96
5.2.2	Shank structure	100
5.2.3	Fixation structure.....	106
5.2.4	Foot structure	111
5.3	Materials and structural dimensioning.....	112
5.3.1	Materials selection.....	112
5.3.2	Critical component simulation and Design change	113
5.4	Discussion of the results	121
5.4.1	Comparison with Exo-H2	122

5.4.2	SmartOs features	124
5.4.3	Device classification	126
5.5	Pre-prototype production	126
6.	Conclusions and Future work	128
6.1	Conclusions.....	128
6.2	Prospect for future work.....	131
7.	References	133
8.	Appendices.....	146

LIST OF FIGURES

Figure 2-1 - Bones and joints of the foot (adapted from [16])	9
Figure 2-2 - Ligaments of the tibiotalar joint: (a) anterior view, (b) medial view of the ankle, showing the medial collateral ligaments (or deltoid ligaments) of the joint and the posterior part of the tibiofibular syndesmosis, and (c) lateral view of the ankle, showing the lateral collateral ligaments (adapted from [16]).	10
Figure 2-3 - Muscles of the leg and respective tendons: (a) anterior compartment, and (b) lateral compartment. Noting that the fibularis tertius muscle is not referenced due to the fact that is a deep muscle of the anterior compartment (adapted from [16]).	11
Figure 2-4 - Muscles of the leg and respective tendons: (a) posterior compartment, and (b) deep posterior compartment (adapted from [16]).	12
Figure 2-5 - Axis of rotation for the dorsi- and plantarflexion movements, forming an angle of 10° with the frontal plane axis (adapted from [15], [17]).	13
Figure 2-6 - Subtalar joint axes in the (a) superior view and (b) lateral view, demonstrating the range of angles that forms between the subtalar axis and the sagittal and transverse plane (adapted from [15]).	13
Figure 2-7 - Transverse tarsal joint axes: (a) medial (top) and superior (bottom) view of the longitudinal axes and (b) medial and superior view of the oblique axes and its angles formed with the antero-posterior axis of the sagittal and transverse plane (adapted from [26]).	14
Figure 2-8 - Anatomical planes of the human body (a) and the foot (b), being (i) frontal or coronal plane, (ii) sagittal plane and (iii) transverse plane (adapted from [27]).	15
Figure 2-9 - Motion of the ankle joint complex within each anatomical plane: (a) transverse plane, (b) frontal or coronal plane, (c) sagittal plane and (d) three dimensional motions (adapted from [27]).	15
Figure 2-10 - Phases of the normal human gait cycle (adapted from [31], [35]).	17
Figure 2-11 - Vertical ground reaction forces in a normal gait cycle, with gait velocity equal to 0,5 m/s (adapted from [33]).	18
Figure 2-12 - Example of normal ankle joint kinetic curves in the sagittal plane: (a) Ankle joint moments and (b) ankle joint power (adapted from [15])	21

Figure 2-13 - The three rockers occurring during stance phase of the human cycle: (a) the heel (first) rocker; (b) the ankle (second) rocker; (c) the forefoot (third) rocker (adapted from [37]).22

Figure 2-14 - Graphical representation of the ankle joint’s range of motion in the sagittal plane, during a normal gait cycle, and respective gait phase. Positive and negative values concern dorsiflexion and plantarflexion, respectively (adapted from [21]).23

Figure 2-15- The four commonly seen ankle and foot deformities, following a stroke: (a) equinus ankle deformity on the right side, (b) varus ankle abnormality, (c) equinovarus deformity, and (c) striatal toe on the left side [56].25

Figure 2-16 - Gait pattern of individuals with paretic ankle. The red link represents the impaired limb [10].26

Figure 2-17 - GRF mean profiles of the unaffected and affected side in individuals with hemiparesis walking at self-selected (red lines) and fast (blue lines) speeds. The former speed is 0.72 m/s and the fast speed is reported to be 1.08 m/s. The black lines refer to healthy subject walking at self-selected speed (1,26 m/s) (adapted from [67]).27

Figure 2-18 - Kinematics profile of the ankle joint of healthy subjects (dark dotted line) and of the paretic side of patients, walking at a speed of 0.78 m/s (red line) and 0.85 m/s (blue line) (adapted from [67]).28

Figure 2-19 - Kinetics profile of the ankle joint of healthy subjects (dark dotted line) and of the paretic side of patients, walking at a speed of 0.78 m/s (red line) and 0.85 m/s (blue line): (a) ankle joint’s moment profile (with negative plantar flexor moment) and (b) ankle joint’s power (adapted from [67]).28

Figure 3-1 - Example of the resistance training mode on the bicep muscle: (a) Concentric exercise and (b) eccentric exercise [70].30

Figure 3-2 - Muscular and task-oriented focus post-stroke gait rehabilitation: (a) example of a FES device, (b) treadmill training with a harness, and (c) example of a robot-assisted gait training device (Lokomat DGO) [78]–[80].32

Figure 3-3 - Examples of a passive and active ankle foot orthosis: (a) The passive AFO developed by Ottobock and (b) Exo-H2 AFO developed by Technaid [10].33

Figure 3-4 - Passive ankle-foot orthoses: (a) Nonarticulated AFO developed by Ottobock (2017); (b) Articulated AFO, also developed by Ottobock; (c) Posterior leaf spring AFO by

Ottobock and (d) Articulated AFO called “Dorsiflexion assist controlled by spring” (DACs) developed by Yamamoto et al. (1999) [10], [30], [86].35

Figure 3-5 - Semi-active ankle-foot orthoses: (a) The AFO developed by Furusho et al., with an MR brake, that generates the braking torque to keep dorsiflexion; (b) The AFO developed by Svensson et al. with an MR damper to realize the ankle damping at foot down and locking during the swing phase [10].36

Figure 3-6 – Example of an active AFO: Ankle module of the Technaid H2 lower limb robotic exoskeleton powered by an electric motor [83].37

Figure 3-7 - Exoskeletons throughout the years: (a) Concept design of the Yagn’s exoskeleton (1890), and (b) HAL-5 exoskeleton (2012) [8], [88].38

Figure 3-8 - Exoskeletons and ankle-foot orthoses powered by the different types of actuation technologies: (a) Ekso Exoskeleton (Ekso Bionics, USA), actuated by electric motors, (b) An autonomous AFO, powered by a DC motor, developed by Mooney et al. to reduce the metabolic cost of human loaded walking, (c) BLEEX exoskeleton (USA), powered by hydraulic actuator, (d) Sarcos tethered exoskeleton (also denominated XOS 2), actuated by hydraulic actuators, (e) Lower limb orthosis designed by Takahashi et al. that uses artificial pneumatic muscles, and (e) AFO developed by Galle et al. to reduce the metabolic cost of walking, also actuated by PMA [8]–[10].41

Figure 3-9 - Ankle joint mechanical stops: (a) Plantarflexion stop, (b) dorsiflexion stop, and (c) Tamarack flexure joint aligning the medial and lateral axes and a plantarflexion limiter kit, which limits the plantarflexion movement due to the collision of the circled system [96], [97].43

Figure 3-10 - Safety mechanism based on limit switch: (a) Limit switch, (b) schematic representation of a normally open limit switch (the physical contact with the actuator’s piston results in the closure of the circuit), and (c) schematic representation of a normally closed limit switch, which works in opposite to the former (adapted from [101], [102]).44

Figure 3-11 - Kinematic and kinetic sensors used in lower limb exoskeletons and AFOs: (a) IMU board integrated with its components, (b) IMU motion tracking system developed by XSens, (c) Potentiometer, (d) Encoder integrated in a DC motor, (e) Strain gauge goniometer with flexible connecting beam, by Pluxx, (f) Flexible goniometer mounted on

a subject’s knee, (g) Force sensor resistive (FSR), and (h) FSR embedded in an insole (Solemate) (adapted from [84], [103]–[107]).....45

Figure 3-9 - Bioelectric sensors: (a) EMG surface electrodes, (b) EMG indwelling/intramuscular electrodes, and (c) EEG surface electrodes [84], [108], [109]. 46

Figure 3-10 - Commercially available lower limb exoskeletons: (a) HAL for Medical Use, Series ML05 (Cyberdyne); (b) ReWalk Rehabilitation (ReWalk Robotics); (c) Ekso GT (Ekso Bionics); (d) Indego Therapy (Parker Hannifin Corporation); (e) Keeogo (B-TEMIA); (f) HANK (GOGOA Mobility Robots); (g) REX for Clinical Use (Rex Bionics); (h) Exo-H2 (Technaid) [83], [111], [113], [124].....49

Figure 3-11 - Active AFOs: (a) MIT active AFO actuated by a series elastic actuator (SEA) and developed by Blaya et al. [130]; (b) Arizona State AFO powered by a robotic tendon actuator (Boehler et al.) [134]; (c) Powered AFO developed by Ward et al., actuated by a robotic tendon [133]; (d) Michigan ankle orthosis (designed by Ferris et al.) powered by artificial pneumatic muscles [135]; (e) AnkleRobot, developed by Yeung et al., actuated by a servomotor [129]; (f) The neuromechanics-based AFO developed by Takahashi et al. [132].....50

Figure 3-12 – Self-alignment mechanism incorporated in lower limb orthotic devices: (a) Prototype of the mechanism incorporated in the knee joint, developed by Ergin et al. (2011); (b) Mechanism for the S-Assist knee joint, designed by Choi et al. (2016), and (c) Prototype of AssistOn-Ankle device, developed by Erdogan et al. (2016) [136], [139], [144].52

Figure 3-13 – Multiple degree of freedom ankle-foot orthoses developed over the years: (a) Two DoF AFO for robotic rehabilitation, designed by Agrawal et al. (2005); (b) Quasi-passive three DoF AFO developed by Zhang et al. (2015), where IR and ER mean Internal and External Rotation, respectively (adapted from [149], [150]).....54

Figure 3-14 – CAD model of the two-degrees of freedom AFO developed by Ranaweera et al. (2019): (a) Anterior view of the ankle unit’s mechanism; and (b) Range of motion of the ankle unit for plantarflexion and dorsiflexion and inversion and eversion (orthosis in supination mode, meaning PF + In + IR) [145].....55

Figure 3-15 - Pneumatic actuated AFO with two degrees of freedom, developed by Choi et al. (2019): (a) Model of the proposed AFO, being the bolded arrows the force direction applied by the PAMs. Part A is the structure surrounding the calcaneus and foot, part C

surrounds the calf and thigh, and part B is the part that connects to part A and C to form the subtalar joint and the tibiotalar (or talocrural) joint, respectively [147]......55

Figure 3-16 - AFOs composed by different materials: (a) metal and leather AFO; (b) passive posterior AFO composed by polypropylene; (c) Matrix Max with an anterior carbon composite frame and neoprene paddings to ensure a soft interface between the orthosis and the tibial crest, (d) Nexgear Tango ankle joint inserted in an anterior shank frame constituted by carbon-fibre composite and carbon-fibreglass webbing, and (e) construction of an knee-ankle-foot orthosis (KAFO) using prepreg carbon fibre technology [163]–[167].59

Figure 3-17 - Computer Numerical Control (CNC) Machining: (a) CAD software used for the design of the desired part; (b) CAM software to create a digital programming code for posterior control of the machine; (c) Preparation of the CNC machine; (d) CNC Milling; (e) CNC Electrochemical deburring; and (f) CNC Laser cutting machine (adapted from [175], [177], [179]–[181])......62

Figure 3-18 - CNC Machining applied in the orthotics field: (a) Moulds for foot orthoses production; and (b) Four-axis milling CNC machine used in a spinal orthosis mould production [178].63

Figure 4-1 - Objectives Tree of the design of the SmartOs ankle-foot orthosis for gait rehabilitation of post-stroke patients.....65

Figure 4-2 – Black box with the overall function of the SmartOs project, which is to convert the input “Patient with drop foot” into the output “Patient with a stable and comfortable gait, through the integration of an adjustable, stable and wearable active AFO.69

Figure 4-3 – Transparent box of the SmartOs project, containing the sub-functions associated with the design of the proposed rehabilitation device.70

Figure 5-1 – Schematic representation of the SmartOs wearable active orthosis organization into domains, including unique (actuation system – green) and customizable domains (shank, fixation and foot structure – orange, black and grey, respectively).93

Figure 5-2 - Representation of the anthropometric parameters whose values were collected from the literature, as well as the range of values, respective to the distance between the ankle joint and the top of the knee (in red)......95

Figure 5-3 - Articulation/Actuation system CAD model: (a) View of the lateral part of the assembly, (b) view of the encoder’s placement, and (c) motor case.....99

Figure 5-4 – Safety mechanism designed for the SmartOs articulation: (a) Dimensioning of the mechanical stop, showing the limit of 20° in both the posterior and anterior sides of the sagittal plane, and (b) Mechanical stop limits.....100

Figure 5-5 – Three-dimensional model of the SmartOs wearable orthosis left shank structure: (a) Isometric view of the smallest size shank structure, attached to an approximate model of a human leg (1.50 meters height); (b) Isometric view of the largest size shank structure, coupled to a model of a large human leg, and (c) Top view of the same shank structure, where are visible the bends of the sheet metal that are designed to resemble the geometry of the human leg.101

Figure 5-6 – SolidWorks® *Sketched Bend* tool used to create a bend on the shank structure sheet metal, with the bend radius parameter defined accordingly to the manufacture requirements of Orthos XXI.102

Figure 5-7 – Design detail added to facilitate the sheet metal bending process. This way the machine’s punch can be correctly aligned to the bending centrelines defined to achieve a folded-up geometry.....103

Figure 5-8 – Locations to place the EMG surface electrodes necessary for the technology used in the SmartOs project.103

Figure 5-9 – Three dimensional drawing of the middle adjustment strap composed by layers of different materials.104

Figure 5-10 – Wedge part (red) incorporated into the left shank structure: (a) Function of coupling the fixation structure, and (b) Function of warranting the perpendicularity of the fixation structure relative to the axis of rotation of the ankle joint.....105

Figure 5-11 - CAD models of the standard right and left shank structure, respectively. These components were designed by using the smallest and largest size shank structure as a reference.....105

Figure 5-12 – First step of the proximal fixation structure setting process: fastening of the upright to the actuation system through M6 bolts and nuts.106

Figure 5-13 – Final phase of the proximal fixation structure installation: fastening the shank structure to the upright through two M6 bolts, with the possibility to increase the fixation to three bolts.107

Figure 5-14 – Height adaptation ensured by the wedge component (red) integrated on the shank structure. The level-based bolt fixation made in pairs allows for a height adaptation of 4.5 cm.108

Figure 5-15 – Height adaptation system implemented on the SmartOs wearable orthosis, with the standard proximal upright, ensuring the height adjustment from 35 to 39.5 cm. The measurement is executed from the centre of the articulation system to the top of the shank structure.108

Figure 5-16 – Metal plate to incorporate a distal strap, which will serve as an additional fixation location to ensure a proper attachment of the proximal fixation structure to the user.109

Figure 5-17 – Metal foot structure angle of inclination relative to the ground (left value) and the motor connection plate (right value).110

Figure 5-18 – Strain gauge position spots on the sides of the hollow designed on the motor connection plate, to evaluate the strain of the same part during the standard orthosis use.110

Figure 5-19 – Height regulation system implemented on the distal fixation structure. The dimensioning of this system was executed in congruence with the one designed for the established ankle orthosis, Exo-H2.111

Figure 5-20 – Foot structure CAD drawing, showing the shoe’s outsole model to which a medial metal plate is screwed to the distal upright.112

Figure 5-21 – SolidWorks® Linear Static Analysis definition of the simulation’s conditions of the proximal fixation structure: Fixtures, Connections (including Contact Sets and Connectors) and External Loads.115

Figure 5-22 - Linear Static Analysis with SolidWorks® Simulation tool used to assess the proximal fixation structure composed by aluminium alloy 5083-H111: (a) von Mises stress results, (b) Factor of safety (FOS) results regarding the actuation system structure, and (c) FOS results regarding the fixation of the upright to the wedge component and the actuation system with two galvanized steel bolts. The red colour means that the calculated FOS is inferior to the desired FOS.116

Figure 5-23 - Linear Static Analysis with SolidWorks® Simulation tool used to assess the proximal fixation structure: (a) FOS results regarding the actuation system structure composed by Al6082-T651, and (b) FOS results regarding both the fixation of the upright

to the wedge component (with three M6 galvanized steel bolts) and to the actuation system.....	117
Figure 5-24 - Linear Static Analysis with SolidWorks® Simulation tool used to assess the proximal fixation structure: (a) FOS results regarding the fixation of the upright with M6 class 8.8 steel bolts to the wedge component and to the actuation system, (b) FOS results of the bolts when the distal strap fixation is removed, showing that this additional component is needed to ensure a safer connection to the user, and (c) Validation of the distal strap metal plate fixation with M5 screws.....	118
Figure 5-25 - SolidWorks® Linear Static Analysis definition of the distal fixation structure simulation's conditions.....	119
Figure 5-26 - SolidWorks® Linear Static Analysis results: (a) FOS results regarding the motor connection plate composed by Al5083-H111, and (b) FOS results of the galvanized steel bolts.....	120
Figure 5-27 - SolidWorks® Linear Static Analysis results: (a) FOS results regarding the motor connection plate composed by Al6082-T651, (b) FOS after the design changes implemented on the motor connection plate, and (c) FOS results of the class 8.8 steel bolts.....	121
Figure 5-28 - SolidWorks® Linear Static Analysis strain results on the strain gauge opening, showing that the strain gauges can be placed its lateral sides, due to the constant deformation.....	121
Figure 5-29 – SmartOs standard wearable active orthosis CAD model: (a) Isometric view of the assembly for the right ankle, (b) Isometric view of the assembly for the left ankle, and (c) Exploded view of the assembly for the left ankle.....	125
Figure 5-30 – Left shank structure for the standard SmartOs wearable active orthosis, produced in Orthos XXI: (a) Lateral view of the produced component, and (b) SmartOs component attached to a leg of an individual with 1.5 m height.....	127
Figure 8-1 – 3D model of the self-aligning mechanism designed within the BiRD LAB group, to accommodate the ICR of the ankle joint.....	159
Figure 8-2 – Incorporation of the self-aligning mechanism on an <i>OpenSim</i> model (<i>Gait2354_Simbody</i>).....	160
Figure 8-3 – Kinematic definition between the AFO's shank structure and the left tibia of the musculoskeletal model of <i>OpenSim</i>	161

Figure 8-4 - Kinematic definition between the first link of the self-aligning mechanism, which is connected to the shank structure through a *Pin Joint*.161

Figure 8-5 – GUI view of the *OpenSim* with the musculoskeletal model and the AFO with the proposed self-aligning mechanism attached to it.162

Figure 8-6 - Kinematic constraint between the AFO’s foot structure and the calcaneum of the musculoskeletal model of *OpenSim*.162

Figure 8-7 – Plot of the kinematic effect of integrating in a musculoskeletal model an AFO with a self-aligning mechanism and an AFO with a simple hinge, as oppose to the kinematic behaviour of a model without any AFO attached.....163

Figure 8-8 - Plot of the kinetic effect of integrating in a musculoskeletal model an AFO with a self-aligning mechanism and an AFO with a simple hinge, as oppose to the kinetic behaviour of a model without any AFO attached.164

Figure 8-9 – Dimensions and areas of the different bolt’s sizes [218].169

Figure 8-10 – Metric Mechanical-Property classes for steel bolts, disclosing the proof and yield strength of different sizes bolts.170

Figure 8-11 – Friction coefficient *K* of different bolt conditions. Notice that zinc-plated corresponds to the conditioned of galvanized steel bolts.170

LIST OF TABLES

Table 2-1 - Range of motion of the ankle joint movements in the different anatomical planes [14], [15], [17], [29].	16
Table 4-1 - Performance specification method for the SmartOs project.	72
Table 4-2 – Morphological chart with all the solutions proposed to achieve each subfunction of the SmartOs project.	75
Table 4-3 – Summary of the formed conceptual solutions for the SmartOs project, and sub-solutions selected to compose each one.....	82
Table 4-4 – List of the design objectives for the SmartOs project, to be utilized for posterior evaluation of the alternative designs.	85
Table 4-5 – Rank order of the list of objectives determined by each member of the design team. Values that ranged from 6 (highest priority) to 1 (lowest priority) were given to each rank ordered objective.	86
Table 4-6 – Calculation of each objective’s final importance value, based on the rank order determined by each member of the design team.....	86
Table 4-7 – Chart of systematic comparison of pairs of objectives, to obtain the row total, which indicates the rank order of objectives. Note that the value 1 and 0 refer to a more and less important objective, respectively. The value $\frac{1}{2}$ indicates that the objectives are considered equally important.....	87
Table 4-8 – Rank ordered objectives placed in positions of relative importance on a scale of 1 to 10.....	88
Table 4-9 – Eleven-point evaluation scale set to be used for the assessment of the performance of the proposed alternative designs on each objective.	89
Table 4-10 – Weighted objectives evaluation chart for the proposed conceptual solutions regarding the SmartOs project. The <i>utility value</i> is calculated by the multiplication of the objective’s weight by the performance score of that alternative on each objective. The <i>overall utility value</i> is the sum of all utility values concerning each objective. The conceptual solution with the highest value is chosen as the best solution for the project.	90

Table 5-1 - Anthropometric parameters necessary for the dimensioning of the fixation structure, respective description and range of values concerning the height of 1.50 and 1.90 meters, reported in the literature.	94
Table 5-2 – Comparison analysis between the output data of the selected actuation system for the SmartOs wearable active orthosis and the required data for a human ankle joint.	98
Table 5-3 - Mechanical properties of the aluminium alloys available and currently used for production in ORTHOS XXI [196]–[200].	113
Table 5-4 – Technical specifications of the SmartOs wearable active orthosis standard prototype, including the features that are set to be provided by the system.	124
Table 8-1 – Overview of the passive, semi-active and active ankle-foot orthoses [10], [30], [34].	146
Table 8-2 - Exoskeletons commercially available and its technical and commercial features.	148
Table 8-3 – Overview of the developed active AFO for rehabilitation found in the literature review.	154

LIST OF ABBREVIATIONS AND ACRONYMS

A

AFO Ankle-foot orthosis

AHA American Heart Association

AAN Assist as Needed

ABS Acrylonitrile butadiene styrene

AM Additive manufacturing

AEMPS Spanish Agency of Medicines and Health Products

B

BoNT Botulinum toxin

C

CE European Conformity

CAD Computer Aided Design

CAM Computer-aided Manufacturing

CNC Computer Numerical Control

CFRP Carbon fibre reinforced plastics

D

DC Direct Current

DGO Driven Gait Orthosis

DOF Degree of Freedom

DMLS Direct Metal Laser Sintering

E

EEG Electroencephalogram

EMG Electromyographic

EVA Ethylene-vinyl acetate

EDM Electronic Discharged Machine

F

FEA Finite Element Analysis

FES Functional electrical stimulation

FEM Finite Element Method

FSR force sensor resistor
FDA Food and Drug Administration
FRP Fibre-reinforced plastics
FDM Fused deposition modelling
FOS Factor of Safety

G

GRF Ground reaction forces
GT Gait Trainer
GUI Graphical User Interface

H

HAL Hybrid Assistive Limb
HDPE High-density polyethylene

I

IBV Instituto de Biomecânica de Valencia
IMU Inertia measurement unit
ICR Instantaneous Centre of Rotation

L

LOM Laminated object manufacturing

M

MGT Mechanized Gait Trainer
MR Magneto-rheological

P

PMA Pneumatic muscle actuators
PE Polyethylene
PA Polyamide
PP Polypropylene
PUR Polyurethane
PLA Polylactic acid

R

ROM Range of Motion

S

SPAVC Sociedade Portuguesa do Acidente Vascular Cerebral

SEA Series elastic actuator

SLS Selective laser sintering

SLM Selective laser melting

SLA Stereolithography

STL Stereolithography

T

TGA Australian Therapeutic Goods Administration

V

VSA Variable stiffness actuators

W

WHO World Health Organization

GLOSSARY

- Anterior** Anatomical term used to describe the body structure meaning the front side of the body.
- Body weight line** Line vertical to the centre of gravity, along which the body weight acts vertically downwards.
- Cadence** Total number of full cycles taken within a given period of time.
- Calf** Back portion of the lower leg.
- Distal** Anatomical term used to describe the body structure meaning away from or farthest from the trunk or the point or origin of a part.
- Lateral** Anatomical term used to describe the body structure meaning away from the midline of the body.
- Longitudinal** Running lengthwise, in the direction of the long axis of the body or any of its parts.
- Medial** Anatomical term used to describe the body structure meaning toward the midline of the body.
- Midline of the body** Imaginary line down the middle of the body that splits it into equal left and right parts.
- Posterior** Anatomical term used to describe the body structure meaning back side of the body.
- Proximal** Anatomical term used to describe the body structure meaning toward or nearest the trunk or the point of origin of a part.
- Shank** The part of an animal's or a person's leg between the knee and ankle.
- Step length** Distance measured from the point of foot contact to the point of contralateral foot contact.
- Stride length** Linear distance covered by one gait cycle, i.e. of both the right and the left step.

1. INTRODUCTION

A cerebrovascular accident (also known as stroke) is a sudden disease that affects a limited part of the brain, causing the death of its cells due to lack of oxygen derived from a blockage of blood flow (ischaemic stroke), or due to a rupture of an artery of the brain (haemorrhagic stroke) [1], [2].

Thus, following a stroke, hemiplegia (paralysis of one of the sagittal half of the body), weakness, spasticity (excessive stiffness of the muscles), loss of coordination of the limb movement, as well as joint deformity can impair the patient's ability to independently walk due to an asymmetrical and abnormal gait pattern [2]–[5]. These motor sequelae affect the load-bearing ability of the limb and hinder the foot clearance during swing phase of the gait, in which the foot needs to propel itself forward [3], [4], [6]. This last condition has the name of drop foot and it's caused by the impairment of the muscles responsible for the lifting of the front part of the foot [4], [6].

Herewith, individuals with this pathologic condition require gait rehabilitation sessions. Therefore, in order to assist the restoration of the normal gait pattern and improve safety during walking, an ankle foot orthosis (AFO) is often prescribed as a form of treatment of post-stroke gait. Several studies have studied the effect of the use of an AFO by stroke patients and it was reported that using this kind of device on the affected limb can improve gait biomechanics and speed, balance and mobility [4], [5], [7]–[10]. Furthermore, there are several commercially available robotic devices (which includes exoskeletons and orthoses) that are recommended for individuals with hemiplegia due to stroke, providing them the ability to ambulate or to rehabilitate themselves.

This master dissertation is introduced in a project entitled SmartOs, whose main goal is the development of a wearable lower limb active orthosis for human gait training and rehabilitation, aimed for individuals with impaired walking. The project takes place at Universidade do Minho, in the Bioinspired Robotic Devices Laboratory (BiRD Lab) in the Center of MicroElectroMechanical Systems (CMEMS) group. Hereupon, this master thesis focuses on the rehabilitation of one lower limb joint, consisting of the conceptual and detailed design, and evaluation of a wearable active ankle-foot orthosis. The SmartOs

ankle orthosis design focal points are the following: the attachment system to the user's leg that should warrant the adaptability to both limbs (right and left), the fixation apparatus, which must ensure the adjustability within a defined user height range, and, finally, the coupling structure to the user's impaired foot. Furthermore, the actuation/articulation system is also addressed, however is worth mentioning that this part was executed by a SmartOs design team member. In a subsequent phase, an overall system validation will be performed in a simulated environment.

Finally, the presented master dissertation will culminate in the production of some components of the final ankle-foot orthosis system, being this phase executed in partnership with a Portuguese manufacturer, ORTHOS XXI, which focuses its production on orthopaedic and hospital material since 1985.

1.1 CONTEXT AND MOTIVATION

Worldwide, statistics claim that one in six people will suffer from a stroke, consisting in the second leading cause of death and the third leading cause of disability, according to World Health Organization (WHO) [1]. Portugal is the west European country with the highest rate of stroke-related mortality, mainly in population with ages inferior to 65 years old, as reported by SPAVC (Portuguese acronym that stands for *Sociedade Portuguesa do Acidente Vascular Cerebral*) [2]. In addition, cerebrovascular accidents are the principal cause of death and disability in Portugal [2], [11]–[13]. In agreement to SPAVC, 30% of the stroke victims lose their life and of those who survive, 40% feature an impairment which can manifest itself through motor, cognitive, behavioural and sensory sequelae [2]. The last three secondary effects of the stroke concern disabilities such as overall mental processes, memory problems, depression, anxiety and loss of sensibility in a certain part of the body [2]. Although these sequelae are important to consider, this dissertation will not discuss these concepts, but only the motor sequelae.

To accommodate these motor problems, stroke survivors are prescribed physical therapy, which includes the use of an ankle-foot orthosis (AFO) to enhance walking function by providing stability and foot clearance of the hemiparetic leg, during the swing phase of the gait. Moreover, one of the most noticeable problems of conventional ankle foot orthosis and exoskeletons is the misalignment occurring between the rehabilitation

device and the human joint. This misalignment of the joint axes often causes detrimental parasitic forces on the patient, which beget discomfort, pain or even long term injury due to repetitive use, jeopardizing the effectiveness and usability of the medical device. Due to this, it becomes imperative that the design of the AFO ensures correspondence of the orthotic device axes with the anatomical axes of the human joint.

Last but not least, to warrant the use of the same orthosis by many stroke patients, who might have impairment on different lower limbs, the design of the AFO should ensure its use on both right and left ankle.

1.2 OBJECTIVES

For the conceptual and detailed design of an active ankle-foot orthosis with an adjustable architecture, it was established certain main objectives. In an initial phase, the principal goal was to do a literature survey concerning the following topics: the anatomy of the ankle joint complex, its biomechanical characteristics (such as the principal ankle joint's axes and its range of motion (ROM)); the phases of the normal human gait and the changes verified on the impaired gait; the rehabilitative devices (including powered lower limb exoskeletons and AFOs) that are commercially available or still in development; the mechanisms proposed by several studies to ensure the compliance of the orthoses articulation; and finally, the current user-orthosis attachment systems of commercial devices, and its production method.

The project's aim is the development of a conceptual solution of an active AFO, which embodies the user-orthosis attachment system that enables the adjustability for both right and left ankle, the fixation/adjustment mechanism to both the user's leg and foot, and the actuation system. This conceptual design of the SmartOs ankle orthosis must ensure the comfort, adaptability to the user anthropometric features, as well as to the affected limb. Furthermore, the final AFO should enable the alignment between the device and the patient's ankle, in order to minimize the residual forces and, therefore, ensure its maximum compliance. The development of the AFO's conceptual solution should follow a project methodology, which includes several project methods such as: the objectives tree method, the function analysis method, the performance specification method, the weighted objectives method, and finally the morphological chart method.

Furthermore, a detailed design of each SmartOs wearable orthosis's modules must be completed, after which, the validation of its critical components in a simulated environment (SolidWorks®) it is essential. For this, the stress that result from the maximum applied load, as well as the Factor of Safety (FOS) must be assessed, in order to ensure a safe and reliable design. The design process will be accomplished in partnership with the Portuguese orthopaedic manufacturer, ORTHOS XXI, and with University of Porto.

1.3 ORTHOS XXI

Orthos XXI is a Portuguese manufacturer company, belonging to the universe of orthopaedic and hospital material. Founded in 2007, Orthos XXI succeeds Ortomaia, which activity began in 1985. Throughout this time, Orthos XXI has grown and consolidated, starting to broaden its horizons and converting itself into a recognized and a reference company. As a result of agreements with reputed national and international companies, Orthos XXI has become a European manufacturer of an increasingly wide range of products, participating regularly in international promotion and trade activities, in fairs and congresses in the health sector.

The quality of Orthos XXI's products can be confirmed in the best national hospitals. The majority of the products are classified as class 1 medical devices and bear the CE marking in accordance with Community Directives 93/42/EEC and 2007/47/EC, being notified to Infarmed. Many of these company's products are tested by accredited and independent entities, namely the IBV (*Instituto de Biomecânica de Valencia*), in Spain. Finally, Orthos XXI is also certified according to EN ISO 9001: 2008.

Nowadays, this Portuguese manufacturer has two infrastructures, located in Braga. One of them is the office where the members responsible for the design and development of new products, as well as three assembly lines, upholstery sewing, information systems, commercial and marketing department, repairs, purchasing department, finance department, among others. The other is located in Ave Park, where is manufactured all the metal parts and parts machined by CNC or manual lathes, integrating the departments of tube bending as well, semi-manual and automated welding, painting, mechanical testing, cutting machine laser and bending machine.

Additionally, the department of manufacture of special requests is also located in this infrastructure.

1.4 SMARTOS PROJECT

According to the WHO, 15 million people suffer a stroke every year, and, as reported by the SPAVC, Portugal is the west European country with the highest rate of stroke-related mortality. Of the 20000 cases of stroke incidents that occur every year in Portugal, 30% results in death, and 40% of the survivors feature an impairment (motor, cognitive, behavioural, or sensory). Stroke is a major cause of lower limb spasticity and motor impairments, e.g. equinus foot and varus foot, which generate walking problems, social and work exclusion, limited mobility, and early retirement. It is claimed that associated health and social costs are around 1 million euros (in Europe) and, thereby, faster and more effective treatments of spastic gait are needed to restore the gait function and the independent life of stroke-impaired subjects. Optimal treatment of spastic gait requires a combination of pharmacotherapy (botulinum toxin is mostly used) with prolonged muscle stretching, with a personalized and repetitive gait rehabilitation, adapted and oriented to each patient's needs. Furthermore, the gait training sessions should incentivize the participation of the user/patient, who must be always assessed in an objective manner.

For this purpose, **SmartOs** (Smart, Stand-alone Active Orthotic System) project proposes an innovative robotic technology and personalized solution oriented to gait rehabilitation. SmartOs comprises an active and smart lower limb orthosis, which is synergistically connected to a gait analysis laboratory for personalized and user-oriented rehabilitation (Assist-As-Need). This system is to be combined with a toxin-based intervention in order to enhance the treatment of spastic gait, by providing objective evaluation procedures of spasticity and personalized treatment according to the patients' needs. SmartOs aims to improve the treatments to facilitate walking in spastic subjects, by actively encouraging the user's participation in the therapy. Herewith, SmartOs will develop and validate a **wearable active AFO to assist as needed** during task-oriented gait training, while **monitoring the user**. Moreover, the control framework will incorporate key technologies to ensure a **safe, compliant, and energy-efficient gait** through a **real-time adjustment of the stiffness and damping** properties of the human-orthosis

interface. This wearable technology incorporates different sensorial units such as **TextileLAB** (**FootLAB** to segment the different phases of the human gait, and **MuscLAB** to monitor muscle activity), **MotionLAB**, which included **InertialLAB** to supervise the biomechanical movement and its combination with the EMG information (**MyoLAB**). Lastly, **VibroLAB** is used to monitor and evaluate muscle spasticity.

In conclusion, SmartOs will act as a **wearable mobile lab**, which comprises a **wearable active orthosis and motion lab**, incorporating technological solutions in the domains of **biofeedback** and **artificial intelligence**. Additionally, the proposed AFO should **easily adapt to different anthropometric dimensions, incorporate sensory systems**, which actuate and cooperate in congruence with the human being, all this to satisfy each **impaired subject's needs** and to **enhance gait rehabilitation**.

1.5 THESIS ORGANIZATION

The present master dissertation is structured as follows:

Chapter 2 addresses the biomechanics of the ankle joint and foot complex, where is presented its anatomy and biomechanical features, as well as the kinematic and kinetic information of the normal human gait. The chapter is finalized with the biomechanics of the impaired ankle joint, where its physical, kinematic, and kinetic characteristics are disclosed, as well as normal procedures of gait rehabilitation.

Chapter 3 focuses on the rehabilitative lower limb orthotic devices, starting with the presentation of all types of AFOs that currently exist to then address the wearable lower limb exoskeletons and active AFOs developed over the years. In this section, the conventional actuation used in these devices are explored, along with the safety mechanisms that can be incorporated in association, electronic control systems, and, lastly, a literature review of the powered orthotic devices available on the market or still in development is executed. Moreover, this chapter explores the concept of orthotic articulation compliance and the mean to achieve it, as well as the attachment system, where the aspects of design, material selection and production method are disclosed.

Chapter 4 discloses the conceptual design of the SmartOs wearable active orthosis, in which the necessary project methodologies are used to determine a final conceptual

solution. This solution must comply with the project requirements defined by the SmartOs team.

Chapter 5 addresses the detailed design of the conceptual solution selected in the previous chapter. This chapter will firstly explore the SmartOs design organization and the anthropometric measurements collected from the literature, which will serve as the justification for the design of a standard active AFO as a proof of concept. Further on, the detailed design of the standard SmartOs wearable active orthosis is presented, as well as the validation of the critical components in a simulated environment. This chapter still discusses the obtained results and presents the final SmartOs technical specifications. The production of the pre-prototype is disclosed, with the presentation of the component manufactured.

Finally, **Chapter 6** presents the final conclusions of this master dissertation, as well as the prospects for future work.

2. BIOMECHANICS OF THE ANKLE JOINT AND FOOT

This chapter is dedicated to the literature survey of the anatomical and biomechanical features of the ankle joint complex. It will be disclosed the joints, ligaments and muscles that constitute the ankle complex as well as its anatomical characteristics that influence the type of motion enabled by each one. Herewith, the range of motion of the ankle joint on each anatomical plane will be also addressed, culminating in the description of the normal human walking.

The kinetics and kinematics analysis of the normal gait are a crucial point to approach when the subject at hand is the development of a device, whose main function is to mimic the movement of the lower limb. Thus, these biomechanical parameters will be disclosed, presenting the behaviour of the forces applied to the foot and the ankle joint's moment and power, as well as its range of angles throughout a gait cycle. At last, the impairment resultant of a stroke is briefly explained, disclosing the affected movements.

2.1 ANKLE JOINT COMPLEX

The present section addresses the characteristics of the ankle joint complex, namely the anatomy, which includes the bones and joints that compose it, as well as the ligaments of such joints. Still on this topic, the main muscles of the human leg that ensure ankle and foot motion are disclosed. Moreover, the biomechanics of the normal (nonimpaired) ankle joint is addressed, including the joint's axes of rotation and range of motion.

2.1.1 ANATOMY OF THE ANKLE AND FOOT

The ankle and the foot are comprised by a considerable quantity of bones (26 individual bones), all of which form a total of thirteen joints. Therefore, although frequently referred to as the ankle joint, there are a number of articulations that facilitate foot motion [14], [15]. Hereupon, the ankle joint complex is constituted by the tibiotalar, subtalar,

transverse talar, tarsometatarsal, metatarsophalangeal and interphalangeal joint (see Figure 2-1) [15], [16]. In the present dissertation, only the tibiotalar, subtalar and transverse talar joint will be disclosed once these ankle articulations are the most actively present in the ankle movement during human gait.

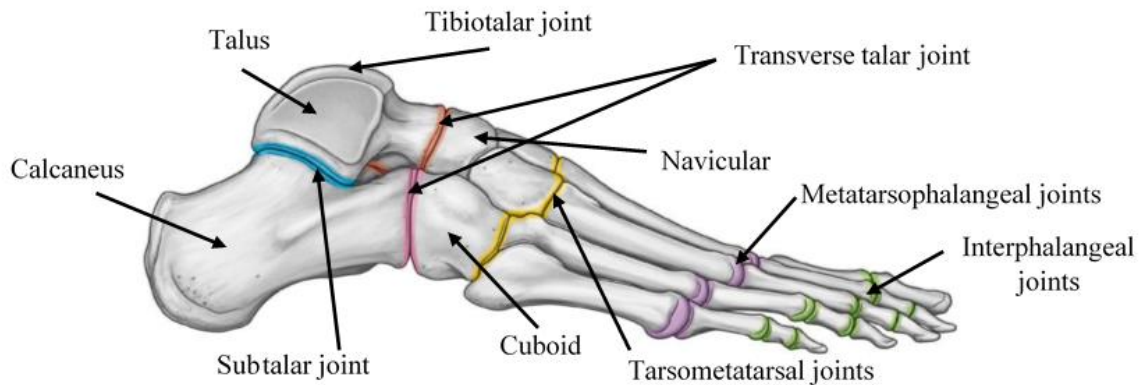


Figure 2-1 - Bones and joints of the foot (adapted from [16])

2.1.1.1 LIGAMENTS OF THE ANKLE JOINT

Besides the ankle's bony structure and joint capsule, the ligamentous support of the ankle joint complex enables it to function with a high degree of stability [15], [17]. The ankle joint comprises a vast number of ligaments, as one can verify in Figure 2-2. However, in this section, only the ligamentous structure of the tibiotalar joint will be addressed. Hereupon, the stability of the talocrural joint is provided by three groups of ligaments: **tibiofibular syndesmosis**, **medial collateral ligaments** (or deltoid ligaments), and **lateral collateral ligaments**.

The **tibiofibular syndesmosis** consists of three main supporting ligaments: the anterior and posterior tibiofibular ligament, and the interosseous ligaments (which is a thickening of the interosseous membrane). This ligamentous structure limits motion between the tibia and the fibula, maintaining stability between the bone distal ends and ensuring that the latter bone of the leg remains held tightly within the incisura of the tibia (Figure 2-2 (a)) [15], [17].

The medial part of the ankle joint is stabilized by the **medial collateral ligaments** (also known as deltoid ligaments), which are composed by the anterior and posterior tibiotalar ligaments, the tibionavicular ligament and the tibiocalcaneal ligament

(Figure 2-2 (b)) [15]–[17]. The function of these ligaments is to provide resistance to eversion motion, being the strongest set of ligaments of the ankle joint [15], [17].

Lastly, lateral ankle stability is conferred by the **lateral collateral ligaments**, which consists of the anterior and posterior talofibular ligament and the calcaneofibular ligament (Figure 2-2 (c)) [15]–[17]. These ligaments are able to reduce inversion motion of the joint, as well as limit external tibial rotation. Furthermore, the anterior and posterior talofibular ligaments withstand high tensile forces under the movements of plantar flexion and dorsiflexion, respectively, and the calcaneofibular ligament is the only connective tissue between the tibiotalar and subtalar joint [15], [17].

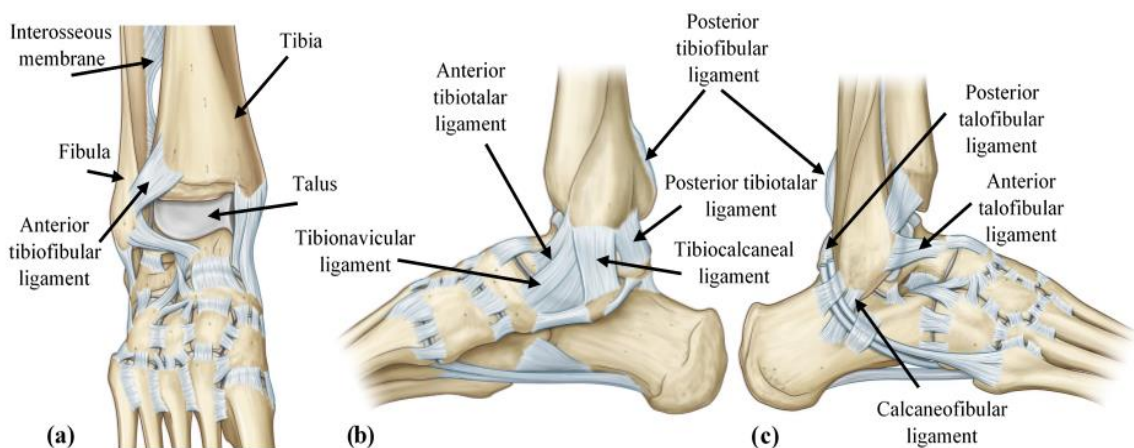


Figure 2-2 - Ligaments of the tibiotalar joint: (a) anterior view, (b) medial view of the ankle, showing the medial collateral ligaments (or deltoid ligaments) of the joint and the posterior part of the tibiofibular syndesmosis, and (c) lateral view of the ankle, showing the lateral collateral ligaments (adapted from [16]).

2.1.1.2 MUSCLES OF THE HUMAN LEG

Regarding the actuators of the ankle and foot motion, there are twelve extrinsic muscles which produce the movement, and that originate within the leg and insert within the foot complex. These can be divided into four compartments: anterior, lateral, posterior and deep posterior compartment [15], [16].

The **anterior compartment** consists of four muscles: tibialis anterior, extensor digitorum longus, the extensor hallucis longus and fibularis tertius. This set of muscles are responsible for producing the dorsiflexion motion, although some also generate other movements. The tibialis anterior and the extensor hallucis longus induce dorsiflexion and

inversion of the foot. Moreover, the fibularis tertius produces dorsiflexion and eversion of the foot, and lastly, the extensor digitorum longus generates dorsiflexion of the ankle [15].

The **lateral compartment** is responsible for the production of plantarflexion and eversion of the foot and is composed by the fibularis longus and the fibularis brevis [15]. Figure 2-3 (a) and (b) illustrates the aforementioned muscles compartments of the ankle, as well as the respective tendons that connect the muscular tissue to the bones.

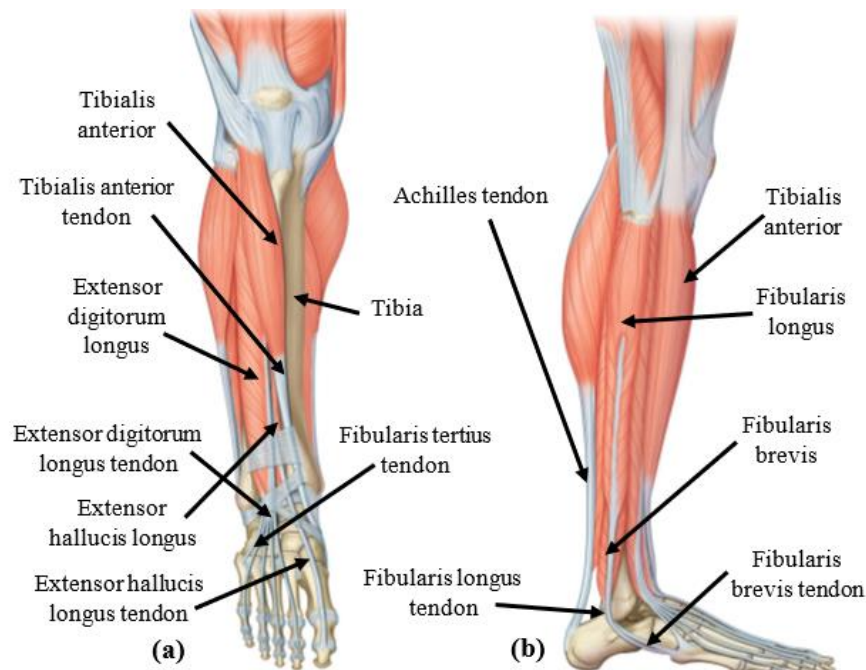


Figure 2-3 - Muscles of the leg and respective tendons: (a) anterior compartment, and (b) lateral compartment. Noting that the fibularis tertius muscle is not referenced due to the fact that is a deep muscle of the anterior compartment (adapted from [16]).

The **posterior compartment** consists of three muscles: gastrocnemius, soleus, and the plantaris (Figure 2-4 (a)). These muscles all contribute to the plantarflexion of the foot. The gastrocnemius and the soleus muscles are attached to the calcaneus through the calcaneal tendon, better known as Achilles tendon, which is responsible for transmitting the force of the strongest ankle plantarflexors [15]–[17].

Finally, the **deep posterior compartment** is in charge of producing plantarflexion and inversion of the foot, being composed by the tibialis posterior, the flexor digitorum longus, and the flexor hallucis longus (Figure 2-4 (b)) [15], [16].

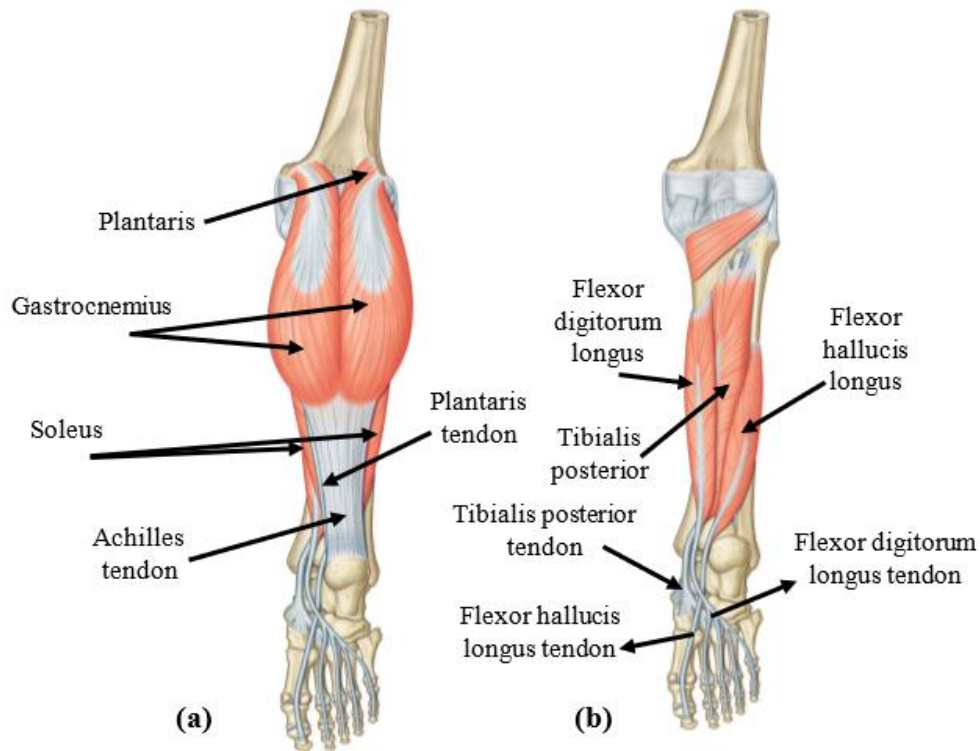


Figure 2-4 - Muscles of the leg and respective tendons: (a) posterior compartment, and (b) deep posterior compartment (adapted from [16]).

2.1.2 BIOMECHANICS OF THE NORMAL ANKLE JOINT

As aforementioned, the ankle joint complex has a number of joints that compose it, although in the present section, only the tibiotalar, subtalar and transverse talar joints will be addressed.

2.1.2.1 AXES OF ROTATION

The **tibiotalar joint** forms the junction between the distal tibia and fibula of the leg and the talus. This joint acts as a hinge joint, contributing to the plantar- and dorsiflexion motion of the foot [15], [17]. However, during these movements, occurs an external and internal rotation of the foot, respectively. Although there has been suggestions that the tibiotalar joint is multi-axial due to these rotations, this joint is indeed uniaxial, but the motion observed occurs as a result of its oblique axis [15]. This axis of rotation happens around the line passing through the medial and lateral malleolus and is angled at 10° to the frontal plane, as is represented in Figure 2-5 [15], [17]. Studies suggest that the

tibiotalar joint axis may alter significantly during the motion of the ankle and can differ between individuals [18].

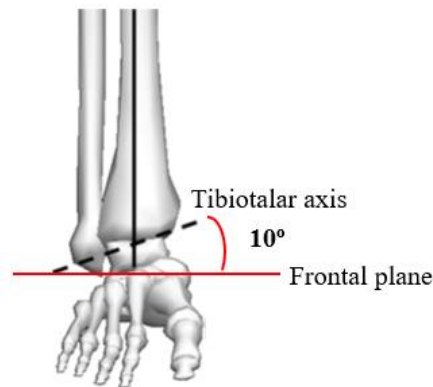


Figure 2-5 - Axis of rotation for the dorsi- and plantarflexion movements, forming an angle of 10° with the frontal plane axis (adapted from [15], [17]).

The **subtalar joint** is comprised by two bones: the talus and the calcaneus. The first one rests on the anterior portion of the calcaneus, enabling primarily the movements of inversion and eversion of the ankle [15]. These movements allow the foot to accommodate to irregular ground and provides shock absorption, being related, as well, to postural control and maintenance of balance [19]–[21]. Similar to the tibiotalar joint axis, the subtalar joint axis is an oblique one. The value of the angles forming between the subtalar axis and the antero-posterior axis, in the sagittal plane and in the transverse plane, varies in the reviewed literature. Hereupon, the former angle varies from 40° to 42° [15], [18], [22] and the angle forming in the transverse plane varies from 16° to 23° [15], [23]–[25]. Figure 2-6 (a) and (b) illustrates the superior and lateral view of the subtalar joint axes and the range of angles that forms between these axes and the sagittal and transverse plane.

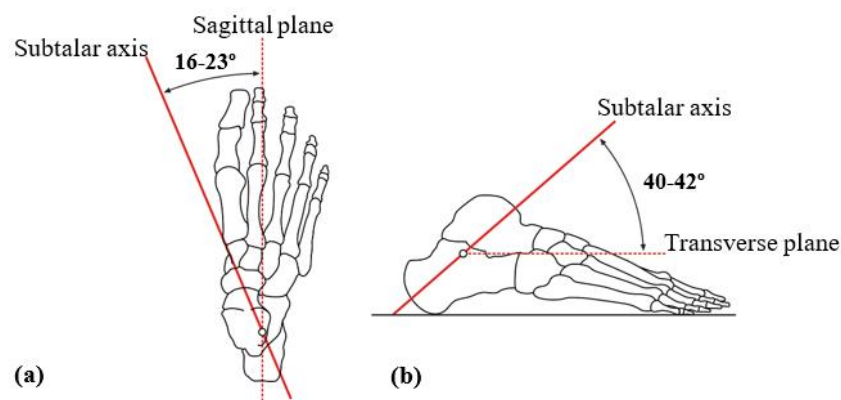


Figure 2-6 - Subtalar joint axes in the (a) superior view and (b) lateral view, demonstrating the range of angles that forms between the subtalar axis and the sagittal and transverse plane (adapted from [15]).

The **transverse tarsal joint**, also called the **Chopart's joint**, combines the junction between the talus and the navicular and the junction between the calcaneus and cuboid [15], [17], [26]. One function of the Chopart's joint is enabling both flexibility and rigidity of the mid-foot during gait, allowing the adaptation to uneven ground and the effective transmission of force from the forefoot to the ground, respectively [17], [26]. This joint possesses two axis of motion: a longitudinal and an oblique axis. The longitudinal axis is oriented 15° upward from the antero-posterior axis in the transverse plane and 9° medially from the same axis, but in the sagittal plane. Along this axis occurs the movements of inversion and eversion. The oblique axis is oriented 52° upward from the horizontal and 57° medially from the antero-posterior axis and motions of plantar- and dorsiflexion occur about this axis [26]. In Figure 2-7 (a) and (b) is represented the medial and superior view of the transverse tarsal joint axes and its angles formed with the sagittal and transverse plane.

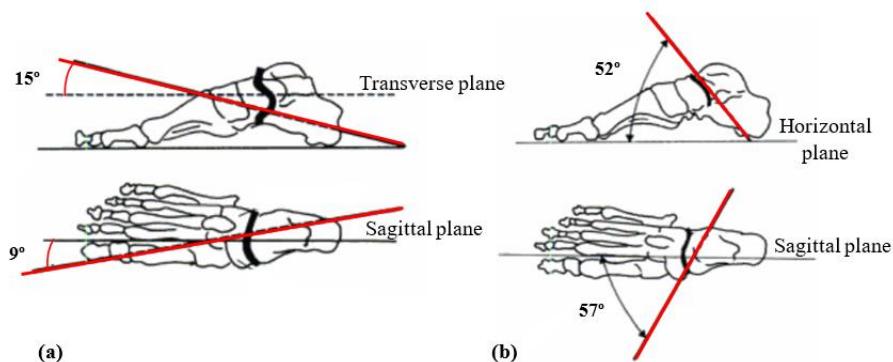


Figure 2-7 - Transverse tarsal joint axes: (a) medial (top) and superior (bottom) view of the longitudinal axes and (b) medial and superior view of the oblique axes and its angles formed with the antero-posterior axis of the sagittal and transverse plane (adapted from [26]).

2.1.2.2 MOTION OF THE ANKLE JOINT

The ankle joint is considered a joint with three rotational degrees of freedom (DOF) around three perpendicular intersecting axes [14], [15]. The motion mode of the human ankle joint includes **plantar-** and **dorsiflexion**, **ad-** and **abduction** and **eversion** and **inversion**. The former occurs in the sagittal plane, ad- and abduction takes place in the transverse plane and, finally, eversion and inversion occurs in the frontal or coronal plane (see Figure 2-8 (a) and (b), and Figure 2-9 (a), (b), and (c)) [14], [15], [17]. Moreover, these motions can combine and create three dimensional motions called supination and

pronation, which are the combination of plantarflexion, inversion and adduction, and dorsiflexion, eversion and abduction, respectively (Figure 2-9 (d)) [15].

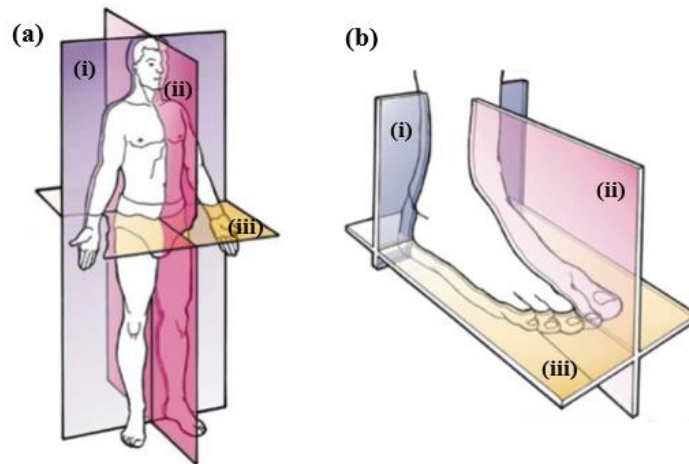


Figure 2-8 - Anatomical planes of the human body (a) and the foot (b), being (i) frontal or coronal plane, (ii) sagittal plane and (iii) transverse plane (adapted from [27]).

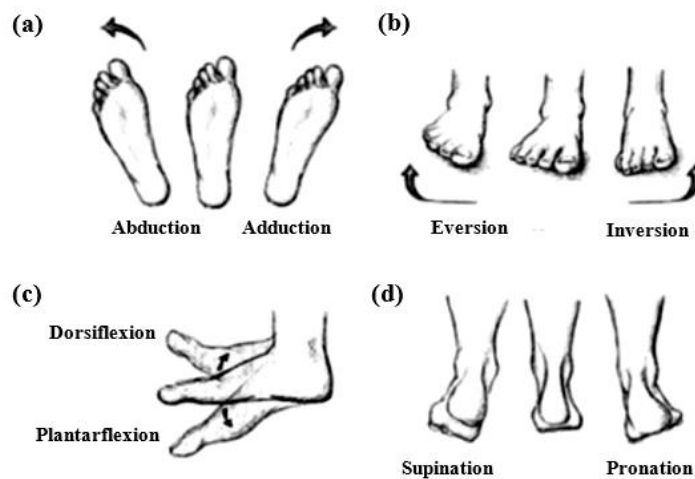


Figure 2-9 - Motion of the ankle joint complex within each anatomical plane: (a) transverse plane, (b) frontal or coronal plane, (c) sagittal plane and (d) three dimensional motions (adapted from [27]).

The tibiotalar joint is able to perform dorsiflexion with a range of 10 to 20° and plantarflexion with a range of 40 to 55°, although only 10° of dorsiflexion and 15 to 20° of plantarflexion are needed for normal locomotion [14], [15], [17], [28]. The subtalar joint is capable to invert by 20 to 23° and evert by 5 to 12° in the normal foot. Moreover, the subtalar joint contributes as well, with a few degrees, to the plantar and dorsiflexion [15], [17].

Finally, the transverse tarsal joint shares a common axis of motion with the subtalar joint, being considered as a part of the same functional unit. Herewith, the transverse tarsal joint contributes for the movements inversion and eversion, as well as is

responsible for the transformation of tibial rotation into forefoot supination and pronation, alongside with the subtalar joint [15], [26]. Regarding ab- and adduction values of range of motion, the literature isn't clear. However, some publications refer to a range of 25 to 30° for both ab- and adduction and others to a range of 20° for adduction and 10° for abduction [14], [29]. Table 2-1 summarizes the values of the range of motion of the ankle joint movements in each anatomical plane.

Table 2-1 - Range of motion of the ankle joint movements in the different anatomical planes [14], [15], [17], [29].

Plane	Motion	Range of motion
Sagittal	Dorsiflexion	10-20°
	Plantarflexion	40-55°
Transverse	Adduction	25-30°
	Abduction	25-30°
Frontal or Coronal	Inversion	20-23°
	Eversion	5-12°

2.2 HUMAN GAIT

The knowledge of the normal human gait as well as its biomechanical measures is crucial for the development of lower limb active orthoses [7], [30]. Walking gait is divided into a stance and a swing phase, being its start and finish point typically represented by the heel strike on the same foot, as is illustrated in Figure 2-10 [7], [30]–[34]. The stance and swing phase represents the period of time when the foot is in contact with the floor and when the foot is not in contact with the ground, respectively [33].

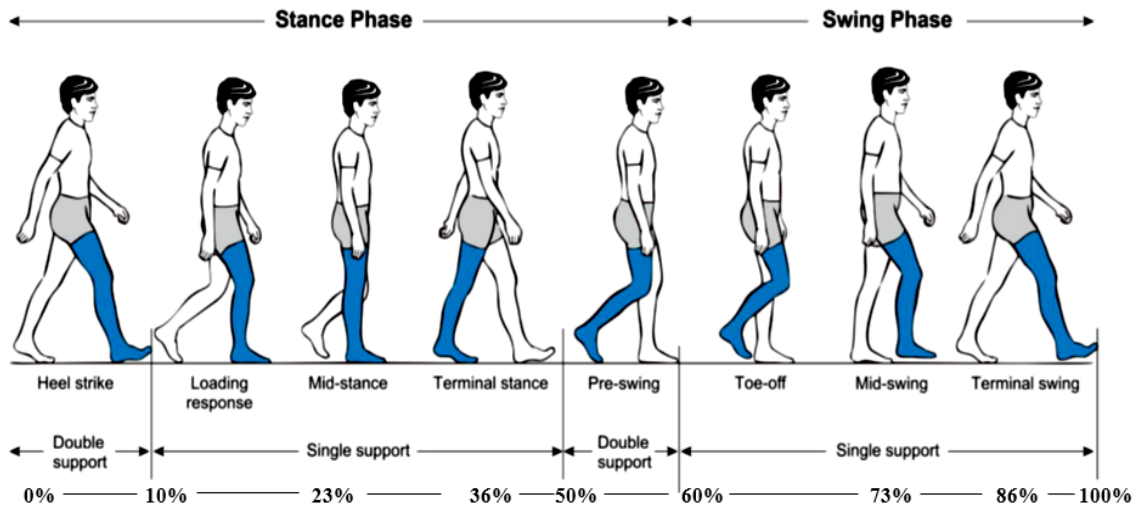


Figure 2-10 - Phases of the normal human gait cycle (adapted from [31], [35]).

The stance phase occupies 60% of the gait cycle and is subdivided into initial contact or heel strike, loading response or foot flat, mid-stance, terminal stance or heel off and pre-swing. At the beginning and end of this phase, both feet are on the ground, consisting of two double support periods of the gait cycle, which last for approximately 10 to 12% of the phase, each one [7], [17], [30], [31]. Moreover, the swing phase lasts for 40% of the gait cycle and is subdivided into initial swing or toe-off, mid-swing and terminal swing, terminating the gait cycle with heel strike of the same foot [7], [17], [31]–[33], [35], [36]. This phase is defined as the period in which the foot isn't in contact with the ground and the limb prepares for subsequent foot contact [37].

2.2.1 KINETICS OF NORMAL HUMAN WALKING

Kinetics is a biomechanical discipline that consists in the study of the forces and moments that are associated with motion of the bodies [35], [38]. In a simulation context, in order to find the moments and forces at each joint during walking, an inverse dynamics analysis must be accomplished [33], [39]. This form of gait analysis is a method for computing joint forces, moments and powers, being the last two determined through the combination of kinematics and ground reaction forces (GRF) [35], [39]. Thus, the main task of the inverse dynamics is to find the joint torques and muscle forces that result in a posterior motion [33].

Herewith, kinetic analysis of the human gait can resort to the investigation of ground reaction forces, which are generated from the impact of the body weight with the ground. This force influences the movement of the entire body, as is the main force acting on the body during human walking, and can be an important descriptor of pathological gait [33], [35], [36], [40]–[42]. Force platforms are used to acquire the three dimensional GRF components in medial-lateral, antero-posterior and vertical direction [33], [41], [43]. These components of the GRF result of the body mass movement in all three direction, which culminate in a much higher in magnitude vertical GRF, when compared to the other shear forces. For this reason, only the vertical GRF is investigated and used to identify specific foot movement characteristics [33], [41]. The equation that describes the ankle's reaction forces is expressed in terms of Newton's Second law of motion, and is typically represented through a M-shaped or double peak graph, which shows the GRF normalised to body weight during a nonimpaired gait cycle (Figure 2-11) [33], [44], [45].

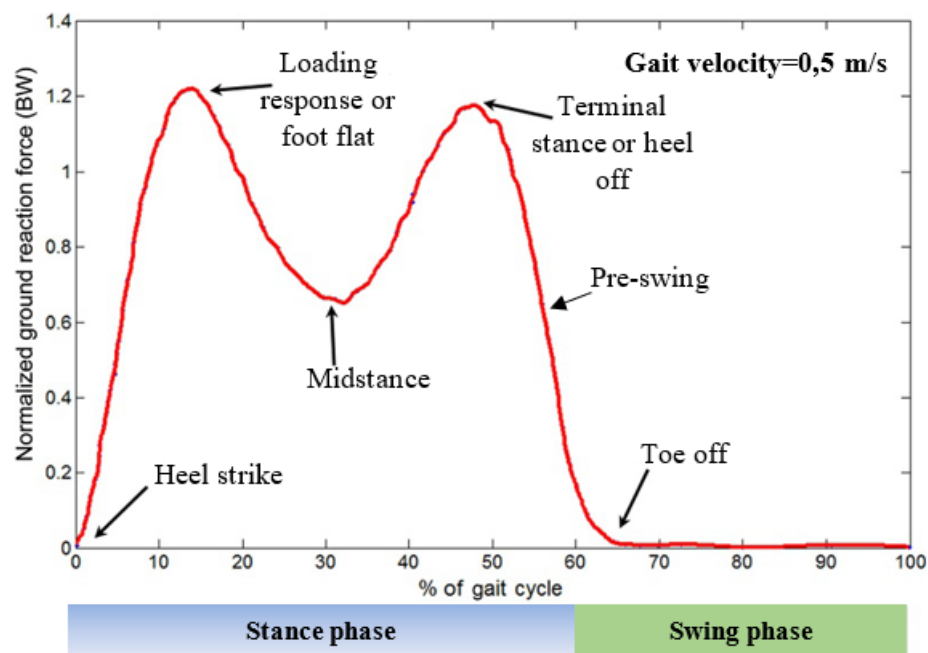


Figure 2-11 - Vertical ground reaction forces in a normal gait cycle, with gait velocity equal to 0,5 m/s (adapted from [33]).

At the initiation of the gait cycle with the heel strike, the energy of the impact forces is absorbed by the soft tissues of the heel and, due to that, the foot complex can be considered as a viscoelastic absorber with the soft heel pad in series with a stiff calcaneus bone [30], [46]. Herewith, data as showed that the ground reaction force will be zero and then increase steadily towards its first peak at the foot flat stage [32], [33],

[46]. The single-support phase begins with the loading response stage, where the whole foot is in contact with the ground and the opposite leg is experiencing a swinging motion [32], [33]. Here, the vertical GRF applied has to be larger than body weight in order to support it and decelerate the downward motion of the body mass [32], [33], [35]. The value of the GRF at this stage can reach 120% of the body weight, as represented in Figure 2-11 [33].

After the first peak, the vertical GRF decreases corresponding to the mid-stance phase, in which the opposite foot is in mid-swing phase and, therefore, the entire body weight is supported by the stance leg [33], [35]. However, at this instant, the centre of mass of the body is upward, creating an upward acceleration that allows a vertical GRF of less than a body weight to support the human body. Hereupon, at this phase, the GRF reaches 63% of body weight [33], [47].

When the heel lifts away from the ground, the vertical GRF rises once more, reaching a value of approximately 125% of body weight to support the body, which is experiencing a forward and upward acceleration in order to propel its centre of mass for the posterior swing phase [32], [33], [35], [36]. Still on this phase, the heel of the opposite foot makes contact with the ground and begins to bear some weight, finally triggering the decrease of the vertical ground reaction force until it reaches zero, at the point of toe-off, when the foot leaves the ground [32], [33], [35].

Moreover, as mentioned above, the three-dimensional ankle joint moments are obtained from the kinematics analysis and the ground reaction forces, as the GRF imposes an external moment on the joint [35], [39], [45]. A moment is then defined as the ability of a force to rotate a body about a certain axis and, relatively to the ankle joint, this moment results of muscular and ligaments forces that causes the joint movement. Furthermore, its study is effectuated by using the Euler's equations of motion presented next [35], [45], [48]. Similarly to the analysis of GRF, joint moments are often normalized to body weight, as well as to leg length [45].

$$\text{Equation 1: } M_x = I_{xx}\alpha_x + (I_{zz} - I_{yy}) \times \omega_y\omega_z$$

$$\text{Equation 2: } M_y = I_{yy}\alpha_y + (I_{xx} - I_{zz}) \times \omega_z\omega_x$$

$$\text{Equation 3: } M_z = I_{zz}\alpha_z + (I_{yy} - I_{xx}) \times \omega_x\omega_y$$

Where, M_x , M_y and M_z are the external angular moments applied to the limb segment in the x, y and z directions; I_{xx} , I_{yy} and I_{zz} are the mass moments of inertia about the principle axes; w_x , w_y and w_z and α_x , α_y and α_z are the angular velocities and accelerations of the limb segment's centre of mass, respectively.

Hereupon, as represented in Figure 2-12 (a), the ankle moment curve demonstrates a brief dorsi-flexor moment at heel strike, which corresponds to the negative value on the curve and serves to control the foot lowering onto the ground and therefore prevent the foot from slapping the floor [15], [35]. This is possible thanks to the dorsiflexors muscles, which eccentrically contract (contraction while lengthening) [15]. This minimum value of joint moment can go down to 0,3 Nm/kg, based on reviewed literature [15], [35], [45], [48]. At the end of stance phase, the peak value for the plantarflexor moment (positive value on the curve) corresponds to the concentric contraction of the plantarflexors muscles, limiting the ankle dorsiflexion movement around a range of angles [15], [35]. This maximum value ranges from 1 to 2 Nm/kg, in the reviewed literature [15], [35], [45], [48]. Towards the toe-off phase, the moment decreases progressively reaching 0 Nm/kg [15], [35], [45].

Furthermore, once the joint angular accelerations, velocities and, therefore, the moments are determined, ankle joint powers can be computed though equation 7, represented next [45]:

$$\text{Equation 4: } P_x = M_x \times w_x$$

$$\text{Equation 5: } P_y = M_y \times w_y$$

$$\text{Equation 6: } P_z = M_z \times w_z$$

$$\text{Equation 7: } \sum P = P_x + P_y + P_z$$

Where, P_x , P_y and P_z are the joint powers in the x, y and z directions, respectively and $\sum P$ is the total joint power.

This joint power corresponds to the rate of energy delivered by the muscles to move a joint and its variation results from the absorption and generation of power by the same muscles that occur during gait [15], [35], [45]. The pattern of a normal kinetic curve,

demonstrating the variation of power delivered during a gait cycle is illustrated in Figure 2-12 (b). Through a close look, one can noticed a peak of absorptive power, which corresponds to the negative value on the curve and extends through the initial phases of gait [15], [35], [45], [49]. This peak correlates with a power absorption from the plantarflexors that eccentrically contract during the heel and ankle rockers (addressed in the next section) [15]. According to the reviewed literature, this minimum value can reach between 0,5 and 1,2 W/kg [15], [35], [45], [49]. At the end of the stance phase, occurs a peak of positive joint power corresponding to the third rocker, which infers a generation of power by the plantarflexors in order for the lower limb to propel forward towards the toe-off phase [15], [35]. This maximum ankle joint power can go up to 3,3-5 W/kg [15], [35], [45], [49].

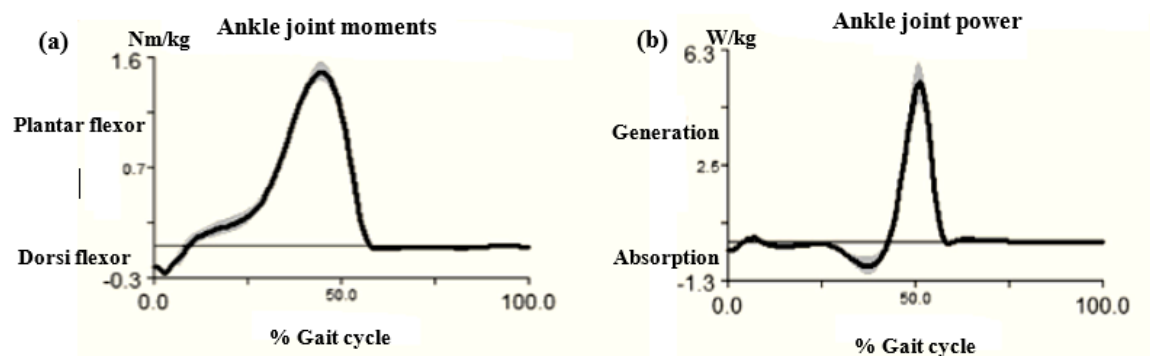


Figure 2-12 - Example of normal ankle joint kinetic curves in the sagittal plane: (a) Ankle joint moments and (b) ankle joint power (adapted from [15])

2.2.2 KINEMATICS OF NORMAL HUMAN WALKING

Kinematics of human walking englobes the analysis of bodies in motion alone, that is without considering the forces actuating on the body [35], [38]. Herewith, an ankle kinematic study allows the description of the body movement during gait, analysing positions, angles, velocities and accelerations of the ankle joint [35].

In 1992, Perry described the rocker theory which analysed the human gait in relation to foot motion in the sagittal plane during stance phase [17]. This wheel-like rolling motion of the ankle has the main function of progression of the leg over the supporting foot. The foot rockers include the heel rocker, ankle rocker and forefoot rocker, as illustrated in Figure 2-13 [17], [35], [37]. The first rocker corresponds to a

deceleration rocker and occurs as the heel contacts the floor at heel strike and progresses until the foot plantarflexes and brings the forefoot into contact with the ground [35], [37]. Here, the ankle experiences plantarflexion [35]. Furthermore, the ankle rocker begins with foot flat (or loading response) and extends to when muscle action restrains further dorsiflexion, comprising the mid-stance phase. This stage corresponds to a deceleration rocker as well and is the period when momentum forces the tibia to rotate forward from a state of plantarflexion to a dorsiflexed position [35], [37]. Finally, the forefoot, or third rocker, coincides with the terminal stance or heel off phase and, at this instant, only the forefoot is in contact with the ground. This one is an acceleration rocker to prepare for the limb advancement in pre-swing, allowing the propulsion of the body during gait [17], [35], [37]. In this phase, the ankle moves rapidly from the position of dorsiflexion to a certain degree of plantarflexion [35].

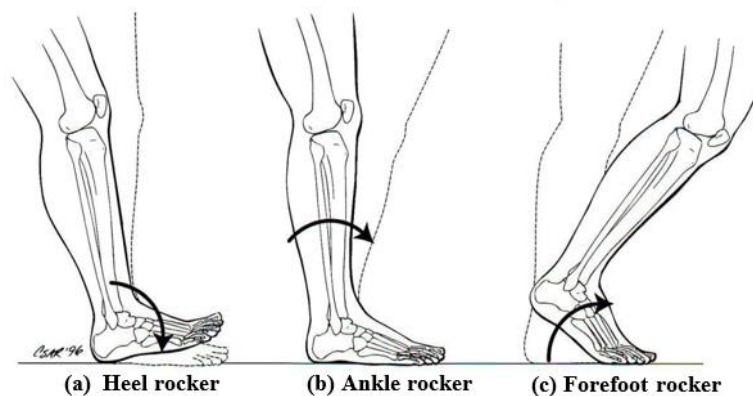


Figure 2-13 - The three rockers occurring during stance phase of the human cycle: (a) the heel (first) rocker; (b) the ankle (second) rocker; (c) the forefoot (third) rocker (adapted from [37]).

During the swing phase, the leg acts as a pendulum controlled by the mass moment of inertia and the ankle dorsiflexes in order to enable the foot to clear the ground and avoid stumbling or tripping phenomena [15], [37]. Initial swing begins with toe-off and, as the ankle experiences plantarflexion, the phase extends to the instant when the swinging limb is aligned with the opposite stance limb. The mid-swing phase begins with this alignment and enables the leg to move forward ahead of the body weight line, while the ankle is in dorsiflexion to permit foot clearance, terminating when the swinging limb is in front of the stance limb and the tibia is in a vertical position [37], [50]. Finally, terminal swing constitutes the last third of the swing phase and the period when the leg begins to

touch the ground and the ankle moves into a neutral position, initiating the next cycle with heel strike [31], [37], [50].

After an extensive review of the literature concerning studies that proposed graphical representations of the range of motion of the ankle joint in the sagittal plane, during a normal gait cycle, it was possible to conclude that the ankle joint motion follows a certain pattern [15], [20], [21], [32], [35], [49], [51]–[55]. However, these studies showed incoherence regarding some of the dorsi-/plantarflexion angle' values. This fact can be explained considering the inter-subject variability of the ankle range of motion, even among anthropometrically similar individuals [21]. Nevertheless, the following Figure 2-14 shows an example of a kinematic graph of the ankle joint's range of angles of dorsi-/plantarflexion during a normal gait cycle.

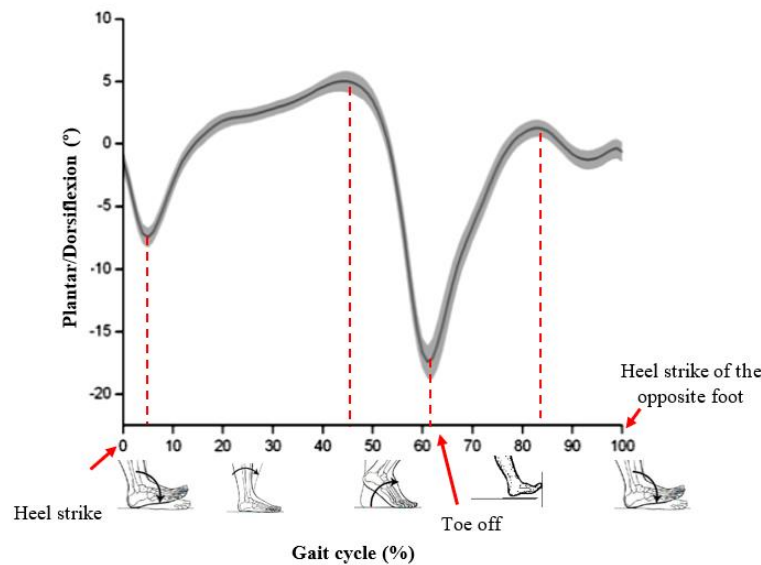


Figure 2-14 - Graphical representation of the ankle joint's range of motion in the sagittal plane, during a normal gait cycle, and respective gait phase. Positive and negative values concern dorsiflexion and plantarflexion, respectively (adapted from [21]).

2.3 BIOMECHANICS OF IMPAIRED ANKLE JOINT

The present section discloses the biomechanics of the impaired ankle joint. The deformities of the ankle following a stroke will be discussed, as well as its effects on individual's gait.

2.3.1 ANKLE JOINT POST-STROKE

Following a stroke, spasticity of the ankle and foot muscles is very recurrent, which results in deformities of the ankle, being the most common the equinus, varus, equinovarus, and striatal toe deformities. This phenomena also has consequences on the control of the ankle movement during gait, as the activation of the affected muscles is more diffuse and divergent [56]–[58]. In order to manage spasticity of the ankle and foot muscles, interventions with botulinum toxin (BoNT) injections are commonly used, which has been reported to ameliorate gait pattern of post-stroke patients [56], [58]. Next, the most common ankle deformities derived from a stroke are addressed.

An **equinus** ankle deformity is a condition that is characterized by the ankle and foot being held in the plantarflexed position and by the difficulty subjects have with voluntary dorsiflexion (Figure 2-15 (a)). This abnormality is caused by spasticity of the muscles responsible for plantarflexion motion (also called plantarflexors) [52]. As mentioned in Section 2.1.1.2, these muscles are the gastrocnemius and soleus muscles, which belong to the posterior compartment of the leg muscles [11], [52]. During gait, subjects with an equinus ankle deformity experience drop foot, which is the incapacity to perform dorsiflexion motion of the ankle and, therefore, the inability to lift the foot during the swing phase [52], [53].

A **varus** ankle is held in a varus position, i.e. inversion position (Figure 2-15 (b)), due to the fact that both tibialis anterior and tibialis posterior muscles experience spasticity [52]. Herewith, since these muscles are responsible for dorsiflexion and inversion, and plantarflexion and inversion, respectively, the effect of its simultaneous activation results in ankle inversion stiff position [11], [52]. The individuals with a varus ankle are not able to perform dorsiflexion and eversion in its full range of motion, and, during stance phase, they support the weight on the anterior lateral part of the foot [52].

An **equinovarus** abnormality is reported to be the most common deformity of the ankle and foot complex following a stroke. The ankle is fixed in a plantarflexed and inverted position (Figure 2-15 (c)), once it's primarily caused by spasticity of the plantarflexors and invertors muscles. The subjects with this deformity endure their weight on the lateral front part of the foot [52]. Lastly, the **striatal toe** deformity is characterized

by the hyperextension of the hallux (commonly known as great toe, Figure 2-15 (d)) and is caused by the spasticity of the extensor hallucis longus.

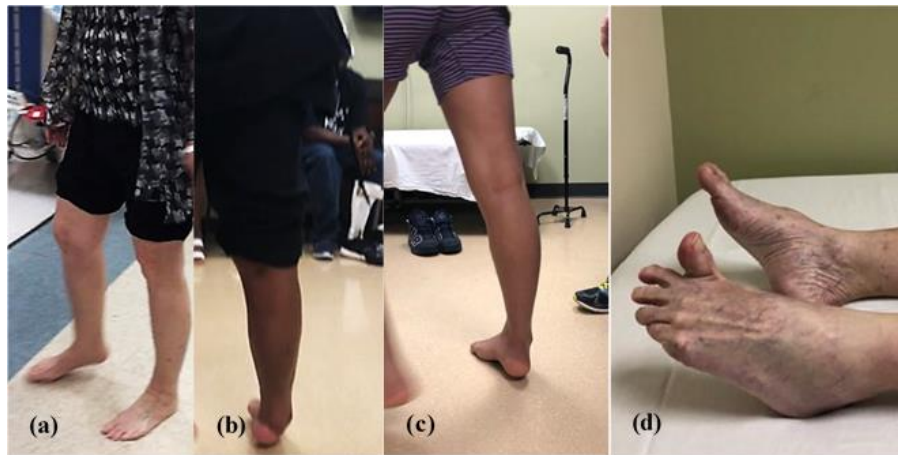


Figure 2-15- The four commonly seen ankle and foot deformities, following a stroke: (a) equinus ankle deformity on the right side, (b) varus ankle abnormality, (c) equinovarus deformity, and (d) striatal toe on the left side [56].

2.3.2 IMPAIRED HUMAN GAIT

As mentioned above, 40% of the stroke survivors feature an impairment which can manifest itself through motor, cognitive, behavioural and sensory sequelae [2]. Concerning the motor disabilities after a stroke, individuals often experience hemiplegia (paralysis of one of the sagittal half of the body) or hemiparesis (weakness of one side of the body), sensory disorders, muscle weakness and spasticity, joint deformity and abnormal coordination [3], [4], [59], [60]. Furthermore, the ease of clearing the floor during the swing phase of the gait and forward propulsion in the stance phase are also affected (Figure 2-16). This abnormality is called drop foot and is induced by the impairment of the muscles responsible for the lifting of the front part of the foot [3]–[5], [60]. This condition leads to the metabolic deficiency of the gait, increasing the risk of falling [4], [5].

One of the main characteristics of post-stroke gait is the reduced walking speed. Studies report that the average self-selected gait velocity for stroke survivors is lower than normal ambulation's velocity, which can range from 0.23 m/s to 0.73 m/s [57], [61]. Through various studies that depicted walking speeds and the associated outcomes, a gait speed of more than 0.80 m/s and 0.90 m/s have been suggested to be necessary for

community ambulation (e.g. crossing the street in time), and to perform household activities, respectively [57], [62]. Due to this decrease of gait velocity, both stride length and cadence are lower, comparing to the values corresponding to able-bodied subjects [57], [61]. Additionally, it's worth noticing the differences in the proportions of stance and swing phase of a gait cycle in people with hemiplegia. Firstly, the stance phase of both the affected and unaffected sides is longer in duration, occupying a greater proportion of the gait cycle when compared to a normal walking cycle at normal speed. Furthermore, the stance phase is longer on the unaffected side than on the impaired side, and, lastly, a greater proportion of the gait cycle is spent in double support than that of healthy subjects' gait at normal speeds [61].

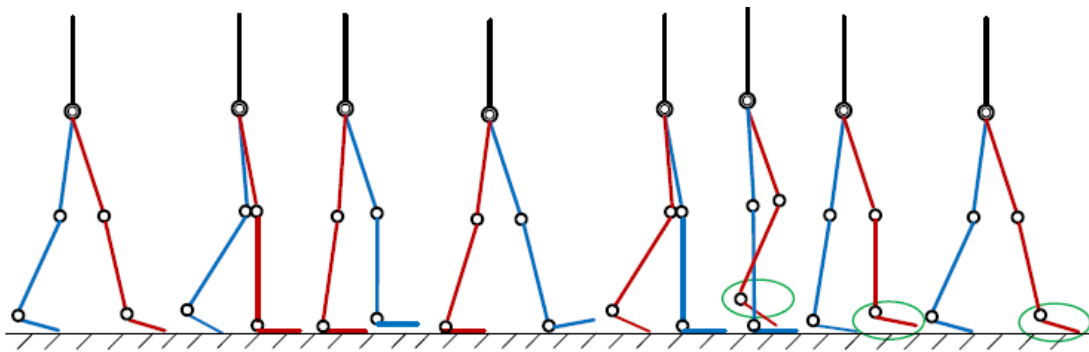


Figure 2-16 - Gait pattern of individuals with paretic ankle. The red link represents the impaired limb [10].

In association with the reduced gait velocity, temporal and spatial inter-limb asymmetries are another feature of the stroke related impaired gait [57]. As mentioned above, the stance time of the impaired limb is shorter than that of the healthy side, and, on the other hand, the swing time of the affected limb is longer than that of the unaffected limb. In addition, on the impaired side, the pre-swing phase is on average more prolonged than the loading response phase. Thereafter, because of the decreased swing time of the unaffected limb, the spatial asymmetry is often characterized by its shorter stride length. Herewith, the asymmetries ratio of stance and swing time for both the healthy and impaired limb, as well as their step length, have a significant negative correlation with the stroke survivors' self-selected gait speed [57], [63], [64].

The loss of balance during gait is common in individuals who have suffered a stroke, and this problem has been related to the spatial-temporal asymmetry, characteristic of impaired gait [57], [65]. Thus, both step length and swing time

asymmetries have been correlated to the negative effect on an individual's balance during walking at comfortable and high speeds [64].

The ground reaction force analysis has been used as a method of identification and assessment of the gait pattern of stroke survivors [57], [66], [67]. Post-stroke gait presents a degree of asymmetry of vertical GRF between the affected and unaffected limb, which has been correlated with the degree of asymmetry of temporal measures during gait and its speed [57], [66]. Kim et al. studied these correlations in a group of individuals with chronic stroke and verified that the vertical GRF of the impaired limb significantly decreased when compared to the healthy side [66]. Additionally, it has been reported that the asymmetry of the vertical GRF between the affected and unaffected limb, at both self-selected and fast speeds, is greater at the end of the stance phase when compared to its beginning. Figure 2-17 shows the vertical GRF mean profiles in individuals with hemiparesis at both speeds. It's worth noticing that the values for the first two GRF peaks (V-P1 and V-P2) are greater on the affected side than on the healthy side, and that the asymmetry increased with speed only for the third peak (V-P3) [67].

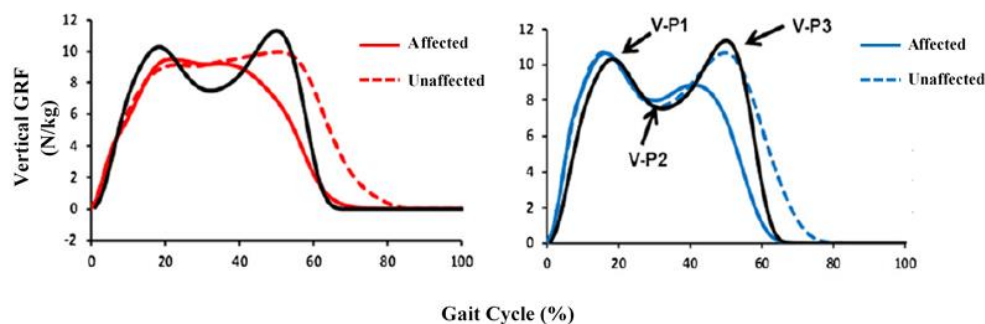


Figure 2-17 - GRF mean profiles of the unaffected and affected side in individuals with hemiparesis walking at self-selected (red lines) and fast (blue lines) speeds. The former speed is 0.72 m/s and the fast speed is reported to be 1.08 m/s. The black lines refer to healthy subject walking at self-selected speed (1,26 m/s) (adapted from [67]).

The kinematics and kinetics characteristics of each lower limb's joint are essential to describe the gait pattern post-stroke and, therefore, assess the patient's ambulatory condition [57], [61], [67]. At the end of the stance phase (toe-off), it's noticeable a decrease in the peak angle value of the ankle's plantarflexion, as well as during the swing phase, where the dorsiflexion amplitude is lower relative to the normal ankle kinematics (Figure 2-18) [61], [67]. To compensate for the decline in the range of angles of the ankle joint, the knee and hip joints present changes in its kinematics, such as a decrease in knee flexion, circumduction of the leg, or exaggerated hip flexion. These compensatory

strategies adopted by stroke survivors allow adequate foot clearance during the swing phase [67].

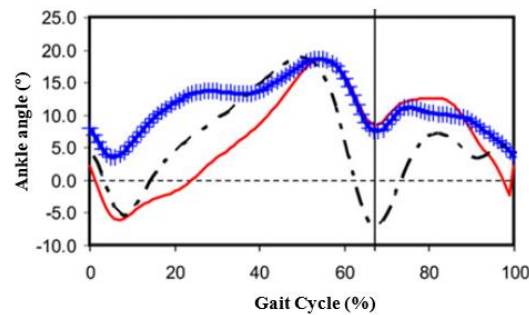


Figure 2-18 - Kinematics profile of the ankle joint of healthy subjects (dark dotted line) and of the paretic side of patients, walking at a speed of 0.78 m/s (red line) and 0.85 m/s (blue line) (adapted from [67]).

Moreover, similar to the kinematic changes concerning post-stroke gait, the net positive moment and power of the ankle joint on the affected side have a profile comparable with that of healthy individuals, although it's noticeable a decrease in amplitude [57], [61], [67]. The hip flexors muscles contribute more to the energy generation than the plantarflexors muscles of the leg while walking, especially during the pre-swing phase, to increase swing initiation [57], [67]. Thus, through the analysis of the graphs in Figure 2-19 (a), one can notice the decrease in plantarflexor moment (negative) on the affected limb, during the end of the stance phase. Besides, the ankle joint's power graph in Figure 2-19 (b) shows the decrease in power generation during the pre-swing phase [57]. Furthermore, although in a lower extent, the kinetics variables of the healthy side also suffer changes, being the ratio of energy produced by leg muscles on the unaffected side compared with the affected side is around 60:40 [67].

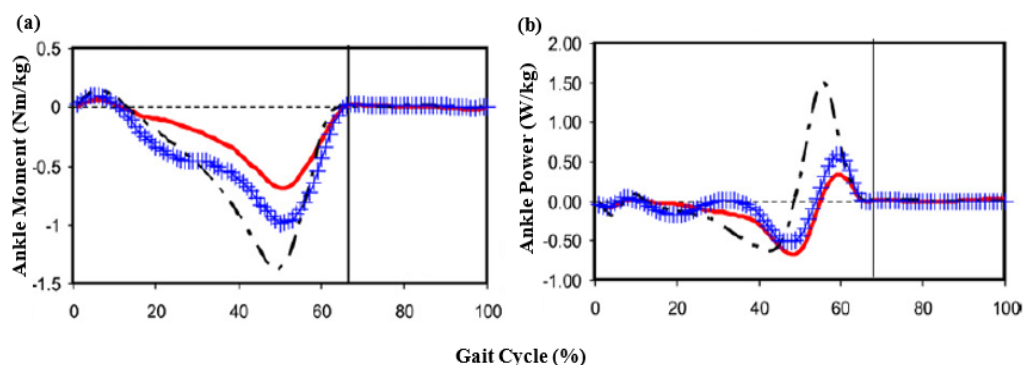


Figure 2-19 - Kinetics profile of the ankle joint of healthy subjects (dark dotted line) and of the paretic side of patients, walking at a speed of 0.78 m/s (red line) and 0.85 m/s (blue line): (a) ankle joint's moment profile (with negative plantar flexor moment) and (b) ankle joint's power (adapted from [67]).

3. REHABILITATIVE LOWER LIMB ORTHOTIC DEVICES

This chapter focuses on the literature survey of the rehabilitative lower limb exoskeletons, as well as powered orthoses that are both commercially available and still in development.

Firstly, the gait rehabilitation procedures are addressed, as well as the various types of ankle-foot orthoses and the distinction between each one. Next, an insight into the wearable active orthoses is given. In this section, the actuation systems that incorporate such devices are explored, and the different types of actuators are compared, disclosing each one's advantages and disadvantages. Furthermore, this section addresses the mechanical and electronic components, which are usually implemented on active AFOs to warrant a safe use, while monitoring his/her biomechanical activity. The section includes the literature and market research of commercially available lower limb exoskeletons and powered ankle-foot orthosis for rehabilitation, as well as orthotic devices that are still in an approval phase or in a development stage.

Moreover, the chapter addresses an issue concerning rehabilitative lower limb orthoses, the misalignment between the user ankle's axis and the rehabilitative device's axis. On this note, the solutions developed over the past years to tackle this problem are disclosed. Hence, it will be presented the currently developed self-aligning mechanism, as well as the multiple DOF AFOs.

Finally, the chapter ends with the presentation of an important aspect regarding the development of an AFO: its structure design. Thus, the orthosis geometrical shape, material selected to compose it, and the production method chosen to manufacture the device's structure are disclosed.

3.1 GAIT REHABILITATION

The restoration of strength, motor coordination and the overall ability to walk are considered the key rehabilitation goals for stroke survivors [2], [65]. Strategies for improvement of the post-stroke gait can be described considering either muscular or a task-oriented focus,

although these two are often covered together in rehabilitation strategies [57]. Muscular focus includes muscle strength training and functional electrical stimulation (FES) and the task-oriented focus comprises the treadmill training, electromechanical and robot-assisted gait training, and the use of AFOs. The effect of the chosen strategy on the patient is often determined based on the subject's speed before and after the treatment [68].

Lower extremity muscular strength training has been recommended by the American Heart Association (AHA) guidelines for post-stroke adult gait rehabilitation [57], [58]. Evidence shows that providing lower limb resistance training (which involves eccentric and concentric exercises, see Figure 3-1 (a) and (b) as an example for the arm muscle) to individuals who are 6 months after stroke, results in the improvement of gait speed and total distance walked, as well as increasing strength and functional performance, such as stair climbing, chair stand, and balance [57], [58], [68]. On this note, studies have shown that, when compared to concentric contractions, the eccentric contractions were a more effective training mode, since it provided the greatest gains in neuromuscular activation and power of the affected leg muscles, as well as it improved the subjects' walking speed [69].

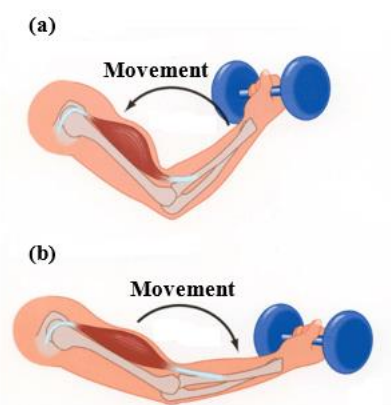


Figure 3-1 - Example of the resistance training mode on the bicep muscle: (a) Concentric exercise and (b) eccentric exercise [70].

FES consists in the application of predetermined frequencies and amplitudes of electrical currents to nerves and muscles in the affected region, in order to generate muscle contraction [57], [71], [72]. This treatment has been used to correct drop foot in hemiplegics since the 1960s, and since then the improvements on gait and on the effort of walking, as well as on walking speed have been reported by researchers [71]–[74]. Several studies have shown that FES (Figure 3-2 (a)), associated with conventional rehabilitation (physiotherapy), can reduce spasticity, and even delay it if it is started early after stroke (up until 3 months afterward), increase muscle tone and strength, improve balance and joint voluntary

movement, and can provide better paretic lower limb functional recovery [71]–[73]. Moreover, the recommended therapy time of FES is 30 minutes, 5 days per week, and an increase in the dorsiflexion torque is reported in these studies, along with improvements in pace, stride rate, step length, as well as with a decrease in single swing rate [73], [74]. Finally, FES not only improves walking ability, but also produces lasting ameliorating effect after the treatment [74].

With the objective of enabling repetitive gait and coordinated stepping practice, treadmill training is often chosen as a post-stroke gait rehabilitation [57], [58], [68], [75]. This type of treatment can resort to body weight support (usually with a harness) or not, and is performed with the help of therapists to assist the paretic lower extremity in stepping, as illustrated in Figure 3-2 (b) [58], [68]. When compared with no intervention or with an intervention without a walking component, treadmill training has shown improvement in walking speed and distance among ambulatory individuals who have suffered a stroke [58]. Furthermore, studies suggest that patients who are earlier after stroke are more likely to experience motor recovery with mechanically assisted walking with body weight support than with over-ground walking (ambulation in an actual environment, like hallways) [58], [68]. On this note, it has also been shown that high-intensity treadmill training has a better therapeutic effect than at slower speed, which improves the maximum walking speed and even enhances cardiovascular fitness [68], [75].

Robots and electromechanical-assisted training devices have also been used to promote gait recovery after stroke. As oppose to body-weight supported treadmill training, in which the patient's legs are guided by a therapist, electromechanical-assisted gait rehabilitation offers continuous support for the legs by robotic orthoses, allowing for reduced physical and time demands on therapists. Moreover, the robotic support in a physiological gait pattern enables the improvement of the repetition accuracy and the extension of the training duration, as compared to manual treadmill training [57], [58], [76]. Herewith, these robotic devices have the potential to collect joint kinematic and kinetic data simultaneously with walking, providing computerized feedback of the current performance of the patient, which habitates for better training effect [57], [76]. This type of gait rehabilitation in combination with physical therapy has shown to be effective to achieve independent walking and to improve the balance of patients who are within the first three months after stroke and those who are unable to walk [58]. The Lokomat Driven Gait Orthosis illustrated in Figure 3-2

(c) (DGO, Hocoma Medical Engineering Inc, Zurich, Switzerland), the Mechanized Gait Trainer (MGT) and the Gait Trainer (GT) 1 and 2 (Reha-Stim, Berlin, Germany), the AutoAmbulator (HealthSouth, Birmingham, Alabama), and the LOPES (Lower-extremity Powered ExoSkeleton, Laboratory Biomechanical Engineering, University of Twente, Enschede, the Netherlands) are the current commercially available devices [57], [58], [77].

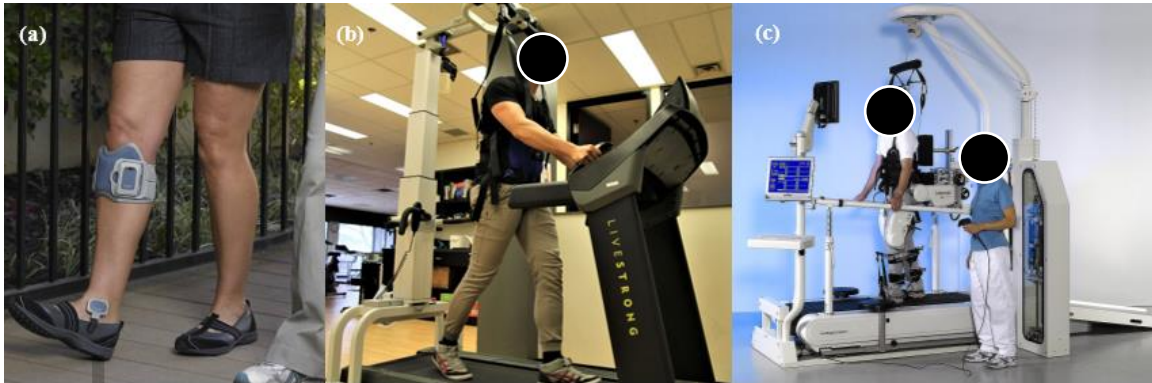


Figure 3-2 - Muscular and task-oriented focus post-stroke gait rehabilitation: (a) example of a FES device, (b) treadmill training with a harness, and (c) example of a robot-assisted gait training device (Lokomat DGO) [78]–[80].

Finally, the use of an ankle-foot orthosis in stroke rehabilitation has revealed itself to be an effective method to improve the walking ability and balance, as well as controlling spasticity and compensating for motor impairments in the lower limb [3]–[5], [7], [57], [58], [76], [77], [81], [82]. An AFO provides medio-lateral stability during gait by limiting tibiotalar and subtalar movement, facilitating foot clearance and heel strike in the swing phase. Both the passive (without actuation) and the active (powered by actuation systems) AFOs present results of increasing the ankle dorsiflexion performance during the stance and swing phase, preventing foot drop [3], [4], [7], [76], [77], [82].

Concerning the passive AFOs, the American Heart Association (AHA) guidelines for post-stroke adult gait rehabilitation recommends its use in individuals with remediable gait impairments and for a period of time of at least three months, since it has been shown that AFO users had better mobility while wearing the orthosis. Moreover, studies claim a favourable impact of AFOs on walking disability, improving its speed, the step length, as well as on overall ankle kinematics, kinetics and energy cost [58], [76]. Studies conducted to analyse the effect of the orthosis design on walking after stroke also claim that, while a rigid AFO (that limits both plantar and dorsiflexion) and an articulated orthosis (that restricts plantarflexion) both correct the excess plantarflexion during swing, the rigid AFO impeded

walking ability for individuals with a normal range of motion. On the other hand, the articulated AFO with plantarflexion resistance allowed the largest excursion of dorsiflexion in stance phase, as well as improved the gait speed and step length [3], [4]. Relatively to the effect of a hinged AFO on post-stroke gait, it was shown that it can significantly improve functional mobility, stride length, cadence and gait speed, while ensuring the comfort to the users [77]. Despite these promising results, passive lower limb orthosis inhibit normal push off during walking, begets dependency and reduces gait adaptability and rehabilitation [58], [82].

Therefore, active AFOs (or ankle rehabilitation robots) provide for power assistance at the ankle joint, which facilitates ankle locomotion and enables stroke survivors to regain walking capabilities [7], [30], [82], [83]. These robot-assisted AFOs can help the walking capacity of patients presenting drop foot, by actively assisting ankle dorsiflexion on over-ground walking for foot clearance during the swing phase, as well as it can minimize the occurrence of foot slap (excessive plantarflexion) at initial contact of the foot with the ground [82]. The high intensity and repetitive nature of the robot promotes an experience-driven adaptation of the damaged motor structures, allowing for a more effective gait training [8], [30], [82]. Figure 3-3 (a) and (b) illustrates two examples of a passive and active AFO, respectively.

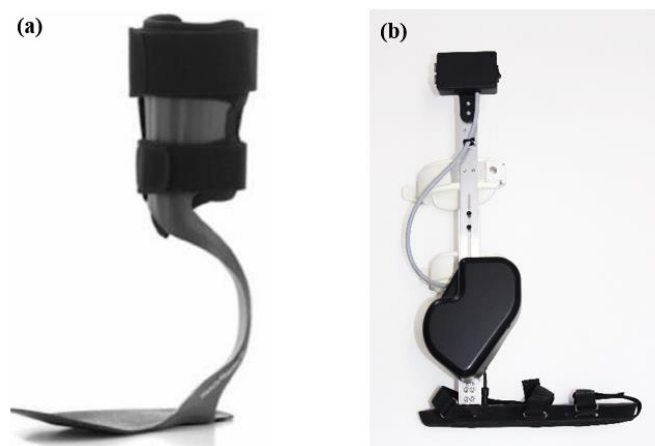


Figure 3-3 - Examples of a passive and active ankle foot orthosis: (a) The passive AFO developed by Ottobock and (b) Exo-H2 AFO developed by Technaid [10].

These rehabilitation robots can be categorized into platform-based and wearable ankle rehabilitation robots [8], [82]. The platform-based ankle rehabilitation robot are stationary robots whose main goal is focused on motion therapy and on strengthening the muscles [82]. The latter, on the other hand, is defined as a wearable mechanical device, designed around

the shape and the function of the human body, which actuates movement of the ankle joint, in order to be used to perform gait training with a programmable control that integrates the cognitive ability of the operator [8], [82]. For this type of robot, the actuator, gait event detection, and control strategies are key factors for the effectiveness of ankle and gait rehabilitation for stroke patients [82]. The actuator has a definitive role in the wearable ankle rehabilitation robot, since it determines the performance of these robots, in terms of the assistive torque, efficiency, and portability [8], [82]. This topic will be further discussed on the next chapter.

In association with the actuator system, the gait event detection can be used to stimulate functional assistance, and the control strategies implemented in a gait rehabilitation device aim to reflect the physical interaction between the user and the device, as well as to create a safe, compliant, and a natural human-computer interaction environment [82], [84]. This topic will also be further discussed, along with the types of ankle foot orthosis that have been developed and the comparison between each one. Concerning the active AFOs, it will be addressed the different actuation systems, and each one's benefits and disadvantages, as well as the commercially available and under development wearable ankle robots and exoskeletons.

3.2 PASSIVE, SEMI-ACTIVE AND ACTIVE ORTHOSES

Existing ankle-foot orthosis include three types of devices: passive (with nonarticulated or articulated joints), semi-active and active [10], [30], [34]. Passive orthoses don't incorporate in its system any electronic control element other than mechanical elements, such as springs or dampers to control the ankle-foot complex, or any power source [30], [34]. These AFOs' main goal is to provide assistance to the user by preventing unwanted foot motion with direct physical resistance, being the most popular daily-wear device thanks to its compactness, durability, lightweight and simplicity of the design [10], [30], [34]. However, the motion control limited by passive components of passive AFOs are not capable of adapting to changing environments and have restricted functionality for disabled people [10], [34]. Figure 3-4 illustrates some of the many passive AFOs designs, articulated and nonarticulated, developed by Ottobock and a research team led by Sumiko Yamamoto [85].



Figure 3-4 - Passive ankle-foot orthoses: (a) Nonarticulated AFO developed by Ottobock (2017); (b) Articulated AFO, also developed by Ottobock; (c) Posterior leaf spring AFO by Ottobock and (d) Articulated AFO called “Dorsiflexion assist controlled by spring” (DACs) developed by Yamamoto et al. (1999) [10], [30], [86].

Concerning the nonarticulated passive orthoses (Figure 3-4 (a) and (c)), these devices are usually single piece, composed by flexible and lightweight thermoformable or thermoplastic materials, such as polypropylene and carbon graphite composites [30], [34]. This type of orthosis determines the motion control characteristics through its material properties and geometry [30]. The design of these AFOs can vary from highly rigid to flexible: the former holds the ankle in a fixed position, restricting plantarflexion completely, and the latter has a spring-like behaviour, being able to store energy during deformation and enhance push-off during the pre-swing phase. The use of rigid nonarticulated AFOs has shown to cause excessive knee flexion moment during loading response, in order for the user to be able to clear the toes during swing phase, resulting in walking instability. On the other hand, the flexible design, like the carbon fibre AFO, has proven to decrease the energy expenditure of the impaired patient, improving pathological gait. Nevertheless, nonarticulated passive AFOs do restrict some normal movements of the ankle joint, which affects the functional recovery [10], [30], [34].

Relatively to the articulated passive AFOs (Figure 3-4 (b) and (d)), the materials that compose it are the same as in the case of fixed AFOs, but it includes a joint with a hinge, flexion stops, and stiffness control elements, like springs, oil dampers and others, which provide better motion control [10], [30], [34]. These mechanical components have shown to prevent drop-foot successfully by providing dorsiflexion assisting force or locking the ankle in a suitable position [10], [34]. Nonetheless, the functionality of these AFOs is limited, and the user might experience deficient dynamic balance and unnatural gait pattern. A direct positive torque supply is necessary for the patient to propel the body forward [10], [30]. Consequently, an

AFO shouldn't just rely on passive elements, such as springs, since this type of control presents limited robustness [30].

In order to overcome the limitations of passive ankle-foot orthoses, semi-active AFOs have been developed to provide assistance for patients with drop foot, without the supply of active torque [10], [30], [34]. This type of AFO can only dissipate, store and release available energy, using computer control to vary the compliance/damping and flexibility of the ankle joint in real-time [10], [30], [87]. Semi-active AFOs integrate into its system magneto-rheological (MR) brake or damper, which can ensure controllable braking torque, by modulating the current applied to them. This component has shown to be crucial to warrant the ankle damping at the foot down, as well as locking it during the swing phase. The results of the studies regarding semi-active AFOs show not only the effectiveness to prevent drop foot, but also the improvement of the user's comfort while walking [10], [30]. Figure 3-5 (a) and (b) show two examples of semi-active articulated AFOs developed by research teams led by Furusho et al. and Svensson et al. [10].

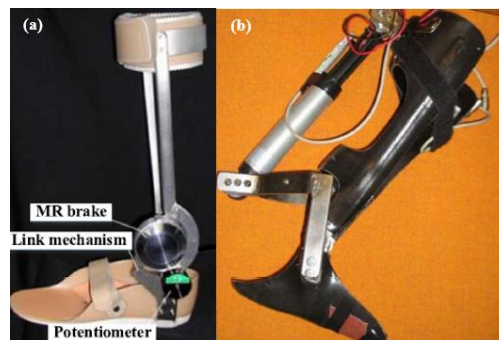


Figure 3-5 - Semi-active ankle-foot orthoses: (a) The AFO developed by Furusho et al., with an MR brake, that generates the braking torque to keep dorsiflexion; (b) The AFO developed by Svensson et al. with an MR damper to realize the ankle damping at foot down and locking during the swing phase [10].

Regarding active AFOs, these are comprised of one or more actuators and portable or tethered sources of power to move the joint, which associated with a robotic control system, ensure a controllable assistive torque during gait [10], [30], [34]. This type of AFOs also incorporates an electronic system that includes force sensors, angle measurement sensors, accelerometer, potentiometer, and microprocessors [10], [34], [84]. As oppose to the passive AFOs, active ankle orthoses can interact with the walking environment and modulate the ankle movements accordingly [10], [34]. Thus, active AFOs are often prescribed to post-stroke patients, due to the fact that these devices can provide assistance for individuals with hemiplegia, and warrant sufficient toe clearance and, therefore, prevent drop foot during the

swing phase of the gait [7], [10], [30], [34], [84]. Figure 3-6 shows an example of an active AFO. More examples will be further presented in Section 3.3.4.

An overview concerning the characteristics and limitations of passive, semi-active and active ankle-foot orthoses, as well as the report of some examples of developed devices, is present in the appendix **A-Overview information of the different types of AFOs** of this dissertation.



Figure 3-6 – Example of an active AFO: Ankle module of the Technaid H2 lower limb robotic exoskeleton powered by an electric motor [83].

3.3 WEARABLE ACTIVE LOWER LIMB EXOSKELETONS AND ANKLE-FOOT ORTHOSES

The concept of using exoskeletons to enhance human locomotory performance dates back to 1890 when an apparatus for facilitating walking, running and jumping was conceptualized by Nicholas Yagn (Figure 3-7 (a)). This first idea of an exoskeleton consisted of a large bow spring connected between the hip belt and a foot attachment, which stored the energy generated by the weight of the wearer [7], [88]. Throughout the years, the progress in the development of exoskeletons has been noticeable, and in the last sixty years, the fields of gait rehabilitation, assistance and human strength augmentation have demonstrated immense interest in the research and development of powered lower limb exoskeletons and active orthosis [9], [84], [88]–[90]. However, the past two decades have been remarkable in terms of computer technology improvement, faster data processing, reduced equipment size and energy requirements, whereby universities, research institutes, and industrial companies have been actively performing research in this field [9], [89]. As a result, several active exoskeletons and

orthoses have been developed, tested and some certified (an example is illustrated in Figure 3-7 (b)) [7]–[9], [30], [83], [84], [88]–[90].

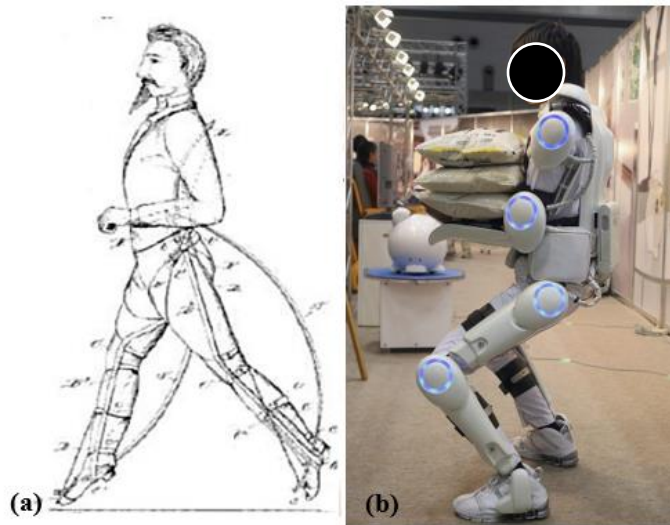


Figure 3-7 - Exoskeletons throughout the years: (a) Concept design of the Yagn's exoskeleton (1890), and (b) HAL-5 exoskeleton (2012) [8], [88].

Despite the distinction between powered exoskeletons and active orthoses not being clear as of yet, in general, the term “exoskeleton” refers to a device that augments the performance of an able-bodied wearer, and the term “active orthosis” is typically used to describe a device used with the purpose of assisting the user, who is suffering from a limb pathology, to recover the motor function, and therefore increase their ambulatory ability [7], [8]. However, the term “exoskeleton” is nowadays often used to describe as well assistive devices, particularly when they enclose several human joints, also being referred as multi-joint exoskeletons [7], [84]. Herewith, a wearable powered exoskeleton/orthosis is defined as an electromechanical device designed around the shape and function of the human body, and that it can be worn by an operator, working in concert with her/his movements [7]–[9], [91]. These devices are equipped with powerful actuators at human joints, as well as with a built-in multisensory system which can acquire the user's motion intentions, in order to accordingly assist the desired movement [8], [9].

Exoskeletons can be classified into four main categories, based on the part of the human body the device provides support: upper limb exoskeletons, lower limb exoskeletons, full-body exoskeletons, and specific joint support exoskeletons (also denominated as orthosis) [9], [84]. Furthermore and as aforementioned, the lower limb exoskeletons are developed for three main scopes of application: gait rehabilitation, human locomotion assistance, and

enhancing physical abilities of an able-bodied human, i.e. human strength augmentation [9]. Concerning the exoskeletons for gait rehabilitation, these can be wearable (also called ambulatory) exoskeletons or tethered/static exoskeletons [7], [84]. On the other hand, as previously mentioned, active orthoses are developed to assist the user with a limb pathology, and ankle-foot orthoses can be divided into two groups: daily-wear devices and patient diagnosis and rehabilitation [30].

Due to the main objective of the SmartOs project, which is the development of a wearable active ankle-foot orthosis intended for ambulatory rehabilitation of post-stroke patients, the scope of this literature review will only include wearable powered lower limb exoskeletons for gait rehabilitation and active orthoses that provide assistance only to the ankle joint. Hence, this section will firstly focus on the actuation technologies conventionally used in exoskeletons and active orthoses. Next, the human-exoskeleton motion assistive techniques and sensor technologies currently implemented in these devices will be briefly reviewed. Lastly, a literature survey of the lower limb exoskeletons and active AFOs will be conducted. This will comprise both commercially available wearable rehabilitation exoskeletons and active ankle-foot orthoses that have either the FDA (Food and Drug Association) approval or the CE (European Conformity) marking and powered wearable AFOs that have been developed worldwide.

3.3.1 CONVENTIONAL ACTUATION IN EXOSKELETONS AND ACTIVE ORTHOSES

Powered lower limb orthotic devices comprise an actuation system in its joint(s) with the prime objective of converting energy into mechanical motion, and, therefore provide positive torque to the user [10], [30], [34], [84], [91], [92]. In robotic applications, different actuators can be used, such as electric, pneumatic (including pneumatic cylinders and pneumatic muscle actuators), hydraulic, piezoelectric, electroactive polymers, variable stiffness actuators (VSA), robotic tendon actuator and series elastic actuator (SEA) [8], [10], [34], [91], [92]. However, many of these actuators technologies can't be used in orthotic devices for human rehabilitation, since that the exoskeleton's actuation systems are required to provide high torques, while operating at low speeds [30], [84], [92]. Herewith, currently, the **electric**, **pneumatic** and **hydraulic** actuators are the technologies predominantly used in exoskeletons and active orthoses [8], [84], [91].

Throughout this section, the main characteristics of these actuation technologies, as well as the advantages and disadvantages of its use in ambulatory orthotic devices will be addressed.

Electric motors are one of the most implemented actuators technologies in powered orthotic devices [8], [84], [91]. The main reasons this type of actuators are preferable in comparison to the others is its higher specific power (ratio between the continuous power and the mass of the actuator), easy control and portability [8], [91]. The latter has been made possible thanks to the development of batteries technologies that allow for a viable untethered orthosis energy source [91]. Moreover, studies suggest that electric motor actuation is able to significantly decrease power consumption when compared to hydraulic actuation [7], [93].

This type of motor is characterized by being low-torque and high-speed output actuators. Having in mind that human motion is powered by relatively high torque acting at low velocities, orthotic systems powered by electric motors require transmission elements (for example gearboxes) to convert the high-speed and low-torque output to the low-speed and high-torques needed in the joint [8], [30], [84], [91]. These transmission elements may constitute a drawback to the actuation system, due to the backlash, noise and friction that causes and because it negatively affects the motor efficiency, backdrivability and size [84], [91]. In addition to this disadvantage, it has been pointed out that the weight of the electric motors is about twice than that of the hydraulic actuation. Besides, the weight of the electrical actuation needs to be centred at the assisted joint [8], [94]. According to the literature, the oxygen consumption rate of a person (performance method for assessment of the effectiveness of an orthotic device) would increase by 30% if a load of two kilograms was placed on each foot [7], [10], [91]. Thus, it's essential to ensure the compactness of the actuator [10], [91]. Figure 3-8 (a) and (b) presents a commercially available electric exoskeleton, certified for rehabilitation use, and an AFO actuated by DC motors, although it was developed for reducing the metabolic cost of walking.

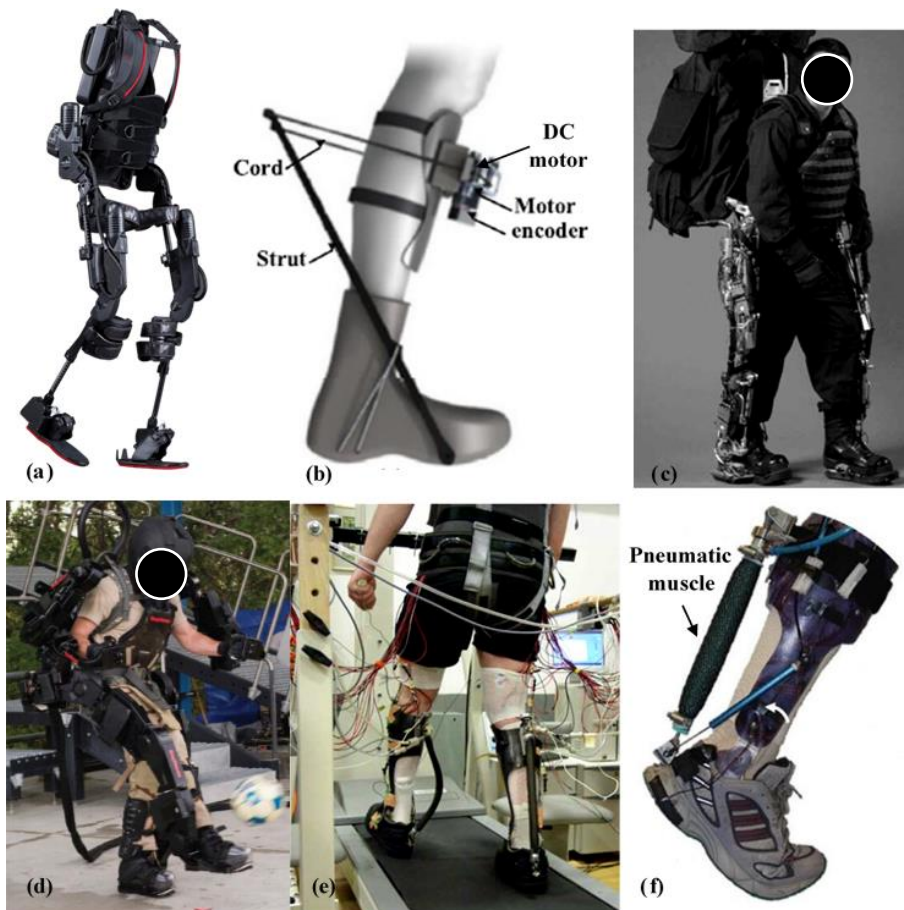


Figure 3-8 - Exoskeletons and ankle-foot orthoses powered by the different types of actuation technologies: (a) Ekso Exoskeleton (Ekso Bionics, USA), actuated by electric motors, (b) An autonomous AFO, powered by a DC motor, developed by Mooney et al. to reduce the metabolic cost of human loaded walking, (c) BLEEX exoskeleton (USA), powered by hydraulic actuator, (d) Sarcos tethered exoskeleton (also denominated XOS 2), actuated by hydraulic actuators, (e) Lower limb orthosis designed by Takahashi et al. that uses artificial pneumatic muscles, and (e) AFO developed by Galle et al. to reduce the metabolic cost of walking, also actuated by PMA [8]–[10].

Regarding **hydraulic actuators**, this type of actuation converts pressurized liquid into mechanical torque, and are powered by pumps or valves [84], [91], [95]. The selection reasons for the use of hydraulic transmission in orthotic devices are its high specific power, fast response to a change in input, silent and precise actuation, impervious to dusty and wet environments, it doesn't have exposed moving components and can have infinitely variable backdrivability [91], [95]. On the other hand, hydraulic motors do present the disadvantage of its dependence on non-portable pressure supplies, which are too heavy and large [91]. As a result, this type of actuation has been limited to tethered orthotic devices with no or low portability, which make its implementation not suitable for lightweight exoskeletons and active orthoses developed for rehabilitation [84], [91]. Herewith, the hydraulic actuated exoskeletons commercially available (Figure 3-8 (c) and (d)) are, mainly, designed for augmentation of the human performance [8], [9]. Furthermore, the inefficiency is another

fundamental limitation of hydraulic actuators, due to the high power losses in pressure drops across hydraulic valves [91].

Pneumatic actuation can be divided into two types: pneumatic cylinders and pneumatic muscle actuators (PMA), also known as artificial pneumatic muscle [8], [30], [91]. In both cases, pneumatic actuators incorporate a variable pressure and volume chamber to convert a pressurized gas into mechanical torque, being powered by air compressors, via solenoid valves [84], [91]. However, artificial pneumatic muscles have some specific characteristics and benefits over a pneumatic cylinder, such as higher specific force (force/weight ratio), lightweight, inherently variable compliance (similar to the human joint) and limited maximum contraction, which ensures the actuation's safety, the softness and the intrinsic elasticity of biological muscle. These characteristics allow for PMA to be used in rehabilitation applications [8], [91], [94]. In addition, along with pneumatic cylinders, PMAs also present a high specific power, provide for a quiet operation and for an inherent compliant actuation, which is an important feature regarding actuation in orthotic devices, as it can absorb position errors and allow impact resistance in gait events, such as heel strike [8], [84], [91], [94].

Nevertheless, similar to the hydraulic actuation, the high inefficiency of the pneumatic actuators is due to the power losses in pressure drops in pneumatic valves, and this type of actuation is not portable. Additionally, the efficiency of pneumatics is worsened by the use of compressible air, which is inherently compliant, making it difficult to efficiently compress it [8], [91]. In the case of PMA, the non-linear and time-varying features impose a control problem, and as a result, its control bandwidth is relatively low, compared to the hydraulic actuation [8], [94]. After an extensive literature review, no pneumatically actuated exoskeletons were found. On the other hand, there were a few ankle-foot orthoses that incorporated PMA, developed both for gait rehabilitation (Figure 3-8 (e)) and for reduce of walking metabolic cost (Figure 3-8 (f)).

3.3.2 SAFETY MECHANISMS

Safety is an essential issue that should be considered during the design of an active AFO for rehabilitation purposes [10], [91], [96]. This requirement dictates that the actuator system

must have a limited range of motion, in order to ensure that angular displacements are not applied on the user's joint, and thereby, don't inflict harm to the patient [10], [91].

Passive metal AFOs present the simplest design of **mechanical stops** to restrict ankle motion to a predetermined range [3], [96]. These mechanical ankle joints can implement a projection on the posterior section within the joint, which limits plantarflexion (Figure 3-9 (a)), or on the anterior section, limiting dorsiflexion motion (Figure 3-9 (b)) [96]. Moreover, the Tamarack flexure joints are considered the most widely used thermoformable orthotic joint for custom articulated AFOs. These joints are implemented in association with the Tamarack plantarflexion limiter, which is an adjustable motion control option, designed to be easily integrated into thermoplastic AFOs (Figure 3-9 (c)) [3], [97], [98].

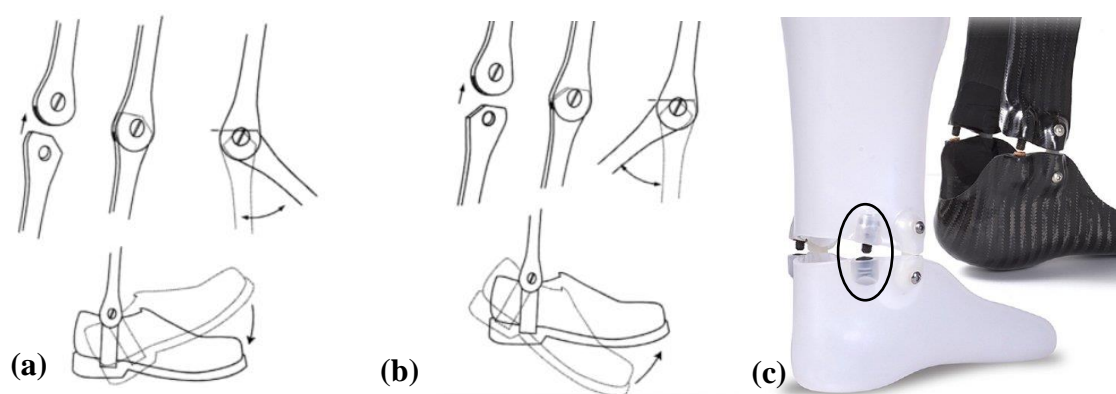


Figure 3-9 - Ankle joint mechanical stops: (a) Plantarflexion stop, (b) dorsiflexion stop, and (c) Tamarack flexure joint aligning the medial and lateral axes and a plantarflexion limiter kit, which limits the plantarflexion movement due to the collision of the circled system [96], [97].

Similarly, for **active AFOs**, the safety is often warranted by the implementation of mechanical limit stops on the extremities of the allowed ROM of the ankle joint [10], [34], [91]. In addition, control algorithms are also developed towards ensuring the safety of the actuation system, alongside with hardware design [10].

The use of **limit switch** as a safety feature is reported in the literature, most specifically, in the field of upper limb orthotic devices [99], [100]. A limit switch is an electromechanical device that operates by a physical force applied to it by an object, being used to define the limit of travel of such object, before being stopped (Figure 3-10 (a)) [101], [102]. When the object enters in physical contact with the actuator's piston, its movement results in the electrical contacts within the switch to either close or open their electrical connection, depending on whether it's a normally open circuit (Figure 3-10 (b)) or a normally closed circuit (Figure 3-10 (c)), respectively [102]. The advantages of limit switches comprise the high

accuracy and repeatability, the suitable use in almost any industrial setting, and low power consumption. On the other hand, this type of device relies on mechanical action and, therefore, they are used in equipment that operates at relatively low speeds. Moreover, its mechanical design premises the mechanical wear and fatigue at which is subjected, indicating that an eventual replacement might be needed [101], [102].

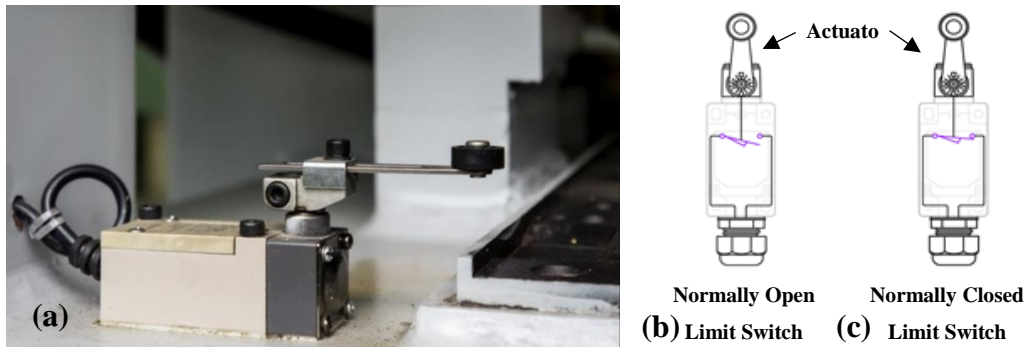


Figure 3-10 - Safety mechanism based on limit switch: (a) Limit switch, (b) schematic representation of a normally open limit switch (the physical contact with the actuator's piston results in the closure of the circuit), and (c) schematic representation of a normally closed limit switch, which works in opposite to the former (adapted from [101], [102]).

3.3.3 ELECTRONIC CONTROL SYSTEMS

Alongside with the studies conducted to improve the performance of lower limb exoskeletons and active orthoses for rehabilitation training, researchers also focused on ameliorating the control strategies, in order to increase the overall comfort and efficiency of the orthotic device [8], [9], [84]. Herewith, **human-exoskeleton motion data acquisition and analysis**, and **motion control algorithms** are critical factors for ensuring that the device provides an intelligent, effective and comfortable assistance and rehabilitation to the wearer [8], [9].

The **control strategies based on the human-exoskeleton interaction** that allow for the prediction of the user motion intention have been shown to be essential for movement rehabilitation purposes [8], [9]. Moreover, measured motion data can also be used to analyse the motion status and gait pattern, and evaluate the motion performance of the wearer [9]. Three types of biomechanical data are generally associated with human motion: kinematic, kinetic, and bioelectric data. The latter one can be applied to detect and assess muscle and brain activity during walking [9], [84]. To measure each of these parameters, different types of wearable sensors are usually incorporated into the exoskeleton or active orthosis system [8], [9], [84].

Kinematic data, such as body posture and joint angles, can be acquired through sensors such as accelerometers, gyroscopes, magnetometers, an inertia measurement unit (IMU, which is a combination of the first three sensors), goniometers, encoders, and potentiometers [9], [84]. Accelerometers, gyroscopes, magnetometers and IMUs directly acquire kinematic measures, such as the linear acceleration of a moving body, which can be integrated to compute its velocity and position, angular motion, posture, and orientation of the human segment. The first three sensors all combined form the IMU (Figure 3-11 (a)) that, with its system consisting of 9 DOF (3 degrees for each sensor), also provides for the position and orientation data of the body segments (Figure 3-11 (b)) [9], [84]. On the other hand, goniometers and potentiometers' principle of work is based on the resistance proportional change with the angle of the joint (Figure 3-11 (c), (e) and (f)). Similar to these sensors, encoders are used to determine kinematic information indirectly, but this wearable sensor provides data about the angular position, speed and acceleration (Figure 3-11 (d)) [84].

Kinetic data includes the information about the human joint torque, ground reaction forces, and interaction force between the user and the exoskeleton [9], [84]. These measures can be acquired through sensors such as force (force sensor resistor, FSR) pressure sensors, that can be embedded in insoles and shoes (see Figure 3-11 (g) and (h)), and torque sensors [8], [9], [84], [103].



Figure 3-11 - Kinematic and kinetic sensors used in lower limb exoskeletons and AFOs: (a) IMU board integrated with its components, (b) IMU motion tracking system developed by XSens, (c) Potentiometer, (d) Encoder integrated in a DC motor, (e) Strain gauge goniometer with flexible connecting beam, by Pluxx, (f) Flexible

goniometer mounted on a subject's knee, (g) Force sensor resistive (FSR), and (h) FSR embedded in an insole (Solemate) (adapted from [84], [103]–[107]).

Bioelectric data, such as electromyographic (EMG) signals and brain signals (electroencephalogram, EEG) can be acquired non-invasively, with surface electrodes, or in an invasive way through indwelling/intramuscular electrodes (for EMG) and invasive brain-machine interface (for EEG) [9], [84]. The selection between both types of EMG sensors (Figure 3-12 (a) and (b)) depends on the properties of the target muscle and application. Therefore, indwelling/intramuscular electrodes can reach all existing muscles and collect fewer surrounding muscles, but this process is expensive, difficult, and painful. In the case of the surface electrodes, although these cannot monitor deeper muscles, they are simple, cheap and pain-free [84]. EMG and EEG signals have been extensively studied to analyse human disabilities and rehabilitation's progress, as well as to predict human motion intentions or to even control wearable robots through EEG-based interface (Figure 3-12 (c)) [8], [9]. However, these two technologies present some limitations, such as the time-consuming calibration of the bioelectric sensors, interferences, generated by either neighbouring sensor nodes or by different cortical areas, and noise [8], [9].

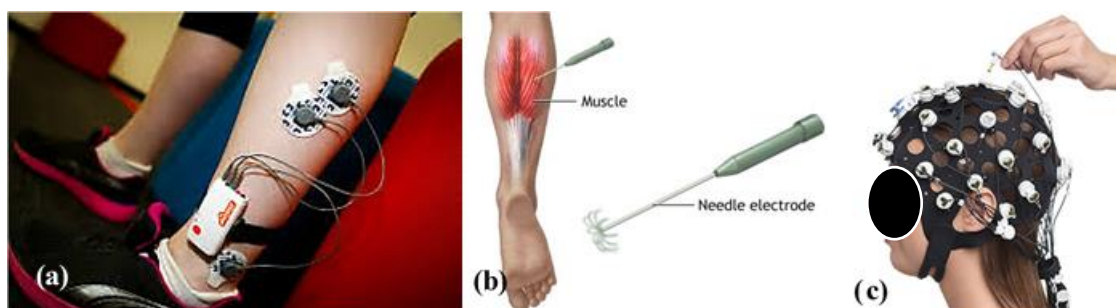


Figure 3-12 - Bioelectric sensors: (a) EMG surface electrodes, (b) EMG indwelling/intramuscular electrodes, and (c) EEG surface electrodes [84], [108], [109].

As aforementioned, in order to ensure that the rehabilitation process is comfortable and effective for the user, powered wearable orthotic devices need to optimize the interaction human-machine. Herewith, these devices can integrate a hierarchical-based control system with three levels: the high-level, mid-level and low-level control [8], [84]. As a brief description, the high-level (perception layer) controller recognizes the user's motion intentions and passes the information to the mid-level controller, which translates this data to the low-level controller. This last one represents the execution layer, as it assists the user, by sending the commands to the actuators [84]. Inside this hierarchical control framework,

motion control strategies can be organized to supply the user with the right rehabilitation procedure [9], [84].

The **motion control strategies** of exoskeletons and active AFOs in gait rehabilitation can be generally divided into two categories: trajectory tracking and assist as needed (AAN). The first approach uses predefined trajectories for the device's joints, which are usually collected from healthy individuals, as control targets for the impaired user. This algorithm presents some flaws, since the wearer is passively trained to follow a predefined trajectory and, therefore, may decrease his/her motor learning and participation in the training. To overcome these difficulties, the AAN strategy only supplies assistance when the wearer needs to accomplish the training tasks. This way, the assistance is intelligently adjusted to the patients' physical condition and efforts in the rehabilitation session, with the objective of incentivising their voluntary participation [9].

3.3.4 ACTIVE LOWER LIMB ORTHOTIC DEVICES

Throughout the years, with special focus on the last two decades, the advances in the field of development of exoskeletons and active AFOs for rehabilitation have been enormous [7]–[9], [89], [90]. This is due to the progress in computer and actuation technology, that allowed for improved human-exoskeleton systems and the device's portability and compactness [7]–[9], [89], [91].

Nonetheless, universities, research institutes and industrial companies have been putting their efforts into the development of lightweight, efficient and overall user-friendly lower limb exoskeletons and active AFOs. Herewith, several orthotic systems for gait rehabilitation purposes have been developed, tested, and some of them even certified by the FDA (Food and Drug Administration) or the CE (acronym from the french *Conformité Européenne*, meaning European Conformity) [7]–[10], [84], [88]–[90], [92].

This section will address lower limb exoskeletons and powered ankle-foot orthosis for **rehabilitation**, which are commercially available, still in an approval phase or in a development stage.

After a literature and market survey, the most ground-breaking and technologically advanced lower limb exoskeletons were selected (see appendix **B- Commercially available powered lower limb exoskeletons**). The same will disclose topics such as the company

responsible for the device, target subjects, device's weight, user's maximum weight, actuation system features (regarding the type of actuation, maximum torque and speed, and actuated joints), control system, sensor technologies implemented, and at last the commercial state (commercially available or research state) and its market price.

HAL-5 (Hybrid Assistive Limb) was developed by the Tsukuba University (Japan), in collaboration with the company Cyberdyne, and is the most widely distributed mobile medical rehabilitation exoskeleton [110], [111]. This exoskeleton comes in two versions: HAL Medical (intended for rehabilitation purposes) and HAL Living Support (aimed at personal assistance) [110]. HAL ML05 Series for Medical Use (Figure 3-13 (a)) is intended for individuals who exhibit sufficient residual motor and movement-related functions of the hip and knee to trigger and control the exoskeleton (through EMG sensors) [112]. Furthermore, it's worth mentioning that HAL for Medical Use is the only robotic medical device that is able to teach the brain how to move the legs [111].

ReWalk was developed by ReWalk Robotics (Israel), and it was the first active exoskeleton to be approved by the FDA and by the Australian Therapeutic Goods Administration (TGA), in 2014. This exoskeleton was certified for both rehabilitation (ReWalk Rehabilitation, Figure 3-13 (b)) and for assistance use (ReWalk Personal 6.0) [113], [114]. One year later, Ekso Bionics (USA) developed **Ekso GT**, which was the first exoskeleton to be approved by the FDA for recovery of patients with stroke (Figure 3-13 (c)) [115], [116]. The same year, **Indego Therapy** exoskeleton (Figure 3-13 (d)) was designed by the Parker Hannifin Corporation (USA) for clinical use in a rehabilitation setting, although a community and home setting version was also constructed, the Indego Personal [113], [117], [118]. Currently, both versions of Indego have a CE Mark and FDA approval, allowing it to be sold commercially in Europe and the U.S [118], [119].

Keeogo (Figure 3-13 (e)) is a powered knee only exoskeleton, designed by B-TEMIA (Canada) for medical applications such as rehabilitative training at a Keeogo certified clinic, and day to day life use [120]. In addition, it's important to clarify that the device is built for individuals who have a lack of endurance while walking and reduced muscle strength, due to conditions such as stroke [113], [120], [121].

In 2016, **HANK** exoskeleton was developed by GOGO Mobility Robots (Spain), and is the premiere lower body rehabilitation exoskeleton designed and manufactured in the European Union. It is also the first European company to have received a CE marking which

enabled the certified clinical use. Nonetheless, this powered exoskeleton comes in both a rehabilitation and personal use version (Figure 3-13 (f)) [122]–[125]. In the same year, Rex Bionics (New Zealand) designed **REX**, which is the first commercial powered exoskeleton that enables the movement in individuals with complete spinal cord paralysis, existing two versions: REX for Clinical Use and REX P for Personal Use [113], [126], [127]. Each leg of REX for Clinical Use has five degrees of freedom: two for each ankle and the hip, and one for the knee, which makes it the only rehabilitation exoskeleton found with two DOF at the ankle joint (Figure 3-13 (g)) [90].

Finally, **Exo-H2** (Technaid, Spain) is a lower limb robotic designed to aid the restoration of the walking ability in subjects that have lost the capacity to do so (Figure 3-13 (h)) [83], [128]. At the time of this dissertation, Exo-H2 is approved by the AEMPS (Spanish Agency of Medicines and Health Products) for investigation purposes.

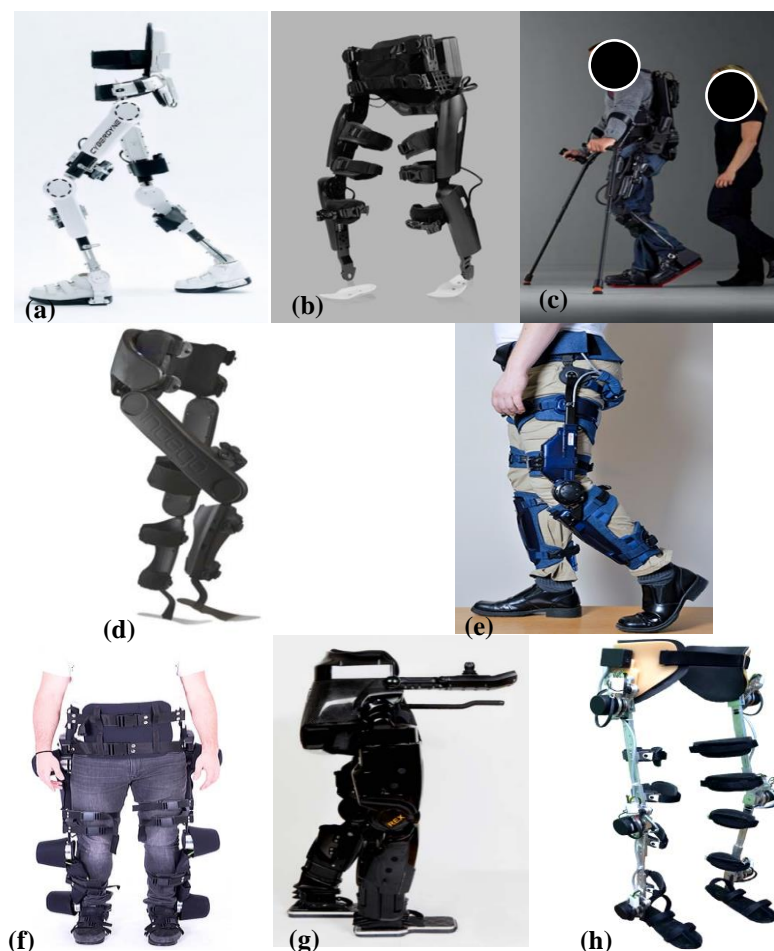


Figure 3-13 - Commercially available lower limb exoskeletons: (a) HAL for Medical Use, Series ML05 (Cyberdyne); (b) ReWalk Rehabilitation (ReWalk Robotics); (c) Ekso GT (Ekso Bionics); (d) Indego Therapy (Parker Hannifin Corporation); (e) Keeogo (B-TEMIA); (f) HANK (GOGOA Mobility Robots); (g) REX for Clinical Use (Rex Bionics); (h) Exo-H2 (Technaid) [83], [111], [113], [124].

In addition to the lower limb exoskeletons, a review of the AFOs developed to aid individuals with paretic ankle and help them during the rehabilitation process was conducted. In the appendix C-Active ankle-foot orthoses for rehabilitation still in a development stage of this thesis is presented a table with the technical characteristics of each AFO collected in the literature, such as its actuation system, maximum applied torque, the sensory system implemented, and if it's a tethered or untethered technology [7], [10], [129]–[131].

All of the AFOs presented in the aforementioned table are still being submitted to clinical tests to validate its effectiveness and, thus, no commercially available AFO was reported in the literature. As a summary of the collected orthoses, **Ferris et al.** and **Takahashi et al.** were the only ones to incorporate PMAs in their AFO's actuation system, whereas the remainders opted for the actuation based on DC motors associated with mechanical and electrical components, such as SEA (AFO by **Blaya et al.**), servomotor (AnkleRobot by **Yeung et al.**), and robotic tendon actuator, in the case of the AFO by **Boehler et al.** and **Ward et al.** [7], [10], [30], [129]–[133]. The presented AFOs are illustrated in Figure 3-14 (a) to (f).

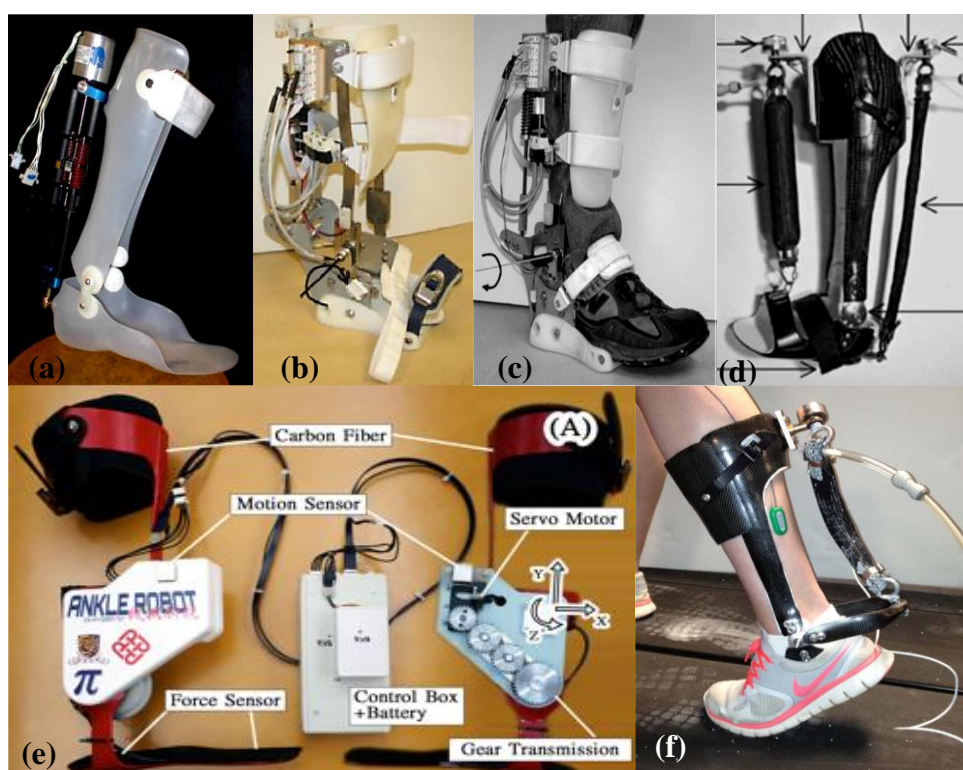


Figure 3-14 - Active AFOs: (a) MIT active AFO actuated by a series elastic actuator (SEA) and developed by Blaya et al. [130]; (b) Arizona State AFO powered by a robotic tendon actuator (Boehler et al.) [134]; (c) Powered AFO developed by Ward et al., actuated by a robotic tendon [133]; (d) Michigan ankle orthosis (designed by Ferris et al.) powered by artificial pneumatic muscles [135]; (e) AnkleRobot, developed by Yeung et al., actuated by a servomotor [129]; (f) The neuromechanics-based AFO developed by Takahashi et al. [132].

3.4 ORTHOSES ARTICULATION COMPLIANCE

This section focuses on the features implemented on the ankle joint of AFOs to ensure an articulation compliance. This is a crucial factor on the design process of an AFO for rehabilitation since it minimizes phenomena such as the misalignment between the device and the patient. After an extensive literature research, self-alignment mechanisms and multiple degrees of freedom AFOs are presented.

3.4.1 SELF-ALIGNMENT MECHANISMS

One of the critical problems conventional exoskeletons face is the misalignment occurring between the orthosis and the human joint [136]–[141]. Misalignment of the joints axes causes detrimental parasitic forces on the patient at the attachment points and at the joints, which can reach up to 250 N and torques up to 1.46 Nm [140], [141]. These forces can cause discomfort, pain or even long term injury due to repetitive use, which jeopardizes the usability of the orthotic device [136], [137], [140], [141]. Furthermore and most crucially, axis misalignments promotes compensatory movements that can inhibit rehabilitation of the user [140]. Hereupon, in order for exoskeletons and orthotic devices to function correctly, is imperative that the design ensures correspondence of the device axes with the anatomical axes of the human joint [137], [140], [142].

Misalignments occur since (i) human joints have complex kinematics and cannot be modelled as simple revolute joints; (ii) the exact location of human joints cannot be determined from the outside without imaging devices and (iii) placement of the human limb in the orthotic device changes from a therapy session to another. Therefore, the device always requires adjustments [137], [140].

Over the years, many orthoses that can perform complex joint movement of the lower limbs have been proposed [136], [139]–[141]. However, mechanisms with the ability to self-align have been more focused on the knee joint than on the ankle joint. Nevertheless, in this section are briefly presented two self-aligning mechanisms for the knee joint and one for the ankle joint, which have been developed for orthotic devices.

Ergin et al. presented a device for robot-assisted rehabilitation that accommodates transitional movements of the knee joint on the sagittal plane and its rotation. The authors

claim that the results indicate the mechanism is adjustable and it's a good candidate to assist performing knee rehabilitation exercises, although the prototype dimensions are not optimized to minimize the footprint of the robot [139].

Choi et al. introduced a novel compact self-aligning knee mechanism for walking assistance devices in order to provide help for the flexion/extension of the knee joint [136]. This system has been integrated in an innovative wearable robot, the Samsung-Assist device Lower-limb type (S-Assist L-type). This device compensates the centre of rotation by adding two redundant DOF to the one DOF revolute joint, having the advantage that the mechanism can perform the motion of the joint without individual deviation relative to the body, which satisfies the wearers that feel minimum resistance during motion [136], [143].

Erdogan et al. presented a reconfigurable, powered exoskeleton for ankle rehabilitation, the AssistOn-Ankle. This device features reconfigurable parallel mechanism for delivery of both range of motion/strengthening and balance/proprioception exercises. The former mechanism is a self-aligning mechanism, useful to cover the whole ROM of the human ankle in an ergonomic manner and for strengthening exercises. On the other hand, the mechanism responsible for balance/proprioception exercises supports the human weight and adjusts the torques transferred to the ankle joint [144].

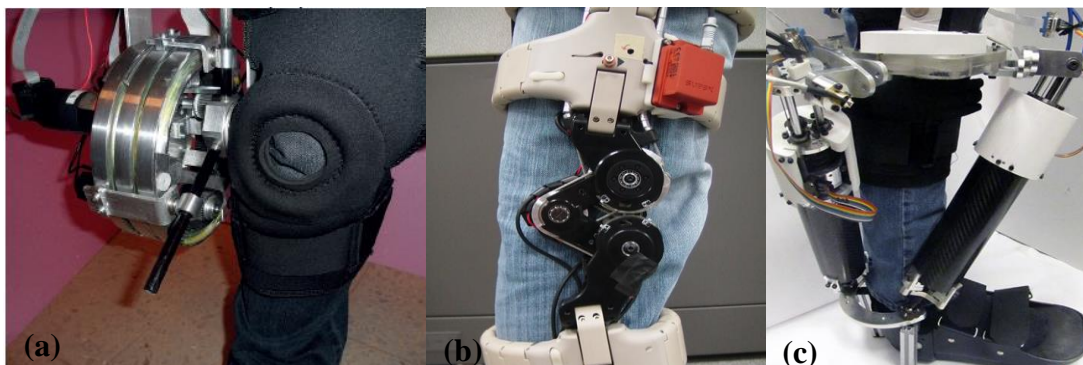


Figure 3-15 – Self-alignment mechanism incorporated in lower limb orthotic devices: (a) Prototype of the mechanism incorporated in the knee joint, developed by Ergin et al. (2011); (b) Mechanism for the S-Assist knee joint, designed by Choi et al. (2016), and (c) Prototype of AssistOn-Ankle device, developed by Erdogan et al. (2016) [136], [139], [144].

3.4.2 MULTIPLE DEGREES OF FREEDOM AFOS

In Section 2.1, the complex biomechanics of the ankle joint was acknowledged by addressing its motion around the three anatomical planes, and the deviation of the axes of rotation. However, as mentioned in the previous section, the ankle joint of rehabilitative orthotic

devices is often designed as a simple revolute joint, considering solely the tibiotalar joint, and restricting the motion provided by the subtalar joint [137], [140], [145]–[148].

The inversion/eversion motion in current developed AFOs is often accommodated only through the flexibility of the material. In addition, regarding the exoskeletons reviewed in this dissertation, only one did implement a two degree of freedom ankle joint (REX exoskeleton, see appendix **B-Commercially available powered lower limb exoskeletons for rehabilitation**). This limitation in normal ankle motion of the subtalar joint does not ensure a natural motion to the ankle, and even adds to the discomfort of wearing the device [146]–[148]. Moreover, the rehabilitation process might be jeopardized once the user does not strengthen the motion around the frontal plane [146], [147].

Over the last two decades, there has been an eagerness to study and develop AFOs that would enhance anatomical conformity, by ensuring an anthropomorphic design with biomimetic features. After an extensive literature review, several studies that proposed multiple DOF AFOs were found [145]–[150]. The present dissertation will disclose three published studies that proposed the development and validation of two DOF AFOs, and one study presented the design of a three DOF AFO for rehabilitation training [145], [147]–[150].

Agrawal et al. proposed an AFO with two degrees of freedom, corresponding to the motions of dorsiflexion/plantarflexion and inversion/eversion. The motion in the sagittal plane is actively controlled by a servomotor, and the frontal plane motion is passive with a torsion spring and a damper. The orientation of each joint axis is fixed according to the anthropometric data of the human ankle. This orthosis is set to assist subjects with ankle dorsiflexors' weakness and the authors claim that the prototype AFO with the subtalar joint (P/S Axis represented in Figure 3-16 (a)) would introduce a greater functionality over current marketed devices [148], [149].

Zhang et al. designed a quasi-passive three DOF AFO, which is proposed to be used in medical institutions for rehabilitation training to improve ankle lesions. The device's main ankle motion mode is the dorsi- and plantarflexion movement (DF and PF, respectively), accompanied by minimal motions of the other two DOF (internal/external rotation and inversion/eversion, see Figure 3-16 (b)). The transmission method involves the combination of a DC motor, an electromagnetic clutch, ball screw, a spring and steel wire, which is pulled to propel the wearer along with the release of spring energy. The authors claim that the

orthosis can warrant low energy consumption and ankle dynamic characteristics similar to those of a natural gait [150].

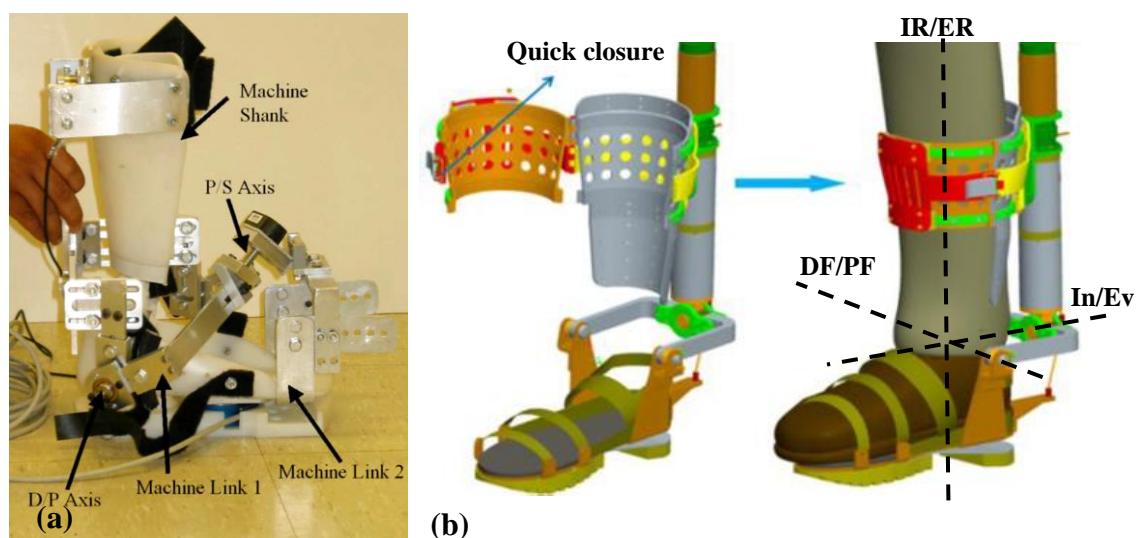


Figure 3-16 – Multiple degree of freedom ankle-foot orthoses developed over the years: (a) Two DoF AFO for robotic rehabilitation, designed by Agrawal et al. (2005); (b) Quasi-passive three DoF AFO developed by Zhang et al. (2015), where IR and ER mean Internal and External Rotation, respectively (adapted from [149], [150]).

Ranaweera et al. proposed in their study a two-degrees of freedom AFO with an anthropomorphic design to minimize mechanical interferences between the user ankle and the orthosis. The authors incorporated biomimetic features, such as a pair of helical spring, introduced on both sides of the joint to imitate the ligaments of the human ankle joint complex (Figure 3-17 (a)). These springs help maintain the foot unit at a neutral position by restricting the motion range for Inversion/eversion through the maximum spring compression (Figure 3-17 (b)). The range of motion is set by the definition of the link lengths and spring heights. Moreover, the ankle unit supports PF and DF about a hinged joint, where the axis of rotation is aligned accurately to the tibiotalar (or talocrural) axis of human ankle, and, throughout the movement, the same unit is able to adjust its centre of rotation. The evaluation of the AFO system revealed its effectiveness in meeting the complex kinematics of the human ankle joint [145].

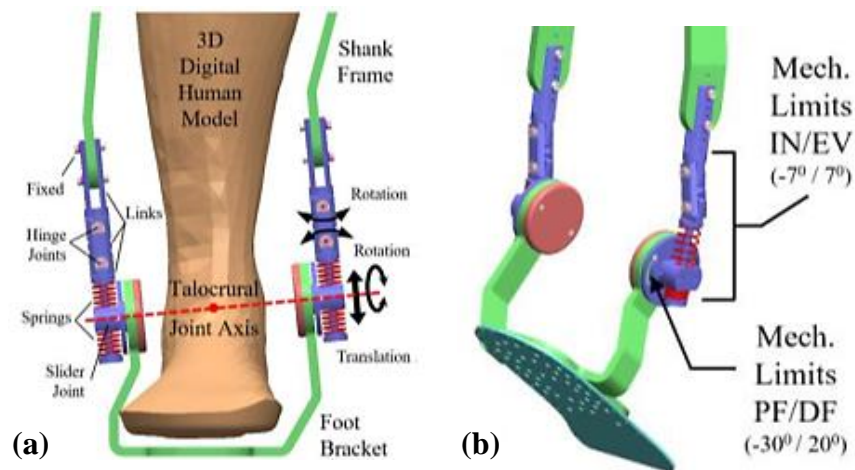


Figure 3-17 – CAD model of the two-degrees of freedom AFO developed by Ranaweera et al. (2019): (a) Anterior view of the ankle unit's mechanism; and (b) Range of motion of the ankle unit for plantarflexion and dorsiflexion and inversion and eversion (orthosis in supination mode, meaning PF + In + IR) [145].

Finally, **Choi et al.** developed a two DOF powered AFO that incorporated the tibiotalar and subtalar joints. The orthosis is actuated by two pneumatic artificial muscle, a longer and a shorter one, being the former responsible for the help of plantarflexion and inversion movement, and the latter aids the plantarflexion and eversion motion, imitating the fibularis longus muscle (see Figure 3-18 (a) and (b)). The authors of the paper state that the addition of a subtalar joint not only minimizes the dislocation of the human ankle relative to the AFO (misalignment) but also has a great advantage in rehabilitation that emphasizes balanced walking, claiming that is a crucial help for stroke patients [147].

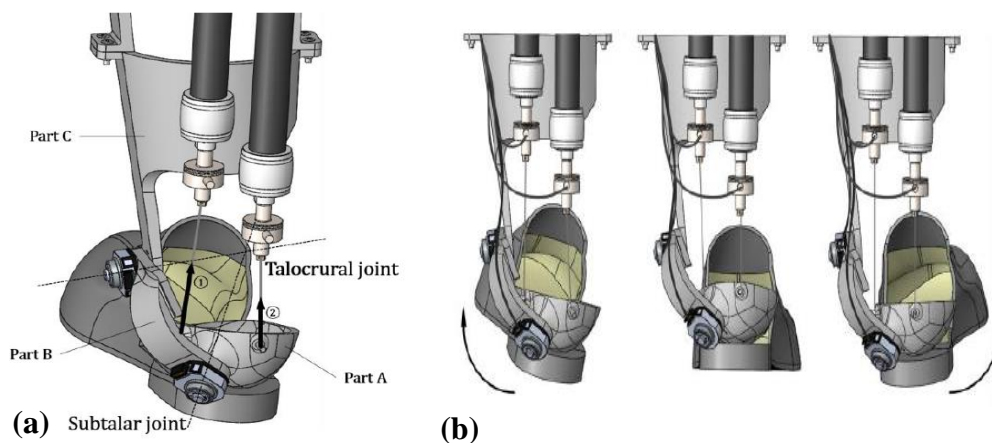


Figure 3-18 - Pneumatic actuated AFO with two degrees of freedom, developed by Choi et al. (2019): (a) Model of the proposed AFO, being the bolded arrows the force direction applied by the PAMs. Part A is the structure surrounding the calcaneus and foot, part C surrounds the calf and thigh, and part B is the part that connects to part A and C to form the subtalar joint and the tibiotalar (or talocrural) joint, respectively [147].

3.5 USER-ORTHOSIS ATTACHMENT SYSTEM

In the previous sections, it was discussed the crucial domains of the development of a wearable active lower limb orthotic device, such as the actuation system and the human-device interface. However, a third aspect of an active AFO development is also tremendously important: the design of its structure. The design of the wearable orthosis can comprise the 3D drawing of its **geometrical shape**, the **selection of the material** that will compose it, as well as the **production method** chosen to manufacture the system [151], [152]. Herewith, the present section will explore different designs of the structure that couples the orthotic device to the user's leg. Furthermore, it will be disclosed the various materials selected to constitute the device, as well as the production method that can be chosen to manufacture the prototype.

3.5.1 DESIGN OF THE GEOMETRICAL SHAPE

When providing a patient with an orthosis oriented for the lower limb, both the design team and the orthotist must have a fundamental understanding of the biomechanical principles inherent to the development of an orthotic device. There are three **biomechanical principles** essential to the design of an orthosis, reported in the literature: the **three-point force systems**, **total contact**, and **kinaesthetic reminders**. These key points are often used in combination to achieve the clinical objectives of a lower extremity orthotic device, such as the management and compensation of deformities and abnormal neuromuscular function. These objectives are always required in the association with the protection of the tissues and healing promotion [153].

A **three-point force system** is used to change the alignment of a joint through the application of two forces working in opposition to a counterforce. The main goal of this system is to help manage the deformities of the joint, by limiting the motion around the joint axes [151], [153]. Furthermore, **total contact** of the device should be taken into account in order to distribute the forces more evenly over the user's lower leg. This biomechanical principle is crucial to warrant that pressures are kept in reasonable magnitudes and thus ensuring that tolerable and safe tensions are experienced by the patient's soft tissues [153]. At last, another important issue concerning the design of an orthosis is the **kinaesthetic reminder**, which will be addressed in Section 3.5.2 [153]–[155].

The geometrical shape of the shank structure or the overall AFO (in case of a passive plastic ankle orthosis) can be drawn by using CAD (Computer Aided Design) software, such as SolidWorks. Various designs of AFO's structure have been reported in the literature, regarding devices that are still in a research phase and commercially available orthoses. However, two types of AFOs designs stand out from the literature survey: the **anterior** and **posterior** AFOs (A-AFO and P-AFO, respectively) [156]–[159]. These types concern mostly passive plastic AFOs, being the posterior leaf spring (Figure 3-4, Section 3.2) the most commonly used and prescribed to individuals with gait disorders, such as hemiplegia [156], [157]. The difference of walking performance regarding the use of an A-AFO or a P-AFO by individuals with drop foot has been studied [156]–[158].

Park et al. reported that A-AFOs were less effective in maintaining ankle dorsiflexion in the sagittal plane during the swing phase when compared to P-AFOs [158]. Furthermore, another study of the kinematic features of rear-foot motion (shank-calcaneus rotation angle) during hemiplegic gait using A-AFOs and P-AFOs claimed that the latter is better than the A-AFOs in enhancing rear-foot dorsiflexion during a gait cycle. However, anterior AFOs did reduce rear-foot inversion in both stance and swing phase, while posterior AFO only decreased it in the swing phase [156].

On the other hand, more recently, a study has been conducted to compare walking energy cost between the use of the two types of AFOs in people with drop foot. This assessment reported that anterior AFOs resulted in lower energy costs of walking, meaning that A-AFOs may enable people with drop foot to walk further with less physical effort relatively to walking with P-AFOs. Additionally, the study showed that walking speed and step length were significantly higher while using A-AFOs compared to using P-AFOs [157]. Lastly, alongside the study conducted by Park et al., it was concluded that the level of perceived comfort was significantly higher when walking with an A-AFO compared with a P-AFO [157], [158]. The comfort is a crucial aspect to enhance people's willingness to use a certain AFO, being more important than the effect of the device on gait and balance [157]. In conclusion, studies show that A-AFOs are more comfortable and, therefore, more likely to improve compliance and walking ability than P-AFOs [157], [158]. The following section presents some examples of both types of AFO designs.

3.5.2 MATERIALS

Another highly important AFO's design parameter is the material selected to compose the **device's structure** [151], [152]. Mechanical properties such as durability, fatigue strength, corrosion and fatigue resistance and weight depend on the material type selected. Hence, an ideal AFO design should implement lightweight materials to ensure that the final product is easy to use, durable, cosmetic, resistant against environmental effects, and to warrant a reasonable cost and an adequate production time [129], [151]. Metal, plastics, synthetic fabrics and composites are the most common materials used for AFO manufacture [96], [151], [152]. In addition, the choice of the material is a determining factor for the manufacturing cost of the AFO [151].

Before the advent of plastics, ankle-foot orthoses were composed by **steel or aluminium with leather** accessories. These AFOs included a steel shoe attachment (also denominated stirrup), ankle joints with a single axis, uprights, and a calf band, also made of a metal or plastic, with a closure leather strap (Figure 3-19 (a)) [96], [152]. The high mass density of metals is counterpointed with its advantageous mechanical properties such as the durability (fatigue resistance), corrosion resistance, and high tensile strength [34], [96], [151], [152].

Plastic AFOs are preferred when compared to metal orthosis, because they are lighter, easy to maintain, more appealing to the user, and they can be more easily casted, moulded or extruded [96], [151], [152]. Plastics include thermoplastics and thermosetting plastics, which are differentiated based on each one's reaction to the application of heat [152], [160]. The most commonly used thermoplastics in orthopaedic appliances are polyethylene (PE), more specifically high-density PE (HDPE), PE foam plus ethylene-vinyl acetate (EVA), polyamide (PA), acrylonitrile butadiene styrene (ABS) and polypropylene (PP) (Figure 3-19 (b)) [152]. On the other hand, epoxy resin, unsaturated polyester resin and acrylic resins are examples of thermoset plastic that may be used in the orthotic field, as they warrant excellent strength and temperature-resistance [151], [152], [160]. The main disadvantages of using plastic in orthopaedic applications are its low tensile strength and ductility (which results in parts that require designs with higher thickness) [160].

Cushioning of the AFO structure (such as the shank structure) is another important aspect of the design process, as it contributes deeply to the comfort of the final product [152],

[153]. Both thermoplastic and thermosetting materials can be used to produce an expanding foam structure, which can be applied to the interface to protect the wearer's skin from the device. Materials such as PE with EVA, and elastomers, e.g. neoprene rubber, soft polyurethane (PUR) foam and silicone are used nowadays as padding of AFOs to provide comfort, as well as shock attenuation (Figure 3-19 (c)) [152]. As aforementioned, **kinaesthetic reminder** is one of the biomechanical principles that deals with the sensation of wearing the device. This concept refers to the sensation of being in physical contact with the orthosis which might also contribute to the achievement of an intended function [153]–[155].

Synthetic fabrics can be classified as being polymeric-base or mineral-base. The former include polyester and polyamide fibres (commonly known as nylon) and the mineral-base fibres comprise fiberglass and carbon fibre [152]. In regard to the latter synthetic fibres, these materials have gained more attention over the last two decades, especially when applied in fibre-reinforced plastics (FRPs), forming **composites** [96], [152], [161]. Composites provide an enhanced strength, at the level of both compressive and flexural stresses, and stiffness to the materials, being carbon fibre reinforced plastics (CFRP) widely selected for the manufacture of the orthotics' frame or structure (Figure 3-19 (c) and (d)) [9], [34], [129], [151], [152], [161], [162].

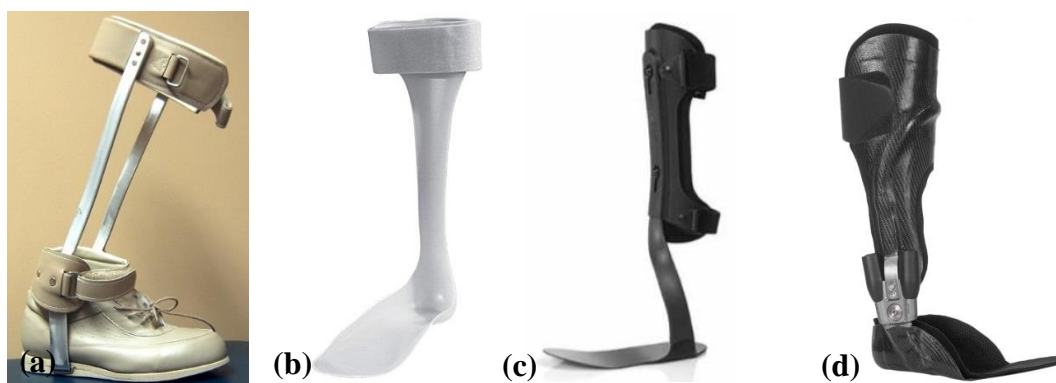


Figure 3-19 - AFOs composed by different materials: (a) metal and leather AFO; (b) passive posterior AFO composed by polypropylene; (c) Matrix Max with an anterior carbon composite frame and neoprene paddings to ensure a soft interface between the orthosis and the tibial crest, (d) Nexgear Tango ankle joint inserted in an anterior shank frame constituted by carbon-fibre composite and carbon-fibreglass webbing, and (e) construction of an knee-ankle-foot orthosis (KAFO) using prepreg carbon fibre technology [163]–[167].

3.5.3 PRODUCTION METHOD

New designs and new materials lead to the development of new manufacturing methods [151]. The most commonly used manufacture processes used in the field of orthotics are

thermoforming, additive manufacturing (commonly known as 3D printing) and resin pre-impregnated fabrics (or prepreg). The former is the process in which a thermoplastic sheet is heated to its softening temperature, and then forced against the contours of a positive mould. Orthotics companies resort to thermoforming method to manufacture passive thermoplastic AFOs, which usually is personalized to the users, but can also be prefabricated [151], [168]. Vacuum moulding technique is reported to be the conventional manufacturing process regarding personalized ankle-foot orthoses. This technique comprises the leg moulding process and the AFO production phases, and it faces a few challenges, such as the long manufacture time, limited design flexibility, consistency of the quality relying on orthotists' skills, and the requirement of multiple clinical visit of the patient [151], [152], [168]–[170].

Additive manufacturing (AM) or 3D-Printing, is a technique that provides a digitalized platform (CAD software) for designing and manufacturing solid parts from digital files and has become the medium of a new technological revolution in the medical field, which includes the development of personalized AFOs [151], [152], [168], [169], [171]. In comparison with the conventional manufacture technique of AFOs, 3D-printing presents a vast number of advantages, such as the increased flexibility in design (as all the information is digitalized in a software), higher dimensional accuracy, reduced labour-intensity, fabrication time (it takes about a full day), and waste of material. Additionally, AM allows the reduction of clinic visits, saving patients' time, the repeatability of the manufacture, and the improvement of the overall performance of the personalized AFO [151], [168], [169], [171].

Prepreg technology is a method of processing that consists in impregnating base materials, such as carbon fibres, with epoxy resins, being the most preferable for orthotic applications, since it's easier to work with and generates lightweight materials [152], [167], [172].

Although the aforementioned technologies are the most used in orthotic laboratories, this section will explore more specifically the production method used in Orthos XXI: Computer Numerical Control (CNC) machining.

3.5.3.1 COMPUTER NUMERICALLY CONTROLLED MACHINING

CNC Machining (Computer Numerical Control) is a manufacturing process where computers run programs that control how the machines will manufacture the desired product [173]–

[177]. The implementation of this technology in industrial factories dates back to the 40s and 50s, when these machines were just NC (Numerical Control) and incorporated motors that moved based on the information input given via punched tape, in which the code was manually punched into data cards. However, once the programming languages started to emerge, these instruments of manufacture evolved to CNC machines, which are fully automated and driven by digital files with the cutting trajectories and tooling's instructions [173]–[175], [177].

The CNC machining process starts with the design of the parts in a CAD (Computer-aided Design) software (Figure 3-20 (a)), in which the necessary technical specifications, such as dimensions and geometries, are defined. The next stage involves the conversion of the CAD file into a CAM (Computer-aided Manufacturing) software, which will extract the part's geometry information and create the digital programming code that controls the CNC machine (Figure 3-20 (b)). Geometric code, referred to as **G-code**, and Machine or Miscellaneous code, also known as **M-code** are the two most well-known CNC programming languages. The former is used to tell a machine **when, where, and how** to move, determining the movement, voltage and speed of the cutting heads. On the other hand, M-code controls the auxiliary functions of the machine, such as use of coolant, tool change, program stops, amongst other tasks. Once the CNC program is generated, the next step is to prepare the CNC machine for operation, which includes the affixation of the workpiece directly into the machine and the attachment of the required tooling used to remove the material from the workpiece (Figure 3-20 (c)). Lastly, the final step is to run the CNC program that instructs the CNC machine to execute the necessary machine operation in order to produce the desired product (Figure 3-20 (d), (e), and (f)) [173], [177]. This process is suitable for a wide range of materials, including metals, plastics, wood, glass, foam, and composites [173], [175], [177]. Moreover, CNC machining finds application in a variety of industries, such as aerospace, electrical, industrial machinery, clothing, automotive, and product design, which includes the fabrication of medical products, with special focus on the orthotics and prosthetics field [173], [175]–[178].

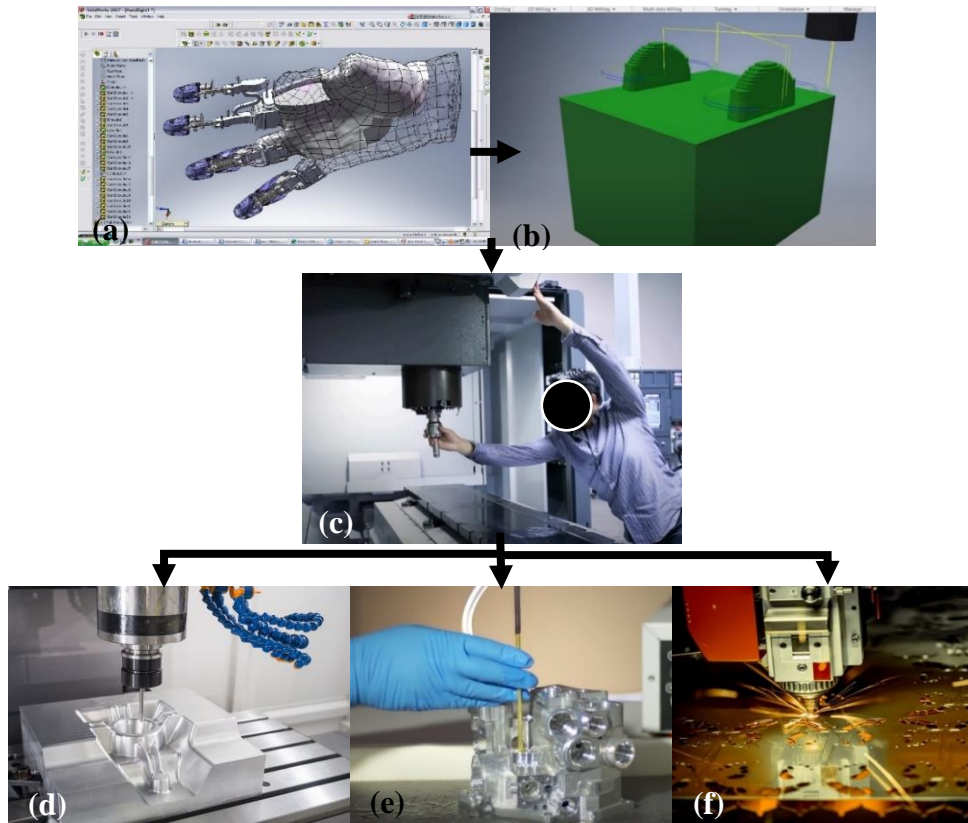


Figure 3-20 - Computer Numerical Control (CNC) Machining: (a) CAD software used for the design of the desired part; (b) CAM software to create a digital programming code for posterior control of the machine; (c) Preparation of the CNC machine; (d) CNC Milling; (e) CNC Electrochemical deburring; and (f) CNC Laser cutting machine (adapted from [175], [177], [179]–[181]).

There are many different types of CNC machines defined according to the machining technologies used to remove the material from the workpiece, including **mechanical**, **chemical**, **electrical**, and **thermal** machining. **Mechanical CNC machining** operations comprises CNC Milling (Figure 3-20 (d)), CNC Lathing or Turning, CNC Drilling, and waterjet cutting. Furthermore, **chemical machining** processes include chemical milling, and engraving; **electrical machining** includes the electrochemical deburring (Figure 3-20 (e)) and grinding; and, finally, **thermal** machining operations comprise Electron Beam machining, CNC Lasers (most typically used on sheet metal, as seen in Figure 3-20 (f)), Plasma Arc cutting, and Electronic Discharged Machines (EDM).

In addition, CNC machines can be characterized based on the directions the cutting tools can move: **2.5**, **3**, **4**, and **5 axis**. The **2.5 axis** cutter is able to remove material from the workpiece not only in the X and Y axes, but also in the Z axis. However, these types of machines cannot perform simultaneous movements on the three axes (only 2 axes together), making it a more limited technology than full three-axis CNC machine. In contrast, **three-axis** machines can move simultaneously on the X, Y and Z planes, which most free-form surfaces require. For

more complex parts, **four** and **five-axis** CNC machines are available as they include the aforementioned degrees of freedom, plus one and two rotary axis movement, respectively [174], [175].

Regarding the orthotic field, **three-axis CNC milling machines** are the most represented machines, while machines with five DOF are rarely encountered in orthotic practice. The reason for this is that CNC machine tools are most commonly used to produce foot orthoses, primarily orthopaedic insoles (Figure 3-21 (a)), whereby three-axis CNC machines satisfies most of the requirements with high degree of completeness. Nonetheless, it has been reported the application of five-axis CNC machining in the medical field, for the manufacture of body moulds and dentures in dentistry (Figure 3-21 (b)). Such systems enable a more functional formation of a continuous surface and complex shapes that resemble a certain part of the body [178].

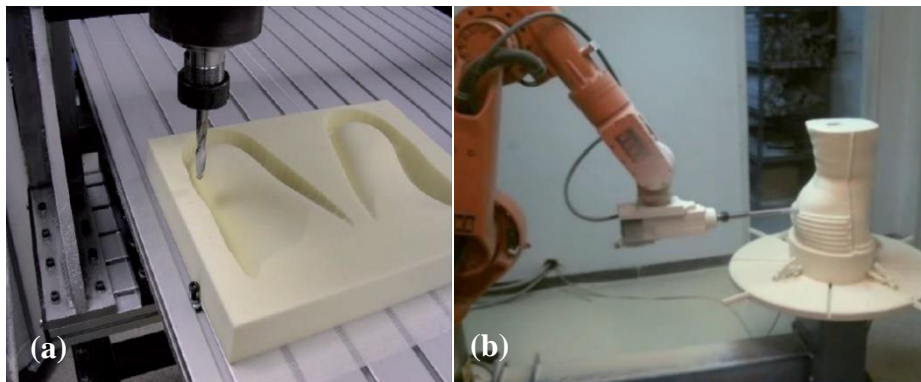


Figure 3-21 - CNC Machining applied in the orthotics field: (a) Moulds for foot orthoses production; and (b) Four-axis milling CNC machine used in a spinal orthosis mould production [178].

4. CONCEPTUAL DESIGN

In this chapter, the development of a conceptual solution for an adaptable wearable active orthosis for powered ankle joint assistance in the sagittal plane is discussed and presented. For this purpose, the design process includes a series of design methods or tools that aid the designer in the concretization of the project: the objectives tree method, the function analysis method, the performance specification method, the morphological chart method and, finally, the weighted objectives method.

The following sections will explore each of these design methods, in order to achieve the main objective that is to develop a final solution that culminates all the requirements projected for the SmartOs ankle orthosis.

4.1 THE OBJECTIVE TREE METHOD

The objective tree method consists in the formulation of the objectives in a diagrammatic form, which elucidates the relation between different objectives. This tool is useful to clarify the objectives of the project and to reach an agreement between clients and members of the design team [182], [183]. To draw a complete tree diagram, one must prepare a list of design objectives collected from the literature review and the discussion with the design team, organise the list into sets of higher-level and lower-level objectives, and finally draw a diagrammatic tree showing the hierarchical relationships and interconnection between the objectives and sub-objectives. Worth noting that each connecting link indicates that a lower-level objective is a means of achieving the higher-level objective to which it's linked. The tree diagram represents a perception of the project's problem structure, being its main aim to make the design objectives more explicit and shed light on how a higher-level objective might be achieved and why a lower-level objective is included [182].

Concerning the presented SmartOs project, the main objective is the design of an adjustable, stable and wearable ankle-foot orthosis, that enables gait rehabilitation in post-stroke patients. From this point forward, a set of objectives were established and these were interconnected with sub-objectives, which represent the means to achieve

the formers. The following Figure 4-1 illustrates the objectives tree of the design of the project's AFO.

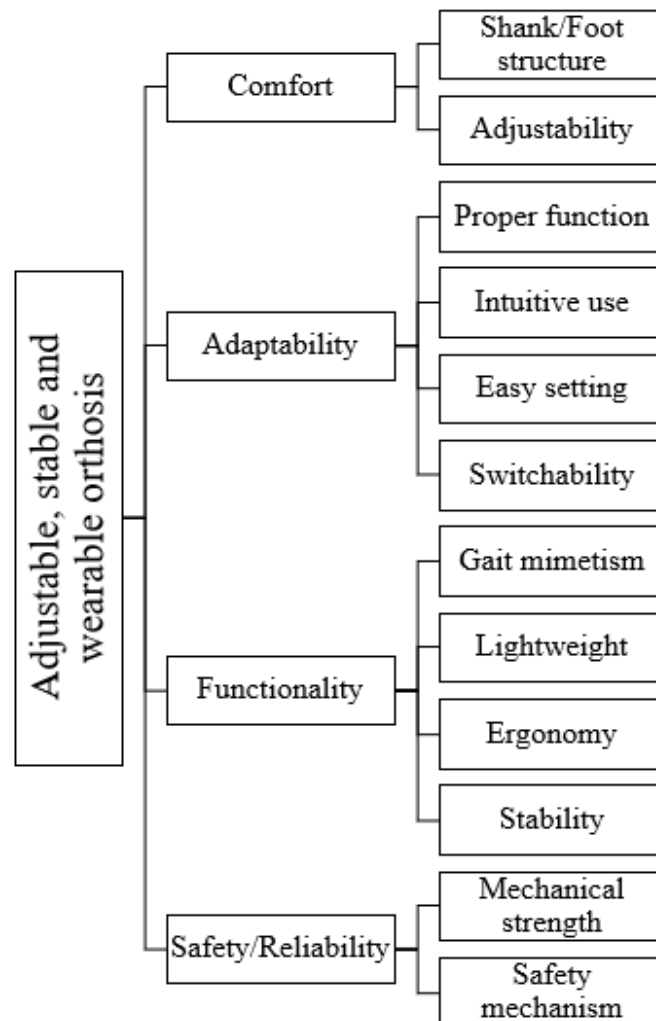


Figure 4-1 - Objectives Tree of the design of the SmartOs ankle-foot orthosis for gait rehabilitation of post-stroke patients.

In order to develop an adjustable, stable and wearable ankle-foot orthosis for rehabilitation of the ambulation capabilities of a stroke survivors, four higher-level objectives were proposed: comfort, adaptability, functionality and safety/reliability. Then, a set of lower-level objectives were established as ways of achieving each of the four objectives. Next, a brief description of each objective and sub-objective is presented:

Comfort: Due to the fact that the AFO is meant to be used in rehabilitation sessions which can last for several minutes, by individuals with impaired gait whose main aim is to restore the ambulation ability, the comfort of the device is of extreme importance. In order to achieve this objective, the designer must consider the shank and foot structure

that couples the orthosis to the user and its adjustability to their anthropometric dimensions.

- Shank/Foot structures: To ensure the comfort of the AFO to the patient, the device must connect to the shank or leg, and the foot of the user in a way that allows for a compliant use. For this sub-objective, it's important to consider the materials of which the structures are composed and the fabrication method (3D printing, thermoforming or CNC machining). Moreover, the biomechanical principles addressed should be taken into consideration as well.
- Adjustability: Another aspect of the AFO's design that is relevant for the user's comfort is its adjustability to the different anthropometric dimensions of each patient that enters a rehabilitation session. Hence, the orthosis's structures must implement systems that allow the user to adjust the AFO to their shank's height and width, and their ankle height.

Adaptability: The device must adapt to the user condition and must be easy for the patient to adapt to the device. Consequently, the AFO should warrant proper function, be intuitive for the user, allow the easy setting to the lower limb and must be switchable to each patient's impaired limb.

- Proper function: In order to achieve a successful gait rehabilitation after a stroke, the users must be submitted to exercises that mimic the human gait movement. For this purpose, the device should incorporate an electronic/mechanical system that enables the compliant and right function of the human ankle. Furthermore, the orthosis must implement a design that prevents robotic gait, contributing as well for the gait mimetism, mentioned later on.
- Intuitive use: Like any other electronic device, the active AFO should be intuitive, easy for the user to learn and adapt to.
- Easy setting: The setting and fitting of the AFO must be executed by the user with the help of the therapist. Herewith, this task should

be easily carried out in a relatively short time, so that the rehabilitation session's time is fully optimized.

- Switchability: One of the requirements concerning the use of a lower limb orthotic device for gait rehabilitation is that users with impairment on different sides (left or right one) can use the same device. Hence, the AFO must include a system that allows its setting on both the right and left leg, enabling gait restoration on a vast community of stroke survivors.

Functionality: Another one of the main objectives of the SmartOs project is to develop an active AFO that can perform its function of gait restoration in post-stroke patients in the best possible way. To achieve this objective, the gait mimetism function of the system incorporating the AFO, as well as its weight, ergonomy and stability must be considered in the design process.

- Gait mimetism: The device should mimic the human ankle movement during a gait cycle in such a way that the user is able to perform the dorsi-/plantarflexion and in-/eversion movement while walking on a horizontal or inclined plane. Therefore, the AFO should provide for the correct kinematic and kinetic assistance, meaning that the range of angles and torque provided must be in accordance with the biomechanical information about the healthy and impaired human ankle. Having these aspects in consideration helps the rehabilitation process, and thus aids the AFO's users regain their quality of life.
- Lightweight: For the purpose of optimizing the energy consumption of the user throughout the rehabilitation session, the AFO should be as lightweight as possible. This sub-objective is a way to achieve the functionality of the device since it allows for a more efficient and less tiresome walking process. Hence, the materials selected to constitute the AFO's shank and foot structure and the overall design must gurantee its weightlessness.

- Ergonomy: In order to achieve a fluid walk, the user must be provided of an ergonomic AFO, with a structural design that enables comfort and compliance.
- Stability: Drag phenomena of the AFO's foot during a gait session must be avoided, in order to prevent the feeling of discomfort on behalf of the user. Furthermore, the alignment between its articulation and the patient's anatomical axis of the ankle is highly important when it comes to ensuring the stability of the patient's ankle and rehabilitation success.

Safety/Reliability: The final key objective of the AFO's design is to warrant the safety of the device use and the reliability of the components that compose its structure. This is attained through the study and analysis of the mechanical strength of the materials selected for the AFO and through the incorporation of a safety mechanism.

- Mechanical strength: The selected materials that will compose the shank and foot structure of the AFO must ensure a mechanical resistance to fracture and strain so that the user feels safe and comfortable during the gait rehabilitation sessions. For this, a Factor of Safety must be defined for the whole device, in order to validate it in congruence with the established value.
- Safety mechanism: To warrant that the kinematic range of the AFO's articulation is in consonance with the biomechanics of the human ankle, and to prevent excessive angular movements, a safety mechanism should be integrated into the AFO's articulation.

4.2 THE FUNCTION ANALYSIS METHOD

Design problems can have different levels of generality or detail, being that the level at which this problem is addressed by the design team is crucial. Herewith, it can be useful for the design team to consider the problem level at which is to work, and the essential functions that a solution type will be required to satisfy. This way facilitates the development of alternative solution proposals that fulfil the functional requirements.

Thus, the function analysis method represents a means of considering and indicate the essential functions that the final product should satisfy, and establish the problem level, by implementing a boundary around these functions [182].

The purpose of the function analysis method is to concentrate on what has to be achieved by the design, and not how it's to be achieved. Hence, the designer must express the overall function for the design in terms of the conversion of inputs into desired outputs, through a simple “black box”. Inside this box, the fundamental purpose of the product or device must be clarified. The overall function is then broken down into a set of essential sub-functions, interconnected to each other and the inputs and outputs, in order to achieve a feasible, working system. The “black box” is made transparent so that the sub-functions and its interconnections are clear, and a system boundary that sets the functional limits for the device is defined [182].

As aforementioned, the main goal of the SmartOs project and this master dissertation is the design of an adjustable, stable and wearable active AFO that allows the gait rehabilitation of post-stroke patients. Thus, the device to be designed must convert the input (a patient with drop foot) into the output (the same patient with a stable and comfortable gait). Figure 4-2 represents the “black box” containing the overall function of this project.

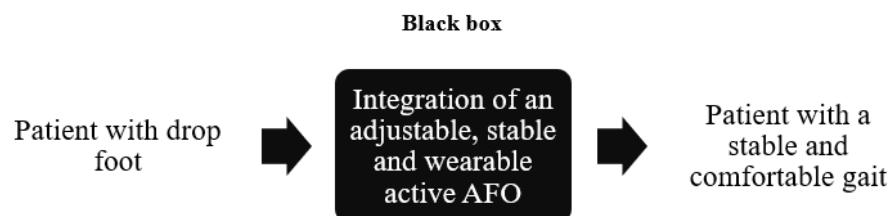


Figure 4-2 – Black box with the overall function of the SmartOs project, which is to convert the input “Patient with drop foot” into the output “Patient with a stable and comfortable gait, through the integration of an adjustable, stable and wearable active AFO.

Once the overall function of the project is established, the sub-functions that comprise all the tasks inside the “black box” are defined. A block diagram consists of all these sub-functions linked together by their inputs and outputs, to warrant the overall function of the device that is being designed. This block diagram is called “transparent box” and it sets the boundary of the system, defining the functional limit for the product which is mandatory to ensure its feasibility. Figure 4-3 represents the “transparent box”

of the present project, containing the sub-functions associated with the design of the SmartOs device.

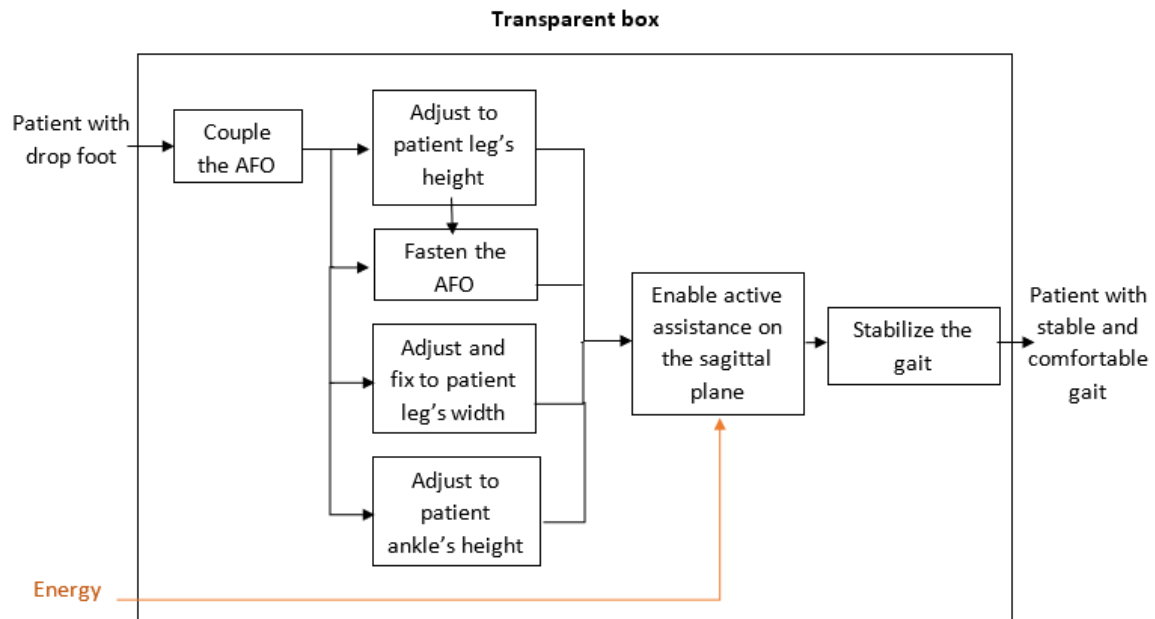


Figure 4-3 – Transparent box of the SmartOs project, containing the sub-functions associated with the design of the proposed rehabilitation device.

The patient who suffered a stroke, which jeopardized his/her ability to walk, and starts a gait rehabilitation procedure must, firstly, couple the AFO to the leg. This AFO is composed by materials that must warrant the safety, comfort and compliance during the rehabilitation sessions. After the coupling of the device on the impaired foot (left or right) it must be adjusted to the patient leg's height, fasten to the desired height that suits the patient, and width. Lastly, the foot structure of the AFO must adjust to the patient ankle's height.

The adjustment sub-functions are essential to ensure the proper alignment of the AFO to the patient's anthropometric features while preventing vertical calf band travel or pistoning (proximal/distal sliding of the AFO's shank structure on the leg), which results in shear forces that may compromise the integrity of the skin and the success of the rehabilitation process [5]. Moreover, the adjustment of the foot structure to the user ankle's height is crucial to ensure the alignment between the axes of the device and the user, before the start of the gait therapy.

Once the gait rehabilitation session is initiated, the AFO must enable active assistance to the ankle joint, during the performance of dorsiflexion and plantarflexion

movements (sagittal plane motion). This sub-function is possible through the incorporation of an actuator on the device's articulation. Herewith, energy (which can be pneumatic, hydraulic or electrical energy) is a necessary input to the mentioned sub-function. In association with the ankle movement assistance, the patient's gait should be stabilized as much as possible, which implies that the user's ankle axis is in conformity with the AFO axis during walking, in order to avoid axis misalignments that promote detrimental parasitic forces and compensatory movements that cause discomfort and inhibit rehabilitation, respectively. Finally, all of these sub-functions must culminate in the crucial output of providing the rehabilitation patient a stable, safe and comfortable gait.

4.3 THE PERFORMANCE SPECIFICATION METHOD

Once the functions of the final device are defined, the next phase of the project is to accurately specify the performance requirements of a design solution. To this end, the performance specification method is used. This method limits the range of acceptable solutions, setting up some boundaries to the solution space within which the design team must focus on, and to posteriorly be used in the evaluation of the proposed solutions. Summarily, the performance specification method aids the designer to define the required performance that a solution has to achieve, and not any particular physical component that may be used to achieve the performance [182].

Herewith, the first steps of this method are to consider and then determine the level of generality at which to operate, considering the most general (product alternatives) down to the least (product features). The highest level grants the design team the freedom to propose different alternative ways of achieving the performance. On another hand, the intermediate level concedes more limited freedom, focusing only on different types of appliances, and, finally, at the lowest level of generality, the designer would be constrained to considering different features, making a modification to existing products. Once the level of generality at which the design process is to proceed has been decided, the required performance attributes need to be identified. These can be similar to or derived from the design objectives and functions, and the main goal is to define a final list of performance requirements that contains all the conditions that a design proposal or solution should satisfy. In other words, the specification should say what a

product must do, not what it must be. Additionally, it may become mandatory to distinguish within this list the attributes or requirements that are demands (D) and those that are wishes (W). Demands comprise all the requirements that must be met, whereas wishes are the attributes which the client, customer or design team would like to meet, if possible [101].

Relatively to the SmartOs project, the lowest level of generality (product features) was determined. This decision is justified considering that the project aims to modify an existing ankle foot orthosis (H2 AFO, Technaid, seen previously in Section 3.2, Figure 3-6), inputting the necessary changes to its structure and actuation, in order to develop a more compliant and comfortable rehabilitation device. The requirements of the product were already set by the **SmartOs team**. Next, Table 4-1 presents the demanded and wished requirements for the wearable active AFO of SmartOs project.

Table 4-1 - Performance specification method for the SmartOs project.

Demands (D) Wishes (W)	Requirements
<p style="text-align: center;">W</p> <p style="text-align: center;">D</p> <p style="text-align: center;">D</p> <p style="text-align: center;">D</p>	<ul style="list-style-type: none"> ▪ <u>Compliant design of the shank structure:</u> <ul style="list-style-type: none"> - 3D printed structure combined with comfortable and lightweight materials; - Adjustable to different users' height (1.5 to 1.9 m); - Adjustable to different users' body mass (45-100 kg); - Mechanical stiffness set according to user's comfort.
<p style="text-align: center;">D</p>	<ul style="list-style-type: none"> ▪ <u>Compliant design of the foot structure:</u> <ul style="list-style-type: none"> - Include lightweight, flexible and comfortable materials;

Demands (D) Wishes (W)	Requirements
<p style="text-align: center;">D</p> <p style="text-align: center;">W</p> <p style="text-align: center;">D</p>	<ul style="list-style-type: none"> - Easily replaceable from the actuation system; - Thickness of the outsole < 1.5 cm; - Adjustable to different foot sizes (EU: 35-45).
<p style="text-align: center;">W</p>	<ul style="list-style-type: none"> ▪ Adaptable design: <ul style="list-style-type: none"> - Switchable to both right and left foot
<p style="text-align: center;">D</p> <p style="text-align: center;">D</p> <p style="text-align: center;">W</p> <p style="text-align: center;">D</p> <p style="text-align: center;">D</p>	<ul style="list-style-type: none"> ▪ Accurate functionality: <ul style="list-style-type: none"> - Electric actuator for ankle joint; - Assisted gait speed (0.5 to 3 km/h); - Nominal torque (35 to 80 Nm); - Alignment between the ankle and orthosis axis; - Lightweight design (<1.3 kg).
<p style="text-align: center;">D</p>	<ul style="list-style-type: none"> ▪ Reliable use: <ul style="list-style-type: none"> - Safety mechanism to limit range of motion (-20 to 20° in the sagittal plane).

4.4 THE MORPHOLOGICAL CHART METHOD

Generating alternatives or solutions is an essential aspect of the design process, as it allows the design team to make a reasoned choice of the final solution, based on a wide combination of means to achieve the planned sub-functions [182].

Hence, the morphological chart method aims to help the design team to identify novel combinations of elements, components or sub-solutions that can be combined

together to form a solution. This number of possible combinations can include existing, conventional solutions, as well as a wide range of variations and completely novel solutions. The main goal of this design method is to widen the search for possible new solutions, by selecting the combinations of sub-solutions from the chart [182], [183].

The morphological chart method must begin with the list of features or functions which are crucial to the product. These are usually expressed in an abstract manner of product requirements or functions. Furthermore, the items in the list should all be at the same level of generality and respect the necessary functions of the desired product (defined with the previous method). To avoid situations of an unmanageably large range of possible combinations of sub-solutions, one must keep the list of functions on about four to eight functions. Posteriorly, for each function, the design team must list the means or sub-solutions by which it might be achieved. For this, the list of means can include not only the existing sub-solutions of the particular product but also new ones that the design team find to be feasible. After the morphological chart is constructed from the previous list, the selection of one sub-solution at a time from each row consists of the complete range of all the theoretically-possible different solution forms for the final product. The final step of this method is to identify the combinations of sub-solutions that form a feasible conceptual solution. It's important to notice that some of these combinations will be either existing solutions, valid new solutions or impossible solutions. Each potential solution can be considered and then hierarchically organized into better solutions (for reasons of cost, performance, novelty, or material availability) that are chosen for further development. Computer aid design is an important tool that helps the designer to search for all the possible combinations of sub-solutions to incorporate in a feasible final product [182].

For the SmartOs project, the morphological chart method was used to generate solutions that would warrant the development of a wearable, adjustable, safe, and feasible active ankle-foot orthosis. The presented sub-solutions for each sub-function were designed during the internship in the company Orthos XXI and comprise all the conceptual ideas gathered by the SmartOs design team. Table 4-2 is the morphological chart containing all the possible means to achieve each sub-function required by the project SmartOs.

Table 4-2 – Morphological chart with all the solutions proposed to achieve each subfunction of the SmartOs project.




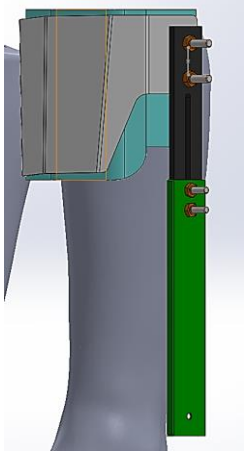
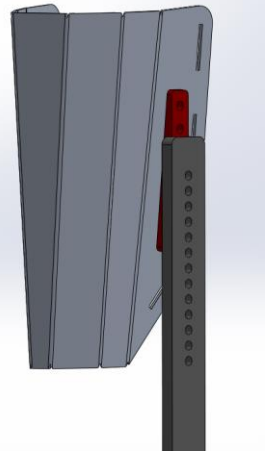
Solutions Subfunctions	1	2	3	4
<p>Couple the AFO</p>	<p><u>Lateral upright and straps</u></p> 	<p><u>Anterior shank structure</u></p> 	<p><u>Lateral shank structure</u></p> 	<p>...</p>
<p>Adjust to patient leg's height</p>	<p><u>Slider and upright system</u></p> 	<p><u>Upright with bolt fixation</u></p> 	<p>...</p>	<p>...</p>

Table 4-2 – Morphological chart with all the solutions proposed to achieve each subfunction of the SmartOs project (cont.).

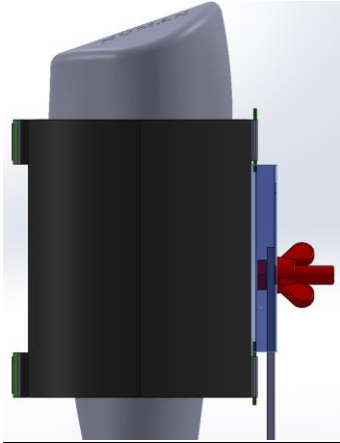
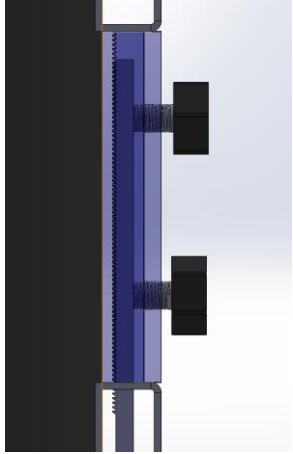
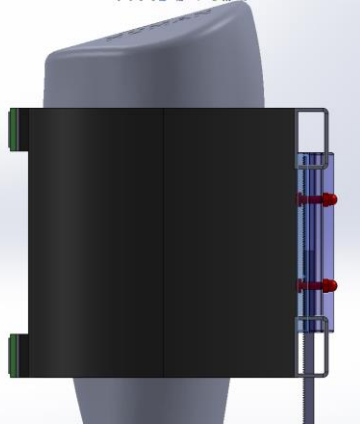
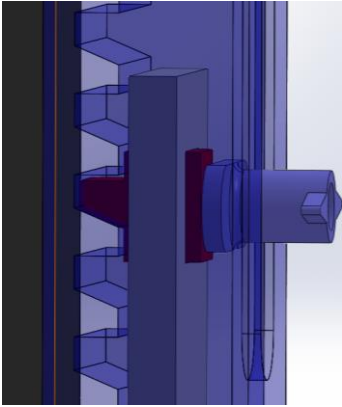
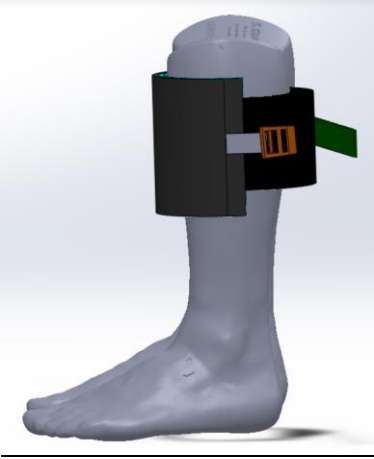
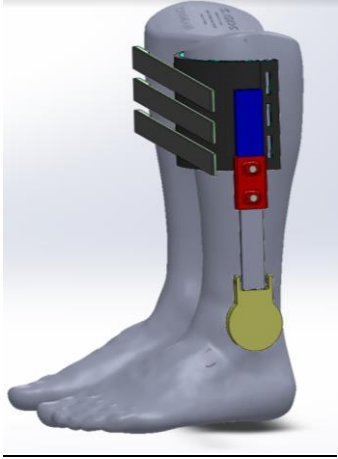
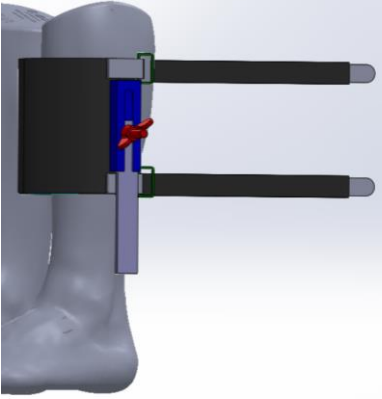

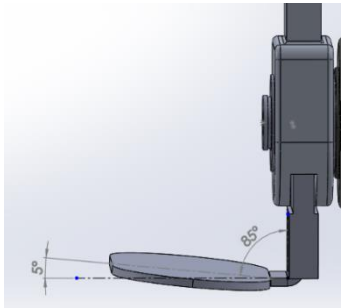
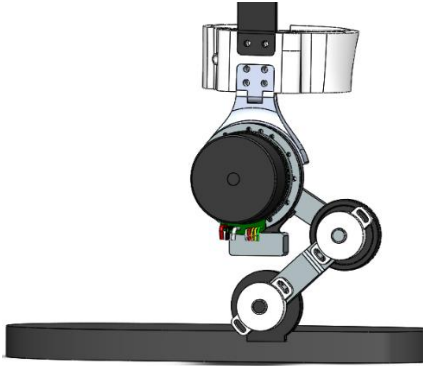

Solutions Subfunctions	1	2	3	4
Fasten the AFO	<p><u>Bolt and nut fixation</u></p> 	<p><u>Locking teeth structure with handles</u></p> 	<p><u>U-shaped bar with locking teeth structure</u></p> 	<p><u>Locking teeth mechanism with insertable component (red)</u></p> 
Adjust and fix to patient leg's width	<p><u>Strap with buckle</u></p> 	<p><u>Strap and shank structure's holes</u></p> 	<p><u>Strap and metal clip system</u></p> 	<p>...</p>

Table 4-2 – Morphological chart with all the solutions proposed to achieve each subfunction of the SmartOs project (cont.).

Solutions Subfunctions	1	2	3	4
<p>Adjust to patient ankle's height</p>	<p>Shoe insert with height adaptation (Exo-H2 ankle) and w/o tibiotalar tilt</p> 	<p>Shoe insert with height adaptation and tibiotalar inclination</p> 	<p>...</p>	<p>...</p>
<p>Enable active assistance on the sagittal plane</p>	<p>PMA</p>	<p>Servomotor with gearbox</p>	<p>SEA</p>	<p>...</p>
<p>Stabilize the gait</p>	<p>Self-aligning mechanism</p> 	<p>Two-Degree of freedom articulation (with silent blocks)</p> 	<p>...</p>	<p>...</p>

The means to achieve the subfunction **Couple the AFO** comprise three different designs of the user-orthosis attachment or coupling system: a **lateral upright with straps**, an **anterior** and **lateral shank structure**, coupled on the anterior and lateral side of the patient's leg, respectively. The former design is already implemented on the ankle module of the Exo-H2. One of the aspects of the design of this ankle orthosis that was set to be improved was exactly the coupling system, which was considered to be quite uncomfortable for the wearer. Thus, the SmartOs design team formed two different concepts of an attachment system that were both based on the incorporation of a structure onto the shank of the patient. These solutions were considered having in mind the biomechanical principle of the **total contact** (with the leg in this case), which demonstrates that, for the same force, an increase of the contact area results in the mitigation of pressure.

The subfunction **Adjust to the patient leg's height** can be accomplished through a system consisting of a **slider (green component) and an upright (black part)**, which is fixed to the shank structure and would be pushed through the slider, in order to adapt the height of the AFO to the point most comfortable for the patient. Moreover, another solution proposed was a system consisting of an **upright with a series of bolt fixations**. In contrast with the first solution, which embodies a continuous adaptation, this last solution is a series system, with several levels of height adaptation, that ensures higher mechanical safety of fixation compared to the continuous adaptation solution.

Alongside the solution of the height fixation system consisting of a bolt and nut, three other solutions were designed to realize the subfunction **Fasten the AFO**. The system with two handles would exert tension on the upright and lock itself in a locking teeth structure, which is incorporated in the shank structure. Moreover, solution three would comprise a U-shaped structure through which the upright would slide and locked by the tension created by tightening of the red bolt. This system would also incorporate a locking teeth structure to generate more friction and prevent unlocking situations. Finally, the proposed solution four is a higher-scale locking teeth mechanism and would function through the connection of the red component with the complementary teeth of the structure fixed to the shank system. To avoid a situation of a detachment of the red part, the user would have to rotate the exterior component (blue part) so that it's horizontal, as represented in the image.

In order to **Adjust and fix the AFO to the patient leg's width**, three solutions were proposed. The first solution is a system composed of a strap attached to a soft material cushion, which would be adjusted through a buckle fixed on the shank structure. Furthermore, a system with three or more straps cushioned with a soft material and positioned on the posterior side of the patient's leg. The extremities of the straps would have a layer of VELCRO® hook, which would go through the holes of the shank structure and then looped back to fix on the VELCRO® loop of the strap. Finally, the final proposed solution would be similar to the latter, but instead of the straps going through the holes on the shank structure, they would be looped back around a metal clip attached to the structure.

The subfunction **Adjust to patient ankle's height** can be realized through the implementation of a metal shoe insert. The first proposed solution would be the one already incorporated in the ankle module of the Exo-H2, which has a height adaptation system, similar to the one that allows for the adaptation of the leg's height, but with a lower range. To ensure better alignment of the orthosis axis of rotation with the user ankle's axis, the Orthos design team suggested the design of several shoe inserts, with the same working principle as that of the Exo-H2, but with different sizes. Additionally, this shoe insert would also comply with the tibiotalar axis, which is anatomically inclined, as mentioned in Section 2.1.2.1. The inclination value of the component would have to be defined correspondingly to the range of inclination of the tibiotalar joint (set to be maximum 5°).

The means to achieve the subfunction **Enable active assistance on the sagittal plane** can comprise all of the conventional actuation implemented in exoskeletons and active orthoses. However, it was selected the most suitable actuation systems that have been used in orthotic devices, especially on AFOs (see Section 3.3.4 and the appendix C- **Active ankle-foot orthoses for rehabilitation still in a development stage**). Herewith, to enable a powered assistance for dorsiflexion and plantarflexion motions, one can consider actuators such as PMA, servomotor, and a SEA. PMAs present the advantage of being lightweight and similar to the human muscle (biomimetic feature). In addition, SEAs were considered for the present project in an earlier stage, due to its capability of storing energy in the spring connected to the DC motor, which can be released in the propulsive stage of the gait. Nevertheless, the SmartOs team ruled out any actuation system other

than an electric motor, as it was defined as *Demanded* in the previous section. Furthermore, due to the mechanical requirements of the human ankle (high torque and low velocities), a gearbox must be incorporated in association with the DC motor. Hence, the servomotor (brushless DC motor assembled with a gearing set, control circuit, a position feedback component - encoder or potentiometer) would be preferable because it is a known efficient solution. So, the space of solutions for this subfunction can be reduced to only one feasible solution – the servomotor.

The final subfunction that the final product should accomplish is **Stabilize the gait**. This can be achieved through a self-aligning mechanism, which would operate in a similar way as the mechanisms addressed in Section 3.4.1. The CAD model of the mechanism represented in Table 4-2 was designed previously by a member of the SmartOs team and studied during the present master dissertation. This study was conducted with the aid of an open source software dedicated to model musculoskeletal systems and dynamic simulation of movement – *OpenSim* – with the main goal of assessing the validity of the proposed self-aligning mechanism. The principle of the designed self-aligning mechanism is to mitigate misalignments between the axes of the orthosis and the human ankle, by compensating the centre of rotation with the addition of two redundant DOF to the one DOF revolute joint. This mechanism was inspired on the knee self-aligning mechanism developed by Choi et al. (see Figure 3-15 (b) in Section 3.4.1). Unfortunately, the results of the executed simulations to evaluate the mechanism were not promising enough to develop the apparatus (see appendix **D-Self-aligning mechanism validation**). Hereupon, the proposed self-alignment mechanism was discarded from the design's feasible solutions.

As mentioned in Section 3.4.2, two degrees of freedom systems are reported to minimize the dislocation of the human ankle relative to the AFO, presenting a great advantage for gait rehabilitation. Therefore, the incorporation of a flexible component was proposed by the Orthos design team. This part would allow the movements of inversion and eversion to be performed in a passive manner, alongside with the actuated movements in the sagittal plane. Regarding what flexible component would be selected to ensure the passive DOF, a spring and a silent block were suggested. Although, the silent block was considered a more accessible solution, in terms of cost and production.

In the following section, the feasible combinations of sub-solutions will be identified to set out the complete range of conceptual solutions. This will be executed by selecting the valid sub-solutions for each sub-function and combining them into conceptual solutions that may be considered for future development.

4.4.1 CONCEPTUAL SOLUTIONS

The morphological chart constructed in this section comprises the complete range of all the possible different solutions for the final product. As aforementioned, the complete range of solutions consists of the combinations made up by selecting one sub-solution at a time from each row of sub-functions. Therefore, the total number of combinations is very large. In this case, the complete set of possible solutions' combination is $3 \times 2 \times 4 \times 3 \times 2 \times 3 \times 2 = 864$. This combinatorial explosion calls for a drastic reduction of the sub-solutions considered.

Herewith, the space of solution was reduced as follow:

- The sub-function of **Couple the AFO** can only be achieved by solution 2 (anterior shank structure), due to the fact that is the concept that best respects the biomechanical principle of total contact area, being the most feasible solution;
- The means to achieve the sub-function **Adjust to patient leg's height** is reduced to only solution 2 (upright with bolt fixation) for the reasons of mechanical safety mentioned above;
- Because of the previous selected solution, sub-function **Fasten the AFO** should only be accomplished by solution 1 (bolt and nut fixation);
- Even though the Orthos team found the second solution more preferable, the sub-function **Adjust to patient leg's width** can be realized through solutions 1 and 2, discarding this way the sub-solution 3. The first solution was selected to be further studied in the posterior method due to the decision of the SmartOs team, that also considered the solution to be feasible;
- The sub-function of **Adjust to patient ankle's height** can be accomplished by both solutions 1 and 2. Solution 1 is already implemented in a developed

AFO, so it's a solution that is known to be practical, and thereby, must be evaluated along with the novel solution proposed;

- As mentioned above, the sub-function **Enable active assistance on the sagittal plane** can be reduced to only one solution, the servomotor;
- Lastly, as aforementioned, the proposed self-alignment mechanism was discarded from the design's feasible solutions. Therefore, only the sub-solution of incorporating a two-degree of freedom system will be considered to achieve the sub-function **Stabilize the gait**.

Hereupon, the total number of possible combinations of sub-solutions is immensely reduced to $1 \times 1 \times 1 \times 2 \times 2 \times 1 \times 1 = 4$ **conceptual solutions**. The following Table 4-3 presents a summary of the conceptual solutions that will be further studied in the weighted objectives method, and the sub-solutions selected to compose each one.

Table 4-3 – Summary of the formed conceptual solutions for the SmartOs project, and sub-solutions selected to compose each one.

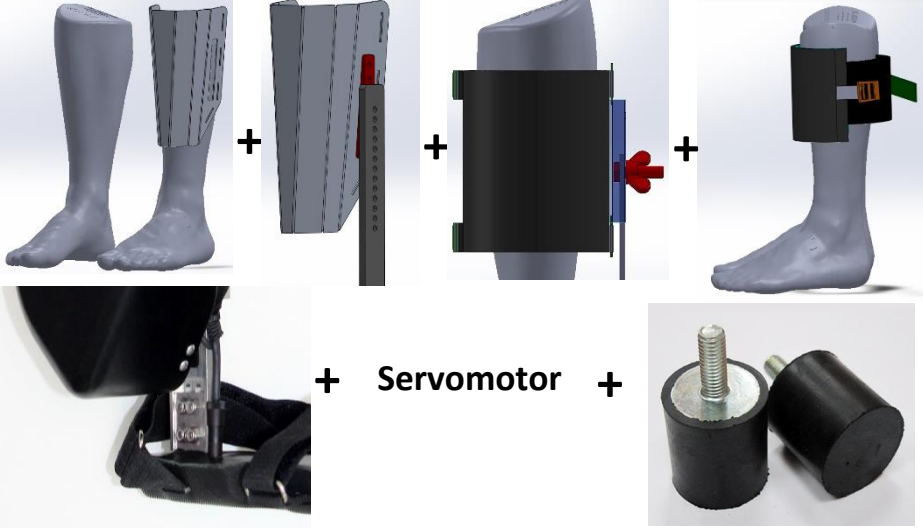
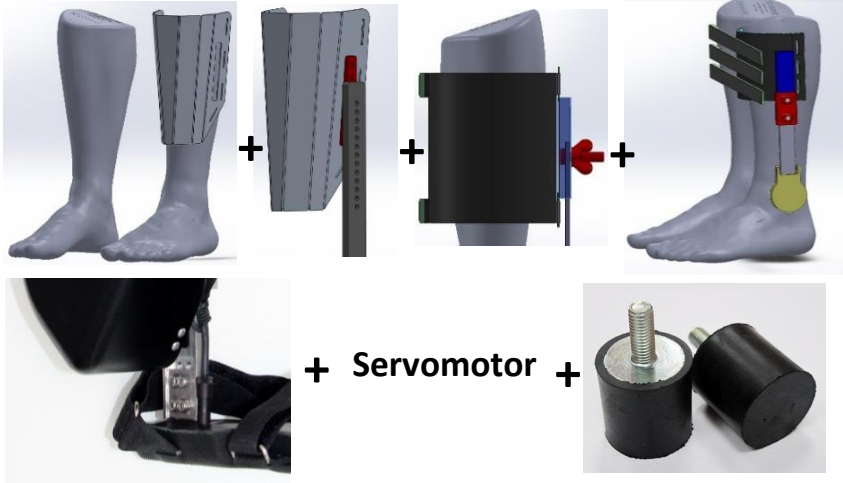
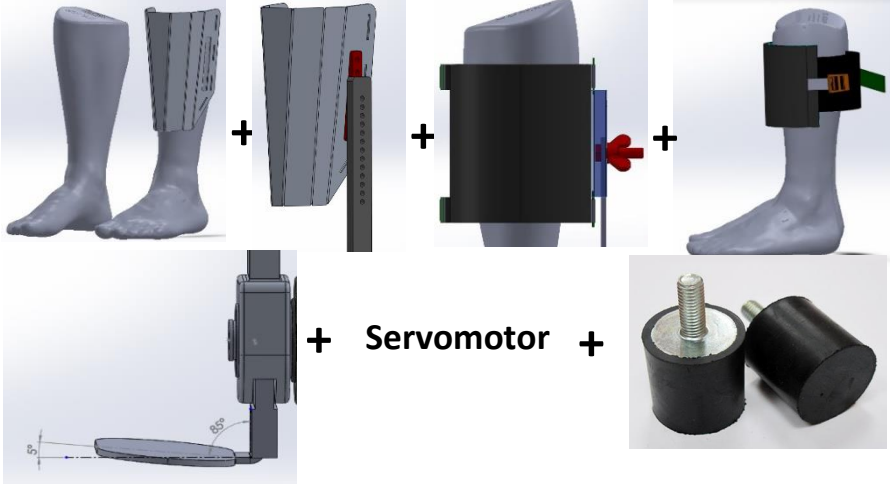
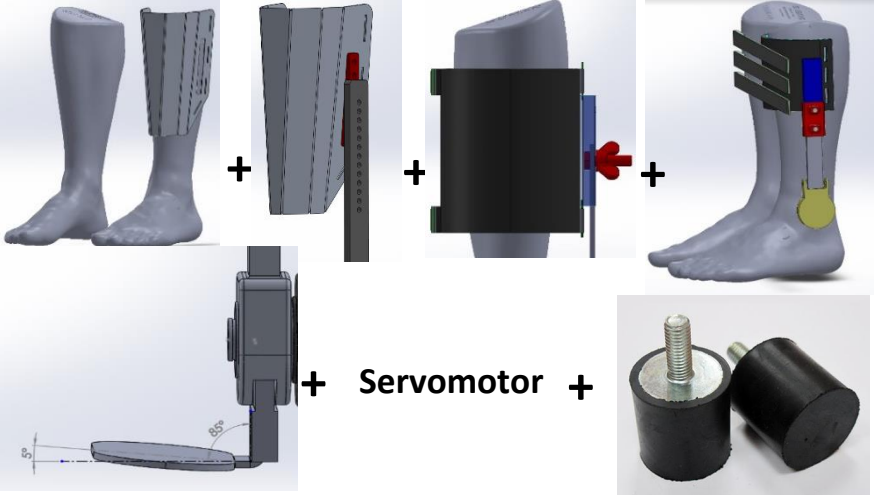
Conceptual Solutions	Sub-solutions selected
1	

Table 4-3 – Summary of the formed conceptual solutions for the SmartOs project, and sub-solutions selected to compose each one (cont.).

Conceptual Solutions	Sub-solutions selected
<p style="text-align: center;">2</p>	 <p style="text-align: center;">+ Servomotor +</p>
<p style="text-align: center;">3</p>	 <p style="text-align: center;">+ Servomotor +</p>
<p style="text-align: center;">4</p>	 <p style="text-align: center;">+ Servomotor +</p>

4.5 THE WEIGHTED OBJECTIVES METHOD

Once the range of alternative designs for a product is set, the design team is faced with the task of selecting the best one. This choice can indeed be made by guesswork, intuition, experience or even by arbitrary decision. However, it's better that such decision is based on some more rational, or at least open procedure. The evaluation of the alternatives or conceptual solutions must be executed by considering the objectives defined for the project. The result of this assessment is to determine the value or utility of a design proposal with respect to the design objectives. Hence, it's necessary to characterize each objective, in order to obtain the value of importance in comparison with each other, i.e. to weight the objectives [182].

The weighted objectives method provides a mean of assessing and comparing conceptual solutions, using differentially weighted objectives. This method is based on the numerical scores assigned to the performance of alternative designs measured against the defined project's objectives, which are also given a numerical weight [182], [183].

The first step of the weighted objectives method is to list once again the design objectives. Even though these objectives were established with the objectives tree method, in a later stage of the design process, the early set of objectives may well have become modified or may not be entirely appropriate to the designs that have been created. Subsequently, this list of objectives should be rank ordered by systematically comparing pairs of objectives, one against the other. The process of comparison can be done by using a simple chart, in which each objective is considered in turn against each other and given the value of **1** or **0**, depending on whether the first objective is considered more or less important than the second. Moreover, if any pair of objectives is regarded as equally important, a $\frac{1}{2}$ value is assigned. Once all pairs of comparison are made, the row totals indicate the rank order of the objectives, being the highest priority objective the one with the highest value [182].

The next step is to assign a numerical value to each objective that represents its weight relative to the other set of objectives. There are several ways to perform this task. A simple way of doing this is to place the objectives in positions of relative importance on a scale of 1 to 10, or 1 to 100. So, this way if an objective is given for instance the maximum

value of 10, then the other are placed in the positions with value relative to this. Consequently, if an objective is given the value of 7, it means that it was valued as about 70% of the importance of latter objective. Furthermore, it's necessary to establish performance parameters or utility scores for each of the objectives. For this, a points scale can be created, in which each parameter is assigned a utility score representing the worst to best possible performance range [182].

Finally, the final stage of the evaluation is to consider each alternative design proposal and assess its performance, by calculating it based on the established parameters. The performance scores on each parameter for each alternative design should take into account the different weights of each objective. Thus, the **utility value** of an alternative design is calculated by multiplying the performance scores by the weight value of each objective. These utility values are then used as a basis of comparison between the alternative designs, which can be ranked in order of overall performance. The participation of all members of the design team is recommended to ensure a consensus regarding the selection of the final solution [182].

Herewith, in order to be able to evaluate the alternative designs proposed in Section 4.4.1 it is necessary to have a set of criteria, which must be based on the design objectives. The full set of objectives established with the tree of objectives method is no longer appropriate at a later stage of the design process, as many of the defined objectives have become deprioritized, at least for a first prototype. With this in mind, the new list of objectives was created by selecting from Figure 4-1 the design requirements that were more vastly considered during the gathering of solutions by the design team. Table 4-4 provides the design objectives to be used for evaluation of the conceptual solutions.

Table 4-4 – List of the design objectives for the SmartOs project, to be utilized for posterior evaluation of the alternative designs.

A	Structure's comfort
B	Adjustability
C	Mechanical strength
D	Lightweight
E	Proper function
F	Stability

With the new list of design objectives established, it is necessary to assess them in terms of relative importance. Therefore, a systematic comparison between pairs of objectives should be done in order to obtain the relative weights. It is important to refer that this design method was accomplished as a team effort, as the members of the design team gave their perspective on the priority of each defined objective. As is normal, each member of the design team gave different priorities to the defined objectives. Therefore, in order to account for every opinion inside the team and to reach a team consensus, the average importance given to each objective was calculated. Table 4-5 presents the rank order of the objectives defined by each member of the design team.

Table 4-5 – Rank order of the list of objectives determined by each member of the design team. Values that ranged from 6 (highest priority) to 1 (lowest priority) were given to each rank ordered objective.

Team	Objective's importance					
	6	5	4	3	2	1
Team member #1	E	B	F	A	D	C
Team member #2	E	A	C	D	B	F
Team member #3	E	A	F	D	B	C

Subsequently, each rank ordered objective was submitted to a calculation of its importance value, which is nothing more than the average value assigned by the team members. Table 4-6 clarifies this importance value calculation, which it will serve as a guideline to the definition of the final rank order of the list of objectives.

Table 4-6 – Calculation of each objective's final importance value, based on the rank order determined by each member of the design team.

Objective	Importance value calculation
A	$\frac{5 \times 2 + 3 \times 1}{3} \approx 4,33$
B	$\frac{5 \times 1 + 2 \times 2}{3} = 3$
C	$\frac{1 \times 2 + 4 \times 1}{3} = 2$
D	$\frac{3 \times 2 + 2 \times 1}{3} \approx 2,67$

Table 4-6 – Calculation of each objective’s final importance value, based on the rank order determined by each member of the design team (cont.).

Objective	Importance value calculation
E	$\frac{6 \times 3}{3} = 6$
F	$\frac{4 \times 2 + 1 \times 1}{3} = 3$

With the importance value of each objective calculated based on the opinion of each member of the design team, the final rank order of the objectives list is set through a systematic comparison of pairs of objectives, as it’s explained above. The relative importance of each pair of objectives is determined by the values calculated in Table 4-6. As a result, Table 4-7 represents the chart used to rank order the different objectives.

Table 4-7 – Chart of systematic comparison of pairs of objectives, to obtain the row total, which indicates the rank order of objectives. Note that the value 1 and 0 refer to a more and less important objective, respectively. The value $\frac{1}{2}$ indicates that the objectives are considered equally important.

Objectives	A	B	C	D	E	F	Row total
A	-	1	1	1	0	1	4
B	0	-	1	1	0	$\frac{1}{2}$	2,5
C	0	0	-	0	0	0	0
D	0	0	1	-	0	0	1
E	1	1	1	1	-	1	5
F	0	$\frac{1}{2}$	1	1	0	-	2,5

Once the rank order of the objectives is settled, a numerical value is assigned to each objective. This value represents its weight relative to the other objectives. As aforementioned, there are several ways of doing this, of which it was chosen a simple scale of 1 to 10, where the objectives are placed in positions of relative importance. This step is important to convert the ordinal rank order scale of Table 4-7 into an interval value scale, which can be used for later arithmetic operations. Table 4-8 represents the scale of 1 to 10, where the rank ordered objectives were appointed in relative positions.

Table 4-8 – Rank ordered objectives placed in positions of relative importance on a scale of 1 to 10.

Weight	Objective
10	E
9	
8	A
7	
6	
5	B, F
4	
3	D
2	
1	C

Herewith, it is now possible to conclude that the most important objective is **E** (proper function), which has been given the value 10. The other objectives are then given values relative to this. Hence, the objective **A** is valued as 80% of the importance of objective **E**; objective **B and F** were given the same importance, which is five times more important than objective **C** (mechanical strength); and objective **D** is valued as 30% less important than objective **E**.

With the relative weightings of each objective assigned, it becomes necessary to convert the statements of objectives into parameters of performance that can be measured. Thus, through an eleven-point scale (0 to 10) it is possible to compare qualitative parameters, which represents the worst to best possible performance range. The utility scores are then used to classify the performance on the established parameters or objectives of each alternative design proposal. The eleven-point scale used to evaluate the performance of the proposed conceptual solutions for each objective is represented in Table 4-9. Finally, the final stage of this method is to evaluate each alternative design proposal in terms of its performance in the established objectives. In order to accomplish this, the point scores or performance measures on each objective for each conceptual solution must take into account the different weights of each objective. Therefore, the **performance score** is multiplied by the **weight value** of each objective, which provides the result that indicates the relative **utility value** of that alternative for each objective.

Table 4-9 – Eleven-point evaluation scale set to be used for the assessment of the performance of the proposed alternative designs on each objective.

Eleven-point scale	Objective
0	Totally useless solution
1	Inadequate solution
2	Very poor solution
3	Poor solution
4	Tolerable solution
5	Adequate solution
6	Satisfactory solution
7	Good solution
8	Very good solution
9	Excellent solution
10	Perfect or ideal solution

These utility values are then summed for each alternative design and used to compare the proposed conceptual solutions. The total score of the overall performance or utility value of each conceptual solution allows the design team to choose the best alternative, which is the one with the highest sum value. Herewith, Table 4-10 presents the weighted objectives evaluation chart, through which the best conceptual solution for the development of an active AFO for rehabilitation is selected.

In regard to the structure's comfort objective, all solutions consider metallic and soft materials; however, conceptual solutions 3 and 4 ensure a more compliant use of the device, due to the system that couples it to the shoe. This one takes in high consideration the adaptation to the user's ankle joint, which allows for a more comfortable gait. Moreover, solution 3 comprises a width adjustment system composed of a larger area of softer materials, which might provide for a more comfortable attachment.

Table 4-10 – Weighted objectives evaluation chart for the proposed conceptual solutions regarding the SmartOs project. The *utility value* is calculated by the multiplication of the objective’s weight by the performance score of that alternative on each objective. The *overall utility value* is the sum of all utility values concerning each objective. The conceptual solution with the highest value is chosen as the best solution for the project.

Objective	Weight	Conceptual solutions							
		1		2		3		4	
		Performance score	Utility value	Performance score	Utility value	Performance score	Utility value	Performance score	Utility value
Structure’s comfort	8	6	48	5	40	8	65	7	56
Adjustability	5	3	15	3	15	9	45	9	45
Mechanical strength	1	4	4	9	9	4	4	9	9
Lightweight	3	7	21	8	24	4	12	6	18
Proper function	10	5	50	5	50	7	70	7	70
Stability	5	4	20	4	20	7	35	7	35
Overall utility value			158		158		231		233

As aforementioned, solutions 3 and 4 provide for more efficient adjustability, which take into account the anthropometric dimensions of individuals with heights that range from 1.50 and 1.90 meters. While with the first two solutions only one footplate with a certain height regulation would be designed, on the last two, several shoe inserts would be developed to cover the full range of a human ankle's height and thus try to avoid any phenomena of misalignment between the device and the user.

Concerning the mechanical strength objective, all the proposed conceptual solutions would integrate practically the same resistant materials on their structure. Nevertheless, solutions 1 and 3 would incorporate a plastic buckle which would be submitted to the stress caused by the width adjustment. Therefore, even though this sub-solution would provide for more comfortable use, it also would be more subjected to yield.

Although the design of several footplates with different heights tackles the misalignment problem, the larger footplates (with a higher upright) also increase the weight of the device, when compared to the incorporation of a single dimensioned footplate. Hence, solutions 1 and 2 perform better at this objective. Furthermore, solutions 2 and 4 are benefited by their width adjustment system that implements cuts on the shank structure, which aids the decrease of the device's weight.

All of the proposed conceptual solutions comprise the two-degree of freedom articulation, which would be an important component to guarantee the device proper function. However, solutions 3 and 4 incorporate the footplate, which considers the tibiotalar inclination and implements an adjustment system that prevents misalignment. Hereupon these concepts are considered to be a good solution when compared to the ones that do not ponder the anatomical axis. Finally, for the same reason, these conceptual solutions were also assessed as better solutions to ensure orthosis stability.

Herewith, once the overall utility value calculation was finished, the conceptual solution 4 was defined as the best solution to further develop. However, as it will be explained next, it was not possible to design all the parts of the conceptual solution. So, the next chapter will address the detailed design of the selected conceptual solution, with the exception of one part.

5. DETAILED DESIGN

This chapter discloses the detailed design of the conceptual solution selected in the previous chapter for further development. It starts with the clarification of the design process organization regarding the SmartOs wearable structure, followed by the design of each part, disclosing the 3D drawing made in CAD software, SolidWorks®. Furthermore, a structural analysis is performed with the subsequent FEM (Finite Element Method) simulations that allow for design improvements of critical components that fail the tests. These design changes comprise the selection of the materials available for manufacture in Orthos XXI that ensure a better mechanical performance.

Even though that the actuation/articulation system was not part of this thesis scope, the selected electric actuator and gearbox are presented, as well as the electrical components that must be associated with it. Hence, the 3D CAD model is disclosed, but it's important to note that this part of the SmartOs design was developed by a member of the SmartOs design team.

The standard version of the first SmartOs wearable active orthosis prototype is presented, and a comparison of its technical specifications with those of the Exo-H2 ankle module is carried out. Finally, the manufacture of the orthosis pre-prototype is presented, disclosing the initiation of the whole device production.

It is also important to note that the two-degree of freedom apparatus (silent blocks) mentioned in the previous chapter, was not designed as the design team considered that this component wasn't a high priority function to accomplish. Nevertheless, this mechanism was placed in consideration for a future work.

5.1 SMARTOS DESIGN ORGANIZATION

As mentioned in Section 1.4, the SmartOs project comprises four aspects which the final device will ensure. The design of the **wearable active orthosis** is the domain focused by the SmartOs design team, being the main goal the development of the device's structure that warrants a proper attachment and assistance to the wearer. Thereby, one of the first steps into the design process was the structuration and organization of this project's aspect. Hence, the design of the wearable active ankle-foot orthosis was divided into

different parts and assigned it to each design team member. This organization allowed for a more efficient and dynamic working process, which resulted in the assembly of a whole set of solutions provided by different team members.

Herewith the wearable active orthosis was divided into four domains: the shank structure, the fixation structure, the actuation system, and the foot structure. The actuation system domain is unique and the only part that is not customizable to the user's needs. The rest of the orthosis domains comprise the necessary sizes in order to satisfy the user's anthropometric requirements (Figure 5-1).

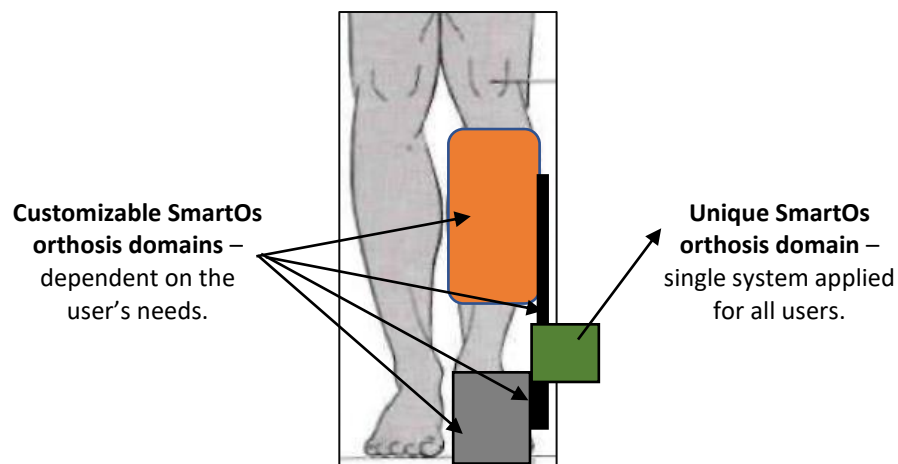


Figure 5-1 – Schematic representation of the SmartOs wearable active orthosis organization into domains, including unique (actuation system – green) and customizable domains (shank, fixation and foot structure – orange, black and grey, respectively).

The module of the **shank structure** includes the 3D drawing of the orthosis's component that will attach to the patient/user's shank, as well as the necessary parts to associate with it, in order to couple to the fixation structure. Furthermore, this aspect also includes the adjustment and fixation system of the shank structure to the user leg's width and the material considered and selected to ensure a proper cushioning of the same part.

The design of the **fixation structure** comprises the drawing of the CAD model regarding both the proximal and distal fixation components, which must ensure an efficient fixation of the shank structure to the actuation system, and the latter to the foot structure, respectively. Moreover, the fixation structure must also include the orthosis adaptation to the user leg and ankle's height. Lastly, the design process wouldn't be completed without the fixation structure 3D drawing validation through simulation tools provided by SolidWorks® software.

The **foot structure** aspect of the wearable active orthosis design includes the shoe selection and the attachment method to couple it to the distal fixation structure. All of the mentioned aspects were assigned to the Orthos XXI design team.

Lastly, the **actuation system** domain was attributed to the University of Porto design team and comprises the DC motor and gearbox selection most suitable for the proposed application. In addition, the 3D drawing of the structure, in which the actuator is to be embedded, is also a crucial task of this design aspect.

5.1.1 ANTHROPOMETRIC DIMENSIONS

As aforementioned, the fixation structure module of the SmartOs wearable orthosis should implement a height adaptation function, to comply with the user's height requirements of the SmartOs project (see Section 4.3). Herewith, a literature study was conducted to obtain the anthropometric values necessary to dimension the fixation structure. Several studies were consulted, addressing not only the anthropometric measures of Portuguese people but also of foreign individuals, especially from the EUA and European countries [184]–[190]. Table 5-1 presents the anthropometric values regarding the human knee and ankle height, and the calf circumference, for individuals with height that range from 1.50 and 1.90 meters.

Table 5-1 - Anthropometric parameters necessary for the dimensioning of the fixation structure, respective description and range of values concerning the height of 1.50 and 1.90 meters, reported in the literature.

Anthropometric parameters and description	Range of values (mm)
Ankle height – Vertical distance between the standing surface and the level of the ankle circumference.	52 – 82[184]–[187]
Knee height – Vertical distance between a footrest surface and the top of the knee of a seated subject. The knee is flexed 90 degrees.	400 – 600[188], [189]
Calf circumference – Maximum horizontal circumference of the calf.	270 – 450[189], [190]

Once the shank structure module is set to be coupled to the user's shank, the height adjustment system needs to approximately comply with the range regarding this anthropometric feature. The previous table discloses the values required for this definition, which can be computed by subtracting the range of values concerning the *ankle height* from the values of the *knee height*. This way, it is known the adaptation that the fixation structure adjustment complex needs to accomplish, which is **17** centimetres (Figure 5-2).

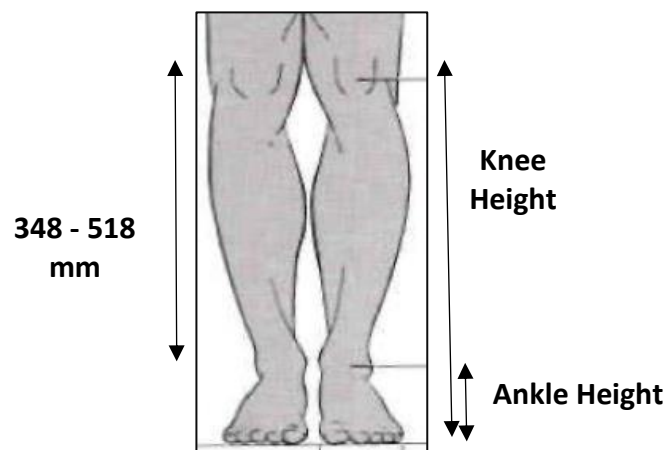


Figure 5-2 - Representation of the anthropometric parameters whose values were collected from the literature, as well as the range of values, respective to the distance between the ankle joint and the top of the knee (in red).

Having defined the adjustment requirement, and due to its high value, the idea proposed by the Orthos XXI design team was to design various sizes of both components that compose the fixation structure, in order to ensure the defined adaptation. However, because the design of several fixation structure sizes implicates a different mechanical dimensioning for each component, it was decided that a proof of concept must be designed first. The proof of concept is developed to demonstrate/verify the feasibility of the SmartOs wearable active orthosis. This orthosis standard version would be projected for **male** users with an **average Portuguese height**, and it would be instrumented with the required electronic components. This way, the design team is able to produce a first standard prototype, optimize and validate it, to further on produce the components necessary to comply with the height adjustment requirement.

According to [191], a male Portuguese average height is 1.73 metres, and thus, the fixation structure will be designed having in mind the approximate anthropometric values for such user's height. Hence, the following section discloses the detailed design of each

of the aspects concerning the development of the proof of concept or standard SmartOs wearable active orthosis.

5.2 COMPUTATIONAL MODELLING OF THE SOLUTION

This section discloses the three-dimensional model construction of the standard SmartOs prototype. The CAD software used is both the versions 2013 and 2019 of SolidWorks®, in order to ensure compatibility with the version used in Orthos XXI Company and the version used by the other members of the design team.

5.2.1 ACTUATION/ARTICULATION SYSTEM

The actuation/articulation system is the only domain of the SmartOs wearable active orthosis that is not customizable to each user's needs, i.e. a single module is applied to all wearers. The rest of the SmartOs modules described posteriorly are to be coupled to both the proximal and distal sides of the articulation system.

Herewith, the first step to develop the actuation system is the electric motor selection. To accomplish this, the human ankle mechanical requirements were explored in order to select the DC motor that better complied the user's needs. So, according to the reviewed literature mentioned in Section 2.3.2 (Figure 2-19 (a)), the necessary torque to provide for a post-stroke patient, in order for him/her to perform a normal stance phase, is approximately 0.8 Nm per kg of the body mass (difference between the peak plantarflexion values at the velocity of 0.78 m/s). Thus, theoretically the provided torque range should be within 36 and 80 Nm (see project requirements in Section 4.3).

Furthermore, the modifications in the ankle angular velocity at various speeds were studied in healthy subjects [192]. This study reported that, at minimum assessed gait velocity of 0.4 to 0.59 m/s (1.44 to 2.12 km/h) the highest mean angular velocity occurs at the pre-swing phase and it's 130 ± 22.87 °/s. Moreover, at the gait velocity of 0.8 to 0.99 m/s (2.88 to 3,56 km/h), the highest mean angular velocity is 234.10 ± 39.81 °/s. As it's specified in Section 4.3, the assisted gait speed is required to range between 0.5 and 3 km/h (0.83 m/s). Thus, the maximum angular velocity for the gait speed of 3 km/h would be **4.09 ± 0.69 rad/s** and, for the required speed of 0.5 km/h, the angular velocity would be less than **2.27 ± 0.4 rad/s**. Due to lack of more information regarding

the angular speed at the minimum required gait velocity, this value was taken into account as a reference for the selection of the actuation system.

Having the ankle nominal torque and angular velocity determined, one can analyse the several commercially available DC motors which are able to conform to these requirements. Hence, the Maxon® motor EC 60 flat 60 mm, brushless, with 200 W (part number 614949) was chosen to integrate the SmartOs active orthosis. The motor data, namely the nominal speed and torque, is presented in appendix E - **Selected DC motor specifications**. Due to the excessively elevated nominal speed (3240 rpm, or 339.3 rad/s), a gear system is required to reduce this speed, and subsequently increase the output torque. The gear units from Harmonic Drive® were regarded as being the best technology to incorporate onto the actuation system, due to its compact design, lightweight and high load capacity. The gear unit CSD Series was selected, more specifically CSD-25-100-2A-GR, which has a mass of 0.24 kg and has a gear ratio of 100.

Table 5-2 discloses the output information of the motor associated with the gear unit. Regarding the **speed**, the actuation system is able to provide 32.4 rpm (3.39 rad/s) of angular speed, which is within the required kinematic range. Moreover, in theory, the DC motor can provide for 6000 rpm of speed if the right voltage is supplied (48V as a reference). Nevertheless, the maximum input speed of the gear unit (with grease lubrication, which is the recommended for the application) is 5600 rpm (see appendix F- **Harmonic Drive® gear unit specifications and efficiency tables**). Hence, the combined output speed of 5.86 rad/s can be achieved, in the case of high-voltage supply.

As to the **torque**, although the DC motor provides for 0.536 N.m of nominal torque, the efficiency of the gear unit at the speed of 3500 reduces it by approximately 60% (see appendix F- **Harmonic Drive® gear unit specifications and efficiency tables**, at 20°C temperature). Thus, the output nominal torque is 32.16 Nm, which is below the required ankle torque. However, a Maxon® collaborator recommends that the DC motor provides 2 to 3 times the nominal torque (1.608 N.m) [193], which corresponds to a maximum output torque of 96.5 N.m at the lowest efficiency of 60%. Once this value is not superior to the repeatable peak torque of the gear unit (110 N.m), it's safe to state that the actuation system can supply for the required torque.

The Exo-H2 implements an EC 60 flat 68 mm, brushless, with 100 W (see appendix G- **Exo-H2 system specifications, efficiency table and side calculations**) associated with a

harmonic drive with a gear ratio of 160 (CSD-20-160-2A-GR). Herewith, the provided nominal torque, at the lowest efficiency of 50% (see the same appendix, at 20°C temperature), was 17.7 N.m and the angular velocity was 24.1 rpm. When analysing the **speed**, the selection of a lower gear ratio allowed for greater output nominal speed (34.4% increase). As to the **torque**, with the new actuation system, the nominal torque was increased by 81.7% and the recommended torque would be 0.663 N.m, which corresponds to a recommended maximum output torque of 53.04 N.m. Therefore, the increase of the power to 200 W and the decrease of the gear ratio allowed an increase of 81.9% of the maximum output torque. These calculations are explored in appendix **G-Exo-H2 system specifications, efficiency table and side calculations**.

Table 5-2 – Comparison analysis between the output data of the selected actuation system for the SmartOs wearable active orthosis and the required data for a human ankle joint.

DC motor: EC 60 flat, 200W		Harmonic gear: CSD-25-100-2A-GR					Combined Output	Required kinematic inputs		Required kinetic inputs
		Gear ratio	Efficiency (20°C, at 3500 rpm)	Nominal torque	Peak torque	Input speed		Gait speed		Peak torque
								0.5 km/h	2.88 - 3,56 km/h	
Nominal Speed	3240 rpm	100	-	-	-	5600 rpm	$\frac{3240}{100} =$ 32.4 rpm (3.39 rad/s)	<2.27± 0.4 rad/s	4.09 ± 0.69 rad/s	-
Maximum Speed at 48V DC	6000 rpm									
Nominal Torque	536 mN.m	60% (approx.)	47 Nm	-	-	0.536×100 $\times 0.6$ $= 32.16 \text{ N.m}$	-	-	36 – 80 N.m	
Peak Torque (Maxon® recommen- dation)	2-3 × Nominal Torque	<60%	-	110 Nm	-	1.6×100 $\times (< 0.6)$ $< 96.5 \text{ N.m}$				

It is worth mentioning that these theoretic output values are fully dependent of the selected battery and controllers, which are not addressed in the present dissertation.

The selected Maxon® DC motor already incorporated hall sensors, which are mainly used to detect the rotor orientation by measuring variations in the magnetic field but can also be used to measure speed. However, an encoder should be also incorporated

to provide data about the angular position, speed, and acceleration of the joint. Several encoders were considered and, between the absolute modular angular encoder MCS 15 and the AkSiM-2™ rotary absolute encoder, the latter one was selected [194]. This encoder stood out for its compactness, with a ring design developed for applications with limited installation space, which is crucial to guarantee a low width of the articulation system.

Hereupon, the 3D drawing of the actuation/articulation system is presented in Figure 5-3 (a) and (b). The encoder was mounted on the output of the motor to measure the joint kinematic values (Figure 5-3 (b)). Moreover, this system will be encased with a structure in order to protect the actuation components against dust (Figure 5-3 (c)). This assembly comprises a proximal and a distal plate to ensure the connection between the actuation system and the proximal and distal fixation structure, respectively.

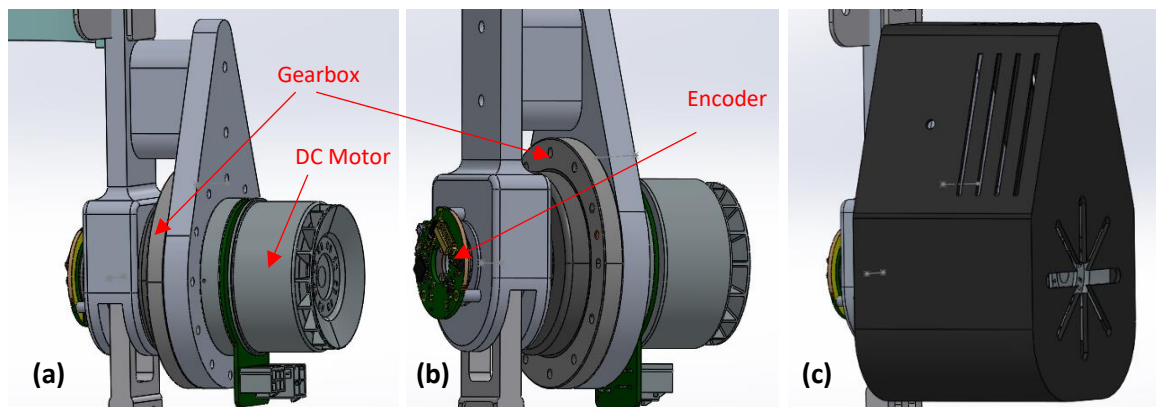


Figure 5-3 - Articulatio/Actuation system CAD model: (a) View of the lateral part of the assembly, (b) view of the encoder's placement, and (c) motor case.

As it is specified in Section 4.3, a safety mechanism has to be implemented in order to limit the range of motion of the system's distal upright. Herewith, a mechanical stop, similar to the ones addressed in Section 3.3.2, was designed to restring the distal part's movement within -20° and 20° , as illustrated in Figure 5-4 (a). To prevent a metallic collision between the components, a rubber material will be placed on the faces highlighted in Figure 5-4 (b).

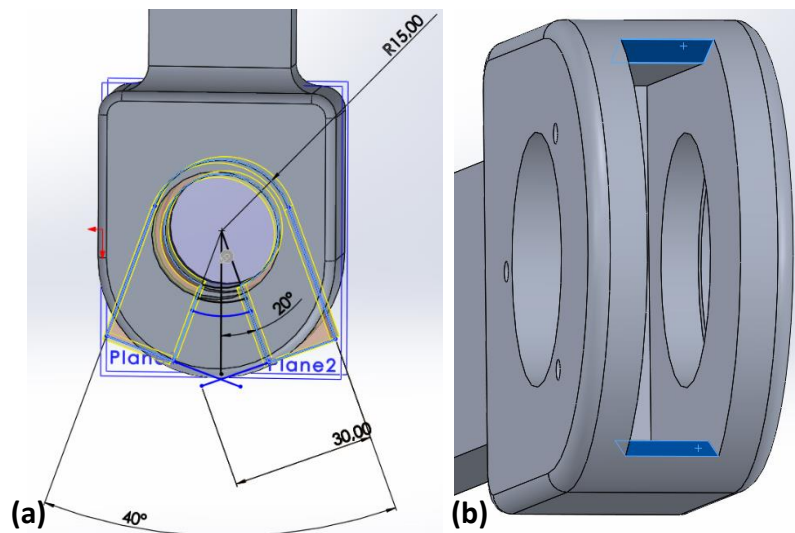


Figure 5-4 – Safety mechanism designed for the SmartOs articulation: (a) Dimensioning of the mechanical stop, showing the limit of 20° in both the posterior and anterior sides of the sagittal plane, and (b) Mechanical stop limits.

5.2.2 SHANK STRUCTURE

As mentioned above, the shank structure is the most proximal component of the SmartOs orthosis, which serves to provide a fixation spot on the user's impaired leg. Thus, this component is essential to ensure an efficient coupling of the device on the wearer, which ultimately contributes to the mitigation of misalignment and to the proper active assistance to the patient's ankle.

For the present master dissertation, an interview with an orthopaedist of Viana do Castelo's hospital was conducted with the purpose of acquiring more insight regarding orthopaedic devices for post-stroke patients. Besides to ensure the comfort of use, Dr. Rita Proença claimed that the orthotic system must respect the ankle's axis of rotation, the shank structure should be coupled to the proximal part of the leg (a few centimetres below the knee), and must permit the adjustment to the height and width of the patient's leg.

One of the attachment structure key aspects defined early on by the Orthos XXI design team was to guarantee a high contact area, as a way of better distributing the stress applied on the user's shank. It was also decided that the shank structure should be attached to the anterior side of the user's leg once it is claimed to provide for more comfortable coupling (as addressed in Section 3.5.1). Furthermore, with the same

purpose it was thought that the shank structure should adapt and fixate to the leg through the maximum number of straps. Hereupon, the shank structure was set to have such a length that would cover approximately $\frac{2}{3}$ of the patient's leg.

Once this idea was established, the 3D drawing of the shank structure could be initiated. Since the standard shank structure should comply with a leg of an average height person, two versions of a shank structure were designed in congruence with a short and large leg, to have a reference for the medium size. Hence, to aid the 3D drawing dimensioning it was downloaded a 3D model of a human leg and created a model based on a leg of a person with 1.50 meters height (once there was not any model available online). The model based on a small human leg was set to be the approximate positive mould for the smallest size (Figure 5-5 (a)). Moreover, after the dimensioning of the online 3D leg model on the SolidWorks® software, it was determined that this would serve as a positive mould for the largest size shank structure (Figure 5-5 (b)). With the smallest and largest shank structures created, the standard size would be designed with the respective intermediate value of length and width. It is worth noting that the shown 3D drawings are designed for the left leg.

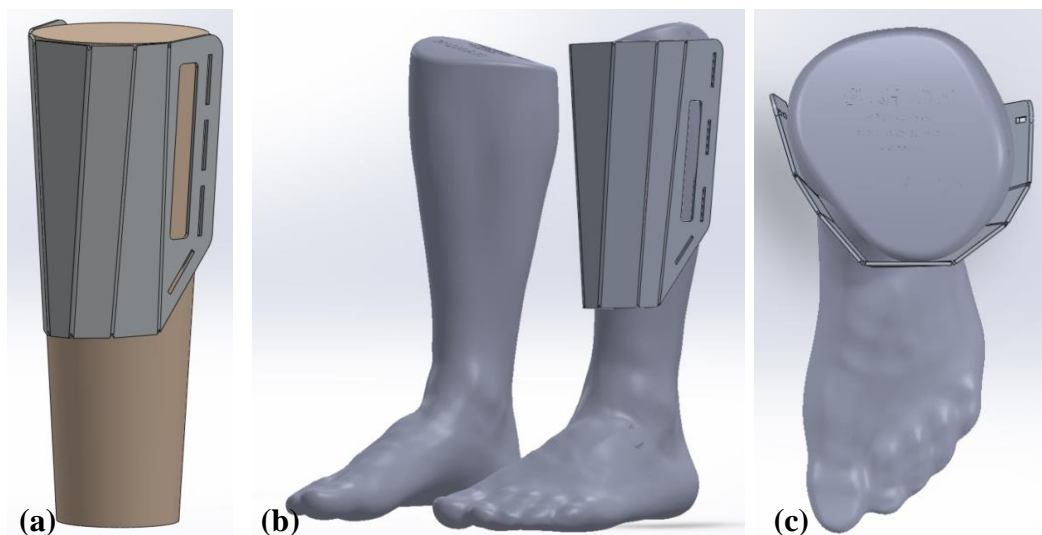


Figure 5-5 – Three-dimensional model of the SmartOs wearable orthosis left shank structure: (a) Isometric view of the smallest size shank structure, attached to an approximate model of a human leg (1.50 meters height); (b) Isometric view of the largest size shank structure, coupled to a model of a large human leg, and (c) Top view of the same shank structure, where are visible the bends of the sheet metal that are designed to resemble the geometry of the human leg.

To avoid circumstances of mechanical mal-functioning, the Orthos XXI design team established that metal would be the material selected to compose the shank structure.

Thus, the SolidWorks® tool *Sheet Metal* was used to design the component once this tool comprises features useful for the adequate drawing and posterior manufacture. For example, the *Sheet Metal* feature *Sketched Bend* allows the designer to add bend lines to the sheet metal so that the part has a folded-up geometry, which should be as approximate as possible to the geometry of the human shank. Through the assembly of the structure with the human shank models available, the bend lines were dimensioned in accordance with the most befitting geometry (Figure 5-5 (c)). Figure 5-6 illustrates the *Sketched Bend* tool used to achieve the shank structure folded-up form, and the input bend parameters. The bend radius parameter had to be defined in congruence with the manufacture requirements of Orthos XXI, which could be consulted in the company's bending table (see appendix **H-ORTHOSXXI bending specifications table**). This table discloses the force needed to be applied by the machine's punch onto a sheet metal with a defined thickness, in order to create a bend with a certain bend radius, tap length and matrix "V" width. Thus, for a sheet metal with a thickness of 2 mm, the advisable bend radius is 2,5 mm, as is shown in Figure 5-6 signalized in bold red.

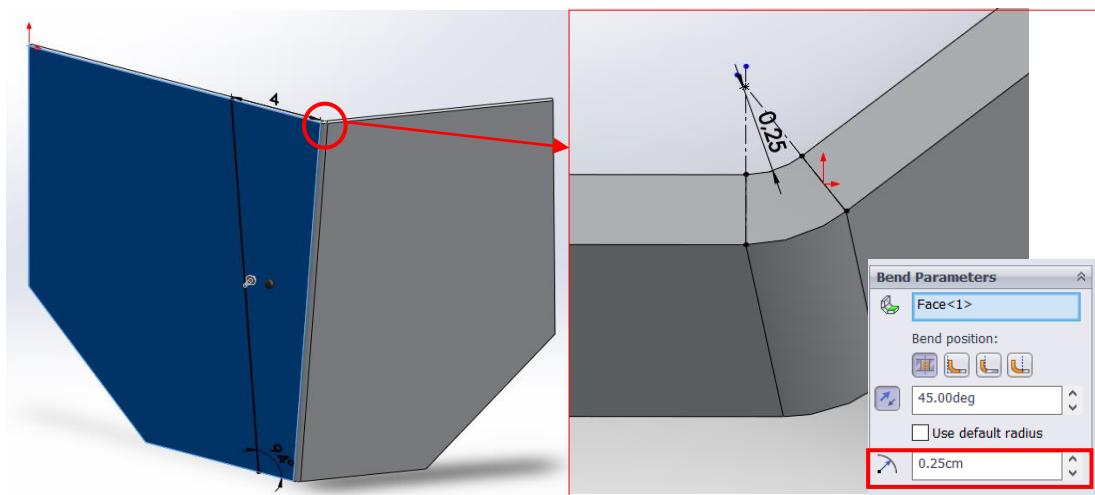


Figure 5-6 – SolidWorks® *Sketched Bend* tool used to create a bend on the shank structure sheet metal, with the bend radius parameter defined accordingly to the manufacture requirements of Orthos XXI.

Furthermore, in order to facilitate the manufacture process, certain design details can be added to the CAD model. As it's represented in Figure 5-7, triangle-shaped cuts were made on the top and bottom part of the shank structures so that the bending machine's punch is properly aligned with the bending centreline defined in the 3D drawing.

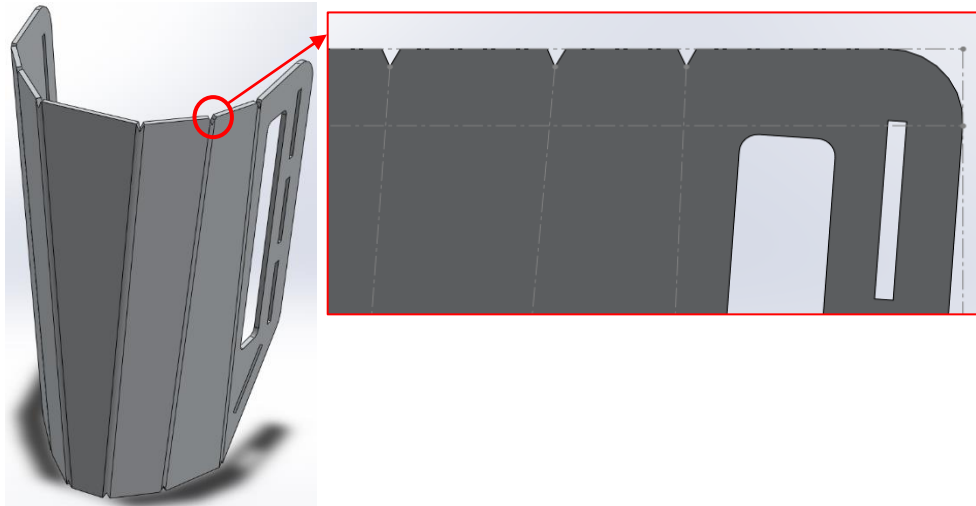


Figure 5-7 – Design detail added to facilitate the sheet metal bending process. This way the machine’s punch can be correctly aligned to the bending centrelines defined to achieve a folded-up geometry.

As it can be observed in the previous figures, four cuts were made on the shank structures, through which straps are going to be inserted for the adjustment of the width. The straps designed were inspired on the straps used in the XSens Motion Capture technology for sensors placement in the human body. Similarly, in addition to the function of adjustment, the straps are also meant to fixate EMG sensors in a specified location of the leg i.e. on the gastrocnemius medialis muscle (Figure 5-8 (a)). Furthermore, another EMG surface electrode needs to be placed on the anterior part of the user’s leg, to measure the activity of the tibialis anterior muscle (Figure 5-8 (b)). Herewith, the shank structure needs to be prepared in a way that considers this electronic component, which is discussed below.

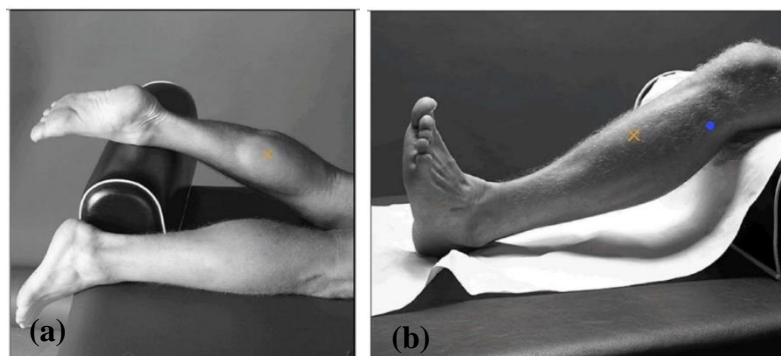


Figure 5-8 – Locations to place the EMG surface electrodes necessary for the technology used in the SmartOs project.

Hence, three groups of straps were formed: the top one, the lower one, and the middle straps, being that each strap group has its length defined in accordance to the leg

circumference values. The middle straps have the additional functionality of having to fixate the EMG sensor (surface electrode) on the calf muscle. Figure 5-9 shows the 3D drawing of a middle strap, composed by the same three different materials used in the XSens strap. The middle strap serves to fasten the shank structure around the half portion of the user's leg with a largest circumference. Having this in mind, according to the values presented in Table 5-1, the width adjustment ranges from 13.5 cm to 22.5 cm, consisting of an adaptation of 9 cm in width, which can be achieved.

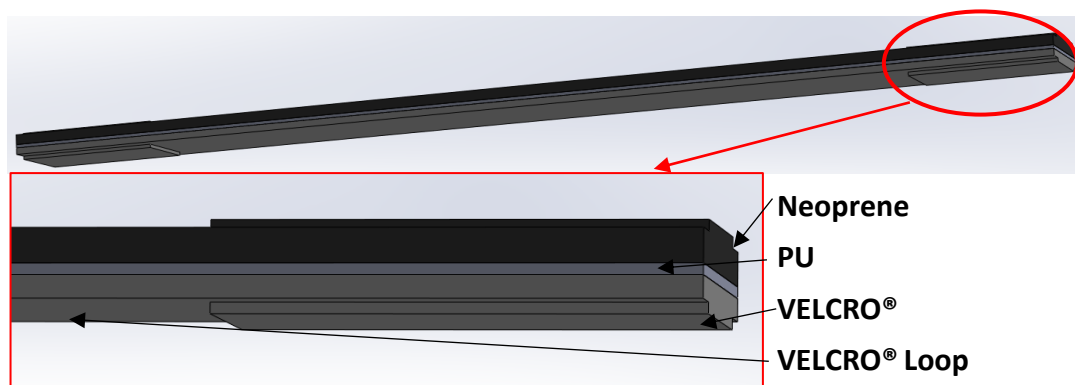


Figure 5-9 – Three dimensional drawing of the middle adjustment strap composed by layers of different materials.

As aforementioned, another EMG sensor needs to be placed on the anterior part of the user's leg. The shank structure requires a lining with a soft material that ensures a comfortable attachment to the user, but also that enables the proper functioning of the EMG sensors. One of the problems reported by the BiRDLAB team member regarding the use of neoprene in straps is that this material overheats, which might cause problems to the EMG electrode. Therefore, the solution found to prevent this phenomena to happen on the middle straps was to reduce the thickness of the neoprene layer as much as possible (2 mm). However, if neoprene was to be used for the cushioning of the shank structure, it wouldn't be advisable to reduce it to such thickness, once the component is in contact with the bony prominence part of the human leg. Thus, gel silicone pads were considered, since its use can be found in several applications that involve skin-contacting sheets to prevent pressure sores [153].

The shank structure incorporates a piece which has the function of coupling the fixation structure, addressed in the next section (Figure 5-10 (a)). Moreover, this part is designed to have a wedge form to assure that the fixation structure is perpendicular to

the ground, and thereby, to the ankle's axis of rotation, as is represented in Figure 5-10 (b).

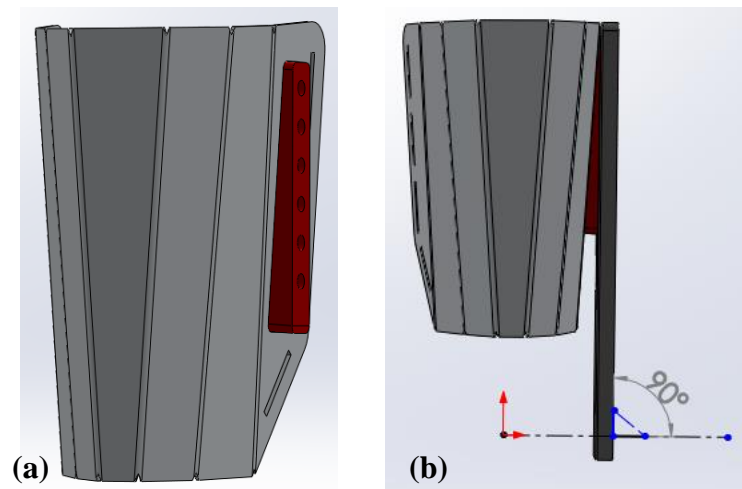


Figure 5-10 – Wedge part (red) incorporated into the left shank structure: (a) Function of coupling the fixation structure, and (b) Function of warranting the perpendicularity of the fixation structure relative to the axis of rotation of the ankle joint.

This section addressed the detailed design of the two sizes of the shank structure that serve as a reference for the design of the **standard** shank structure. In addition, to warrant the accomplishment of the requirement defined in Section 4.3 “Switchable to both right and left foot”, another shank structure for the right leg was designed. The 3D drawing is in all similar, with the exception of the wedge component location that is attached to the right side of the shank structure, as seen in the following Figure 5-11.

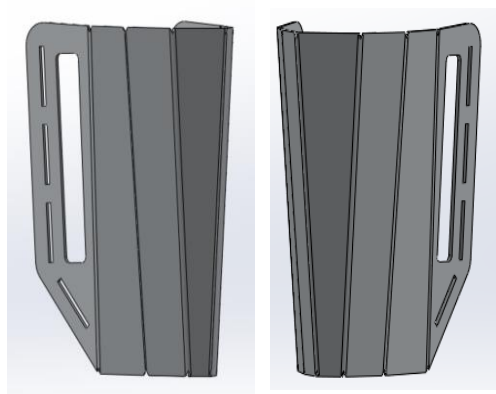


Figure 5-11 - CAD models of the standard right and left shank structure, respectively. These components were designed by using the smallest and largest size shank structure as a reference.

5.2.3 FIXATION STRUCTURE

The fixation structure component of the SmartOs wearable orthosis comprises the proximal upright, which allows the connection between the shank structure and the orthosis articulation, and the distal upright that link the latter with the foot structure. The present subsection addresses the setting process of the fixation structures into the other components of the wearable orthosis, as well as the height regulation system.

5.2.3.1 PROXIMAL FIXATION STRUCTURE

Starting up with the proximal fixation structure, this orthosis part must provide the connection between the actuation/articulation system and the shank structure by fixating them with a series of bolts. This rather simple linking method came about to solve a problem regarding the fixation system of the Exo-H2, which implemented a continuous height regulation structure (two bars pushed one inside the other – sliding system). This system was reported to experience some wear and failure, which jeopardized the entire fixation structure. Figure 5-12 and Figure 5-13 show the installation process of the standard proximal upright into the orthosis articulation system and the shank structure. The first step of the setting is to couple the lower part of the upright to the top part of the actuation system by using M6 bolts and nuts to hold both structures together (Figure 5-12).

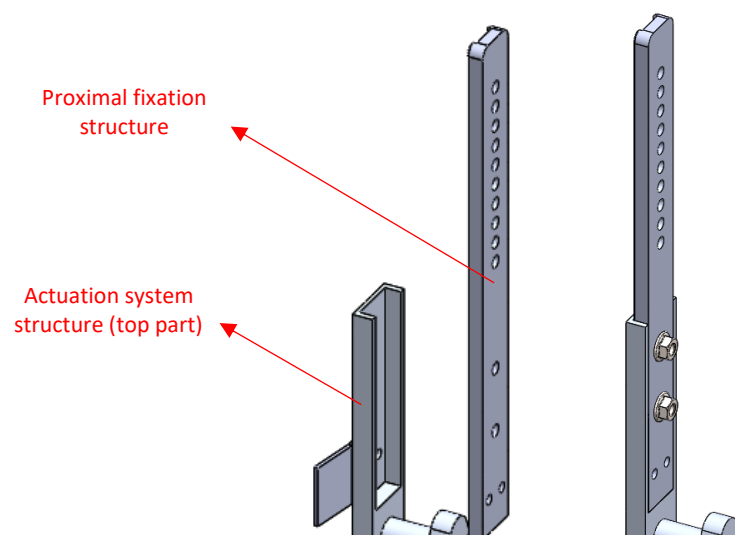


Figure 5-12 – First step of the proximal fixation structure setting process: fastening of the upright to the actuation system through M6 bolts and nuts.

Subsequently, the connection of the proximal upright to the wedge component of the shank structure is executed with two hex M6 bolts, being possible to extend to a fixation with three bolts. These mechanical components are inserted through the inside of the shank structure and tightened with a selected nut from the lateral side (Figure 5-13).

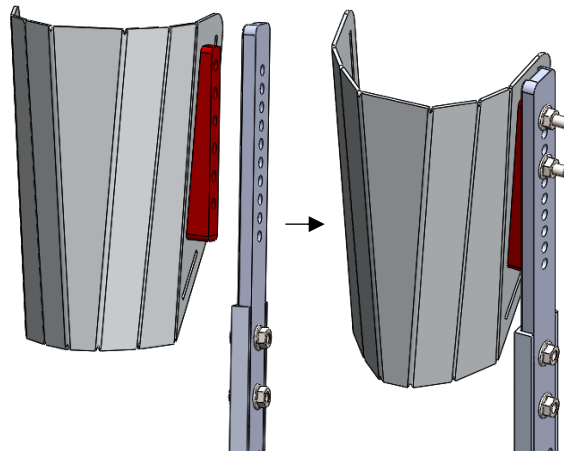


Figure 5-13 – Final phase of the proximal fixation structure installation: fastening the shank structure to the upright through two M6 bolts, with the possibility to increase the fixation to three bolts.

After a group discussion concerning the placement location of the shank structure, it was defined that the top part of this component would be placed approximately 10 cm below the top part of the knee. This definition would serve as a reference for the height regulation system, to validate the accomplishment of the defined range of height values for the standard fixation structure. Having this in mind, the shank height of a person can be measured from the lateral malleolus of the ankle joint to a point below the knee joint. According to the study conducted by Arezes et al. the knee height of a person with an average height of 1.70 m is 53 cm [188]. Furthermore, by subtracting this value to the approximate ankle height of a person with the same stature, the shank height can be computed. The estimated value of 46.3 cm was obtained.

The standard shank structure designed would have the wedge component welded to it, which allows a height adaptation of 4.5 cm, as is illustrated in Figure 5-14. The height fixation is done in pairs through the fastening of bolts, which are distanced 1.5 cm apart from the next level. Thus, this apparatus consists in a level-based height adaptation and a pair fixation system, which is suggested to enhance the overall adjustment technique, preventing bolts' loosening and wear.

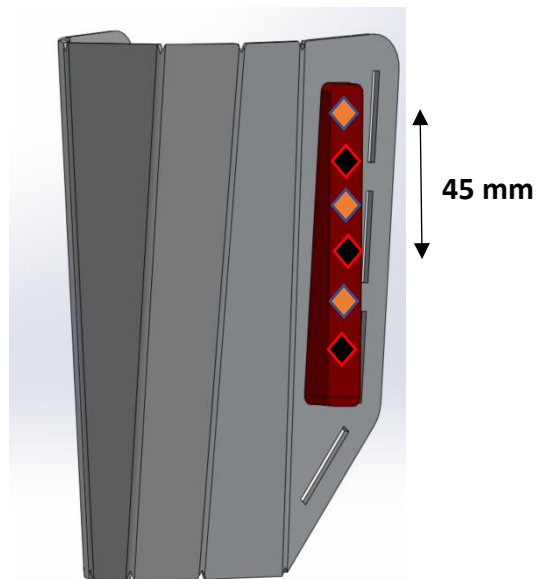


Figure 5-14 – Height adaptation ensured by the wedge component (red) integrated on the shank structure. The level-based bolt fixation made in pairs allows for a height adaptation of 4.5 cm.

Having in mind the reference point settled for the shank structure placement mentioned above and the height adaptation ensured by the same structure, the proximal fixation structure should provide for a height adjustment ranging from **35 to 39.5** cm. Herewith, Figure 5-15 illustrates the process of the height regulation system designed for the standard SmartOs wearable orthosis.

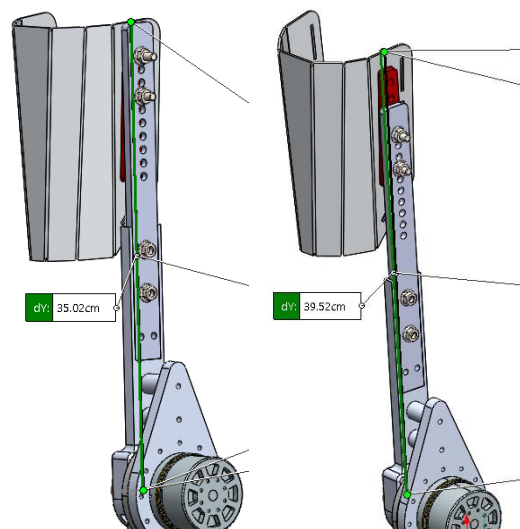


Figure 5-15 – Height adaptation system implemented on the SmartOs wearable orthosis, with the standard proximal upright, ensuring the height adjustment from 35 to 39.5 cm. The measurement is executed from the centre of the articulation system to the top of the shank structure.

After a discussion amongst the members of the SmartOs design team on whether the shank structure's straps were sufficient to ensure a proper attachment of the proximal

fixation structure to the user, the conclusion reached was that another strap was needed. This strap must be located as close as possible to the orthosis articulation to guarantee a more rigid fixation. Hence, a metal plate was designed to be screwed on the proximal motor bar, to which it will be attached a distal strap (Figure 5-16 (a)). The idea is similar to the one implemented on Exo-H2 (Figure 5-16 (b)).

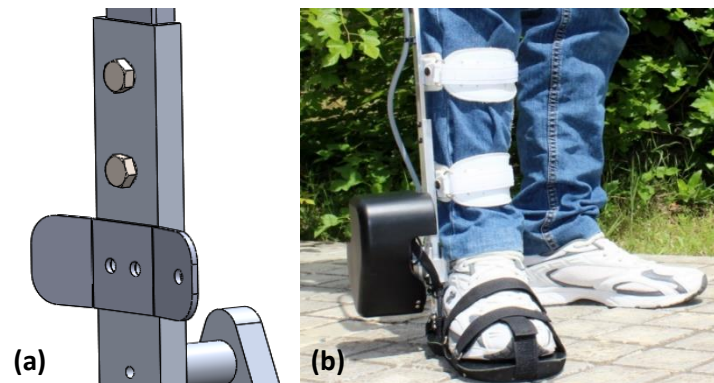


Figure 5-16 – Metal plate to incorporate a distal strap, which will serve as an additional fixation location to ensure a proper attachment of the proximal fixation structure to the user.

5.2.3.2 DISTAL FIXATION STRUCTURE

There are two important aspects regarding this structure of the SmartOs wearable orthosis: its capability to align and comply the orthosis axis of rotation with the ankle joint's tibiotalar axis of rotation. The former ability is achieved by the regulation system within the sheet metal shoe insert. The adjustment of the actuation system is a crucial feature of the device, as it ensures the proper alignment between the active assistance and the patient's anatomical axis of rotation. Herewith, it becomes essential as well that the height regulation system of the distal fixation structure warrants a flexible and reliable adaptation. Having this in mind, as opposed to the proximal fixation structure, it was implemented a continuous height adaptation system (sliding system), fastened through bolts to the plate that ensures the connection with the motor.

Additionally, the compliance of the device axis of rotation with the tibiotalar axis of rotation is accomplished through the inclination of the bottom part of the metal shoe insert. The degree of tilt of the structure was debated amongst the SmartOs consortium members, especially with LABIOMEPE director Professor João Paulo Vilas-Boas, resulting in the decision of implementing a maximum degree of inclination of 5° (Figure 5-17). The

arguments presented in favour of the selected inclination were as follows: one should never try to perfectly imitate an anatomical joint, as it is immensely complex; one should always try to ensure the compliance of devices that are set to be used by an individual; and finally, the only way to validate a concept is to test it.

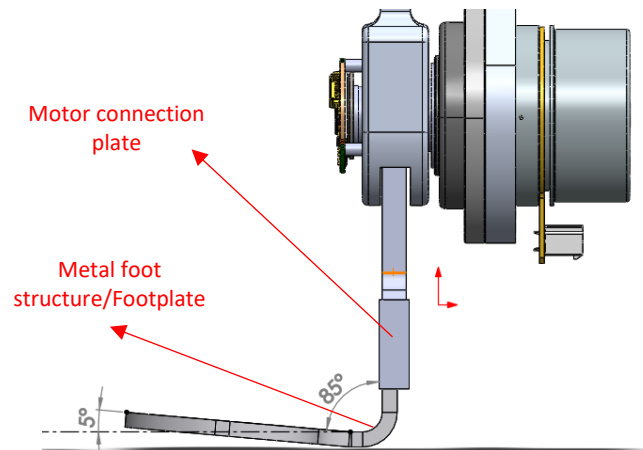


Figure 5-17 – Metal foot structure angle of inclination relative to the ground (left value) and the motor connection plate (right value).

An opening had to be designed on the motor connection plate for the strain gauge. It was advisable to incorporate this latter component into the part that experiences a constant strain, in order for this device to measure the deformation more effectively (Figure 5-18). Subsequently, the metal foot structure would be coupled to this component through M6 bolts to ensure a safe fixation.

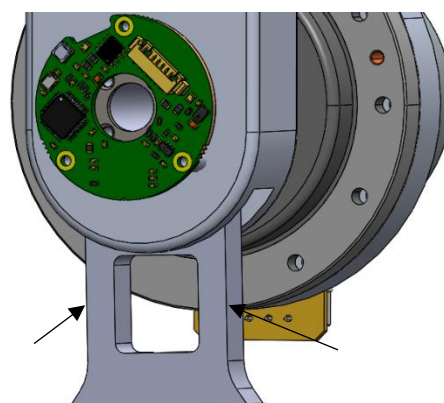


Figure 5-18 – Strain gauge position spots on the sides of the hollow designed on the motor connection plate, to evaluate the strain of the same part during the standard orthosis use.

As mentioned above, a continuous height adaptation system (sliding system) was implemented on the distal fixation structure to warrant a more flexible regulation. To

ensure a safer fixation, 4 bolts were implemented and, so, this system is projected to regulate **5 mm** in height, as it is illustrated in Figure 5-19.

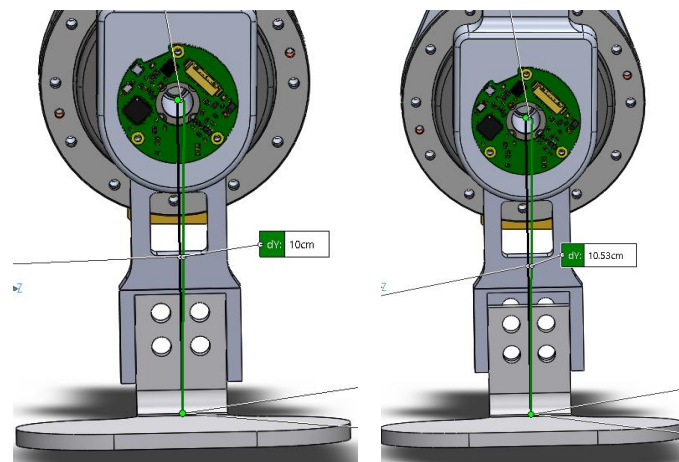


Figure 5-19 – Height regulation system implemented on the distal fixation structure. The dimensioning of this system was executed in congruence with the one designed for the established ankle orthosis, Exo-H2.

5.2.4 FOOT STRUCTURE

Another problem related to walking with the Exo-H2 reported by the BiRDLAB team was the discomfort felt with the implemented solution for the foot structure. The Exo-H2 incorporated articulated footplates into rubber outsoles, on top of which the user would attach and fix their shoe with VELCRO® straps.

To come up with a solution to this adverse characteristic, the Orthos XXI design team suggested the use of a shoe instead of an outsole. The metal plate showed in the previous section would be inserted into the sole of the selected shoe and safely screwed to it. This concept is based on the foot structure implemented on HAL-5 (see Figure 3-13 (a) of Section 3.3.4). The shoe would be customizable to each user, which would consist in not only a more comfortable solution but also a more hygienic one. Figure 5-20 illustrates the foot structure, showing a model of the shoe's outsole, fixated to the distal upright through a medial metal plate. These two components are fastened with two M3 screws. An insole with embedded FSR is set to be placed on this structure to monitor the interaction with the floor. This information is further used for the segmentation of the different gait phases.

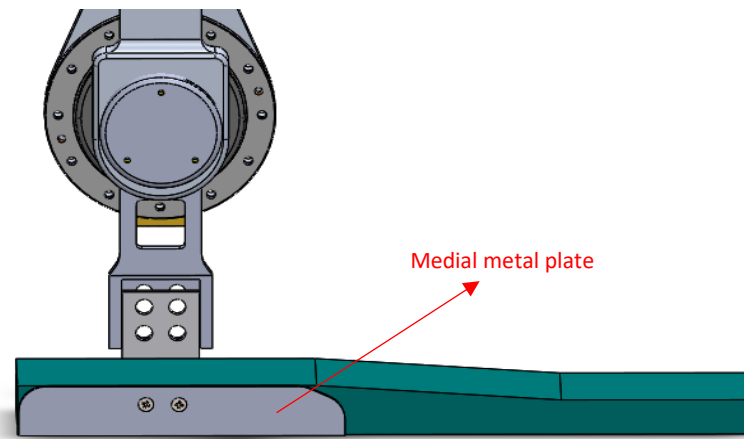


Figure 5-20 – Foot structure CAD drawing, showing the shoe's outsole model to which a medial metal plate is screwed to the distal upright.

5.3 MATERIALS AND STRUCTURAL DIMENSIONING

As already referred, the design and construction of the wearable ankle-foot orthosis integrated in the SmartOs project was based on a produced active AFO – Exo-H2 (Technaid S.L., Spain). The necessary design changes to the already established exoskeleton were made, in order to ensure that the new prototype would respond positively to some of the problems faced by the H2. Herewith, the materials chosen to compose some of the components were different than those of the H2, as it's discussed in the next subsection.

Furthermore, once the standard version of the SmartOs wearable orthosis CAD model was developed, it became necessary to submit the critical components of this model to a finite element analysis (FEA) to assess their performance in pre-defined situations. Thus, the SolidWorks® Simulation tool (more specifically, the linear static analysis) was used to test the 3D drawing.

5.3.1 MATERIALS SELECTION

Exo-H2 lower limb exoskeleton's principal structure materials are stainless steel and aluminium alloy 7005. According to the information available online, the several existing types of stainless steel present a volumetric mass density that ranges from 7.6 to 8 g/cm³, which corresponds to an excessively heavy metal. On the other hand, the type 7005 aluminium's mass density is around 2.9 g/cm³. Moreover, this 7000-series aluminium alloy presents a Young's modulus of 70000 MPa, a Poisson's ratio of 0.33 and a yield strength that ranges from 95 to 350 MPa [195].

Due to the rather low mass density and good mechanical properties, aluminium was the metal selected to compose the SmartOs structure. The three aluminium alloys currently used for production in ORTHOS XXI are: Al 5083, Al 5754, and Al 6082. However, another aluminium alloy with a higher mechanical strength was considered to compose the structure's components subjected to higher tensions: Al 7075. Table 5-3 presents the mechanical properties of the mentioned aluminium alloys, which are necessary inputs for the SolidWorks® static simulation.

Table 5-3 - Mechanical properties of the aluminium alloys available and currently used for production in ORTHOS XXI [196]–[200].

Aluminium alloy	Mechanical Properties			
	Elastic (or Young's) Modulus (MPa)	Poisson's Ratio	Mass Density (g/cm ³)	Yield Strength (MPa)
Al 5083-H111	71000	0.33	2.66	115
Al 5754-H111	70500	0.33	2.68	80
Al 6082-T651	70000	0.33	2.70	240
Al 7075-T651	71000	0.32	2.80	475

5.3.2 CRITICAL COMPONENT SIMULATION AND DESIGN CHANGE

Once the standard version of the SmartOs wearable orthosis was achieved, its CAD model had to be subjected to a validation process, to ensure its reliability. Thus, the components submitted to the highest loads, and which fracture or yield would lead to the compromise of the whole device, were selected to be tested.

SolidWorks® Simulation is a FEA program built into the software's interface that allows designers to test their designs and iterate on them. This program comprises several simulation tools such as linear static, fatigue, thermal, frequency analysis and much more. The simulation tool selected was the linear static analysis, which subjected the components to steady-state load conditions to quickly analyse and iterate designs based on stress, displacement, strains and factor of safety results [201]. The linear static analysis makes a few assumptions such as that loads are applied slowly and gradually until they reach their full magnitudes, where they remain constant; all materials in the model

comply with the Hooke's law (stress is directly proportional to strain); and that the induced displacements are small enough to ignore the change in stiffness caused by loading [202].

From the various components of the SmartOs orthosis, it was selected for simulation those which its yield would compromise the whole device's function. Hence, both the proximal and distal fixation structures were submitted to a static simulation, to ensure that the performance of such parts under the maximum load would not jeopardize the patient's safety.

5.3.2.1 PROXIMAL FIXATION STRUCTURE

Regarding the proximal fixation structure, it was defined that it should support a torque of approximately 65 N.m (twice the actuation system's nominal output torque) without experiencing yielding. The project team decided to not use the maximum torque required (80 N.m) to avoid oversizing the mechanical structure. Thus, the standard upright was tested, simulating with different materials to assess which one would warrant a superior FOS. Moreover, the bolts that hold the parts together are also analysed to evaluate the best fixation conditions.

To simulate the proximal upright, the shank structure was excluded from the analysis, since it would save processing time, and the wedge component was fixed. The *Fixed Geometry* option sets all translational degrees of freedom to zero, and, once the wedge component is welded to the shank structure, this option was used on the face coincident with it. Additionally, the same option was used on the distal strap metal plate, to simulate the fixation with this piece.

Regarding the contact condition, the *Global Contact* and *Bonded* option was selected to save computing time, and this way the whole assembly acts as one part. In order to simulate a more realist condition and also to reduce the computing time, *Contact Sets (No Penetration and Surface to Surface Contact)* were defined to ensure that both the coincident faces of the wedge component with the upright, and the latter one with the actuation system are in contact. Moreover, a *Bonded Contact Set* was defined between the distal strap and the actuation system so that the fixation between these two components is not computed. This fixation will be validated further on.

To assess the bolts that would link the upright, wedge component and the actuation system plate, *Bolt Connectors* were used. This functionality allows the definition of the bolts' strength data and pre-load conditions, which provides a more realistic analysis. Herewith, for each bolt connector, the tensile stress area and the pre-load conditions were defined in accordance with the tables presented in **I-Bolts mechanical properties information**. The calculation of the pre-load condition was executed through the following mathematical equations:

$$\text{Equation 1: } F_i = 0.75 \times F_p$$

$$\text{Equation 2: } F_p = A_t \times S_p$$

$$\text{Equation 3: } T = K \times F_i \times d$$

where, F_i is the axial pre-load, F_p is the proof load, A_t is the tensile stress area, S_p is the proof strength, K is the friction coefficient, d is the bolt diameter, and, finally, T is the pre-tension applied to the bolt. The proof load is computed through the values presented in Figure 8-9 and Figure 8-10, and the value of the friction coefficient can be discovered in Figure 8-11. Galvanized steel bolts have a friction coefficient of 0.2. The definition of the simulation's conditions of the proximal upright is illustrated in Figure 5-21.

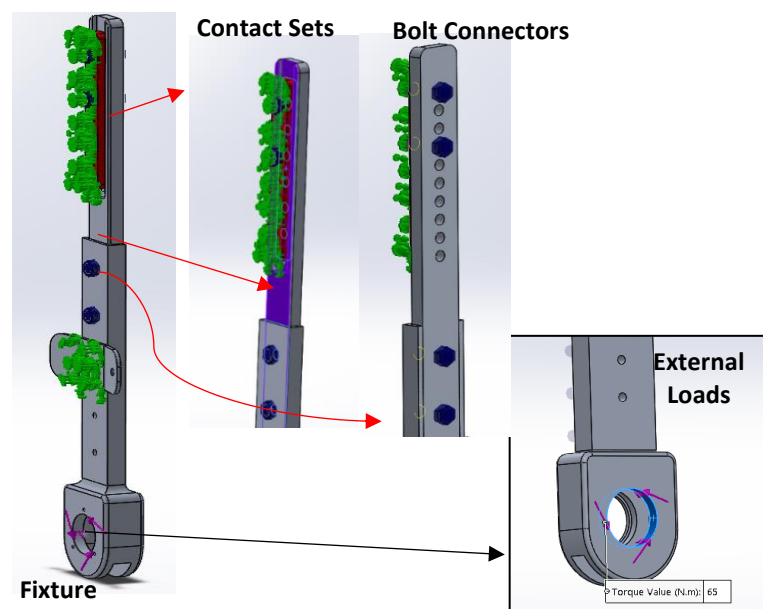


Figure 5-21 – SolidWorks® Linear Static Analysis definition of the simulation's conditions of the proximal fixation structure: Fixtures, Connections (including Contact Sets and Connectors) and External Loads.

Once the simulation conditions were established, it was defined the discretization of the model with parabolic tetrahedral solid elements (*High quality mesh*). Parabolic

elements are reported to yield better results, as they represent curved boundaries more accurately and produce better mathematical approximations. A *Standard mesh* was set with an element global size of 5 mm, in order to save computational resources and the resolution time.

A first FEA analysis was conducted with aluminium alloy 5083-H111 as the composition material of all structural components and galvanized steel as the bolts' material (yield strength of approximately 204 MPa and computed pre-load of 4.1 N.m). Figure 5-22 (a) shows the von Mises stress obtained and Figure 5-22 (b) and (c) present the FOS results of the actuation system structure and the upright fixation method with the wedge component (with two bolts M6), respectively. The highest von Mises stress was applied on the actuation system upright and, as one can verify with Figure 5-22 (b), the minimum FOS of this structure is 1.282. Since it is advisable that the FOS is superior to 1.5, the aluminium alloy selected needs to have a superior yield strength. Furthermore, Figure 5-22 (c) shows that fixating the structures with two M6 galvanized steel bolts does not provide for a reliable FOS, and, thus, a third bolt needs to be incorporated to distribute the tensions more effectively. Therefore, the second trial of simulations will assess Al6082-T651 as the structure material and a fixation with three M6 bolts.

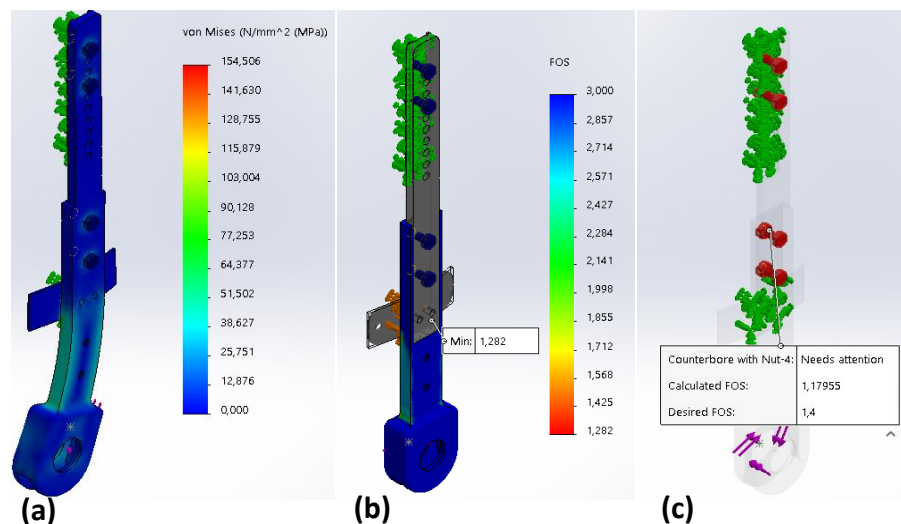


Figure 5-22 - Linear Static Analysis with SolidWorks® Simulation tool used to assess the proximal fixation structure composed by aluminium alloy 5083-H111: (a) von Mises stress results after applying a torque of 65 Nm, (b) Factor of safety (FOS) results regarding the actuation system structure, and (c) FOS results regarding the fixation of the upright to the wedge component and the actuation system with two galvanized steel bolts. The red colour means that the calculated FOS is inferior to the desired FOS.

Figure 5-23 (a) shows the improvement achieved with the change of the material that composes the actuation system connection, where the calculated FOS increased to 2.671. In contrast, the additional M6 galvanized steel bolt still does not provide for the desired FOS, as the computed value range from 1.1 to 1.18 (Figure 5-23 (b)).

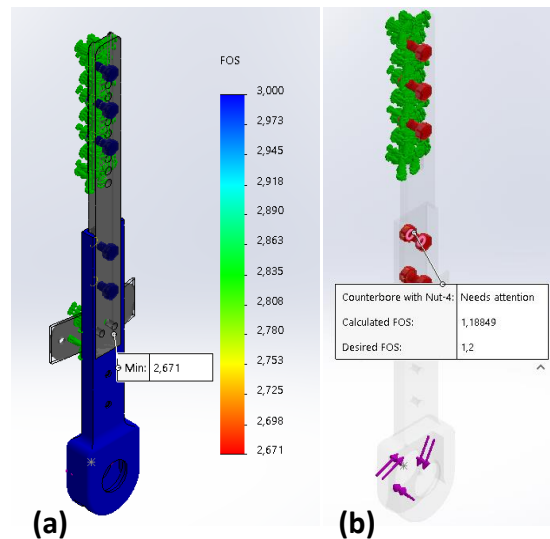


Figure 5-23 - Linear Static Analysis with SolidWorks® Simulation tool used to assess the proximal fixation structure: (a) FOS results regarding the actuation system structure composed by Al6082-T651, and (b) FOS results regarding both the fixation of the upright to the wedge component (with three M6 galvanized steel bolts) and to the actuation system.

Since it was noticeable that the yield strength of the steel had to be increased, a bolt of class 8.8, which is a medium carbon steel, quenched and tempered, was selected. Although in the Shigley's table, presented in the appendix **I-Bolts mechanical properties information**, a class 8.8 bolt size ranges from M16 to M36, in accordance with ISO898-1:1999, this property class of steel bolts ensures a minimal yield strength of 640 MPa to all sizes below 16 mm (diameter) [203], [204]. The pre-load had to be updated with the class 8.8 proof strength values. Hence, a final simulation was carried out with two property class 8.8 M6 bolts to validate this design change.

Figure 5-24 (a) illustrates the increase of the FOS when this type of bolts is incorporated. Although the computed FOS was not 1.5, it was concluded amongst the design team that the fixation would still be reliable. In addition, a simulation was performed to evaluate the distal fixation with the additional strap, by removing the *Fixed*

Geometry option from the metal plate of the strap. Results show that this fixation is needed to warrant a safe shank structure's fixation (Figure 5-24 (b)).

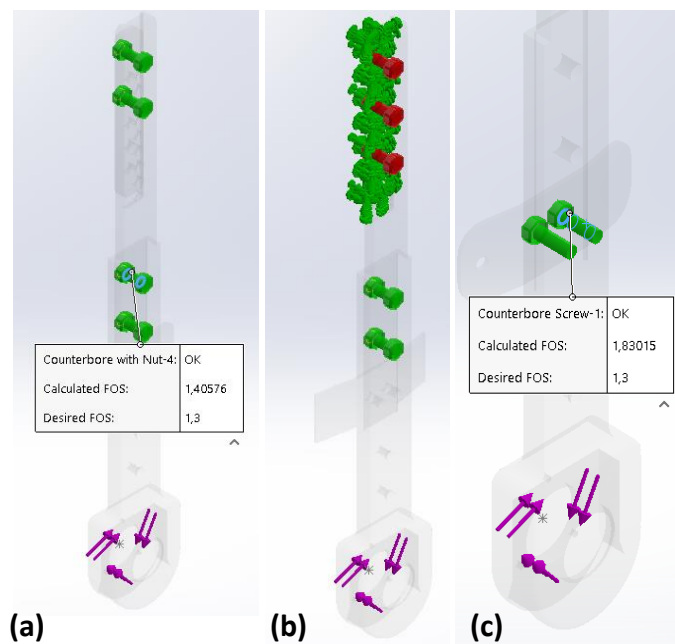


Figure 5-24 - Linear Static Analysis with SolidWorks® Simulation tool used to assess the proximal fixation structure: (a) FOS results regarding the fixation of the upright with M6 class 8.8 steel bolts to the wedge component and to the actuation system, (b) FOS results of the bolts when the distal strap fixation is removed, showing that this additional component is needed to ensure a safer connection to the user, and (c) Validation of the distal strap metal plate fixation with M5 screws.

Finally, the fixation of the metal plate for the distal strap to the structure was assessed separately to save computing resources and time. Herewith, two M5 screws were defined to perform the fixation, and the simulation FOS results show that these components are able to ensure a proper fixture (Figure 5-24 (c)).

5.3.2.2 DISTAL FIXATION STRUCTURE

Similarly, the distal fixation structure was submitted to a static simulation to evaluate its performance with the torque of 65 N.m. The results of the von Mises stress, displacement and FOS were assessed, and the necessary design changes were conducted in order to obtain the most favourable FOS.

To simulate only the results of the maximum torque exerted by the actuator, the *Fixed Geometry* option was applied onto the bottom face of the footplate. Moreover, due to the program's incapacity to define *Bolt Connectors* in a situation of continuous bolt hole, *Rigid Connectors* were used to simulate the footplate fixation to the motor

connection plate. Furthermore, a *Global Contact of No Penetration* was defined to the components of the assembly which were initially touching. This way is prevented the interference between the motor connection plate and the metal foot structure. *Contact Sets* were defined between the non-touching faces of the footplate and the bolts representative components. The *Bonded* option was selected so that the stresses are more concentrated in the location of interaction between the motor connection plate and the bolts since these parts are joined together (“welded”) with the footplate (Figure 5-25).

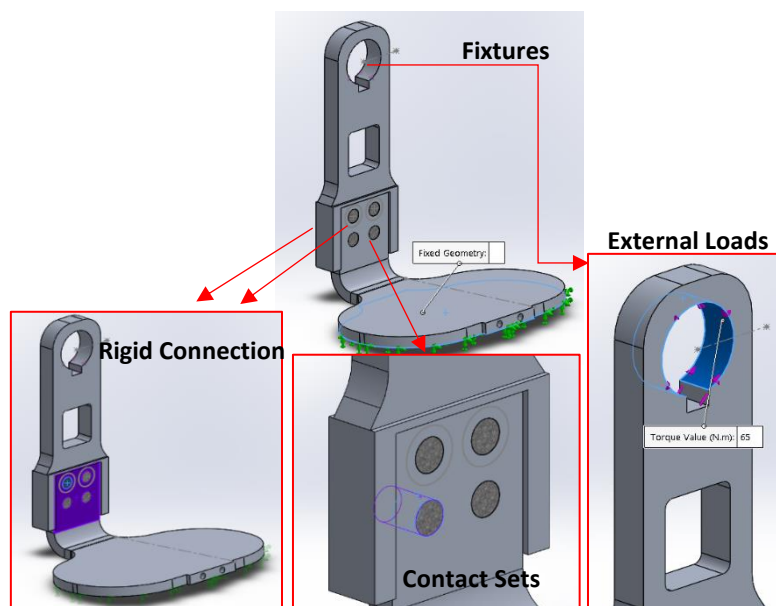


Figure 5-25 - SolidWorks® Linear Static Analysis definition of the distal fixation structure simulation's conditions.

The quality of the mesh was also established at the high option, but with the parabolic element global size set to 3 mm and the option *Curvature-based mesh* selected, so that the mesher creates more elements in higher-curvature areas automatically (without need for mesh control). In addition, since the metal foot structure/distal upright was modeled with sheet metal features, the simulation program automatically treated the part as a sheet metal. This means that the part was converted to a shell mesh which greatly reduces the overall size of the mesh, as the shell elements only mesh the exterior surfaces of the sheet metal geometry and take into account the thickness during the calculation [205].

Moreover, the aluminium alloys used for the first test were Al5754-H111 for the shoe insert and Al5083-H111 for the motor connection plate. The first aluminium type

was used because it's the material currently used in ORTHOS XXI for the CNC Laser of sheet metals with thickness below 8 mm. In addition, it's important to note that the distal upright's thickness is 5 mm, which is twice the thickness defined for the Exo-H2 footplate. The material primarily selected for the bolts was galvanized steel. Figure 5-26 (a) shows the FOS results regarding the motor connection plate, where one can verify that a change of material must be implemented, in order to ensure that the working stress is higher than the material's yield strength. In addition, the factor of safety results concerning the galvanized steel bolts also show that these components would yield under such loads (FOS of 0.863, see Figure 5-26 (b)).

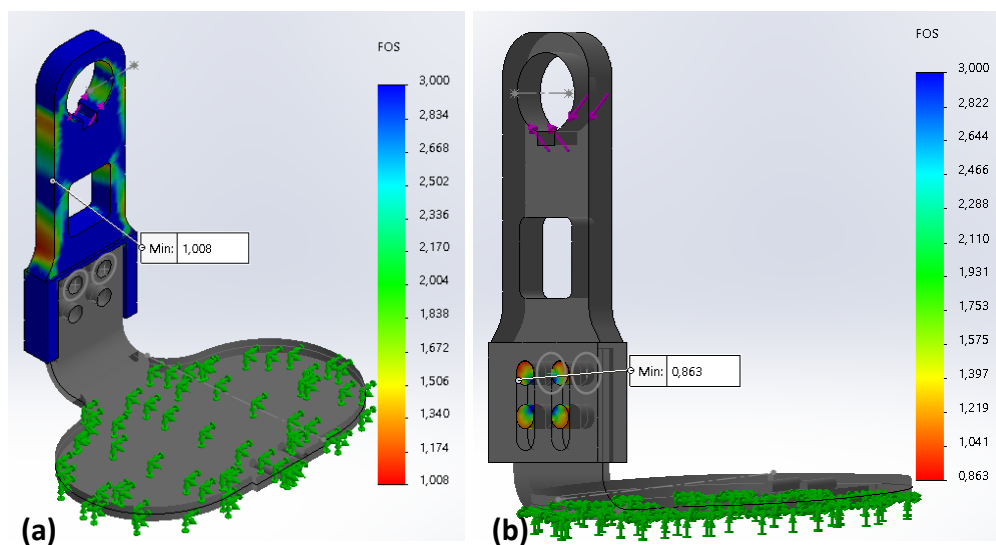


Figure 5-26 - SolidWorks® Linear Static Analysis results: (a) FOS results regarding the motor connection plate composed by Al5083-H111, and (b) FOS results of the galvanized steel bolts.

Having these results in mind, the aluminium alloy selected for the motor connection plate was changed to Al6082-T651 and the pieces representing the bolts were defined as being class 8.8 steel bolts. Figure 5-27 (a) shows that the minimum FOS of 1.29 is found on the strain gauge opening, indicating that the higher stresses are concentrated on the edge of this hollow. Therefore, a design change was implemented, in which the rounded corners of the strain gauge opening were increased, as well as the lateral edges. This way, a minimum FOS of 1.573 was achieved (Figure 5-27 (b)). Finally, the minimum FOS regarding the bolts was immensely increased from 0.863 to 1.55, which consists of a satisfactory result, once it represents that the class 8.8 bolt fixation is able to ensure a safe connection between the parts (Figure 5-27 (c)).

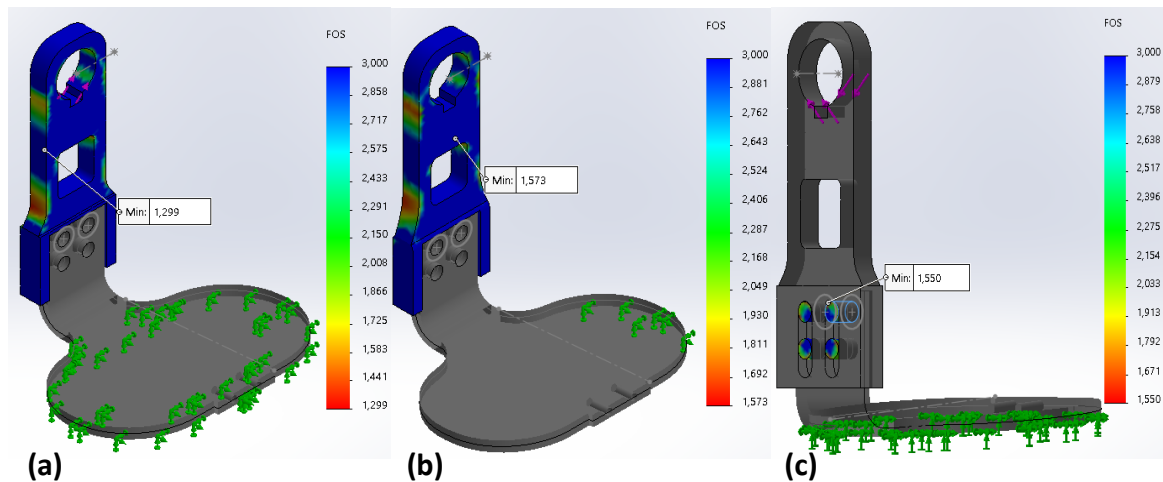


Figure 5-27 - SolidWorks® Linear Static Analysis results: (a) FOS results regarding the motor connection plate composed by Al6082-T651, (b) FOS after the design changes implemented on the motor connection plate, and (c) FOS results of the class 8.8 steel bolts.

Lastly, the strain gauge must be integrated in a place that experiences constant deformation. Thus, the strain was computed and, as illustrated in Figure 5-28, the deformation remained constant on the lateral sides of the device's opening, which is indicative that the strain gauge is placed correctly.

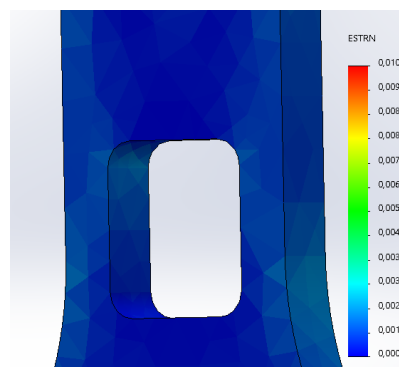


Figure 5-28 - SolidWorks® Linear Static Analysis strain results on the strain gauge opening, showing that the strain gauges can be placed its lateral sides, due to the constant deformation.

5.4 DISCUSSION OF THE RESULTS

The present master dissertation main purpose was to design and validate a first prototype of the SmartOs wearable structure, which assembled four components, each with a different function. With the CAD model developed and validated in a simulation environment, a design comparison with the Exo-H2 can be executed to assess the solutions implemented to tackle the main exoskeleton's problems. Herewith, this section will disclose the principal improvements achieved with the standard SmartOs design.

Lastly, the SmartOs wearable ankle-foot orthosis features are presented, which include the actuator specifications (motor and gearbox), structure materials, the implemented sensory system and the device's weight.

5.4.1 COMPARISON WITH EXO-H2

The SmartOs wearable active orthosis was designed with the Exo-H2 problems in mind, in order to improve certain functionalities of the exoskeleton. One of the main issues regarding the established orthosis was the fixation mechanism of its uprights, which experienced bolts loosening and wear, as reported by the BiRD LAB team. To tackle this problem, the continuous height adaptation of the Exo-H2 was replaced with a discontinuous regulation system. The orthosis's level-based height regulation system was suggested to enhance the overall adjustment technique by preventing bolts loosening and wear, and, therefore, allow a safer connection to the user.

Furthermore, the distal fixation structure of the Exo-H2 incorporated bolts M4 to fixate the footplate to the motor connection. This fixation was also reported to experience loosening of the bolts, which resulted in the overall discomfort felt by the users. To address this issue, superior size bolts were incorporated.

Concerning the materials selected to compose the orthosis structure, the aluminium alloys available for production in Orthos XXI were tested to verify which one worked better in the simulated components. Besides, aluminium was the preferable material to implement on the SmartOs prototype, due to its low mass density, which is almost three times less than the mass density of the stainless steel, used in the Exo-H2. Moreover, through the static simulations it was also possible to conclude that steel bolts of the class 8.8 are a good solution to incorporate on the fixation structure.

The shank structure was designed with a higher area of contact than the one provided by the leg's straps of Exo-H2. This solution was implemented in order to comply with the biomechanical principle of total contact area, which should be increased to warrant that pressures are kept in reasonable magnitudes, and thus to provide the most comfortable attachment. Furthermore, through the simulations carried out on the proximal fixation structure, it was possible to conclude that the incorporation of a strap

close to the orthosis's articulation was indeed needed. With the additional strap, the fixation of the device to the user is more rigid and safer.

Regarding the actuation/articulation system, the selected actuation system (DC motor and gear unit) is able to provide more nominal torque, maximum torque, and nominal speed than that of the actuation system selected for the Exo-H2. This is a positive result, once it permits a full active assistance to lighter and heavier patients when considering the maximum torque recommended by a Maxon® collaborator. Additionally, although the weight of the selected harmonic drive was almost twice as high as the one incorporated in Exo-H2, the mass of the DC motor and gearbox was reduced from 483 to 384 g. However, the width of the whole articulation system was increased by about 5 mm, due to the positioning of the encoder on the output of the motor. Nevertheless, this magnetic encoder, selected to replace the potentiometer implemented on the Exo-H2, presents a higher accuracy.

One other aspect of the Exo-H2 that needed to be ameliorated was the foot structure. Although the shoe structure has only been considered but not selected, nor the footplate opening has been machined, it is suggested that the incorporation of a shoe into the orthosis would ensure more comfortable use and gait. This is claimed because the outsole and the straps used to fasten the user's shoe of the Exo-H2 are replaced by one shoe unit, which would be customizable to each user's foot size. This way the same outsole would not be worn by several users, as each one would get their own machined shoe, which would warrant not only a more comfortable use but also a more hygienic one.

Finally, the designed orthosis represents a standard version of the SmartOs wearable active orthosis oriented for average height Portuguese people, which implicates that the adaptation feature to the required range of user's heights was not fulfilled. Nonetheless, once this proof of concept is constructed, tested, and validated, the height adaptation functionality would be ensured by the manufacture of several sizes of both the proximal and distal fixation structure. Similarly, the shank structure would also be customizable.

5.4.2 SMARTOS FEATURES

This section presents the final CAD model of the SmartOs wearable active orthosis developed by the design team, which includes both the University of Porto and Orthos XXI design team (Figure 5-29 (a), (b) and (c)). Finally, Table 5-4 is provided to summarize the main technical features of the SmartOs orthosis standard prototype.

Table 5-4 – Technical specifications of the SmartOs wearable active orthosis standard prototype, including the features that are set to be provided by the system.

Standard SmartOs – Smart, Stand-alone Active Orthotic System		
Number of DOF	1 active in the sagittal plane	
Target Market	Post-stroke gait rehabilitation	
Materials	Aluminium alloys 5754-H111, 6082-T651	
Mass (kg)	1.294	
Actuation System	Actuator	Servomotor (DC motor + Harmonic Drive)
	Nominal Torque (N.m)	32.16
	Nominal Speed (rad/s)	3.39
Sensory System to be implemented	Strain Gauge (for deformation measurement during use); FSRs (for gait event detection); EMGs (for monitoring muscle activity).	

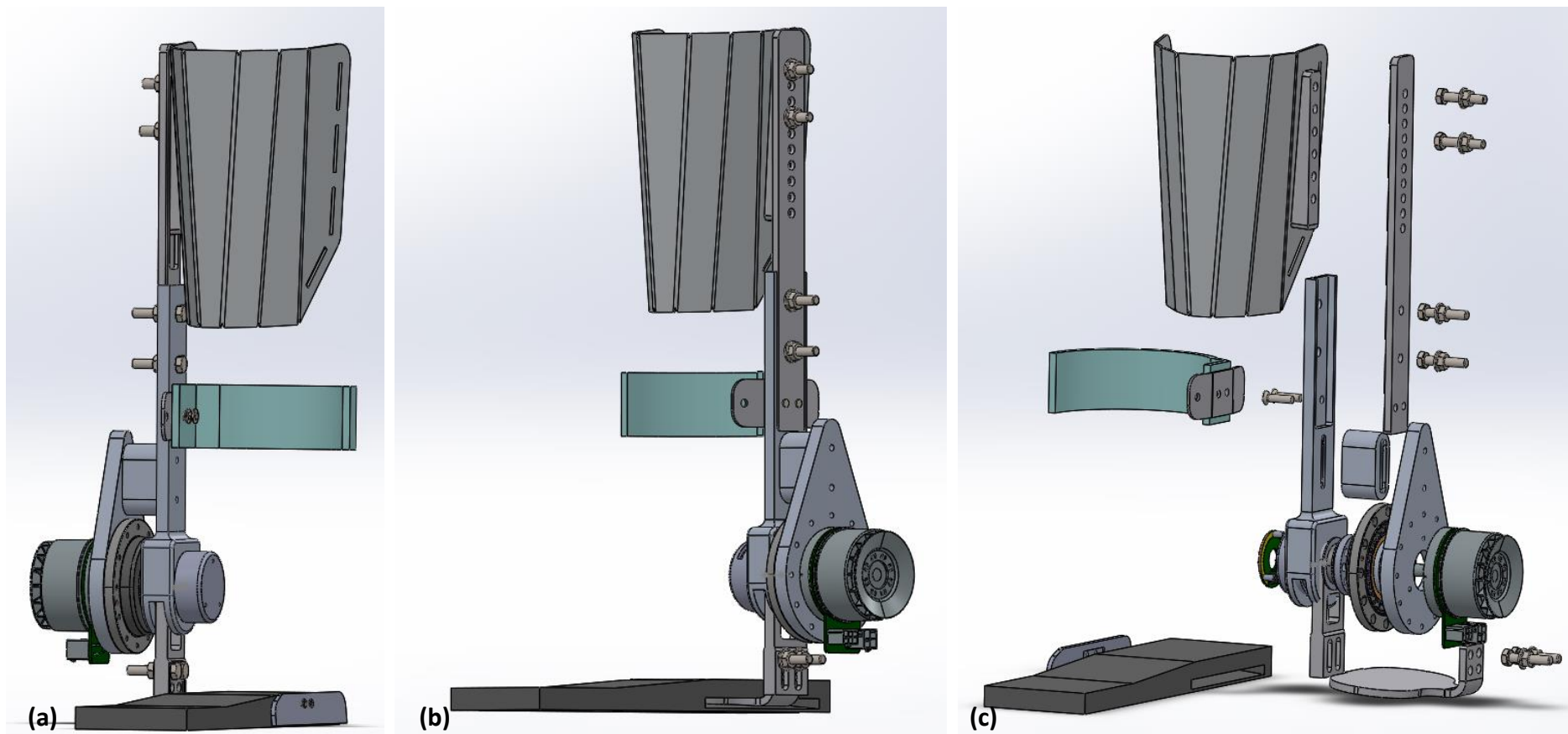


Figure 5-29 – SmartOs standard wearable active orthosis CAD model: (a) Isometric view of the assembly for the right ankle, (b) Isometric view of the assembly for the left ankle, and (c) Exploded view of the assembly for the left ankle.

5.4.3 DEVICE CLASSIFICATION

The FDA has established three regulatory classes (I, II and III) based on the level of control necessary to ensure the safety of the medical device. According to this federal agency, a powered lower extremity exoskeleton is classified into class II (General and Special Controls), meaning that the device requires premarket notification 510(k), which is a regulatory requirement stating that it must be demonstrated that the device is substantially equivalent to one legally in commercial distribution in the United States [206].

Regarding the criteria applied in Portugal, with the amendment of Directive 93/42/EEC by Directive 2007/47/EC, of the European Parliament and of the Council, of 5 September, this new directive has been transposed into national law through the following diploma: Decree-Law 145/2009, of 17 June, establishes the rules to be followed by research, manufacture, marketing, entry into service, surveillance and advertising of DM and their accessories and transposes it to the internal legal order Directive 2007/47/EC, of the European Parliament and of the Council, of 5 September.

Decree-Law 145/2009, of 17 June, divides medical devices into four classes of risk: Class I medical devices (low risk); Class IIa medical devices (medium risk); Class IIb medical devices (medium risk) and Class III medical devices (high risk). Through the analysis of the classification criteria presented in Annex IX, the SmartOs orthosis seems to be a **Class IIb medical device**, once it is an active medical device that, because of its features, is susceptible to supply or exchange energy to and from the body in a potentially dangerous way, considering the nature, density, and place of application of energy. In this case, the evaluation of conformity should follow the requirements stated in the Annex II of the Decree-Law [207]. Nevertheless, this classification needs further evaluation by the Orthos XXI team and regulatory entities.

5.5 PRE-PROTOTYPE PRODUCTION

Due to lack of manufacture resources of the Orthos XXI Company, the standard prototype of the SmartOs wearable active orthosis was not possible to be produced and assembled.

Nevertheless, both the Maxon® DC motor and the Harmonic Drive® gear unit have been ordered and the production is set to start once these components arrive.

Although the whole assembly was not manufactured, it was possible to produce the shank structure to verify its dimensions and to assess its coupling in different legs. The material used to manufacture it was aluminium alloy 5754-H111 and the bending process was performed in a one DOF CNC machine (Figure 5-30 (a)). Additionally, the opening for the wedge components and the straps, were cut in a CNC Laser with two DOF. Figure 5-30 (b) shows the shank structure attached to a leg of an individual with 1.5 m height. However, the same component was tried out in other individuals with the average height and its coupling was reported to be comfortable and satisfactory.

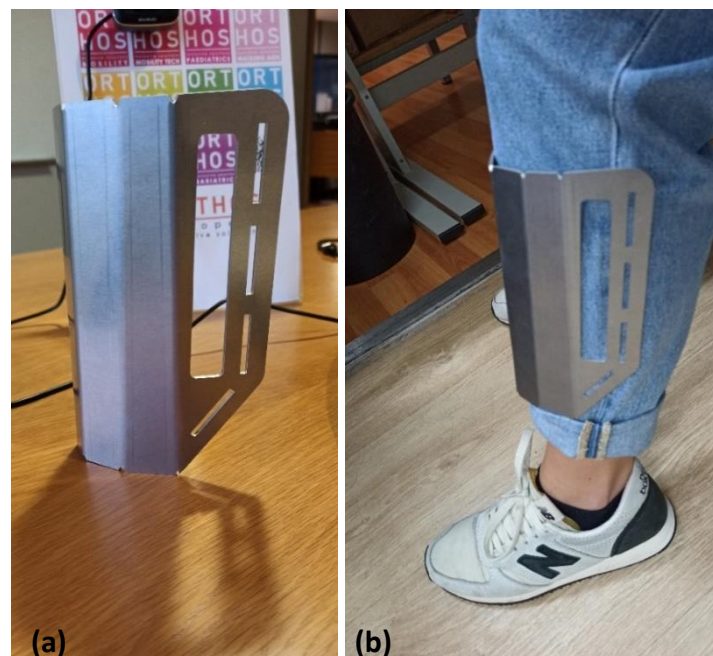


Figure 5-30 – Left shank structure for the standard SmartOs wearable active orthosis, produced in Orthos XXI: (a) Lateral view of the produced component, and (b) SmartOs component attached to a leg of an individual with 1.5 m height.

6. CONCLUSIONS AND FUTURE WORK

This chapter discloses the conclusions drawn from the present master's dissertation and the curricular internship developed in the Portuguese company Orthos XXI, as well as the prospect for future work.

6.1 CONCLUSIONS

This master's dissertation initiated with the literature review regarding the anatomy and biomechanics of the human ankle joint, and the rehabilitative lower limb orthotic devices. From the former, it is possible to conclude about the high complexity of the ankle joint and how the gait kinematics and kinetics are affected by the stroke phenomena. Chapter 3 disclosed the many components that integrate a lower limb orthotic device, from which it was possible to understand the work that has been done in the past years, not only to provide an intelligent and controlled active assistance to impaired individuals but also to ensure the compliance between the user and the orthosis's articulation, through self-alignment mechanisms or even through multiple degrees of freedom articulations.

In this master thesis, the conceptual solutions for the SmartOs wearable active orthosis's required functions were proposed. To accomplish this, several design methodologies were used. These methods revealed to be reliable tools, that facilitate the design process and provide for an organized collection of ideas to answer the project's problems and goals. The performance specification method disclosed the SmartOs project requirements, in which the wished and demanded features were defined. Thus, it becomes necessary to conclude about the specifications that were accomplished and about those that were not.

Firstly, regarding the **compliance of the shank structure** design, it was wished a 3D printed structure that comprised lightweight materials. However, after a group discussion amongst the Orthos XXI design team, it was decided that a metal structure with low thickness and lined with a comfortable, soft material would provide not only for a

comfortable attachment to the user's leg but also a safer one, due to the high mechanical strength of the aluminium alloys. Furthermore, the produced aluminium shank structure was attached to several individuals that considered the component to be lightweight. Nevertheless, further tests are required to assess the comfort provided by its use.

In addition, the adjustability of the orthosis to users with stature within the range of 1.50 and 1.90 meters was demanded. The idea was to design several proximal and distal upright sizes, which would be easily coupled and detached from the articulation/actuation system. This way, the final SmartOs orthosis would be a configurable device, that comprised a single unit applied to all users (the actuation system) and three other modules, customizable to the patient's needs. This adaptation approach would ensure a shank height regulation of 17 centimetres, which would be an increase in 23% comparing to the height adjustment of the Exo-H2 (13 centimetres). Similarly, the distal fixation structure would be able to warrant the adjustment necessary to comply with the ankle height range, which would represent an important improvement when compared to the Exo-H2, which only permits regulation of about 5 millimetres. Furthermore, the manufacture of several distal upright sizes contributes to the mitigation of the misalignment between the actuation system's axis of rotation and the user ankle's axis of rotation. Although the concept of manufacturing different fixation structure's sizes still stands amongst the Orthos XXI design team, it was decided that was better to first produce a **standard SmartOs orthosis prototype** (oriented for average height Portuguese individuals), in order to validate the actuation and electronic systems, and the overall comfort of the device. Herewith, the proposed standard version allows the shank's height regulation of about 4.5 centimetres, with the possibility of increasing this adaptation up to 6 centimetres. This represents a decrease in height regulation when compared to the one implemented in Exo-H2. However, the proposed fixation system would ensure a more reliable fastening, with less wear and yield phenomena in regard to the bolts. Moreover, the distal fixation structure ensures a regulation of 5 millimetres, which is similar to that of the Exo-H2.

To achieve the **compliance of the foot structure**, it was demanded by the SmartOs team that the structure would include lightweight and comfortable materials, be easily replaceable from the actuation system and adjustable to different foot sizes. The solution of comprising a shoe would ensure all of these demands, due to the fact that it would be

acquired in a specialized shoe company that already guarantees comfort and customizable characteristics. Besides, the incorporation of a shoe selected for a certain patient would warrant a more hygienic solution than that of the Exo-H2 (an outsole worn by all users). Furthermore, the solution of machining the shoe's outsole, in order to incorporate the distal upright/footplate, would allow the easy detachment and attachment of the foot structure from the actuation system. This way, it would be possible to couple the most appropriate shoe and configure the orthosis to be used on a certain patient. Nonetheless, the wished requirement of the outsole thickness will not be accomplished since a shoe with an appropriate outsole thickness is needed to ensure its safe machining.

Moreover, the **adaptability** of the SmartOs orthosis consisted of ensuring its attachment to the patient's impaired limb (right or left). This wished requirement was fulfilled through the design of two symmetric shank structures, which would ensure the coupling of the remaining SmartOs modules on the lateral side of this structure. Additionally, the foot structure solution would also ensure that the shoe for the impaired foot would be the one selected to be machined. Herewith, the use of the SmartOs wearable orthosis would not be limited by the impaired limb of the patient, as it happened with the Exo-H2.

Concerning the **accurate functionality** of the device, all the wished and demanded requirements were accomplished, with the exception of the alignment between the orthosis and user ankle's axes of rotation. Although the distal upright was designed to comply with the tibiotalar axis of rotation, its height regulation system does not ensure the adjustment of the actuation system to be aligned with the ankle axis of rotation. As aforementioned, this task is set as a further development, with the production of the orthosis's customizable parts. Moreover, the integration of a silent block was suggested in the conceptual design since it would ensure the flexibility of the orthosis's joint, allowing the motion in the coronal plane, which is suggested to mitigate misalignment occurrences. Similar to the customizable parts, this solution is set for further development.

The selected electric actuation system, which comprises a Maxon® DC motor and a Harmonic Drive® gearbox, is able to provide for the required gait speed and the wished torque. This project phase was accomplished with the help of an engineer of Maxon®

Company, who ensured these requirements would be guaranteed if the correct battery and controller were chosen. Furthermore, the mass of the structure is 1.294 kg, which is within the demanded requirement.

Finally, the **reliable use** requirement was achieved through the incorporation of a safety mechanism into the actuation structure, which limits the range of motion from -20 to 20° in the sagittal plane.

Thus, the detailed design of all SmartOs proof of concept modules was disclosed in Chapter 5, in which, both the implemented novelties (the shank and foot structure, and the distal upright) and improvements are addressed. In this chapter, through the static simulation performed in SolidWorks®, it was selected the aluminium alloys that best enhanced the mechanical performance of the critical components. The aluminium alloy 6082-T651, used for manufacture of machined pieces at Orthos XXI, was selected to comprise the majority of the SmartOs structural components, guaranteeing a factor of safety of at least 1.5. Furthermore, class 8.8 steel bolts were chosen as the best fixation components due to its high mechanical strength.

Due lack of time, derived from the delay of both the curricular internship at Orthos XXI and the SmartOs project, it was not possible to produce the standard SmartOs active orthosis. Nevertheless, the production process has been forwarded and both the Maxon® DC motor and the Harmonic Drive® gear unit have been ordered.

6.2 PROSPECT FOR FUTURE WORK

As aforementioned, the rest of the standard SmartOs active orthosis components are already set for production at Orthos XXI. After the orthosis is manufactured and the ordered actuation system arrives, the device's assembly will be performed. The battery and controller will be selected by another project team member, and, posteriorly, the orthosis validation will be executed, to assess the overall comfort, as well as the actuation and electronic system. The cushioning of the shank structure (with silicone gel) will also have to be produced and fixated to the component.

After the orthosis validation, the different sizes of the fixation structure will be dimensioned and designed, in order to comply with the required range of user's height.

These customizable components must also be validated, through the evaluation of its height adjustment system on several users with different statures.

Finally, the incorporation of silent blocks will be studied to further implement in a second orthosis prototype. Moreover, its functionality must be assessed in order to verify if the flexibility provided by such components allows more natural movement of the ankle joint on the frontal/coronal plane.

7. REFERENCES

- [1] W. Johnson, O. Onuma, M. Owolabi, and S. Sachdev, "Stroke: A global response is needed," *Bull. World Health Organ.*, vol. 94, no. 9, pp. 634A-635A, 2016.
- [2] C. Jorge, "O essencial sobre o Acidente Vascular Cerebral," 2016. [Online]. Available: https://static.lvengine.net/spavc2013/lmgs/pages/PUBLICO/GUIA AVC POPULACAO_final.pdf. [Accessed: 10-Jan-2020].
- [3] S. J. Mulroy, V. J. Eberly, J. K. Gronely, W. Weiss, and C. J. Newsam, "Effect of AFO design on walking after stroke: Impact of ankle plantar flexion contracture," *Prosthet. Orthot. Int.*, vol. 34, no. 3, pp. 277–292, 2010.
- [4] M. Yamamoto, K. Shimatani, M. Hasegawa, and Y. Kurita, "Effect of an ankle-foot orthosis on gait kinematics and kinetics: case study of post-stroke gait using a musculoskeletal model and an orthosis model," *ROBOMECH J.*, vol. 6, no. 1, pp. 0–6, 2019.
- [5] S. Fatone, S. A. Gard, and B. S. Malas, "Effect of Ankle-Foot Orthosis Alignment and Foot-Plate Length on the Gait of Adults With Poststroke Hemiplegia," *Arch. Phys. Med. Rehabil.*, vol. 90, no. 5, pp. 810–818, 2009.
- [6] A. S. Association, "Foot Drop." [Online]. Available: <https://www.stroke.org/en/about-stroke/effects-of-stroke/physical-effects-of-stroke/physical-impact/foot-drop>. [Accessed: 10-Jan-2020].
- [7] A. M. Dollar and H. Herr, "Lower extremity exoskeletons and active orthoses: Challenges and state-of-the-art," *IEEE Trans. Robot.*, vol. 24, no. 1, pp. 144–158, 2008.
- [8] W. Huo, S. Mohammed, J. C. Moreno, and Y. Amirat, "Lower Limb Wearable Robots for Assistance and Rehabilitation: A State of the Art," *IEEE Syst. J.*, vol. 10, no. 3, pp. 1068–1081, 2016.
- [9] B. Chen *et al.*, "Recent developments and challenges of lower extremity exoskeletons," *J. Orthop. Transl.*, vol. 5, pp. 26–37, 2016.
- [10] B. Chen, B. Zi, Y. Zeng, L. Qin, and W. H. Liao, "Ankle-foot orthoses for rehabilitation and reducing metabolic cost of walking: Possibilities and challenges," *Mechatronics*, vol. 53, no. June, pp. 241–250, 2018.
- [11] CUF, "AVC - Acidente Vascular Cerebral." [Online]. Available: <https://www.saudecuf.pt/mais-saude/doencas-a-z/avc-acidente-vascular-cerebral>. [Accessed: 10-Jan-2020].
- [12] M. Correia *et al.*, "Prospective community-based study of stroke in Northern Portugal: Incidence and case fatality in rural and urban populations," *Stroke*, vol. 35, no. 9, pp. 2048–2053, 2004.
- [13] M. Correia, M. R. Silva, R. Magalhães, L. Guimarães, and M. C. Silva, "Transient ischemic attacks in rural and urban northern Portugal: Incidence and short-term prognosis," *Stroke*, vol. 37, no. 1, pp. 50–55, 2006.
- [14] T. C. Chang and X. D. Zhang, "Kinematics and reliable analysis of decoupled parallel mechanism for ankle rehabilitation," *Microelectron. Reliab.*, vol. 99, no. March, pp. 203–212, 2019.
- [15] C. L. Brockett and G. J. Chapman, "Biomechanics of the ankle," *Orthop. Trauma*, vol.

- 30, no. 3, pp. 232–238, 2016.
- [16] R. L. Drake, “Gray’s Atlas of Anatomy,” *Clinical Anatomy*, vol. 21, no. 8. pp. 845–845, 2008.
- [17] E. J. C. Dawe and J. Davis, “(vi) Anatomy and biomechanics of the foot and ankle,” *Orthop. Trauma*, vol. 25, no. 4, pp. 279–286, 2011.
- [18] A. Lundberg, O. K. Svensson, G. Nemeth, and G. Selvik, “The axis of rotation of the ankle joint,” *J. Bone Jt. Surg. - Ser. B*, vol. 71, no. 1, pp. 94–99, 1989.
- [19] C. W. CHAN and A. RUDINS, “Foot Biomechanics During Walking and Running,” *Mayo Clin. Proc.*, vol. 69, no. 5, pp. 448–461, 1994.
- [20] X. Guan *et al.*, “Effects of Ankle Joint Motion on Pelvis-Hip Biomechanics and Muscle Activity Patterns of Healthy Individuals in Knee Immobilization Gait,” *J. Healthc. Eng.*, vol. 2019, 2019.
- [21] C. Moriguchi, T. Sato, and H. Gil Coury, “Ankle movements during normal gait evaluated by flexible electrogoniometer,” *Rev. Bras. Fisioter.*, vol. 11, no. 3, 2007.
- [22] R. C. Ward, *Foundations of Osteopathic Medicine*. 2010.
- [23] K. A. Kirby, “Subtalar joint axis location and rotational equilibrium theory of foot function,” *J. Am. Podiatr. Med. Assoc.*, vol. 91, no. 9, pp. 465–487, 2001.
- [24] J. R. Jastifer and P. A. Gustafson, “The subtalar joint: Biomechanics and functional representations in the literature,” *Foot*, vol. 24, no. 4, pp. 203–209, 2014.
- [25] A. Robinson, J. W. Brodsky, and J. P. Negrine, “Biomechanics of the Foot and Ankle,” in *Core Topics in Foot & Ankle Surgery*, 2018, pp. 22–43.
- [26] M. Nordin and V. Frankel, *Basic biomechanics of the musculoskeletal system*. Lippincott Williams & Wilkins, 2001.
- [27] Footmaxx, “Basic Biomechanics.” [Online]. Available: <https://www.footmaxx.com/invest/basic-biomechanics>. [Accessed: 06-May-2020].
- [28] B. Hintermann, *Total Ankle Arthroplasty: Historical Overview, Current Concepts and Future Perspectives*. 2005.
- [29] D. B. Thordarson, *Foot and Ankle*. 2004.
- [30] K. A. Shorter, J. Xia, E. T. Hsiao-Wecksler, W. K. Durfee, and G. F. Kogler, “Technologies for powered ankle-foot orthotic systems: Possibilities and challenges,” *IEEE/ASME Trans. Mechatronics*, vol. 18, no. 1, pp. 337–347, 2013.
- [31] W. Pirker and R. Katzenschlager, “Gait disorders in adults and the elderly,” 2016.
- [32] J. S. Kawalec, *Mechanical testing of foot and ankle implants*. Elsevier Ltd., 2017.
- [33] A. Alamdari and V. Krovi, *A Review of Computational Musculoskeletal Analysis of Human Lower Extremities*, no. June. 2016.
- [34] M. Alam, I. A. Choudhury, and A. Bin Mamat, “Mechanism and design analysis of articulated ankle foot orthoses for drop-foot,” *Sci. World J.*, vol. 2014, 2014.
- [35] A. Bonnefoy-Mazure and S. Armand, “Normal gait,” *Pediatr. Clin. North Am.*, vol. 40, no. 3, pp. 645–657, 2015.
- [36] T. Marasovič, M. Cecič, and V. Zanchi, “Analysis and interpretation of ground reaction forces in normal gait,” *WSEAS Trans. Syst.*, vol. 8, no. 9, pp. 1105–1114, 2009.
- [37] Z. O. Abu-faraj, G. F. Harris, P. A. Smith, and S. Hassani, *Human Gait and Clinical Movement Analysis Human Gait and Clinical Movement Analysis*, no. December. 2015.
- [38] A. Lundberg, “Kinematics of the ankle and foot: In vivo roentgen stereophotogrammetry,” *Acta Orthop.*, vol. 60, no. S233, pp. 1–26, 1989.

- [39] J. Dicharry, "Kinematics and kinetics of gait: From lab to clinic," *Clin. Sports Med.*, vol. 29, no. 3, pp. 347–364, 2010.
- [40] J. Richards, A. Chohan, and R. Erande, "Biomechanics," in *Tidy's Physiotherapy*, 2013, pp. 331–368.
- [41] C. Z. C. Hasan, R. Jailani, N. M. Tahir, and H. M. Desaa, "Vertical ground reaction force gait patterns during walking in children with autism spectrum disorders," *Int. J. Eng. Trans. B Appl.*, vol. 31, no. 5, pp. 705–711, 2018.
- [42] S. Winiarski and A. Rutkowska-Kucharska, "Estimated ground reaction force in normal and pathological gait," *Acta Bioeng. Biomech.*, vol. 11, no. 1, pp. 53–60, 2009.
- [43] S. E. Oh, A. Choi, and J. H. Mun, "Prediction of ground reaction forces during gait based on kinematics and a neural network model," *J. Biomech.*, vol. 46, no. 14, pp. 2372–2380, 2013.
- [44] J. W. Wannop, J. T. Worobets, and D. J. Stefanyshyn, "Normalization of ground reaction forces, joint moments, and free moments in human locomotion," *J. Appl. Biomech.*, vol. 28, no. 6, pp. 665–676, 2012.
- [45] J. G. Webster, Z. O. Abu-Faraj, G. F. Harris, P. A. Smith, and S. Hassani, *Human gait and Clinical Movement Analysis*, no. December. 2015.
- [46] L. Ren, D. Howard, L. Ren, C. Nester, and L. Tian, "A Phase-Dependent Hypothesis for Locomotor Functions of Human Foot Complex," vol. 5, pp. 175–180, 2008.
- [47] D. A. Winter, *Biomechanics and Motor Control of Human Movement*. 2009.
- [48] H. J. Carrapatoso Oliveira, "Inverse Dynamic Analysis of the Human Locomotion Apparatus for Gait," no. November, 2016.
- [49] T. Tengman and J. Riad, "Three-dimensional gait analysis following achilles tendon rupture with nonsurgical treatment reveals long-term deficiencies in muscle strength and function," *Orthop. J. Sport. Med.*, vol. 1, no. 4, pp. 1–9, 2013.
- [50] N. Gurusamy, I. Elamvazuthi, N. Yahya, P. D. Ridzuan, and J. Province, "Biomechanical Energy Harvesting from Human Lower Extremity Gait: A Comparative Analysis," 2017.
- [51] A. Zissimopoulos, S. Fatone, and S. A. Gard, "Biomechanical and energetic effects of a stance-control orthotic knee joint," *J. Rehabil. Res. Dev.*, vol. 44, no. 4, pp. 503–513, 2007.
- [52] E. Sanchis-Sales, J. L. Sancho-Bru, A. Roda-Sales, and J. Pascual-Huerta, "Dynamic flexion stiffness of foot joints during walking," *J. Am. Podiatr. Med. Assoc.*, vol. 106, no. 1, pp. 37–46, 2016.
- [53] M. C. Morais Filho, R. A. dos Reis, and C. M. Kawamura, "Evaluation of ankle and knee movement pattern during maturation of normal gait," *Acta Ortop. Bras.*, vol. 18, no. 1, pp. 23–25, 2010.
- [54] K. Shamaei, M. Cenciarini, and A. M. Dollar, "On the mechanics of the ankle in the stance phase of the gait," *Proc. Annu. Int. Conf. IEEE Eng. Med. Biol. Soc. EMBS*, pp. 8135–8140, 2011.
- [55] J. Weir and N. Chockalingam, "Ankle joint dorsiflexion: Assessment of true values necessary for normal gait," *Int. J. Ther. Rehabil.*, vol. 14, no. 2, pp. 76–82, 2007.
- [56] S. Li, "Ankle and Foot Spasticity Patterns in Chronic Stroke Survivors with Abnormal Gait," *Toxins (Basel)*, vol. 12, no. 10, 2020.
- [57] C. Beyaert, R. Vasa, and G. E. Frykberg, "Gait post-stroke: Pathophysiology and rehabilitation strategies," *Neurophysiol. Clin.*, vol. 45, no. 4–5, pp. 335–355, 2015.

- [58] C. J. Winstein *et al.*, *Guidelines for Adult Stroke Rehabilitation and Recovery: A Guideline for Healthcare Professionals from the American Heart Association/American Stroke Association*, vol. 47, no. 6. 2016.
- [59] T. Akbas, R. R. Neptune, and J. Sulzer, "Neuromusculoskeletal simulation reveals abnormal rectus femoris-gluteus medius coupling in post-stroke gait," *Front. Neurol.*, vol. 10, no. APR, 2019.
- [60] M. P. Afonso, "Modelling the gait of healthy and post-stroke individuals," no. September, pp. 12–13, 2015.
- [61] S. J. Olney and C. Richards, "Hemiparetic gait following stroke. Part I: Characteristics," *Gait Posture*, vol. 4, no. 2, pp. 136–148, 1996.
- [62] A. Middleton, S. L. Fritz, and M. Lusardi, "Walking speed: The functional vital sign," *J. Aging Phys. Act.*, vol. 23, no. 2, pp. 314–322, 2015.
- [63] K. K. Patterson, W. H. Gage, D. Brooks, S. E. Black, and W. E. McIlroy, "Evaluation of gait symmetry after stroke: a comparison of current methods and recommendations for standardization.," *Gait Posture*, vol. 31, no. 2, pp. 241–246, Feb. 2010.
- [64] M. D. Lewek, C. E. Bradley, C. J. Wutzke, and S. M. Zinder, "The relationship between spatiotemporal gait asymmetry and balance in individuals with chronic stroke," *J. Appl. Biomech.*, vol. 30, no. 1, p. 31–36, 2014.
- [65] C. Arienti, S. G. Lazzarini, A. Pollock, and S. Negrini, "Rehabilitation interventions for improving balance following stroke: An overview of systematic reviews," *PLoS One*, vol. 14, no. 7, pp. 1–23, 2019.
- [66] C. M. Kim and J. J. Eng, "Symmetry in vertical ground reaction force is accompanied by symmetry in temporal but not distance variables of gait in persons with stroke," *Gait Posture*, vol. 18, no. 1, pp. 23–28, 2003.
- [67] S. Nadeau, M. Betschart, and F. Bethoux, "Gait analysis for poststroke rehabilitation: The relevance of biomechanical analysis and the impact of gait speed," *Phys. Med. Rehabil. Clin. N. Am.*, vol. 24, no. 2, pp. 265–276, 2013.
- [68] R. Dickstein, "Rehabilitation of Gait Speed After Stroke :," pp. 649–660, 2008.
- [69] D. J. Clark and C. Patten, "Neurorehabilitation and Neural Repair Following Stroke," 2013.
- [70] M. Ekblom, "Eccentric Vs. Concentric training. Which Is Better?" [Online]. Available: <https://www.ebtoofficial.com/build-muscle/eccentric-vs-concentric/>. [Accessed: 30-Jun-2020].
- [71] S. K. Sabut, C. Sikdar, R. Kumar, and M. Mahadevappa, "Functional electrical stimulation of dorsiflexor muscle: Effects on dorsiflexor strength, plantarflexor spasticity, and motor recovery in stroke patients," *NeuroRehabilitation*, vol. 29, no. 4, pp. 393–400, 2011.
- [72] G. You, H. Liang, and T. Yan, "Functional electrical stimulation early after stroke improves lower limb motor function and ability in activities of daily living," *NeuroRehabilitation*, vol. 35, no. 3, pp. 381–389, 2014.
- [73] T. Yan, C. W. Y. Hui-Chan, and L. S. W. Li, "Functional electrical stimulation improves motor recovery of the lower extremity and walking ability of subjects with first acute stroke: A randomized placebo-controlled trial," *Stroke*, vol. 36, no. 1, pp. 80–85, 2005.
- [74] B. Xu, T. Yan, Y. Yang, R. Ou, and S. Huang, "Effect of normal-walking-pattern-based functional electrical stimulation on gait of the lower extremity in subjects with

- ischemic stroke: A self controlled study," *NeuroRehabilitation*, vol. 38, no. 2, pp. 163–169, 2016.
- [75] S. G. Brauer, S. S. Kuys, J. D. Paratz, and L. Ada, "Improving physical activity after stroke via treadmill training and self management (IMPACT): A protocol for a randomised controlled trial," *BMC Neurol.*, vol. 18, no. 1, pp. 1–8, 2018.
- [76] S. F. Tyson, E. Sadeghi-Demneh, and C. J. Nester, "A systematic review and meta-analysis of the effect of an ankle-foot orthosis on gait biomechanics after stroke," *Clin. Rehabil.*, vol. 27, no. 10, pp. 879–891, 2013.
- [77] S. F. Tyson and H. A. Thornton, "The effect of a hinged ankle foot orthosis on hemiplegic gait: Objective measures and users' opinions," *Clin. Rehabil.*, vol. 15, no. 1, pp. 53–58, 2001.
- [78] MSN, "Functional electrical stimulation (FES)." [Online]. Available: <https://www.mstrust.org.uk/a-z/functional-electrical-stimulation-fes>. [Accessed: 01-Jul-2020].
- [79] L. Lünenburger, G. Colombo, and R. Riener, "Biofeedback for robotic gait rehabilitation," *J. Neuroeng. Rehabil.*, vol. 4, no. May 2014, pp. 0–11, 2007.
- [80] D. Friesen, "Body Weight Supported Treadmill Training in Neurological Rehabilitation." [Online]. Available: <https://propelphysiotherapy.com/neurological-injuries/body-weight-supported-treadmill-training-in-neurological-rehabilitation>. [Accessed: 02-Jul-2020].
- [81] S. F. Tyson and R. M. Kent, "Effects of an ankle-foot orthosis on balance and walking after stroke: A systematic review and pooled meta-analysis," *Arch. Phys. Med. Rehabil.*, vol. 94, no. 7, pp. 1377–1385, 2013.
- [82] B. Shi *et al.*, "Wearable ankle robots in post-stroke rehabilitation of gait: A systematic review," *Front. Neurorobot.*, vol. 13, no. August, pp. 1–16, 2019.
- [83] M. Bortole *et al.*, "The H2 robotic exoskeleton for gait rehabilitation after stroke: Early findings from a clinical study Wearable robotics in clinical testing," *J. Neuroeng. Rehabil.*, vol. 12, no. 1, pp. 1–14, 2015.
- [84] P. Oliveira, "A Real-Time Architecture for Smart Wearable Orthoses System," *Univ. do Minho*, 2017.
- [85] S. Yamamoto, M. Ebina, S. Kubo, T. Hayashi, Y. Akita, and Y. Hayakawua, "Yamamoto1999.Pdf." pp. 24–28, 1999.
- [86] Ottobock, "C-Brace - Reshaping the future." [Online]. Available: <https://www.ottobock.co.uk/orthopaedic-rehabilitation/lower-limb-orthoses/c-brace®/>. [Accessed: 29-Jan-2020].
- [87] R. Cardoso and M. T. Silva, "Design, Analysis and Simulation of a Novel Device for Locomotion Support," *Biosyst. Biorobotics*, vol. 15, pp. 833–837, 2017.
- [88] S. Nancy and N. Hussein, "A Review of Lower Limb A Review of Lower Limb Exoskeletons," no. January 2016, 2017.
- [89] A. Esquenazi, M. Talaty, and A. Jayaraman, "Powered Exoskeletons for Walking Assistance in Persons with Central Nervous System Injuries: A Narrative Review," *PM R*, vol. 9, no. 1, pp. 46–62, 2017.
- [90] A. D. Gardner, J. Potgieter, and F. K. Noble, "A review of commercially available exoskeletons' capabilities," *2017 24th Int. Conf. Mechatronics Mach. Vis. Pract. M2VIP 2017*, vol. 2017-Decem, pp. 1–5, 2017.
- [91] A. J. Veale and S. Q. Xie, "Towards compliant and wearable robotic orthoses: A review of current and emerging actuator technologies," *Med. Eng. Phys.*, vol. 38,

- no. 4, pp. 317–325, 2016.
- [92] Y. Hong *et al.*, “Lower extremity exoskeleton: review and challenges surrounding the technology and its role in rehabilitation of lower limbs,” *Aust. J. Basic Appl. Sci.*, vol. 7, no. 7, pp. 520–524, 2013.
- [93] P. Felix, J. Figueiredo, C. P. Santos, and J. C. Moreno, “Powered knee orthosis for human gait rehabilitation: First advances,” *ENBENG 2017 - 5th Port. Meet. Bioeng. Proc.*, no. January, pp. 2–6, 2017.
- [94] M. K. Habib, “Human-Inspired Robotic Exoskeleton for Post-Stroke Gait Rehabilitation,” in *Handbook of Research on Advancements in Robotics and Mechatronics*, 2014, pp. 316–376.
- [95] R. Daniel and T. Paulus, “Introduction to Gate Drives,” in *Lock Gates and Other Closures in Hydraulic Projects*, 2019, pp. 705–784.
- [96] J. E. Edelstein and J. Bruckner, “Ankle-Foot Orthoses,” in *Orthotics: A Comprehensive Clinical Approach*, 2002, pp. 39–54.
- [97] BECKER, “Tamarack Plantar Flexion Limiter Kit.” [Online]. Available: <https://www.beckerorthopedic.com/Product/AnkleComponents/ThermoplasticAnkleJoints/741-ML>. [Accessed: 25-Nov-2020].
- [98] BECKER, “Tamarack Habilitation Technologies.” [Online]. Available: <https://www.beckerorthopedic.com/Spotlight/Tamarack>. [Accessed: 25-Nov-2020].
- [99] M. Giannini, “Project Progress Report,” in *Journal of Rehabilitation Research and Development*, 1990.
- [100] H. R. Lehneis, “Application of External Power in Orthotics,” pp. 13–16, 2008.
- [101] T. Mortenson, “Limit Switch Explained | Working Principles,” 2020. [Online]. Available: <https://realpars.com/limit-switch/>. [Accessed: 30-Nov-2020].
- [102] E. Edwards, “Limit Switch Characteristics.” [Online]. Available: <https://www.thomasnet.com/articles/instruments-controls/limit-switches/>. [Accessed: 30-Nov-2020].
- [103] J. Luo, “Solemate.” [Online]. Available: <https://moooooonaluo.github.io/personal-website/solemate.html>. [Accessed: 24-Oct-2020].
- [104] E. Zheng, B. Chen, X. Wang, Y. Huang, and Q. Wang, “On the design of a wearable multi-sensor system for recognizing motion modes and sit-to-stand transition,” *Int. J. Adv. Robot. Syst.*, vol. 11, no. 1, 2014.
- [105] S. Diao, X. Chen, and J. Luo, “Development and Experimental Evaluation of a state dependent coefficient based state estimator for functional electrical stimulation-elicited tasks,” no. April 2016, pp. 1–20, 2018.
- [106] A. A. Mohamed, J. Baba, J. Beyea, J. Landry, A. Sexton, and C. A. McGibbon, “Comparison of strain-gage and fiber-optic goniometry for measuring knee kinematics during activities of daily living and exercise,” *J. Biomech. Eng.*, vol. 134, no. 8, 2012.
- [107] Plux, “Goniometer (GON).” [Online]. Available: <https://plux.info/sensors/290-goniometer-gon-820201214.html>. [Accessed: 24-Oct-2020].
- [108] Shimmer, “Shimmer3 EMG Unit.” [Online]. Available: <https://www.shimmersensing.com/products/shimmer3-emg-sensor>. [Accessed: 24-Oct-2020].
- [109] BrainSupport, “Uma breve introdução ao EEG e aos tipos de eletrodos.” [Online]. Available: <https://www.brainlatam.com/blog/uma-breve-introducao-ao-eeg-e->

- aos-tipos-de-eletrodos-717. [Accessed: 24-Oct-2020].
- [110] ExoskeletonReport, “HAL Lower Limb.” [Online]. Available: <https://exoskeletonreport.com/product/hal-lower-limb/>. [Accessed: 22-Oct-2020].
- [111] Cyberdyne, “HAL for Medical Use (Lower Limb Type).” [Online]. Available: https://www.cyberdyne.jp/english/products/LowerLimb_medical.html. [Accessed: 20-Oct-2020].
- [112] M. J. Hoffmann, “HAL for Medical Use - Food And Drug Administration,” 2017. [Online]. Available: https://www.accessdata.fda.gov/cdrh_docs/pdf17/K171909.pdf.
- [113] ISCR, “Powered Lower Limb Exoskeletons for Spinal Cord Injury,” 2016.
- [114] J. Hamilton, “EVALUATION OF AUTOMATIC CLASS III DESIGNATION (DE NOVO) FOR ARGO REWALK™,” 2013.
- [115] ExoskeletonReport, “Ekso GT.” [Online]. Available: <https://exoskeletonreport.com/product/ekso-gt/>. [Accessed: 20-Oct-2020].
- [116] “Ekso GT™ Robotic Exoskeleton Cleared by FDA for Use With Stroke and Spinal Cord Injury Patients,” 2016. [Online]. Available: <https://www.globenewswire.com/news-release/2016/04/04/825424/0/en/Ekso-GT-Robotic-Exoskeleton-Cleared-by-FDA-for-Use-With-Stroke-and-Spinal-Cord-Injury-Patients.html>. [Accessed: 27-Jan-2020].
- [117] “FDA approves Vanderbilt-designed Indego exoskeleton for clinical and personal use,” 2016. [Online]. Available: <http://news.vumc.org/2016/03/10/fda-approves-vanderbilt-designed-indego-exoskeleton-for-clinical-and-personal-use/>. [Accessed: 27-Jan-2020].
- [118] Food and Drug Administration, “Indego approval letter,” 2017.
- [119] ExoskeletonReport, “Indego.” [Online]. Available: <https://exoskeletonreport.com/product/indego/>. [Accessed: 20-Oct-2020].
- [120] B-Temia, “WHAT IS KEEOGO? More Than Walking.” [Online]. Available: <https://keeogo.com/about-keeogo/what-is-keeogo>. [Accessed: 04-Nov-2020].
- [121] “Keeogo Target Indications.” [Online]. Available: <https://keeogo.com/about-keeogo/indication-and-clinical-benefits>. [Accessed: 28-Jan-2020].
- [122] GOGOA, “HANK – LOWER LIMBS EXOSKELETON.” [Online]. Available: <http://gogoa.eu/products/robotic-neuro-rehabilitation/hank-for-clinical-rehabilitation/>. [Accessed: 28-Jan-2020].
- [123] Gogoa, “Hank Exoskeleton.” [Online]. Available: <https://www.gogoa.eu/hank>. [Accessed: 10-Nov-2020].
- [124] ExoskeletonReport, “HANK.” [Online]. Available: <https://exoskeletonreport.com/product/hank/>. [Accessed: 10-Nov-2020].
- [125] D. Kirsh, “Gogoa Mobility Robots wins CE Mark for Hank exoskeleton,” 2018. [Online]. Available: <https://www.medicaldesignandoutsourcing.com/gogoa-mobility-robots-wins-ce-mark-for-hank-exoskeleton/>. [Accessed: 10-Nov-2020].
- [126] ExoskeletonReport, “REX.” [Online]. Available: <https://exoskeletonreport.com/product/rex/>. [Accessed: 20-Oct-2020].
- [127] REXBionics, “REX PROVIDES ROBOTIC ASSISTANCE FOR REHABILITATION, EXERCISE AND WALKING.” [Online]. Available: <https://www.rexbionics.com/rex-for-clinical-use/>. [Accessed: 20-Oct-2020].
- [128] B. S. Rupal, S. Rafique, A. Singla, and E. Singla, “Lower-limb exoskeletons : Research

- trends and regulatory guidelines in medical and non-medical applications,” no. December, pp. 1–27, 2017.
- [129] L. Yeung, C. Ockenfeld, M. Pang, H. Wai, and O. Soo, “Design of an Exoskeleton Ankle Robot for Robot-Assisted Gait Training of Stroke Patients *,” pp. 211–215, 2017.
- [130] J. a Blaya, H. M. Herr, T. Supervisor, D. J. Newman, W. C. Flowers, and A. Sonin, “Force-Controllable Ankle Foot Orthosis (AFO) to Assist Drop Foot Gait,” *Mech. Eng.*, no. June, 2003.
- [131] G. S. Sawicki, K. E. Gordon, and D. P. Ferris, “Powered lower limb orthoses: Applications in motor adaptation and rehabilitation,” *Proc. 2005 IEEE 9th Int. Conf. Rehabil. Robot.*, vol. 2005, no. July, pp. 206–211, 2005.
- [132] K. Z. Takahashi, M. D. Lewek, and G. S. Sawicki, “A neuromechanics-based powered ankle exoskeleton to assist walking post-stroke : a feasibility study,” pp. 1–13, 2015.
- [133] J. Ward, T. Sugar, A. Boehler, J. Standeven, and J. R. Engsborg, “Stroke survivors’ gait adaptations to a powered ankle-foot orthosis,” *Adv. Robot.*, vol. 25, no. 15, pp. 1879–1901, 2011.
- [134] A. W. Boehler, K. W. Hollander, T. G. Sugar, and D. Shin, “Design , Implementation and Test Results of a Robust Control Method for a Powered Ankle Foot Orthosis (AFO),” pp. 2025–2030, 2008.
- [135] D. Ferris and B. Hannaford, “An Ankle-Foot Orthosis Powered by Artificial Pneumatic Muscles,” no. May 2014, 2005.
- [136] B. Choi *et al.*, “A self-aligning knee joint for walking assistance devices,” *Proc. Annu. Int. Conf. IEEE Eng. Med. Biol. Soc. EMBS*, vol. 2016-October, pp. 2222–2227, 2016.
- [137] A. Stienen, E. Hekman, F. van der Helm, and H. van der Kooji, “Self-Aligning Exoskeleton Axes Through Decoupling of Joint Rotations and Translations,” *Trans. Robot.*, vol. 25, no. 3, pp. 628–633, 2009.
- [138] T. Kobayashi, M. S. Orendurff, G. Hunt, F. Gao, L. S. Lincoln, and K. B. Foreman, “The effects of alignment of an articulated ankle-foot orthosis on lower limb joint kinematics and kinetics during gait in individuals post-stroke,” *J. Biomech.*, 2018.
- [139] M. A. Ergin and V. Patoglu, “A Self-Adjusting Knee Exoskeleton for Robot-Assisted Treatment of Knee Injuries,” pp. 4917–4922, 2011.
- [140] B. Celebi, M. Yalcin, and V. Patoglu, “ASSISTON-KNEE : A Self-Aligning Knee Exoskeleton,” pp. 996–1002, 2013.
- [141] L. E. Amigo, A. Casals, and J. Amat, “Design of a 3-DoF Joint System with Dynamic Servo-Adaptation in Orthotic Applications,” pp. 3700–3705, 2011.
- [142] Y. Niu, Z. Song, and J. Dai, “Kinematic analysis and optimization of a planar parallel compliant mechanism for self-alignment knee exoskeleton,” *Mech. Sci.*, vol. 9, no. 2, pp. 405–416, 2018.
- [143] Y. Lee *et al.*, “Biomechanical Design of a Novel Flexible Exoskeleton for Lower Extremities,” *IEEE/ASME Trans. Mechatronics*, vol. 22, no. 5, pp. 2058–2069, 2017.
- [144] A. Erdogan, B. Celebi, A. C. Satici, and V. Patoglu, “Assist On-Ankle: a reconfigurable ankle exoskeleton with series-elastic actuation,” *Auton. Robots*, vol. 41, no. 3, pp. 743–758, 2017.
- [145] R. K. P. S. Ranaweera and R. A. M. Abayasiri, “Design and Analysis of An Anthropomorphic Two-DoF Ankle-Foot Orthosis,” *2019 5th Int. Conf. Control. Autom. Robot.*, vol. 1, pp. 802–807, 2019.
- [146] J. Carberry, G. Hinchly, J. Buckerfield, E. Tayler, T. Burton, and R. Vaidyanathan,

- “Parametric Design of an Active Ankle Foot Orthosis with Passive Compliance.”
- [147] H. S. Choi, C. H. Lee, and Y. S. Baek, “Design of a Pneumatic Actuated Ankle-Foot Orthosis which has Talocrural and Subtalar Joint,” *2019 IEEE 16th Int. Conf. Rehabil. Robot.*, pp. 276–281, 2019.
- [148] A. Agrawal, S. K. Banala, S. K. Agrawal, and S. A. Binder-macleod, “Design of a two degree-of-freedom ankle-foot orthosis for robotic rehabilitation Design of a Two Degree-of-freedom Ankle-Foot Orthosis for Robotic,” no. July, 2005.
- [149] S. A. Binder-macleod, “Design of a Novel Two Ankle-Foot Orthosis,” vol. 129, no. November 2007, pp. 1137–1143, 2016.
- [150] Y. Zhu, J. Fan, and J. Zhao, “Design of a quasi-passive 3 DOFs ankle-foot wearable rehabilitation orthosis,” no. January 2016, 2015.
- [151] H. K. Surmen, N. E. Akalan, and Y. Z. Arslan, “Design, Manufacture, and Selection of Ankle-Foot-Orthoses,” *Encycl. Inf. Sci. Technol. Fourth Ed.*, no. January, pp. 298–313, 2017.
- [152] M. S. Wong, B. H. Beygi, and Y. Zheng, “Materials for Exoskeletal Orthotic and Prosthetic Systems,” in *Encyclopedia of Biomedical Engineering*, 2019, pp. 352–366.
- [153] B. Coppard and H. Lohman, “Introduction to Orthotics,” in *Introduction to Orthotics - E-Book: A Clinical Reasoning and Problem-Solving Approach*, 2015, pp. 36–40.
- [154] D. Patrick, “Orthotics,” in *Geriatric Rehabilitation Manual*, 2007, pp. 465–466.
- [155] J. D. Hsu, J. W. Michael, and J. R. Fisk, “Principles and components of spinal orthoses,” in *AAOS Atlas of Orthoses and Assistive Devices*, 2008, pp. 93–96.
- [156] C. C. Chen *et al.*, “Kinematic features of rear-foot motion using anterior and posterior ankle-foot orthoses in stroke patients with hemiplegic gait,” *Arch. Phys. Med. Rehabil.*, vol. 91, no. 12, pp. 1862–1868, 2010.
- [157] F. Menotti, L. Laudani, A. Damiani, P. Orlando, and A. Macaluso, “Comparison of walking energy cost between an anterior and a posterior ankle-foot orthosis in people with foot drop,” *J. Rehabil. Med.*, vol. 46, no. 8, pp. 768–772, 2014.
- [158] J. H. Park, M. H. Chun, J. S. Ahn, J. Y. Yu, and S. H. Kang, “Comparison of gait analysis between anterior and posterior ankle foot orthosis in hemiplegic patients,” *Am. J. Phys. Med. Rehabil.*, vol. 88, no. 8, pp. 630–634, Aug. 2009.
- [159] Robert H. Meier, David C. Ruthsatz, and Daniel Cipriani, “Impact of AFO (ankle foot orthosis) Design on Calf Circumference,” *Low. Extrem. Rev.*, vol. 6, no. 10, pp. 29–35, 2014.
- [160] THOMAS, “Comparison of Thermoset Versus Thermoplastic Materials.” [Online]. Available: <https://www.thomasnet.com/articles/plastics-rubber/thermoset-vs-thermoplastics/>. [Accessed: 07-Nov-2020].
- [161] M. Asim *et al.*, “Processing of hybrid polymer composites—a review,” in *Hybrid Polymer Composite Materials*, 2017, pp. 1–22.
- [162] S. H. Collins, M. B. Wiggin, and G. S. Sawicki, “Reducing the energy cost of human walking using an unpowered exoskeleton.”
- [163] A. Bassett, “Orthotics.” [Online]. Available: <https://www.orthobullets.com/foot-and-ankle/12278/orthotics>. [Accessed: 08-Nov-2020].
- [164] SPS, “Orthoses Ankle/Foot.” [Online]. Available: <https://www.spsco.com/media/wysiwyg/Orthotic-Catalog/1-AFO.pdf>. [Accessed: 08-Nov-2020].
- [165] BECKER, “Drop Foot Splint Full Foot.” [Online]. Available: <https://www.beckerorthopedic.com/Product/PrefabricatedOrthoses/LowerLimb/>

615. [Accessed: 08-Nov-2020].
- [166] Ottobock, "17AD100 Nexgear Tango ankle joint - Fabricating an ankle-foot orthosis and installing the modules." [Online]. Available: <https://professionals.ottobock.no/document;jsessionid=F583C6A6299D135A7EAE D77CEA2A3564.node0?mediaPK=9359125315614&attachment=true>. [Accessed: 08-Nov-2020].
- [167] O. Technika, "PREPREG ORTHOSES." [Online]. Available: <http://www.orthopedic-pro.com/produkte/prepreg-orthoses/>. [Accessed: 10-Nov-2020].
- [168] R. K. Chen, L. Chen, B. L. Tai, Y. Wang, A. J. Shih, and A. Arbor, "Additive Manufacturing of Personalized Ankle-Foot Orthosis," no. April 2017, 2014.
- [169] Y. A. Jin, J. Plott, R. Chen, J. Wensman, and A. Shih, "Additive manufacturing of custom orthoses and prostheses - A review," *Procedia CIRP*, vol. 36, no. February 2015, pp. 199–204, 2015.
- [170] P. R. Programme, "Manufacturing guidelines."
- [171] Y. H. Cha *et al.*, "Ankle-Foot Orthosis Made by 3D Printing Technique and Automated Design Software," vol. 2017, 2017.
- [172] Ottobock, "Prepreg technology." .
- [173] THOMAS, "Understanding CNC Machining." [Online]. Available: <https://www.thomasnet.com/articles/custom-manufacturing-fabricating/understanding-cnc-machining/>. [Accessed: 16-Nov-2020].
- [174] M. Lynch, "A Brief Explanation of CNC Machines and How They Work." [Online]. Available: <https://wiki.mcneel.com/rhino/cncbasics>. [Accessed: 16-Nov-2020].
- [175] B. Warfield, "What is CNC Machining and CNC Machines? [2020 Easy Guide]." [Online]. Available: <https://www.cnccookbook.com/what-is-cnc-machining-and-cnc-machines/>. [Accessed: 16-Nov-2020].
- [176] AstroMachineWorks, "What Is CNC Machining? An Overview of the CNC Machining Process," 2017. [Online]. Available: <https://astromachineworks.com/what-is-cnc-machining/>. [Accessed: 16-Nov-2020].
- [177] A. Velling, "What Is CNC Machining? Working Principles, Capabilities & More," 2020. [Online]. Available: <https://fractory.com/what-is-cnc-machining/>. [Accessed: 16-Nov-2020].
- [178] K. Obrovac, M. Klaić, T. Staraveski, T. Udiljak, and V. J. Obrovac, "Application of Machine Tools in Orthoses Manufacture," vol. 524, pp. 141–157, 2020.
- [179] ConcerningReality, "What is CNC Machining and How Does it Work?," 2018. [Online]. Available: <https://www.youtube.com/watch?v=FNyEXjRmDtl>. [Accessed: 16-Nov-2020].
- [180] R. Ronquillo, "Understanding Laser Cutting." [Online]. Available: <https://www.thomasnet.com/articles/custom-manufacturing-fabricating/laser-cutting-technology/>. [Accessed: 16-Nov-2020].
- [181] SMEMedia, "Electrochemical Deburring - Spider Company," 2016. [Online]. Available: <https://www.youtube.com/watch?v=PM2g3mSmZFc>. [Accessed: 16-Nov-2020].
- [182] N. Cross, "Engineering design methods: Strategies for product design," *Materials & Design*, vol. 16, no. 2. pp. 122–123, 1995.
- [183] G. . Pahl, W. . Beitz, J. Feldhusen, and K. H. . Grote, *Engineering design. [electronic book] : a systematic approach: University of Liverpool Library*. 2007.
- [184] A. Force, S. Command, W.-P. Air, and F. Base, "DISTRIBUTED BY; Natioua" Tacknical

- Inftort Service U. S. DEPARTMENT OF COMMERCE," 1969.
- [185] H. G. Armstrong, "Anthropometry and mass distribution for human analogues. volume 1. military male aviators," *Aerosp. Med. Res. Lab Wright-Patterson ...*, no. 88, pp. 33–38, 1988.
- [186] S. Sánchez-García, C. García-Peñ, M. X. Duque-López, T. Juárez-Cedillo, A. R. Cortés-Núñez, and S. Reyes-Beaman, "Anthropometric measures and nutritional status in a healthy elderly population," *BMC Public Health*, vol. 7, pp. 1–9, 2007.
- [187] S. Nishioka, H. Wakabayashi, and T. Yoshida, "Accuracy of non-paralytic anthropometric data for nutritional screening in older patients with stroke and hemiplegia," *Eur. J. Clin. Nutr.*, vol. 71, no. 2, pp. 173–179, 2017.
- [188] M. P. Barroso, P. M. Arezes, L. G. Da Costa, and A. S. Miguel, "Anthropometric study of Portuguese workers," *Int. J. Ind. Ergon.*, vol. 35, no. 5, pp. 401–410, 2005.
- [189] R. Contini, "Body Segment Parameters, Part II," *Artif. Limbs*, vol. 16, no. 1, pp. 1–19, 1972.
- [190] NASA, "ANTHROPOMETRY AND BIOMECHANICS." [Online]. Available: https://msis.jsc.nasa.gov/sections/section03.htm#_3.3_ANTHROPOMETRIC_AND. [Accessed: 27-Oct-2020].
- [191] N. C. D. Risk and F. Collaboration, "A century of trends in adult human height," *Elife*, vol. 5, pp. 1–29, 2016.
- [192] B. F. Mentiplay, M. Banky, R. A. Clark, M. B. Kahn, and G. Williams, "Lower limb angular velocity during walking at various speeds," *Gait Posture*, vol. 65, no. December, pp. 190–196, 2018.
- [193] U. Kafader, *The selection of high-precision microdrives*. 2007.
- [194] RLS, "AksIM-2™-Off-Axis Rotary Absolute Magnetic Encoder Module." [Online]. Available: <https://www.rls.si/eng/aksim-2-off-axis-rotary-absolute-encoder?partNumbers=MB080SPL20BDNT00%2CMRA080BC055DSE00%2CACCO15>. [Accessed: 01-Jan-2021].
- [195] MakeItFrom, "7005 (AlZn4.5Mg1.5Mn, A97005) Aluminum." [Online]. Available: <https://www.makeitfrom.com/material-properties/7005-AlZn4.5Mg1.5Mn-A97005-Aluminum>. [Accessed: 20-Dec-2020].
- [196] MakeItFrom, "Aluminum Alloys." [Online]. Available: <https://www.makeitfrom.com/material-group/Aluminum-Alloy>. [Accessed: 02-Jan-2021].
- [197] Polylanema Lda., "AW6082 Laminado." .
- [198] Polylanema Lda., "AW 7075." .
- [199] Polylanema Lda., "AW 5083." .
- [200] G.Leal, "5754 H111 | Chapa," p. 5754.
- [201] GoEngineer, "SOLIDWORKS Simulation - Finite Element Analysis (FEA) Software." [Online]. Available: <https://www.goengineer.com/solidworks/simulation/solidworks-simulation>. [Accessed: 02-Jan-2021].
- [202] DassaultSystemes, "Linear Static Analysis." [Online]. Available: https://help.solidworks.com/2018/english/SolidWorks/cworks/c_Linear_Static_Analysis.htm?id=5393cb548d364a3ab8d384a69c9aa9ff#Pg0. [Accessed: 02-Jan-2021].
- [203] JAM BUILDING PRODUCTS, "Mechanical Properties of Steel Bolts, Screws and Studs," p. 4, 2014.

- [204] BoltDepot, “Bolt Grade Markings and Strength Chart.” [Online]. Available: boltdepot.com/fastener-information/materials-and-grades/bolt-grade-chart.aspx. [Accessed: 01-Jan-2021].
- [205] S. Simulation, “Using Sheet Metal Bodies in SOLIDWORKS Simulation.”
- [206] FDA, “Overview of Device Regulation.” [Online]. Available: <https://www.fda.gov/medical-devices/device-advice-comprehensive-regulatory-assistance/overview-device-regulation#510k>. [Accessed: 01-Jan-2021].
- [207] Ministério da Saúde, “DMinistério da Saúde. (2009). Decreto-Lei no145/2009, de 17 de Junho de 2009. Diário Da República, 1.a Série, 115, 3707–3765. <https://dre.pt/application/conteudo/494558creto-Lei n°145/2009, de 17 de Junho de 2009,>” *Diário da República, 1.ª série*, vol. 115, pp. 3707–65, 2009.
- [208] Roboaid, “Cyberdyne HAL-5 – exoskeleton robot.” [Online]. Available: <http://www.robaid.com/bionics/cyberdyne-hal-5-exoskeleton-robot.htm>. [Accessed: 27-Jan-2020].
- [209] E. Watson, “Exoskeletons: What’s New?” [Online]. Available: http://mageerehab.org/wp-content/uploads/2017/10/Exoskeletal-devices_REV.pdf. [Accessed: 10-Nov-2020].
- [210] J. C. Mcleod, S. J. M. Ward, and A. L. Hicks, “Evaluation of the Keeogo™ Dermoskeleton,” *Disabil. Rehabil. Assist. Technol.*, vol. 14, no. 5, pp. 503–512, 2019.
- [211] B-Temia, “Keeogo™ Obtains CE Marking - B-Temia’s Keeogo™ Obtains CE Marking Allowing its Commercialization in EU Countries,” 2019. [Online]. Available: <https://www.prnewswire.com/news-releases/keeogo-obtains-ce-marking---b-temias-keeogo-obtains-ce-marking-allowing-its-commercialization-in-eu-countries-300972245.html>. [Accessed: 04-Nov-2020].
- [212] B-Temia, “B-Temia Inc. Obtains 510(k) Clearance for Keeogo™ from the USA Food & Drug Administration (FDA),” 2020. [Online]. Available: <https://www.prnewswire.com/news-releases/b-temia-inc-obtains-510k-clearance-for-keeogo-from-the-usa-food--drug-administration-fda-301129797.html>. [Accessed: 04-Nov-2020].
- [213] B. Marinov, “GOGO becomes the First European Exoskeleton Company to Receive CE Clearance; Launches 3 New Exoskeletons,” 2018. [Online]. Available: <https://exoskeletonreport.com/2018/10/gogoa-becomes-the-first-european-exoskeleton-company-to-receive-ce-clearance-launches-3-new-exoskeletons/>. [Accessed: 10-Nov-2020].
- [214] S. Delp, A. Habib, and A. Seth, “OpenSim.” [Online]. Available: <https://simtk.org/projects/opensim>. [Accessed: 16-Dec-2020].
- [215] K. N. Salb, D. M. Wido, T. E. Stewart, and D. J. Diangelo, “Development of a robotic assembly for analyzing the instantaneous axis of rotation of the foot ankle complex,” *Appl. Bionics Biomech.*, vol. 2016, 2016.
- [216] K. N. Salb, D. M. Wido, T. E. Stewart, and D. J. Diangelo, “Biomechanical effects of load on foot and ankle mechanics,” *Proc. - 29th South. Biomed. Eng. Conf. SBEC 2013*, pp. 139–140, 2013.
- [217] A. Seth, S. Delp, and A. Habib, “OpenSim Models.” [Online]. Available: <https://simtk-confluence.stanford.edu/display/OpenSim/OpenSim+Models#OpenSimModels-AvailableJointTypes>. [Accessed: 17-Dec-2020].
- [218] R. G. Budynas and J. K. Nisbett, *Shigley’s Mechanical Engineering Design*. .

8. APPENDICES

A. Overview information of the different types of AFOs

Table 8-1 – Overview of the passive, semi-active and active ankle-foot orthoses [10], [30], [34].

Type of orthoses		Characteristics	Limitations	Examples of devices
Passive	Non articulated	<ul style="list-style-type: none"> • Most popular daily-wear device due to its compactness, durability, lightweight and simplicity of design; • Usually single piece; • Fabricated out of lightweight thermoformable or thermoplastic materials; • Can provide assistance in the sagittal plane during gait, while storing energy; • Has proven to decrease walking energy expenditure, improving gait pathology; • Is able to store energy during deformation of its spring-like design, and enhance push-off during the pre-swing phase. 	<ul style="list-style-type: none"> • Restricts normal ankle joint movement, which affects functional recovery; • Might cause excessive knee flexion moment, in order to compensate for toe clearance; • Not able to ensure walking stability; • High risk of tripping. 	<ul style="list-style-type: none"> • WalkOn Reaction AFO, by Ottobock; • WalkOn Flex AFO, by Ottobock; • AFO developed by Ramsey et al.; • AFO developed by Allard et al.; • AFO developed by Wolf et al.; • AFO developed by Bregman et al..
	Articulated	<ul style="list-style-type: none"> • Together with the nonarticulated AFOs, is the most popular daily-wear device; • Fabricated out of lightweight thermoplastics or carbon composite; • Include a joint with a hinge, flexion stops, and stiffness control elements, like springs; • The mechanical components have shown to prevent drop-foot by locking the ankle in a suitable position; • Can provide resistive force, and ankle joint's stiffness, initial angle and range of motion adjustability; • Similarly, it provides assistance to the user by preventing unwanted foot motion with physical resistance. 	<ul style="list-style-type: none"> • Limited functionality; • Motion control determined by passive components, which have limited robustness; • Not able to adapt to changing environment and walking conditions; • The wearer might experience poor dynamic balance and unnatural gait pattern; • Cannot provide direct positive torque for the user during the 	<ul style="list-style-type: none"> • AFO by Ottobock; • AFO by Yamamoto et al.

			propulsive stage of the stance phase.	
Semi active	<ul style="list-style-type: none"> • The effectiveness to prevent drop foot and improve user’s comfort has been shown; • Integrate MR (Magneto-Rheological) dampers or brakes, which can warrant controllable braking torque; • Can manage that motion of the paretic ankle by modulating the damping of the AFOs joint in real-time; • Incorporate potentiometers, force and moment sensors to control the MR brake. 		<ul style="list-style-type: none"> • Don’t provide for active torque to help the user to propel the body forward; • Are not able to reduce the metabolic cost of walking. 	<ul style="list-style-type: none"> • AFO by Furusho et al; • AFO by Svensson et al; • AFO by Shibata et al.
Active	<ul style="list-style-type: none"> • Can provide controllable assistive torque for the wearers in both dorsi- and plantarflexion; • Incorporate actuators and a robotic control system, which make for a more compliant ankle motion; • Are able to interact with unpredictable environments and modulate the ankle movements accordingly; • Can ensure sufficient toe clearance and prevent drop foot during swing phase of the human gait; • Can integrate several types of actuators to generate assistive torque: electric, pneumatic, hydraulic and series elastic actuators (SEA). 		<ul style="list-style-type: none"> • Normally heavy; • Controllers and power supply are worn at the wearer’s waist, which increases the user’s metabolic cost and overall discomfort; • Actuators have an efficiency associated with the elements of transmission, such as the gearbox, in the electric motors case, or with the valves of the hydraulic and pneumatic actuators. 	<ul style="list-style-type: none"> • AFOs by Mooney et al; • AFO by Galle et al; • AFO by Yeung et al.; • AFO by Blaya et al.; • AFO by Ward et al.; • AFO by University of Michigan; • AFO by Arizona State Robotic Gait Trainer; • AFO by Okayama University.

B. Commercially available powered lower limb exoskeletons for rehabilitation

Table 8-2 - Exoskeletons commercially available and its technical and commercial features.

Devices (Year)	HAL For Medical Use - ML05 Series (2012) [112], [113], [208]	ReWalk Rehabilitation (2012) [113], [114], [128]	EksoGT (2013)[113], [116], [118], [209]	Indego Therapy (2013) [113], [118], [128], [209]	Keeogo (2014)[113], [120], [128], [210]–[212]	HANK (2016) [123]–[125], [213]	REX (2016)[113], [126]–[128]	Exo-H2 (2015) [83], [128]
Company	Cyberdyne	ReWalk Robotics	Ekso Bionics	Parker Hannifin Corp	B-TEMIA	GOGOA Mobility Robots	Rex Bionics	Technaid
Target Market	Spinal cord injuries, brain and neuromuscular disorders	Spinal cord injury	Hemiplegia due to stroke, Spinal cord injury	Spinal cord injury	Spinal cord injury, stroke, multiple sclerosis, Knee/hip osteoarthritis	Hemiplegia due to stroke, Spinal cord injury	Complete spinal cord injury, stroke, multiple sclerosis	Hemiplegia due to stroke, Spinal cord injury
Materials	Aluminium alloy and steel	Aluminium and tempered steel	Aluminium, Carbon fibre	Carbon Fibre	NS	Aluminium 7075	Carbon fibre, aluminium	Stainless Steel and aluminium alloy 7005
Weight (kg)	14	25	23	12	6	12	45	11
User Max. Weight (kg)	100	100	100	100	NS	100	100	100

Conclusions and future work

Devices (Year)		HAL For Medical Use - ML05 Series (2012) [112], [113], [208]	ReWalk Rehabilitation (2012) [113], [114], [128]	EksoGT (2013)[113], [116], [118], [209]	Indego Therapy (2013) [113], [118], [128], [209]	Keeogo (2014)[113], [120], [128], [210]–[212]	HANK (2016) [123]–[125], [213]	REX (2016)[113], [126]–[128]	Exo-H2 (2015) [83], [128]
User height range (m)		1.50 – 1.90	1.60 – 1.90	1.60 – 1.90	1.55 – 1.91	NS	1.5 – 1.95	1.42 – 1.93	1.50 – 1.95
Actuation	Actuator	Electric	Electric	Hydraulic	Electric	Electric	Electric	Electric	Electric
	Peak Torque (N.m)	30	125	NS	20	40	35	NS	180 (net torque 35)
	Max. Speed (m/s)	0,56	0,56	0,56	0,56	NS	NS	0,1	0.5
	Actuated Joint	Hip, Knee, Ankle (passive)	Hip, Knee, Ankle (passive)	Hip, Knee, Ankle (passive)	Hip, Knee	Knee	Hip; Knee; Ankle	Hip; Knee; Ankle (2 DoF)	Hip; Knee; Ankle
Battery life; Placement		1h30; User's waist	2h; Backpack or waist	1h; Backpack	1h30; User's waist	1-4h	4h Structure	1h Structure	6h; Backpack

Conclusions and future work

Devices (Year)	HAL For Medical Use - ML05 Series (2012) [112], [113], [208]	ReWalk Rehabilitation (2012) [113], [114], [128]	EksoGT (2013)[113], [116], [118], [209]	Indego Therapy (2013) [113], [118], [128], [209]	Keeogo (2014)[113], [120], [128], [210]–[212]	HANK (2016) [123]–[125], [213]	REX (2016)[113], [126]–[128]	Exo-H2 (2015) [83], [128]
Control System	Self-initiated (EMG detects BES) and remote control	Postural changes for stepping, Remote control worn on the wrist to change modes	Handheld interface for PT; weight shift to initiate steps, SmartAssist software	Uses postural changes to trigger all transition, FES controller, Assist-As-Needed software	Self-initiated (sensors on the joints)	Managed by therapist through an APP on tablet PC or smartphone; EMG and EEG signal to control the exoskeleton; Assist-as-needed and predefined movement patrons	Joystick, computer -brain interface (EEG)	Trajectory tracking; General for all users

Devices (Year)	HAL For Medical Use - ML05 Series (2012) [112], [113], [208]	ReWalk Rehabilitation (2012) [113], [114], [128]	EksoGT (2013)[113], [116], [118], [209]	Indego Therapy (2013) [113], [118], [128], [209]	Keeogo (2014)[113], [120], [128], [210]–[212]	HANK (2016) [123]–[125], [213]	REX (2016)[113], [126]–[128]	Exo-H2 (2015) [83], [128]
Sensory System (Placement)	Force (exoskeleton's foot), EMG (posterior and anterior sides of the user's thigh), Potentiometers (joints), Gyroscopes (backpack), Accelerometer (backpack)	Inclinometer (torso strap), Force (Foot)	Pressure (Crutches), Motion sensors (legs)	Tilt sensors, Force (crutches)	Joint sensors	EMG and EEG sensors;	Inclinometer (structure), 27 on-board microprocessors	Potentiometers, Joint Hall Effect Sensor, Foot/Ground Contact (Heel and Toe)
Data Visualization	HAL Monitor control interface (Screen in real-time)	GUI, Vibratory feedback from backpack and LED indicator on user's wrist controller	Provides visual feedback on the handheld controller and auditory feedback	Provides vibratory feedback and LED indicators on top of hip unit, visible to wearer, Indego App	NS	APP on tablet PC or smartphones to verify personalized patient progress reports	NS	Matlab application (offline); User interface (smartphone)

Conclusions and future work

Devices (Year)	HAL For Medical Use - ML05 Series (2012) [112], [113], [208]	ReWalk Rehabilitation (2012) [113], [114], [128]	EksoGT (2013)[113], [116], [118], [209]	Indego Therapy (2013) [113], [118], [128], [209]	Keeogo (2014)[113], [120], [128], [210]–[212]	HANK (2016) [123]–[125], [213]	REX (2016)[113], [126]–[128]	Exo-H2 (2015) [83], [128]
Use Environment	Flat surfaces (indoor only)	Level surfaces and mild slopes	Indoor, smooth surfaces	Even or uneven terrain up to 5 degrees of inclination	Flat or uneven surfaces	Flat surfaces, slopes and stairs	Flat, horizontal, stable, dry surfaces	NS
Supported Motions	Sit, stand, walk and turn	Sit, stand, walk, and turn	Sit, stand, walk and turn	Sit, stand, walk and turn	Sit, stand, walk, run, turn, crouch, squat, kneel	Walk, sit down, stand up, walk up and down slopes and stairs	Sit, stand, walk, turn, shuffle sideways, exercises to promote mobility (e.g. Squats)	Walk
Patent	US9943458B2 , US8773148B2 , USD749227S1 (<i>design</i>), USD786446S1 (<i>design</i>), WO20100357 06	US9526668B2, US20140196757A1, US20160250093A1, WO2017064720A3, WO2017006322A2, WO2012052988A2, US8905955B2	US8968222B2	--	--	--	US20110066088A 1	--

Conclusions and future work

Devices (Year)	HAL For Medical Use - ML05 Series (2012) [112], [113], [208]	ReWalk Rehabilitation (2012) [113], [114], [128]	EksoGT (2013)[113], [116], [118], [209]	Indego Therapy (2013) [113], [118], [128], [209]	Keeogo (2014)[113], [120], [128], [210]–[212]	HANK (2016) [123]–[125], [213]	REX (2016)[113], [126]–[128]	Exo-H2 (2015) [83], [128]
Commercial Status (Market Price)	CA – FDA approval & CE Marking & TGA (€86.978)	CA – FDA approval & CE marking (€60.781)	CA – FDA approval & CE marking (€117.939)	CA–FDA approval & CE marking (€60.000 -€85446)	CA-FDA approval &CE marking (€36.290 or €907/year)	CE marking (€60.000)	CA-FDA approval & CE marking (€145.171)	AEMPS approval for investigation (–)

Legend: CA – Commercially Available; FDA – Food and Drug Administration; CE – European Conformity; TGA - Therapeutic Goods Administration; NS – Not Specified; BES - Bio-electric signals; PT – Physical Therapist; AEMPS - Spanish Agency of Medicines and Health Products.

C. Active ankle-foot orthoses for rehabilitation still in a development stage

Table 8-3 – Overview of the developed active AFO for rehabilitation found in the literature review.

Devices (Year)		AFO by Blaya et al. (2003) [7], [10], [130]	AFO by Boehler et al. (2008) [10], [134]	AFO by Ward et al. (2011) [10], [133]	AFO by Ferris et al. (2005) [7], [10], [30], [135]	AnkleRobot by Yeung et al (2017) [10], [129]	AFO by Takahashi et al. (2015) [10], [132]
University/Institution		Massachusetts Institute of Technology (MIT)	Arizona State University	Arizona State University, Washington University	University of Michigan	Chinese University of Hong Kong, Hong Kong Polytechnic University	North Carolina State University
Target Market		Drop foot gait (caused by stroke, multiple sclerosis or cerebral palsy)	Stroke survivors	Stroke survivors	Gait study and rehabilitation	Stroke survivors	Stroke survivors
Materials		Polypropylene with a metallic hinge ankle joint	NS	Polypropylene	Carbon fibre and polypropylene shells	Carbon fibre braces	Carbon fibre shank and foot segment
Weight (kg)		3.08	1.75	NS	1.6	1 (0.5 at the ankle, and 0.5 at the user's waist for the control box and battery)	0.53
Actuation	Actuator	SEA (DC motor and a spring)	Robotic tendon actuator (DC motor, custom threaded lead screw, and a spring)	Robotic tendon actuator	PMA's	Servomotor (DC motor, gearing set and control circuit)	PMA's

Conclusions and future work

Devices (Year)		AFO by Blaya et al. (2003) [7], [10], [130]	AFO by Boehler et al. (2008) [10], [134]	AFO by Ward et al. (2011) [10], [133]	AFO by Ferris et al. (2005) [7], [10], [30], [135]	AnkleRobot by Yeung et al (2017) [10], [129]	AFO by Takahashi et al. (2015) [10], [132]
	Peak Torque (N.m)	76.5	60	NS	70 (plantarflexion) and 38 (dorsiflexion)	16.7	25
	Max. Speed (m/s)	1.81	1.25 (selected by the tested able-bodied subject)	NS	1.2 (trial selected)	0.6 (faster speed)	1.09 (selected by tested subject)

Devices (Year)	AFO by Blaya et al. (2003) [7], [10], [130]	AFO by Boehler et al. (2008) [10], [134]	AFO by Ward et al. (2011) [10], [133]	AFO by Ferris et al. (2005) [7], [10], [30], [135]	AnkleRobot by Yeung et al (2017) [10], [129]	AFO by Takahashi et al. (2015) [10], [132]
Control System	<p>Adjusts the joint impedance during different phases of a gait cycle;</p> <p>A spring-damper control is applied to prevent drop-foot during the swing phase.</p>	<p>The spring can store energy and release it to help to propel the body forward;</p> <p>A seven finite state machine was used to control the velocity and stiffness of the AFO (first five states for stance phase, and the last two for swing phase);</p> <p>The switch between states is achieved through the data given by the encoders and force sensors.</p>	<p>The spring can store energy and release it at the propulsive stage for forward progression;</p> <p>No predefined ankle trajectory is defined by the robot, as it only controls the input side of the spring, and the user has to learn to properly store and release the energy.</p>	<p>The AFO is controlled based on the EMG amplitude;</p> <p>Computer software adjusts the air pressure in each artificial muscle so that the force is proportional to the EMG amplitude.</p>	<p>The control algorithm uses the leg tilting ankle and angular velocity for real-time classification of walking conditions: level walking and stair ascending/descending;</p> <p>Furthermore, it uses foot loading pattern to identify the pre-swing phase (when FSRs were unloaded, i.e. foot lifted off from the ground);</p> <p>The level of motor assistance is adjusted according to the walking condition (e.g. higher powered dorsiflexion was provided for stair ascending).</p>	<p>The actuation timing is controlled based on the beginning of the propulsive stage, by collecting EMG signals and GRF data to assist the user ankle;</p> <p>The magnitude of assistance is proportional to the EMG activity of the patient's plantarflexors.</p>
Sensory System (Placement)		Encoder (lead screw and spring);	FSR sensors (heel of AFO foot); motor encoder;	EMG sensors; Tension load sensor;	IMU (shank structure); FSR sensor (AFO foot)	EMG sensors

Conclusions and future work

Devices (Year)	AFO by Blaya et al. (2003) [7], [10], [130]	AFO by Boehler et al. (2008) [10], [134]	AFO by Ward et al. (2011) [10], [133]	AFO by Ferris et al. (2005) [7], [10], [30], [135]	AnkleRobot by Yeung et al (2017) [10], [129]	AFO by Takahashi et al. (2015) [10], [132]
	Potentiometer (ankle joint); GRF sensors (foot), FSR (shoe's heel)	Force sensor (insole)	absolute encoder (ankle joint); rate gyroscope	Force transducers.		GRF sensors (instrumented treadmill)
Use Environment	NS	Flat surfaces but is flexible to walking environment changes	Tested on treadmill (with harness) and overground	Tested on treadmill	Level-ground walking, stair ascending and descending	Tested on treadmill
Tethered/Untethered	Tethered	Tethered	NS	Tethered	Untethered	Tethered
Supported Motions	Ankle motion on the sagittal plane.	Ankle motion in the sagittal plane	Ankle motion in the sagittal plane	Ankle motion in the sagittal plane	Ankle motion in the sagittal plane	Ankle motion in the sagittal plane
Clinical trials	Increased walking speed; Reduced the instances of foot slap; Better symmetry with the healthy leg; Assisted plantarflexion.	Kinematic and kinetic data from a single able-bodied subject; The controller switches states correctly; The actuator generated power comparable to a healthy individual during level walking.	Walking trials with three stroke survivors were conducted; The results verified that the subjects wearing the AFO could increase the cadence, ankle range of motion, and the ability to generate power; Kinematic and kinetic changes were more remarkable while using a	Joint kinematic and PMA force data collected from one healthy participant; Most kinematic profiles were similar for no orthosis and passive orthosis conditions (meaning that the AFO was comfortable); Soleus EMG amplitude reduced while walking with	Tests with three stroke patients were conducted; Results show that the power assistance provided by the AFO could reduce drop foot of the patients during the swing phase.	Five stroke patients were tested; The AFO could increase the plantarflexion torque of the paretic ankle.

Conclusions and future work

Devices (Year)	AFO by Blaya et al. (2003) [7], [10], [130]	AFO by Boehler et al. (2008) [10], [134]	AFO by Ward et al. (2011) [10], [133]	AFO by Ferris et al. (2005) [7], [10], [30], [135]	AnkleRobot by Yeung et al (2017) [10], [129]	AFO by Takahashi et al. (2015) [10], [132]
			treadmill, suggesting that positive results of overground training occur at a slower rate.	assistive plantarflexion torque.		

D. Self-aligning mechanism validation

In an initial phase of the present master dissertation, it was proposed to study a self-aligning mechanism conceptualized and designed within the BiRDLAB group. The study of its functionality would involve the assessment of the kinematic and kinetic effects of incorporating an AFO with the self-aligning mechanism on a musculoskeletal model. To accomplish this, it was used *OpenSim*, a freely available, user-extensible software system for developing musculoskeletal models and for simulating and analysing movement. *OpenSim* was developed by the National Centre for Simulation in Rehabilitation Research (NCSRR) in Stanford University (USA), and allows the creation of dynamic simulations of movement that combine anatomical models with the physics of the musculoskeletal system [214].

The main purpose of the proposed self-aligning mechanism was to accommodate the instantaneous centre of rotation (ICR), that occurs on the ankle joint during the movements around the sagittal plane. Studies have been conducted to explore the magnitude of the deviation in the ICR path [215], [216].

As aforementioned, the three-pulley mechanism designed was inspired on the self-aligning mechanism developed by Choi et al. (see Figure 3-15 (b) in Section 3.4.1), in which an additional passive DOF is created to mitigate the angular misalignment problem. The CAD model of the self-aligning mechanism is illustrated in Figure 8-1.

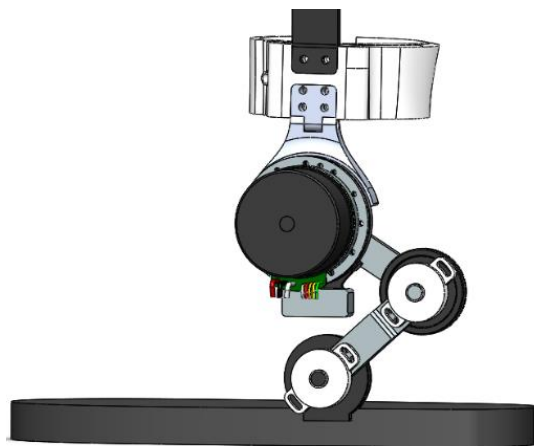


Figure 8-1 – 3D model of the self-aligning mechanism designed within the BiRDLAB group, to accommodate the ICR of the ankle joint.

Herewith, the self-aligning mechanism CAD model was incorporated into the *OpenSim* software and studied through the following steps:

1. Conversion of the components of the mechanism of the SolidWorks CAD model into a STL file;
2. Collection of each body mass, mass centre and inertia matrix through the Mass Properties tool of SolidWorks;
3. Creation of the self-aligning mechanism model with an existing musculoskeletal model (*Gait2354_Simbody*) by writing the necessary code (which includes the information in 2.) in XML, using Notepad ++ as text editor (Figure 8-2). This also includes the definition of the kinematic relationship between all the parts, i.e., to define each of the joints. *OpenSim* provides seven types of joints, which can be seen in [217]. The shank structure of the AFO attached to the left tibia through a *Weldjoint*, so that the bodies are fixed together (Figure 8-3). A *Pin Joint* was then used to characterize the joint between each component of the mechanism, due to the fact that the parts only move on the sagittal plane (Figure 8-4);

```

<length_units>METERS</length_units>
<force_units>N</force_units>
<!--Acceleration due to gravity.-->
<gravity> 0 -9.80665 0</gravity>
<!--Bodies in the model.-->
<BodySet>
  <objects>
    <Body name="ground">
    <Body name="pelvis">
    <Body name="femur r">
    <Body name="tibia r">
    <Body name="talus r">
    <Body name="calc n r">
    <Body name="toes r">
    <Body name="femur l">
    <Body name="tibia l">
    <Body name="talus l">
    <Body name="calc n l">
    <Body name="toes l">
    <Body name="torso">
    <Body name="l AFO cuff">
    <Body name="Driving link">
    <Body name="Mid Pulley">
    <Body name="Bottom Link">
    <Body name="Bottom Pulley">
    <Body name="AFO foot">
  </objects>
</groups />
</BodySet>

```

Figure 8-2 – Incorporation of the self-aligning mechanism on an *OpenSim* model (*Gait2354_Simbody*).

```

<Body name="l_AFO_cuff">
  <mass>0.938899134298787</mass>
  <mass_center> 0 0.25 0</mass_center>
  <inertia_xx>0.0165640955828945</inertia_xx>
  <inertia_yy>0.00414102389572363</inertia_yy>
  <inertia_zz>0.0165640955828945</inertia_zz>
  <inertia_xy>0</inertia_xy>
  <inertia_xz>0</inertia_xz>
  <inertia_yz>0</inertia_yz>
  <!--Joint that connects this body with the parent body.-->
  <Joint>
    <WeldJoint name="tibia_cuff">
      <!--Name of the parent body to which this joint connects its owner body.-->
      <parent_body>tibia_l</parent_body>
      <!--Location of the joint in the parent body specified in the parent reference frame. Default is
      <location_in_parent>0 -0.37563874 0</location_in_parent>
      <!--Orientation of the joint in the parent body specified in the parent reference frame. Euler XY
      <orientation_in_parent>0 0 0</orientation_in_parent>
      <!--Location of the joint in the child body specified in the child reference frame. For SIMM mode
      <location>0 0 0</location>
      <!--Orientation of the joint in the owing body specified in the owing body reference frame. Eul
      <orientation>0 0 0</orientation>
      <!--Set holding the generalized coordinates (q's) that parmeterize this joint.-->
      <CoordinateSet>
        <objects />
        <groups />
      </CoordinateSet>
      <!--Whether the joint transform defines parent->child or child->parent.-->
      <reverse>false</reverse>
    </WeldJoint>
  </Joint>

```

Figure 8-3 – Kinematic definition between the AFO’s shank structure and the left tibia of the musculoskeletal model of *OpenSim*.

```

<Body name="Driving_link">
  <mass>0.0281669740289636</mass>
  <mass_center> 0 -0.04 0</mass_center>
  <inertia_xx>0</inertia_xx>
  <inertia_yy>0</inertia_yy>
  <inertia_zz>0</inertia_zz>
  <inertia_xy>0</inertia_xy>
  <inertia_xz>0</inertia_xz>
  <inertia_yz>0</inertia_yz>
  <!--Joint that connects this body with the parent body.-->
  <Joint>
    <PinJoint name="Cuff_DrivingLink">
      <!--Name of the parent body to which this joint connects its owner body.-->
      <parent_body>l_AFO_cuff</parent_body>
      <!--Location of the joint in the parent body specified in the parent reference frame. Default is (0,0,0).-->
      <location_in_parent>0 0 -0.043</location_in_parent>
      <!--Orientation of the joint in the parent body specified in the parent reference frame. Euler XYZ body-fixed ro
      <orientation_in_parent>0 0 0</orientation_in_parent>
      <!--Location of the joint in the child body specified in the child reference frame. For SIMM models, this vector
      <location>0 0 0</location>
      <!--Orientation of the joint in the owing body specified in the owing body reference frame. Euler XYZ body-fix
      <orientation>0 0 1.047</orientation>
      <!--Set holding the generalized coordinates (q's) that parmeterize this joint.-->
      <CoordinateSet>
        <objects>
          <Coordinate name="Cuff_DrivingLink1">
            <!--Coordinate can describe rotational, translational, or coupled motion. Defaults to rotational.-->
            <motion_type>rotational</motion_type>
            <!--The value of this coordinate before any value has been set. Rotational coordinate value is in rad
            <default_value>0.0845545876884849</default_value>
            <!--The speed value of this coordinate before any value has been set. Rotational coordinate value is
            <default_speed_value>0</default_speed_value>
            <!--The minimum and maximum values that the coordinate can range between. Rotational coordinate rang
            <range>-1.5708 1.5708</range>
            <!--Flag indicating whether or not the values of the coordinates should be limited to the range, abo
            <clamped>true</clamped>
            <!--Flag indicating whether or not the values of the coordinates should be constrained to the curren
            <locked>false</locked>
            <!--If specified, the coordinate can be prescribed by a function of time. It can be any OpenSim Func
            <prescribed_function />
            <!--Flag indicating whether or not the values of the coordinates should be prescribed according to t
            <prescribed>false</prescribed>
            <!--Flag identifies whether or not this coordinate can change freely when posing the model to satisf
            <is_free_to_satisfy_constraints>false</is_free_to_satisfy_constraints>
          </Coordinate>
        </objects>
        <groups />
      </CoordinateSet>
    </PinJoint>
  </Joint>

```

Figure 8-4 - Kinematic definition between the first link of the self-aligning mechanism, which is connected to the shank structure through a *Pin Joint*.

- Adjustment of the necessary location parameters with the help of the GUI (Graphical User Interface) view (Figure 8-5), in order to correct the relative positions of the parts.

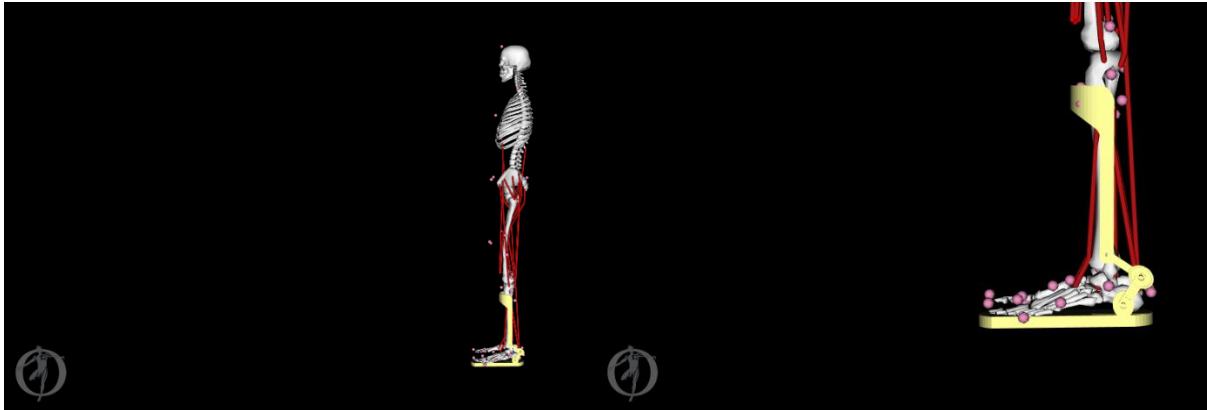


Figure 8-5 – GUI view of the *OpenSim* with the musculoskeletal model and the AFO with the proposed self-aligning mechanism attached to it.

- In order to connect the foot structure of the AFO (*AFO_foot*) to the foot of the musculoskeletal model a constraint must be implemented. *OpenSim* supports three types of constraints (that can be seen in [217]), of which the *Weld Constraint* was chosen so that both bodies have their location and orientation fixed (Figure 8-6);

```
<ConstraintSet>
  <objects>
    <WeldConstraint name="Foot">
      <!--Flag indicating whether the constraint is disabled or not. Disabled means that the constraint is not active i
      <isDisabled>false</isDisabled>
      <!--Specify first of two bodies welded together by the constraint.-->
      <body_1>AFO_foot</body_1>
      <!--Specify second of two bodies welded together by the constraint.-->
      <body_2>calcn_1</body_2>
      <!--Location of the weld in first body specified in body1 reference frame.-->
      <location_body_1>0.1 0.1 0.07</location_body_1>
      <!--Location of the weld in second body specified in body2 reference frame.-->
      <location_body_2>0.102708 0.0308125 0</location_body_2>
    </WeldConstraint>
  </objects>
</ConstraintSet>
```

Figure 8-6 - Kinematic constraint between the AFO's foot structure and the calcaneum of the musculoskeletal model of *OpenSim*.

- Afterwards, the *Inverse Kinematics* tool in *OpenSim* was used to determine the range of angles performed around the sagittal plane by the musculoskeletal model, during two gait cycles (2.5s). Three situations were assessed: a model using an AFO with the self-aligning mechanism, another with an AFO with a simple hinge, and a model without any AFO attached. The results obtained can

be seen in Figure 8-7. As one can verify, the kinematic curve regarding the use of an AFO with a self-aligning mechanism was not similar to the curve concerning the normal walking, without an AFO (24° of difference). This result might also be due to the kinematic constraint defined for the model, which can affect the kinematic behaviour of the model's ankle without any realistic background.

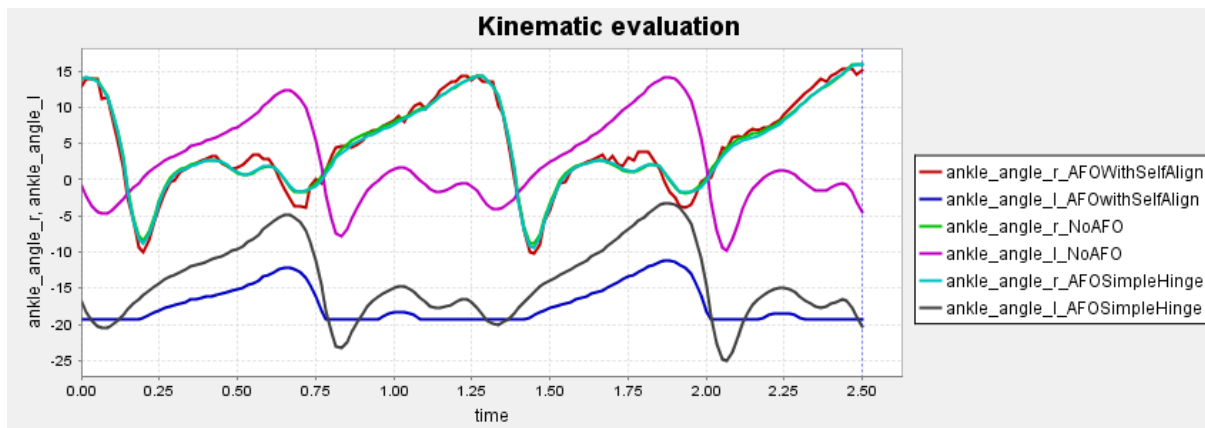


Figure 8-7 – Plot of the kinematic effect of integrating in a musculoskeletal model an AFO with a self-aligning mechanism and an AFO with a simple hinge, as oppose to the kinematic behaviour of a model without any AFO attached.

- Next, the *Inverse Dynamics* tool was used. This *OpenSim* tool calculates the generalized forces necessary to achieve the model desired kinematics. The output file of the inverse kinematics is used as an input in this tool. The same three situations were studied, in order to assess the effect of the self-aligning mechanism on the ankle moment during two gait cycles. The hypothesis tested was if the ankle moment would decrease in the situation of walking with a self-aligning AFO when compared to one with the use of an AFO with a simple hinge. Figure 8-8 shows that the incorporation of an AFO with a simple hinge in the model resulted in higher dorsiflexion peak relative to the incorporation of a self-aligning mechanism and walking without an AFO. Moreover, the use of an AFO with a self-aligning mechanism provided for a similar kinematic behaviour of the ankle joint as the normal walking (*SemAFO* meaning without any AFO).

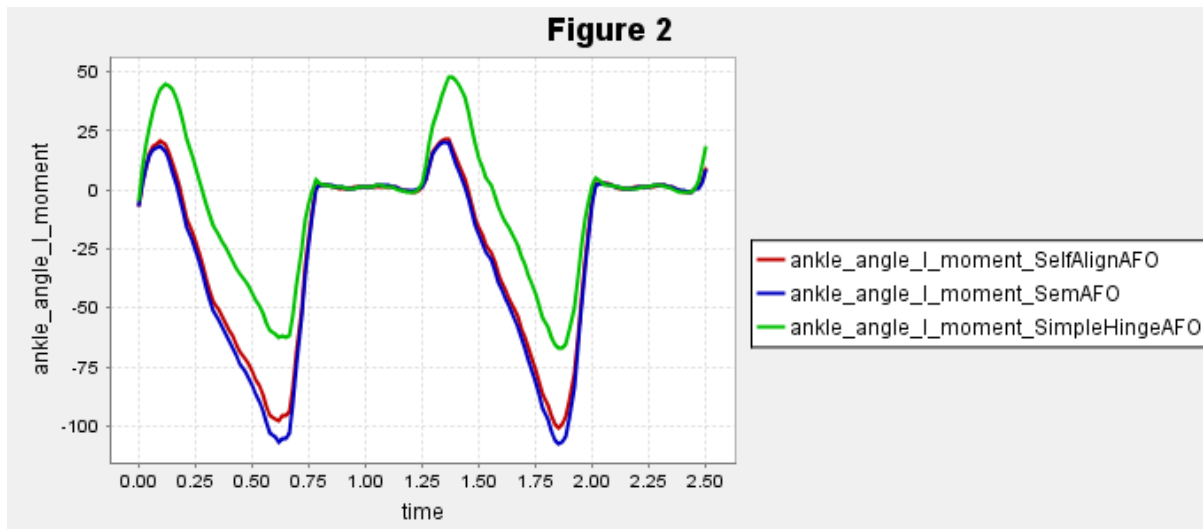


Figure 8-8 - Plot of the kinetic effect of integrating in a musculoskeletal model an AFO with a self-aligning mechanism and an AFO with a simple hinge, as oppose to the kinetic behaviour of a model without any AFO attached.

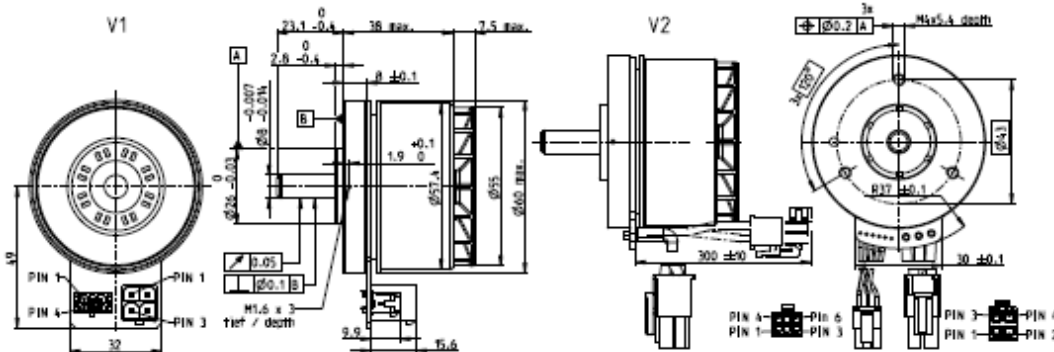
8. These results weren't considered feasible due to limitations regarding the definition of the kinematic behaviour of the self-aligning mechanism. The joint connecting the first link of the mechanism to the shank structure was given the kinematic values of the normal ankle, as a way of imitating the motor actuation. However, the other joints of the mechanism were not given any kinematic values, therefore, the self-aligning mechanism couldn't be simulated properly. In order to achieve a feasible simulations, the mechanism had to be constructed and its kinematic behaviour during gait had to be evaluated. For this reason, the self-aligning mechanism couldn't be considered as a valid solution to accomplish the sub-function **Stabilize the gait**.

E. Selected DC motor specifications

EC 60 flat Ø60 mm, brushless, 200 Watt

Ventilated

EC flat



M 1:2

	Part Numbers		
Stock program			
Standard program			
Special program (on request)			
V1 with Hall sensors	625860	614949	625861
V2 with Hall sensors and cables	647896	642221	647897

Motor Data				
Values at nominal voltage				
1 Nominal voltage	V	12	24	48
2 No load speed	rpm	3760	4300	4020
3 No load current	mA	815	497	224
4 Nominal speed	rpm	2790	3240	3020
5 Nominal torque (max. continuous torque)	mNm	492	536	577
6 Nominal current (max. continuous current)	A	15.7	9.28	4.6
7 Stall torque	mNm	3340	4300	4870
8 Stall current	A	111	81.9	43.2
9 Max. efficiency	%	83.8	85.2	86.3
Characteristics				
10 Terminal resistance phase to phase	Ω	0.108	0.293	1.11
11 Terminal inductance phase to phase	mH	0.0911	0.279	1.28
12 Torque constant	mNm/A	30	52.5	113
13 Speed constant	rpm/V	318	182	84.8
14 Speed/torque gradient	rpm/mNm	1.14	1.01	0.837
15 Mechanical time constant	ms	9.95	8.83	9.29
16 Rotor inertia	gcm ²	832	832	832

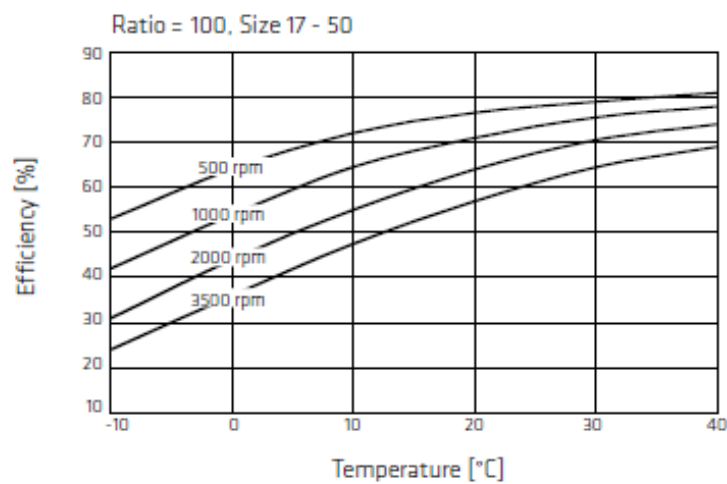
Specifications	Operating Range	Comments		
17 Thermal data		<p>Continuous operation In observation of above listed thermal resistance (lines 17 and 18) the maximum permissible winding temperature will be reached during continuous operation at 25°C ambient. - Thermal limit.</p> <p>Short term operation The motor may be briefly overloaded (recurring).</p> <p>Assigned power rating</p>		
18 Thermal resistance housing-ambient			1.22 K/W	
19 Thermal resistance winding-housing			0.843 K/W	
20 Thermal time constant winding			9.19 s	
21 Thermal time constant motor			44 s	
22 Ambient temperature			-40...+100°C	
23 Max. winding temperature			+125°C	
Mechanical data (preloaded ball bearings)				
24 Max. speed			6000 rpm	
25 Axial play at axial load < 12.0 N			0 mm	
26 Axial play at axial load > 12.0 N			0.14 mm preloaded	
27 Radial play			12 N	
28 Max. axial load (dynamic)			170 N	
29 Max. force for press fits (static) (static, shaft supported)			8000 N	
30 Max. radial load, 5 mm from flange			112 N	
Other specifications				
31 Number of pole pairs			7	
32 Number of phases			3	
33 Weight of motor			360 g	

maxon Modular System		Details on catalog page 38	
Planetary Gearhead	Encoder MILE		
Ø52 mm	512 - 4096 CPT,		
4 - 30 Nm	2 channels		
Page 402	Page 447		
Recommended Electronics:			
Notes	Page 38		
ESCON Module 50/5	487		
ESCON Mod. 50/8 (HE)	488		
ESCON 70/10	489		
DEC Module 50/5	491		
Connector	Part number		
Molex Micro-Fit	43045-0627	43025-0600	
Molex	76829-0104	171692-0104	
Connection cable for V1			
for windings, L = 3 m	520851		
for Hall sensors, L = 3 m	275878		
Calculation does not include saturation effect (p. 61/168)			
*625860 and 647896 cannot be combined with the MILE encoder, because the current limit of the connectors of the MILE circuit board is 13 A.			

F. Harmonic Drive® gear unit specifications and efficiency tables (CSD-25-2A)

Table 10.2

	Unit	CSD-20-2A			CSD-25-2A		
		50	100	160	50	100	160
Ratio	i []	50	100	160	50	100	160
Repeatable peak torque	T_R [Nm]	39	57	64	69	110	123
Average torque	T_A [Nm]	24	34	34	38	75	75
Rated torque	T_N [Nm]	17	28	28	27	47	47
Momentary peak torque standard	T_M [Nm]	69	76	76	127	152	152
Momentary peak torque with enlarged Flexspline bore (BB)	T_M [Nm]	64	64	64	127	135	135
Maximum input speed (oil lubrication)	$n_{in(max)}$ [rpm]	10000			7500		
Maximum input speed (grease lubrication)	$n_{in(max)}$ [rpm]	6500			5600		
Average input speed (oil lubrication)	$n_{av(max)}$ [rpm]	6500			5600		
Average input speed (grease lubrication)	$n_{av(max)}$ [rpm]	3500			3500		
Moment of inertia	J_{in} [$\times 10^{-4}$ kgm ²]	0.090			0.282		
Weight	m [kg]	0.13			0.24		



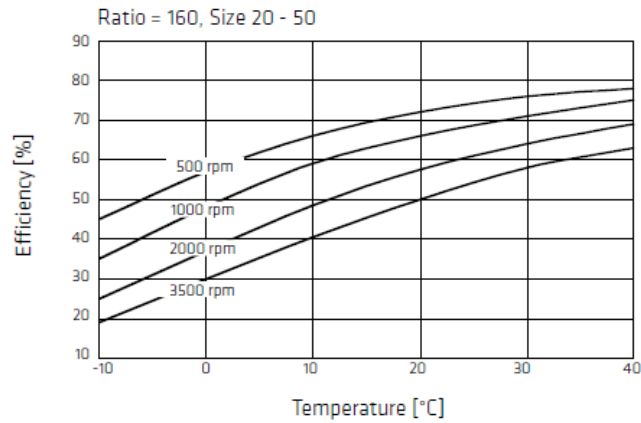
G. Exo-H2 system specifications, efficiency table and side calculations



APPENDIX I : Specifications of the Lower Limb Robotic System.

Lower Limb Robotic System				
Number of Degrees of Freedom	6 degrees of freedom in the sagittal plane. One for hip, knee and ankle in both right and left legs.			
Type of Control	Position, Torque and Admittance in real time control.			
Actuators Strain Wave Gearing (Harmonic Drive)	Ratio	160	i	
	Limit for repeated peak torque	64	T_R [Nm]	
	Limit for average torque	34	T_A [Nm]	
	Rated torque at rated speed 2000 rpm	28	T_N [Nm]	
	Limit for momentary peak torque	76	T_M [Nm]	
	Max. input speed (Oil Lub)	10000	rpm	
	Max. input speed (Grease Lub)	6500	rpm	
	Limit for average input speed (Oil Lub)	6500	rpm	
	Limit for average input speed (Grease Lub)	3500	rpm	
	Moment of inertia	0.09×10^{-4}	[kgm ²]	
	Weight	0.13	[kg]	
	Motors specifications (Hips, Knees and ankles)	1 Nominal voltage	24	V
		2 No load speed	4250	rpm
3 No load current		419	mA	
4 Nominal speed		3850	rpm	
5 Nominal torque (max. continuous torque)		221	mNm	
6 Nominal current (max. continuous current)		4.33	A	
7 Stall torque		3740	mNm	
8 Starting current		78.2	A	
9 Max. efficiency		86	%	
Characteristics:				
10 Terminal resistance phase to phase		0.307	Ohm	
11 Terminal inductance phase to phase		0.188	mH	
12 Torque constant		53.4	mNm/A	
13 Speed constant		179	rpm/V	
14 Speed/torque gradient		1.03	rpm/mNm	
15 Mechanical time constant		13	ms	
16 Rotor inertia	1210	gcm ²		
Communication	CAN buses. Wifi Bluetooth			
Power supply (Charger)	100 – 240 V AC / 50-60 Hz (AC power line)			
Battery LiFePO4	Size (H)	70 ± 2	mm	
	Size (W)	90 ± 2	mm	
	Size (L)	200 ± 2	mm	
	Normal capacity Typ	12.0	Ah	
	Normal capacity Min	11.7	Ah	
	Normal voltage	22.4	V	
	Normal Power	269	Wh	
	Discharging system	8 (const)	A	
	Discharge time (23 ± 3 °C)	≈ 1.5	hour	

Principal structure production material	Stainless Steel and type 7005 aluminum.		
Exoskeleton sensors	Joint Position based on potentiometer: power supply: 5 VDC – range: -100 to 100 degrees – analog output – resolution: 0.5 degree.		
	Joint Interaction Torque: power supply: 5 VDC – range: -40 to 40 Nm – analog output – resolution: 1 Nm.		
	Foot/Ground Contact (heel and toe): power supply: 5 VDC – digital binary output.		
Dimensions	1.180mm tall 150mm long (side view) 230mm wide (front view)		
Weight	approx. 11 kg.		



Nominal Output Speed: $\frac{3850}{160} = 24.1 \text{ rpm}$

Increase (%): $\frac{32.4 - 24.1}{24.1} \times 100 = 34.4\%$

Nominal Output Torque: $221 \times 160 \times 0.5 = 17.7 \text{ N.m}$

Increase (%): $\frac{32.16 - 17.7}{17.7} \times 100 = 81.7\%$

Recommended

Maximum Output Torque: $(221 \times 3) \times 160 \times 0.5 = 53.04 \text{ N.m}$

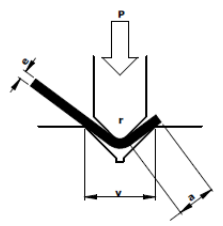
Increase (%): $\frac{96.5 - 53.04}{53.04} \times 100 = 81.9\%$

H. ORTHOSXXI bending specifications table

Espessura da chapa mm (e)	1	1,3	1,6	2	2,5	3	3,5	4	5	6,5	8	10	13	14	16	17	20	22	25	31	35	50	63	78	r
	4	5,5	7	8,5	11	14	15,5	17,5	22	28	35	44	56	63	70	78	88	98	112	140	175	224	280	350	a
0,8	8	6	4																						v
1	14	9	7	5																					
1,25		19	12	9	6																				
1,5			18	14	10	7																			
2				28	19	14	12	11																	
2,5					32	23	21	18	13																
3						36	32	27	19	15															
4							52	38	28	21															
5								63	47	35	26														
6									72	53	39	29													
6,5										84	62	46	34												
7											104	76	56	41	36										
8												105	77	56	48	42									
10													130	94	80	70	62	53	46						
12														123	107	94	80	69	59						
14																134	114	98	83	63					
16																	155	133	112	84					
18																		175	147	107	83				
20																			188	140	106	78			
25																				234	175	128	98		
30																					266	193	146	112	
40																						375	280	211	

P - Força em toneladas p/ metro

TABELA DE QUINAGEM



P - Força em toneladas/metro
e - Espessura da chapa em mm
r - Raio interior em mm
a - Comprimento min. da aba em mm
v - Largura do "V" da matriz

Até 10mm de espessura:
v = 8 x esp.
Acima de 12mm de espessura:
v = 10 x esp.

Os valores da tabela referem-se a quinagem no ar para aço macio de 400-450 N/mm²

(Para outros materiais corrigir os valores proporcionalmente de acordo com a nova tensão de ruptura. Ex. Para **alumínio** com 200N/mm2 (=20kgf/mm2) dividir o valor da tabela por 2.
Para **aço inox** com 700N/mm2 (=70kgf/mm2) multiplicar o valor da tabela por 1,6.)

I. Bolts mechanical properties information

Nominal Maior Diameter d mm	Coarse-Pitch Series			Fine-Pitch Series		
	Pitch p mm	Tensile- Stress Area A _t mm ²	Minor- Diameter Area A _s mm ²	Pitch p mm	Tensile- Stress Area A _t mm ²	Minor- Diameter Area A _s mm ²
1,6	0,35	1,27	1,07			
2	0,40	2,07	1,79			
2,5	0,45	3,39	2,98			
3	0,5	5,03	4,47			
3,5	0,6	6,78	6,00			
4	0,7	8,78	7,75			
5	0,8	14,2	12,7			
6	1	20,1	17,9			
8	1,25	36,6	32,8	1	39,2	36,0
10	1,5	58,0	52,3	1,25	61,2	56,3
12	1,75	84,3	76,3	1,25	92,1	86,0
14	2	115	104	1,5	125	116
16	2	157	144	1,5	167	157
20	2,5	245	225	1,5	272	259
24	3	353	324	2	384	365
30	3,5	561	519	2	621	596
36	4	817	759	2	915	884
42	4,5	1120	1050	2	1260	1230
48	5	1470	1380	2	1670	1630
56	5,5	2030	1910	2	2300	2250
64	6	2680	2520	2	3030	2980
72	6	3460	3280	2	3860	3800
80	6	4340	4140	1,5	4850	4800
90	6	5590	5360	2	6100	6020
100	6	6990	6740	2	7560	7470
110				2	9180	9080

*The equations and data used to develop this table have been obtained from ANSI B1.1-1974 and B18.3.1-1978. The minor diameter was found from the equation $d_s = d - 1,226 869p$, and the pitch diameter from $d_p = d - 0,649 519p$. The mean of the pitch diameter and the minor diameter was used to compute the tensile-stress area.

Figure 8-9 – Dimensions and areas of the different bolt's sizes [218].

Metric Mechanical-Property Classes for Steel Bolts, Screws, and Studs*








Property Class	Size Range, Inclusive	Minimum Proof Strength, † MPa	Minimum Tensile Strength, † MPa	Minimum Yield Strength, † MPa	Material	Head Marking
4.6	M5–M36	225	400	240	Low or medium carbon	
4.8	M1.6–M16	310	420	340	Low or medium carbon	
5.8	M5–M24	380	520	420	Low or medium carbon	
8.8	M16–M36	600	830	660	Medium carbon, Q&T	
9.8	M1.6–M16	650	900	720	Medium carbon, Q&T	
10.9	M5–M36	830	1040	940	Low-carbon martensite, Q&T	
12.9	M1.6–M36	970	1220	1100	Alloy, Q&T	

Figure 8-10 – Metric Mechanical-Property classes for steel bolts, disclosing the proof and yield strength of different sizes bolts.

Bolt Condition	K
Nonplated, black finish	0.30
Zinc-plated	0.20
Lubricated	0.18
Cadmium-plated	0.16
With Bowman Anti-Seize	0.12
With Bowman-Grip nuts	0.09

Figure 8-11 – Friction coefficient K of different bolt conditions. Notice that zinc-plated corresponds to the conditioned of galvanized steel bolts.